An investigation into the potential toxicity of ErbB targeting T4 immunotherapy

Van Der Stegen, Sjoukje

Awarding institution:
King's College London

AN INVESTIGATION INTO THE POTENTIAL TOXICITY OF ERBB TARGETING T4 IMMUNOTHERAPY

Sjoukje Judith Catherina van der Stegen

1052615

Submitted to King's College London for the award of Doctor of Philosophy

CAR Mechanics Group

Research Oncology

Division of Cancer Studies

King's College London

July 2013

Für Opa und Oma

Wir haben es geschafft!

ABSTRACT

The five-year survival rate of patients with head and neck squamous cell carcinoma (HNSCC) has remained stable at 50% over the past five decades. Consequently, new treatment options are required. In approximately 90% of cases, over-expression of the tumour associated antigen ErbB1 is seen. T4 immunotherapy retargets T-cells against the extended ErbB-receptor family and could be beneficial for HNSCC patients. T4 immunotherapy comprises the combined expression of the ErbB-targeting chimeric antigen receptor T28ζ and the chimeric cytokine receptor 4αβ. Human $T4^+$ T-cells have a potent anti-tumour effect. However, ErbB expression is not exclusive to tumour tissue, raising the concern of toxicity in healthy tissue. Here, I have investigated the potential toxicity of T4 immunotherapy in a SCID/Beige immunodeficient mouse model. Human $T4^+$ T-cells are activated by mouse ErbB receptors and consequently destroy both healthy and transformed mouse cells. Intravenous or intra-tumoural $T4^+$ T-cell administration did not result in any clinical or histopathological toxicity. However, intraperitoneal $T4^+$ T-cell administration resulted in severe cytokine release syndrome (CRS). Target recognition in the peritoneal cavity resulted in elevated levels of serum human IL-2 and IFNγ, as well as mouse IL-6. The severity of CRS is hypothesized to be due to a combination of the $T4^+$ T-cell dose, magnitude of target recognition, and macrophage content within the peritoneal cavity. In keeping with this, macrophage depletion ameliorates both IL-6 production and toxicity. Together, these data show that the SCID/Beige mouse is an adequate model to study T4 immunotherapy related toxicity. Furthermore, these results suggest that there may be a window for therapeutic application of $T4^+$ T-cells since anti-tumour efficacy has been demonstrated at lower cell doses without the induction of toxicity. These findings, support progression to a Phase-I clinical trial in which patients with locally recurrent HNSCC are treated with intra-tumoural $T4^+$ T-cells.

TABLE OF CONTENTS

LIST OF FIGURES

LIST OF TABLES

LIST OF ABBREVIATIONS

293T	Cell line derived from HEK293 cells that have been stable transfected with the SV40 T antigen
2B4	Natural Killer Receptor 2B4 (CD244)
435	MDA-MB-435
4αβ	IL-4Rα – IL-2/15Rβ chimeric cytokine receptor
AC	Adherent culture
ACD	Citrate-Dextrose solution
ACT	Adoptive cell therapy
ADCC	Antibody-dependent cell cytotoxicity
ADL	Activities of daily living
AICD	Activation induced cell death
ALL	Acute lymphoblastic leukaemia
APC	Allophycocyanin
ATP	Adenosine triphosphate
BDT	Big Dye Terminator
BG	Background
BLI	Bioluminescent imaging
BMR	Batch manufacturing record
BSA	Bovine serum albumin
BSA	Body Surface Area
C	Constant
C-EST	CAR^+ EBV-specific T-cells
C-NST	CAR^+ non-specific T-cells
$C_2H_4O_2$	Acetic Acid
CA	Capsid
$CaCl_2$	Calcium Chloride
CAIX	Carbonic anhydrase IX
CAR	Chimeric antigen receptor
CASP	Caspase
CBA	Cytometric Bead Array
CBD	Cell-binding domain

CCR	Chemokine receptor
CD44v6	CD44 exon v6
cDNA	Copy DNA
CEA	Carcinoembryonic antigen
Cet-ST	Cetuximab-induced skin toxicity
cG250	chimeric G250
CH_3CO_2K	Potassium Acetate
CIP	Calf Intestinal Alkaline Phosphatase
CIR	Chimeric immune receptor
CLL	Chronic lymphocytic leukaemia
CMV	Cytomegalovirus
CPDA	Citrate phosphatase dextrose adenine
CR	Complete response
CRC	Colorectal cancer
CRF	Clinical research facility
CRS	Cytokine release syndrome
CRUK	Cancer Research UK
CS-1	Cyclin D3 subset 1
CSF-1	Colony-stimulating factor-1
CT	Computerised tomography
CTA	Cancer/testis antigen
CTCAE	Common terminology for adverse events
cTCR	chimeric T-cell receptor
CTE	Constitutive transport element
CTL	Cytotoxic T-lymphocytes
CTLL-2	Interleukin-2 dependent mouse $CD8^+$ T-cell line
CTP	Cytosine triphosphate
DAP10	DNAX-activation protein-10
DAPI	4’,6-diamidino-2-phenylindole
dATP	Deoxyadenosine triphosphate
DC	Dencritic Cells
ddNTP	Dideoxynucleotide triphosphate
DEAE	diethylaminoethyl

dH_2O	Distilled water
DLCL	Diffuse large cell lymphoma
DLT	Dose-limiting toxicity
DMEM	Dulbecco's Modified Eagle Medium
DMSO	Dimethyl Sulfoxide
DNA	Deoxyribonucleic acid
dsDNA	Double stranded DNA
E.Coli	*Escherichia Coli*
EBV	Eppstein-Barr virus
ECD	Energy coupled dye
EDTA	Ethylenediaminetetraacetic acid
EGF	Epidermal growth factor
EGFR	Epidermal growth factor receptor
EGFRvIII	Epidermal growth factor receptor variant III
ELISA	Enzyme linked immunosorbent assay
EMA	European Medicines Agency
EpCAM	Epithelial cell adhesion molecule
EPG	Epithelial glycoprotein
ErbB	Erythroblastosis oncogene B
ERK	Extracellular signal-regulated kinase
EtOH	Ethanol
FACS	Fluorescence activated cell sorting
FAR	Foetal acetylcholine receptor
FasL	Fas ligand
FBP	Folate binding protein
FBS	Foetal Bovine Serum
FcγR	Fc gamma receptor
FcγR	IgG Fc receptor
FDA	Food and Drug Administration
FEP	Fluorinated ethylene propylene
ffLuc	Firefly Luciferase
FITC	Fluorescein isothiocyanate
FL	Follicular lymphoma

FMS	Macrophage colony stimulating factor-1 receptor
FR	Folate receptor
G	Gauge
G250	Renal cell carcinoma-associated antigen 250
GALV	Gibbon-Ape Leukaemia Virus
GD2	Diasialoganglioside-2
Gen	Generation
GM-CSF	Granulocyte macrophage colony-stimulating factor
GMP	Good manufacturing process
gp100	Glycoprotein 100
GTP	Guanidine triphosphate
GvHD	Graft versus Host Disease
GvHR	Graft versus Host Response
h	Human
H29D	Human retroviral packaging cell line derived from HEK293 cell, expressing the MoMLV *gag-pol* genes and the VSV-G *env* gene
H_2O	dihydrogen mono-oxide
H4	Combined expression of HOX and 4αβ
HACA	Human anti-CAR antibodies
HB-EGF	Heparin-binding epidermal growth factor
HBS	HEPES-buffered saline
HCl	Hydrochloric acid
HCM	Human cardiac myocytes
HED	Human Equivalent Dose
HEK	Human embryonic kidney
HEK293	Adenoviral 5-transformed HEK cells
HER	Human Epithelial Growth Factor Receptor/ Homologous EGF Receptor Kinase
HIV	Human immunodeficiency virus
HLA	Human leukocyte antigen
HMEC	Human mammary epithelial cells
HMW-MAA	High molecular weight melanoma-associated antigen
HNSCC	Head and Neck Squamous Cell Carcinoma

HOX	HMGF2 scFv – IgD hinge – IgG_1 Fc and hinge – CD28 – OX40 – CD3ζ MUC1-targeting CAR
HPMEC	Human pulmonary microvascular endothelial cells
HPV	Human Papillomavirus
HRE	Human renal epithelial cells
HRP	Horseradish peroxidase
HS	Human serum
HSCT	Haematopoietic stem cell transplant
HSMM	Human skeletal muscle myoblasts
HUVEC	Human umbilical vein endothelial cells
IC	Intracellular
ICAM	Intracellular adhesion molecule
ICOS	Inducible costimulatory
IFN	Interferon
Ig	Immunoglobulin
IL	Interleukin
IP	Intra-peritoneal
IRES	Internal ribosome entry site
is	*in situ*
IT	Intra-tumoural
ITAM	Immunoreceptor tyrosine-based activation motif
IU	Infectious units
IV	Intravenous
KCl	Potassium Chloride
K_m factor	Weight (kg) / BSA (m^2)
KOH	Potassium hydroxide
L-PHA	Phytohaemagglutinin/Leucoagglutinin
L.Broth	Luria-Broth
LAK-cells	Lymphocyte activating killer cells
LB	Luria-Broth
LC	Liposomal clodronate
LFA	Lymphocyte function associated antigen
LMP	Latent membrane protein

LP	Liposomal PBS
LTR	Long terminal repeat
Lymphodepl	Lymphodepletion
m	Mouse
M	Metastasis
Ma	Matrix
MA	Matrix
mAb	Monoclonal Antibody
MAGE	Melanoma antigen
MAPK	Mitogen-activated protein kinase
MART	Melanoma-associated antigen recognized by T-cells
MBS	Membrane Binding Solution
MDM2	Mouse double minute 2
MeOH	Methanol
MET	Mesenchymal-epithelial transition factor
$MgCl_2$	Magnesium Chloride
$MgSO_4$	Magnesium Sulphate
MHC	Major Histocompatibility Complex
MHRA	Medicines and Healthcare products Regulatory Agency
MLTC	Mixed lymphocyte tumour cell culture
MMP	Matrix metalloproteinases
$MnCL_2$	Manganese Chloride
MoMLV	Moloney murine leukaemia virus
MOPS	3-(N-Morpholino)-propanesulfonic acid
MPC	Magnetic particle concentrator
MPMEC	Mouse Pulmonary Microvascular Endothelial Cells
MPMV	Mason-Pfizer monkey virus
MTD	Maximum tolerated dose
MTT	(3-[4,5-dimethylthiazol-2-yl]-2,5-diphenyltetrazolium bromide
MUC	Mucin
MWS	Membrane Wash Solution
N	Node
NaCl	Sodium Chloride

NaOH	Sodium Hydroxide
NC	Nucleocapsid
NCAM	Neural cell adhesion molecule
NCI	National Cancer Institute
NEB	New England Biolabs
NHBE	Human bronchial/tracheal epithelial cells
NHL	Non-Hodgkin's lymphoma
NIH	National Institutes of Health
NK-cells	Natural killer cells
NKT-cells	Natural killer T-cells
NPC	Nasopharyngeal carcinoma
NRG	Neuregulin
NSCLC	Non-small cell lung cancer
NY-ESO	New York Oesophageal antigen-1
OK-432	multiple cytokine inducer derived from the low-virulence SU strain of *Streptococcus pyogenes*
OK-MC	OK-432 activate PBMCs
OK-SC	OK-432 activated spleen cells
OR	Objective response
OS	Overall survival
OSCC	Oral squamous cell carcinoma
P28ζ	J591 svFv –CD28-CD3ζ PSMA-targeting CAR
P2A	*Porcine tescho* virus-1 2A
P4	Combined expression of P28ζ and 4αβ
PAC	Pancreatic adenocarcinoma
PAP	Prostatic-acid phosphatase
PBMCs	Peripheral blood mononuclear cells
PBS	Phosphate buffered saline
PCR	Polymerase Chain Reaction
PD-1	Programmed death-1
PE	phycoerythrin
PEI	Polyethylenimine
PerCP	Peridinin-chlorophyll-protein complex

PF	Progression-free
PFS	Progression free survival
PG13	Murine retroviral packaging cell derived from NIH 3T3 fibroblasts, containing the MoMLV *gag-pol* genes and the GALV *env* gene
PI3K	phosphatidylinositol 3-kinase
PKC	Protein kinase-C
PLCγ	Phospholipase-Cγ
PLP	PC3-LN3-PSMA
PR	Partial remission
PR	Partial response
PrEC	Prostate epithelial cells
PSCA	Prostate specific cell antigen
PSMA	Prostate specific membrane antigen
PT	Peri-tumoural
R	Receptor
r	Recombinant
RbCl	Rubidium Chloride
RCC	Renal cell carcinoma
RCM	Remaining complete media
RCR	Replication-competent retrovirus
RN	RetroNectin
RNA	Ribonucleic acid
ROR1	Receptor orphan tyrosine kinase receptor 1
rpm	Revolutions per minute
RPMI	Roswell Park Memorial Institute
RR	Response rate
S100	S100 calcium binding protein
SAE	Serious adverse event
SARS	Severe acute respiratory syndrome
SC	Subcutaneous
SCC	Squamous cell carcinoma
scFv	Single chain variable fragment
SCID	Severe combined immunodeficiency

SD	Stable disease
SD	Standard deviation
SDS	Sodium dodecyl sulphate
SOC	Super optimal broth with catabolite repression
SOFA	Sequential organ failure assessment
SPECT	Single photon emission computed tomography
SSX	Synovial sarcoma X
STAT	Signal transducer and activator of transcription
SV40	Simian virus 40
T	Tumour
T1E	EGF/TGFα chimera
T28ζ	T1E-CD28-CD3ζ ErbB-targeting CAR
T2A	*Thosea asigna* virus 2A
T4	Combined expression of T28ζ and 4αβ
T4luc	Combined expression of T28ζ, 4αβ and firefly Luciferase
TAA	Tumour associated antigen
Tag72	Tumour associated glycoprotein 72
TBE	Tris-borate EDTA
TBI	Total body irradiation
TCR	T-cell receptor
TGF	Transforming growth factor
T_H	Helper T-cell
TILs	Tumour infiltrating lymphocytes
T_M	Melting Temperature
TMB	Tetramethylbenzadine
TNF	Tumour necrosis factor
TNM	Tumour Node Metastasis
TNP	2,4,6-trinitrophenyl
TPBG	Trophoblast glycoprotein
Treg	Regulatory T-cells
Tris-Cl	Tris(hydroxymethyl)amino methane
TSA	Tumour-specific antigen
tTa	Tetracycline-transactivator

TTP	Thymidine triphosphate
TTP	Time to progression
UT	Untransduced
v/v	volume/volume
VEGF	Vascular endothelial growth factor
V_H	Variable heavy chain
V_L	Variable light chain
VLA	Very Late Antigen (Integrin α4β1)
VSV-G	Vesicular stomatis virus G
w/v	weight/volume
WT-1	Wilm's Tumour antigen-1
Zap-70	Zeta-chain associated protein 70
α	Anti
β_c	β-chain
γ_c	Common γ-chain

ACKNOWLEDGEMENTS

First and foremost I would like to thank my supervisor *Dr John Maher*. John, thank you for taking me on as an MSc student, and for giving me the opportunity to do this PhD at the end of the 'Spanish Soap Opera'. You were the best supervisor I could have wished for, always available for advice, discussions and a laugh. In the beginning you told me that a PhD is mainly about character building, and there has certainly been some of that. However, most importantly you have taught me to be confident about my ideas and my research, which I am very grateful for. It has been wonderful to work in your CAR Mechanics Group.

Marc (dr D, aka the perfect PhD student) you have been an amazing example to me on how to be a PhD-student. Thank you for teaching me everything when I first came here, and especially for putting up with all my ill-timed questions during your well-deserved lunch breaks. *Rich* (dr B), if you had not suggested that I should and still could apply, I wouldn't have been here right now. I can not thank you enough for that 2 minute conversation (and all the other long random ones which made our days with long incubations last even longer because we got distracted by dry ice-games or ceilidh dancing).

Ana (APPP), thank you for always being an honest and good friend. I am sure we will find a way to keep an eye on each other even if we are no longer in the same lab (I have already appointed spies, be warned). *May* (Maizzie) somehow you managed to make work in the GMP facility fun, despite all our luck with lymphodepleted, cold, or absent blood samples. *Thivyan* (Thiv, Thyrian, Ladyboy) thank you for being an amazing friend, who is there, no questions asked. I am sure you will do great during your PhD and give John some entertaining scenarios to encounter when he walks into the office. Everyone else in the CAR Mechanics Group and BCBG, *Scott, Laura, Sophie, Lynsey, Vincent, Jean, Leticia, Astero, Daniella, Roseanna, Nia, Daisy, Franco, Steve, Deanna, Julia, Sylvain, Debbie, Prof Joy Burchell and Prof Joyce Taylor-Papadimitriou*. Thank you for all your help and laughter and for tolerating my chit-chat and loud-ness around the office (and corridor, and lab, and tea room, basically everywhere).

Everyone at Bart's*, Julie, Jerome, Jane, Julius,* and *Steven Mather*, for allowing me to keep on coming back for more experiments and sharing your always present chocolate/cookies with me.

All the wonderful *students* who visited our lab. You have made me appreciate all the help I got from my supervisors during my projects a lot more. Not just that, you also showed me that the things I learned in Math, actually have a use in life!

My lovely flatmates *Julia*, *Tom*, *Patches*, *Ania*, *Matt*, *Christian* and *KJ* for making no. 53 my home in London.

The *PhD-room bunch*, you made sure life on the office-side never got boring, and that there was always a good story to tell about our nights out.

All my amazing friends, on both sides of the English Channel. I have the best friends anyone could wish for. Thank you for always being there, through the laughs, tears and mischief.

Paps en *Mams,* zonder jullie hulp, steun en stimulans zou ik hier nooit gekomen zijn. Dankjulliewel dat jullie er atlijd voor me zijn. Bedankt voor alle kaartjes, knuffels, pakketjes, ritjes van- en naar het vliegveld en dat er altijd tijd en ruimte was om thuis te komen wanneer ik dat wilde. *Friederike* en *Philip*, ik ben ontzettend trots het sandwich-kind tussen jullie twee te mogen zijn.

Opa und *Oma*, diese These ist euch gewidmet. Danke für alle Telefonate, Briefe und Karten, euer Interesse an allem was ich gemacht habe und euer fester Glaube an mich. Wir haben es geschafft und werden uns jetzt ein neues Ziel setzen müssen. Ich denke jeden Tag an euch.

CHAPTER 1

INTRODUCTION

1.1 Head and Neck Squamous Cell Carcinoma

Head and neck cancer encompasses epithelial malignancies that arise in the paranasal sinuses, oral cavity, nasal cavity, pharynx, and larynx (see Figure 1-1). Approximately 90% of head and neck cancers are squamous cell carcinomas (1). Globally, about 650,000 cases of head and neck squamous cell carcinoma (HNSCC) are diagnosed every year, leading to 350,000 deaths (2) making it the sixth most common cancer (3, 4). The median age of patients at diagnosis is early 60s with a male predominance (2, 5). The mortality rate associated with the disease has remained unchanged over the past 50 years with a 5-year survival rate of approximately 60% (3-5). Contributory factors to poor prognosis include advanced stage of the disease at clinical presentation, significant co-existing co-morbidities, high incidence of second primary carcinomas (6), relapse at the primary site and distant metastases (7). The presence of one or all of these factors renders a significant proportion of patients unsuitable for curative treatment (6).

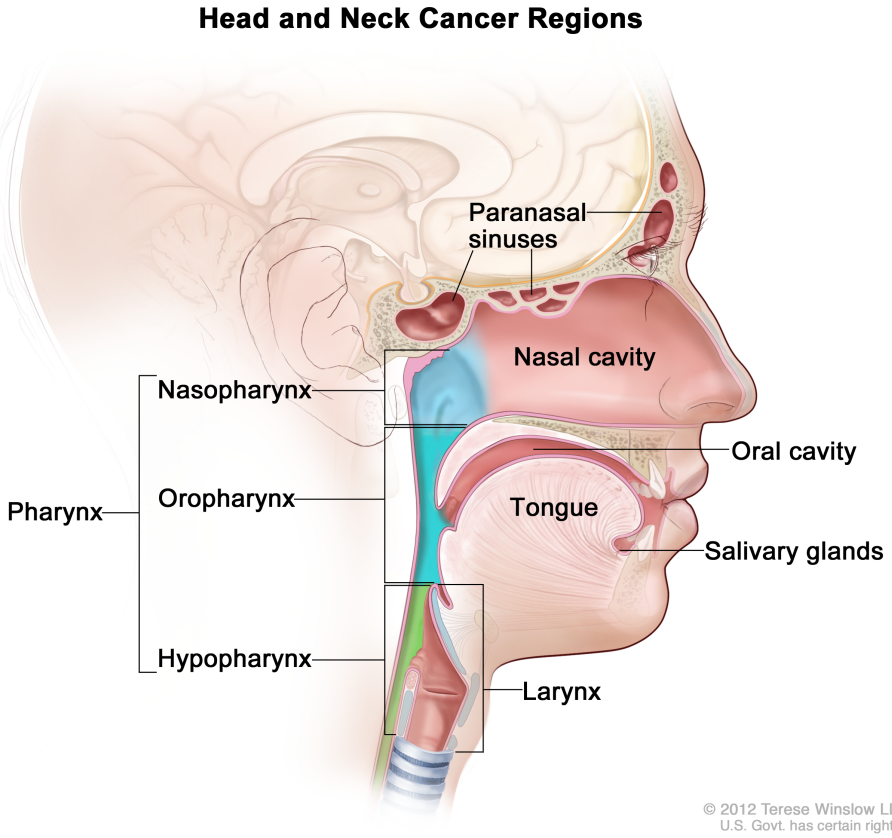

Figure 1-1 Areas of head and neck squamous cell carcinoma
Illustration of the areas in which HNSCC can occur, including the paranasal sinuses, nasal cavity, pharynx (including nasopharynx, oropharynx and hypopharynx), larynx, tongue and salivary glands. © Terese Winslow LCC, U.S. Government has certain rights.

1.1.1 Risk Factors

Head and neck squamous cell carcinoma can be considered as a heterogeneous disease. The majority of patients have one of two distinct risk factor backgrounds, namely high tobacco and/or alcohol consumption and human papillomavirus (HPV) or Epstein-Barr virus (EBV) seropositivity.

1.1.1.1 Tobacco and Alcohol Consumption

Three-quarters of the cases of HNSCC are believed to be related to tobacco consumption (8). Consumption of more than 20 cigarettes a day (9), as well as prolonged exposure to involuntary smoking (for more than 15 years) at home or at work is associated with a higher risk (10). The risk added through tobacco use is larger among women than among men (11). Cessation of smoking at the age of 30 reduces the risk by 90%, whereas stopping smoking at the age of 50 reduces risk by 50% (12). Chewing a variety of products (whether tobacco containing or not) was identified as a risk factor for hypopharyngeal cancer in individuals who had never smoked (13). Alcohol consumption increases the risk of HNSCC independent of the type of alcoholic beverage (14, 15). A combination of tobacco and alcohol use has a synergistic effect to increase the risk of developing HNSCC (14).

1.1.1.2 Human Papillomavirus and Epstein-Barr Virus-Related HNSCC

Infection with oncogenic HPV, mainly HPV type 16 and to a lesser extent type 18, has been associated with the pathogenesis of a subgroup of HNSCC cases (16). The HPV-16 subtype accounts for 90% of HPV-associated HNSCC cases (17). Genomic DNA of oncogenic HPV is detected in approximately 26% of all HNSCC cases, and is most consistently detected in oropharyngeal squamous cell carcinoma (OSSC) (16). Exposure to HPV can precede the appearance of OSCC by 10 years or more. Oral HPV infection is strongly associated with the risk of developing HNSCC, independent of tobacco and alcohol use (16). Among light-drinkers or never smokers, HPV seropositivity is associated with a 30-fold increased risk of developing HNSCC, compared to HPV negativity (18). Due to the different risk-factor profiles, HPV-16-positive and HPV-16-negative HNSCC should be considered as different cancers (19). HPV positivity is a favourable prognostic factor in HNSCC. Tumours that are HPV positive show better responsiveness to radiation and chemotherapy and additionally may be more

susceptible to immune surveillance (20). HPV-positive HNSCC is associated with a lower risk of dying as well as a lower risk of recurrence compared to HPV-negative HNSCC (21). Consequently, HPV status of HNSCC is an important predictive biomarker and needs to be taken into consideration during treatment design (5).

Infection with Epstein-Barr virus (EBV) has also been associated with HNSCC, especially undifferentiated or poorly differentiated nasopharyngeal carcinoma (NPC). The primary EBV-encoded oncogene latent membrane protein (LMP) 1 has been identified as a potential central player in the initiation and progression of NPC. Promotion of cell growth, downregulation of cell-cell adhesion and upregulation of cell motility have all been contributed to LMP1 positivity, increasing the metastatic properties of NPC (22). Plasma EBV DNA levels can be used as a prognostic marker for NPC. Overall survival and relapse-free survival are significantly worse in patients with persistently detectable plasma EBV DNA, compared to patients with undetectable EBV DNA after completion of radiotherapy (23). Similar to HPV seropositivity, there is no confounding effect of EBV-seropositivity in the association between tobacco and alcohol consumption and NPC risk. Tobacco and alcohol consumption can be identified as the cause of over two-thirds of differentiated NPC, whereas EBV-positive tumours are generally poorly differentiated (24, 25).

1.1.1.3 Additional Risk Factors

Independent from the major risk factors presented above, poor dentition (26) and bad oral hygiene (27) have also been associated with the risk of HNSCC. This is possibly related to chronic oral bacterial infections (1). Dietary risks have revealed a positive association with a Western dietary pattern and an inverse association with total fruit and vegetable intake (28, 29). Finally, a low socioeconomic status has also been correlated to the incidence of HNSCC (30)

1.1.2 Current Treatment Options for HNSCC

Treatment of HNSCC is individualised for patients based on multiple clinical factors including primary tumour site, stage and resectability, as well as factors such as swallowing and airway considerations, organ preservation and co-morbidity (5). Tumour stage is determined based on the tumour, node, metastasis (TNM) staging system (see Table 1-1) and can be grouped in stages levelled I to IV (see Table 1-2) (31) Accurate staging is considered the most important factor to guide therapeutic planning (5). Approximately 30% of patients present with early-stage disease (stage I or II) (32) whereas about 60% present with locally advanced disease (stage III or IV). Distant metastasis is present in about 10% of patients at first presentation (5)

Table 1-1 TNM staging of HNSCC

	Tumour (T)	Node (N)	Metastasis (M)
X	Can not be assessed	Can not be assessed	Can not be assessed
is	*in situ*		
0	No evidence	No evidence	No evidence
1	Limited to one site <2cm	1 lymph node <3cm	Distant metastases
2	Limited to one site 2-4cm	1 or more lymph nodes <6cm	
3	Limited to one site >4cm	1 or more lymph nodes >6cm	
4	Invasive tumour		

Exact criteria of TNM staging in HNSCC are determined by the location of the primary tumour, here a summery is given based on the guidelines given in reference (31). TNM: Tumour, Node, Metastasis; *is*: *in situ*

Table 1-2 Tumour stage level I-IV based on TNM stage

	Tumour (T)	Node (N)	Metastasis (M)
0	T*is*	N0	M0
I	T1	N0	M0
II	T2	N0	M0
III	T1-3	N0-1	M0
IV	T4	N0-3	M0-1

Exact criteria of TNM staging in HNSCC are determined by the location of the primary tumour, here a summery is given based on the guidelines given in reference (31). *is: in situ*

1.1.2.1 Early-Stage Disease

The major line of treatment for early stage disease is surgery or radiation therapy. In 90% of stage I patients and 70% of stage II patients, such treatment is curative. The exact approach taken mainly depends on the site of the primary tumour. However, surgery is often preferred to limit the long term complications related to radiation therapy (5).

1.1.2.2 Locally Advanced Disease

A combination of surgery, radiation therapy, chemotherapy or chemoradiotherapy is the first line of treatment for patients with stage III or IV disease. In unresectable locally advanced disease, chemoradiotherapy is the standard of care (32, 33). Tumours are considered unresectable if there is (impending) invasion of major vessels, at the base of the skull or the prevertebral musculature (5).

At least 50% of patients who present with locally advanced disease develop locoregional or distant relapse within 2 years of the treatment. At this stage, few patients are eligible for salvage surgery (34). Local recurrence can be due to outgrowth of residual malignant cells after treatment or due to pre-neoplastic mucosal epithelium which surrounded the primary tumour (32). The main objective of treatment at this stage is symptom palliation and survival extension. The standard first-line treatment for these patients is platinum-based chemotherapy, giving patients a median progression free survival (PFS) of 2.7 months (35). Clinical trials have combined platinum based chemotherapies with the EGFR-targeting antibody Cetuximab. As a first-line treatment, combined therapy with Cetuximab and platinum-based chemotherapy resulted in a significantly prolonged median overall survival (OS), median PFS, and increased response rate (RR) (36). As a result of these data, the FDA (Food and Drug Administration) and EMA (European Medicines Authority) have approved of the use of Cetuximab in the treatment of HNSCC. The use of Cetuximab in treatment of HNSCC is further detailed in paragraph 1.2.4. There is no standard second-line therapy for patients with locally advanced disease. Without treatment, the median survival for patients is 11.5 months after diagnosis (6).

1.1.2.3 Side Effects

Acute as well as late side effects and complications can occur due to treatment of HNSCC. Common acute effects in relation to radiation therapy are mucositis, increased secretions, dysphagia, loss of taste, hoarseness caused by laryngeal oedema and dermatitis (37). Swallowing function can improve within the first year after treatment but may be permanent (38, 39). Other late complications include osteoradionecrosis, dental caries, subcutaneous fibrosis, thyroid dysfunction, sensorineural hearing loss, pharyngeal or oesophageal stenosis and myelitis. In long-term survivors, radiation-induced xerostomia occurs universally (40).

Side effects associated with chemotherapy include anaemia, neutropenia, thrombocytopenia, hypomagnesaemia, fatigue, skin rash, anorexia and infection (36). The combination of platinum-based chemotherapy with Cetuximab has also resulted in short-term side effects in the form of rash and infusion-related reactions (36).

1.2 The ErbB Receptor Family

The avian erythroblastosis oncogene B (ErbB) tyrosine kinase receptor family consists of four members, the epidermal growth factor receptor (EGFR; ErbB1), ErbB2 (Her2/Neu), ErbB3 (Her3) and ErbB4 (Her4) (41). This family constitutes a group of single pass transmembrane growth factor receptors, in which an extracellular ligand-binding domain is linked to an intracellular signalling domain by a hydrophobic, α-helix-structured, transmembrane region (42-44). The ErbB2 and ErbB3 receptors are distinct from the other family members in that no ligand has been discovered for ErbB2 while ErbB3 has an impaired kinase domain (45). ErbB2 is the favoured dimerization-partner for the other ErbB receptors, and ErbB3 can be activated through heterodimerisation with other ErbB-receptors (46). ErbB4 consists of two pairs of naturally occurring isoforms, differing in their juxtamembrane domain and C-termini (47). Involvement of the receptor family in oncogenesis was first suggested by the discovery that the avian erythoblastosis tumour virus encoded an aberrant form of EGFR (48).

1.2.1 Tumour Antigens

The involvement of the ErbB receptor family in cancer renders these molecules candidate tumour antigens. There are different types of tumour antigens. Tumour specific antigen (TSAs) are antigens which are exclusively expressed on tumour tissue, such as mutant caspase (CASP)-8 (49) or EGFRvIII (50). Tumour associated antigens (TAAs) are self-antigen which are expressed on healthy tissue but are aberrantly expressed on tumours (such as the ErbB-receptor family). Some are associated with a specific differentiation stage or lineage (for example carcinoembryonic antigen (CEA) (51) or melanoma antigen (MAGE)-1 (52)). The cancer/testis antigens (CTA) are a group of tumour antigens in which normal organ expression is restricted to germ cells in the testis. In malignancy, gene regulation is disrupted, leading to aberrant expression of these antigens by tumour cells. Cancer/testis antigens include New York oEsophageal antigen (NY-ESO)-1, MAGE-A and synovial sarcoma X (SSX) antigen (53). Finally, there are virally encoded oncogenes (such as HPV-derived E6 or E7 (54)). For clinical applicability, the tumour antigen has to be important for tumour survival and malignant behaviour and should preferably be expressed in a majority of patients (55).

The ErbB receptor family is overexpressed on a vast range of solid tumours, making it an interesting tumour antigen for targeted therapies.

1.2.2 The Role of the ErbB Receptor Family in Healthy Tissues

The main function of the ErbB receptor family in normal tissues is to mediate cell-cell interactions in organogenesis and during adulthood. Absence of any of the four ErbB-receptors is not compatible with life, either due to embryonic lethality or death very shortly after birth (56-59). These outcomes reflect the fundamental roles which these receptors play in the development of heart, brain, lung, gastrointestinal tract, liver and skin (60, 61). Signalling through the ErbB-receptors has two key characteristics. First, activation is ligand dependent (in the absence of mutations or gross over-expression). Second, ErbB receptors are obligate dimers, meaning they can only function in homo- or heterodimeric formations or oligomers thereof.

1.2.2.1 ErbB Receptor Ligands

There are at least 11 different, but structurally related, growth factors that are recognized by the ErbB receptors. Each receptor has its own group of activating ligands (see Figure 1-2). Exclusive ligands for ErbB1 are epidermal growth factor (EGF), transforming growth factor alpha (TGFα) and epigen. Ligands for ErbB1 as well as ErbB4 include heparin-binding EGF (HB-EGF), β-cellulin and epiregulin-1. Ligands for ErbB3 and ErbB4 are neuregulin (NRG) -1 and -2. Neuregulin-3 and -4 are exclusive ligands for ErbB4 (62).

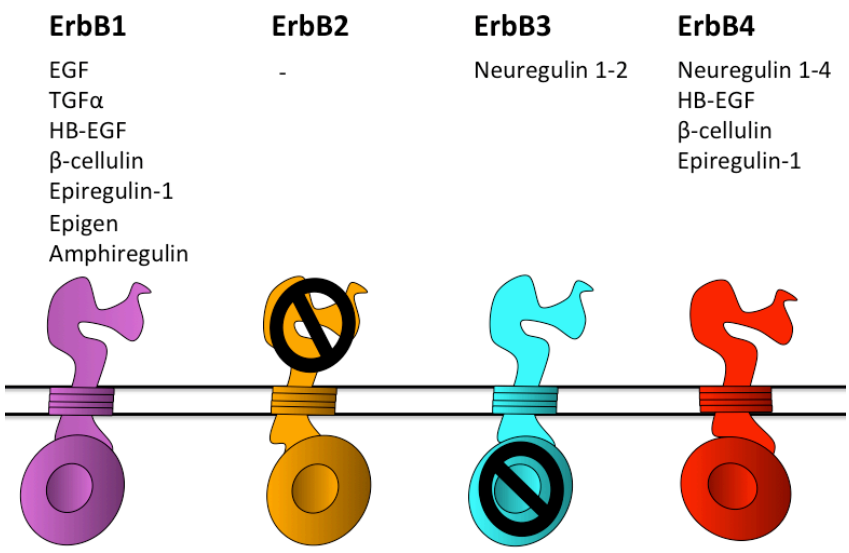

Figure 1-2 ErbB receptors and their ligands
The ligands for each of the four receptors are detailed above each individual receptor. No activating ligand has been identified for ErbB2, and ErbB3 has a substantially impaired kinase domain. EGF: epidermal growth factor, HB-EGF: heparin-binding epidermal growth factor, TGFα: transforming growth factor alpha.

1.2.2.2 ErbB Receptor Activation and Signalling

The extracellular domain of the ErbB-receptors contains the ligand-binding domain. The extracellular domain consists of four separate domains, two large domains (L-domains, also referred to as domain I and III) and two smaller, cysteine rich domains (S-domains, also referred to as domain II and IV) (see Figure 1-3)(63, 64). In the absence of bound ligand, ErbB1, ErbB3 and ErbB4 adopt a 'closed' conformation (see Figure 1-3). In the closed conformation a 'molecular tether' is formed through the interaction of a loop, which protrudes from domain II, with specific residues in domain IV (65-67). This 'molecular tether' can also be formed by binding to domain II of an interacting ErbB-receptor, therefore it is also referred to as the 'dimerisation arm' (68, 69). Upon the binding of a ligand to domains I and III, the receptors undergo conformational rearrangements, resulting in an extended 'open' conformation. The 'open' conformation enables the 'dimerisation arm' to interact with an additional ErbB-receptor (see Figure 1-3). The extracellular domain of ErbB2 differs from the other receptors. ErbB2 is constitutively in the extended, 'open' state, exposing the dimerisation arm (70, 71). Due to this constitutive 'open' state, ligand binding to ErbB2 is sterically hindered (72). However, ErbB2 is the preferred heterodimerisation partner of the other receptors, which can be explained by its constitutive 'open' conformation

(73, 74). Homodimerisation of ErbB2 is prevented by electrostatic repulsion (70). At endogenous expression levels this repulsion is sufficient to prevent homodimerisation. However, when ErbB2 is overexpressed (as seen in many cancers), this repulsion can be overcome through the interaction between other areas of the receptor (75).

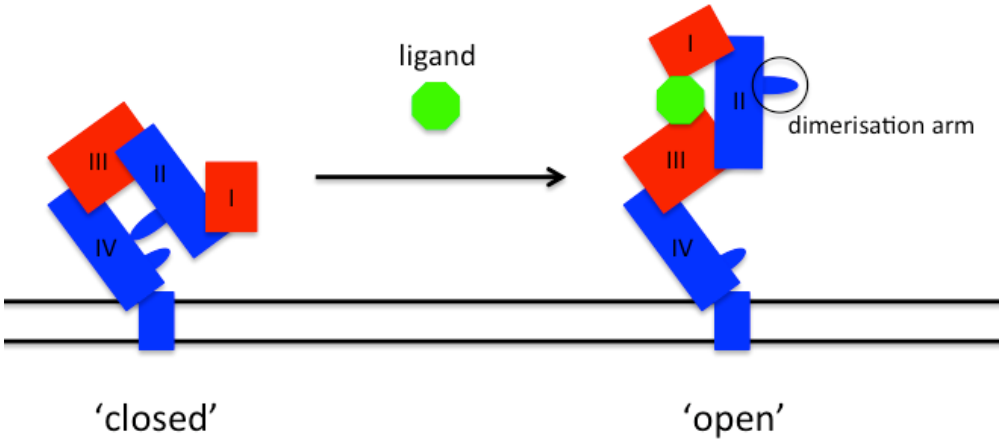

Figure 1-3 The 'closed' and 'open' conformation of ErbB receptors
Upon ligand binding to domain I and III, the ErbB receptors undergo a conformational transformation from their 'closed' to an 'open' conformation. The 'open' conformation exposes the 'dimerisation arm' allowing for dimerization with a second ErbB receptor. Image adapted from (46, 76)

However, it has been shown that the ErbB-receptors can also form inactive homo- and heterodimers in the absence of ligand (77-79). Because of the flexibility of the extracellular domain (with the exception of ErbB2), the preformed dimer may assume one of two structures with either high or low affinity for the ligand, due to their 'open' or 'closed' conformation respectively (66, 67, 71). Ligand-mediated activation of preformed dimers may be explained by the 'rotation/twist'-model proposed by Moriki et al. This model proposes that ligand binding induces flexible rotation or twist of the juxtamembrane region of the receptor, thereby rotating the transmembrane domains and dissociating the dimeric, inactive forms of the intracellular domains. This rotation may be required for the intrinsic catalytic kinase to become accessible to the tyrosine residues in the regulatory domain (79). Ligand-induced interaction of the two dimerisation arms may also induce the 'rotation/twist', rearranging the symmetric structure of the intracellular domains and thereby rearranging the dissociated kinase domains for activation (79, 80).

Ligand-mediated activation of receptor dimers induces the activation of the tyrosine kinase domain contained within the intracellular part of the receptors (81).

This results in the phosphorylation of tyrosine residues in the C-terminal tail, which serve as docking sites for signalling molecules that contain Src homology region 2 (SH2) and phosphotyrosine-binding (PTB) domains (82, 83). The combination of the identity of the ligand, and the dimerisation partner dictates which sites are phosphorylated. In turn, this phosphorylation pattern determines which signalling proteins are engaged, allowing for context-specific responses (84, 85). The main signalling pathways downstream of ErbB activation include the phosphatidylinositol 3-kinase (PI3K)-activated Akt pathway, the Ras-activated mitogen-activated protein kinase (MAPK) pathway, the phospholipase Cγ (PLCγ) pathway and signal transducer and activation of transcription (STATs) pathway (85-87). Signalling through ErbB-receptors results in cell division, migration, adhesion, differentiation and apoptosis. Ligand binding also induces receptor clustering and endocytosis, followed by either recycling back to the cell surface or lysosomal degradation (88, 89). After endocytosis, nuclear translocation of the receptors may also occur where it may regulate gene expression (62, 85, 90). The specific output that results depends on the cellular context, ligand specificity and the nature of ErbB dimers formed (91, 92).

1.2.3 The Role of the ErbB Receptor Family in HNSCC

The ErbB receptor family plays a critical role in growth, survival, invasion, metastasis and angiogenesis in HNSCC tumour cells (93). Cancers exploit the ErbB network through the activation of the signalling network at different layers. This results in the fact that in many tumours, the ErbB signalling pathway is hyperactivated. There are several mechanisms through which this hyperactivation is induced, including the overproduction of ligands and receptors, and/or constitutive activation of receptors as a result of mutations. Four major signalling pathways downstream of the ErbB receptors have been implicated in malignant cells. The first of these is, the Ras-MAPK pathway, which induces the phosphorylation and nuclear translocation of extracellular signal-regulated kinase (ERK) leading to activation of transcription factors and several cytoskeletal proteins (94, 95). The second is, the PI3K-Akt pathway, which induces Akt activation and translocation to the nucleus, resulting in altered gene transcription. In parallel, other cytosolic proteins are activated by this pathway, which promote the expression of mitochondrial anti-apoptotic proteins and caspase inhibitor proteins (96, 97). The third is the phospholipase-Cγ (PLCγ) and protein kinase-C (PKC) pathway in

which the activation of PKC results in cell cycle progression (98). The fourth pathway is termed the signal transducer and activator of transcription (STAT) pathway. Activated STAT proteins regulate the expression of genes that are vital for cell proliferation, survival, transformation and progression to carcinoma (99). In HNSCC, STAT1, STAT3 and STAT5 play significant roles, and STAT3 has been implicated to function as an oncogene (100).

1.2.3.1 ErbB1

Overexpression of ErbB1 is seen in more than 80% of invasive HNSCC cases, compared to normal adjacent mucosa (101). This overexpression is associated with increased ErbB1 copy number and worsened clinical prognosis (102, 103). Local recurrence rate in patients with overexpressed ErbB1 is 70%, compared to 48% in patients with normal ErbB1 expression levels. Furthermore the 5-year survival rate in these patients is reduced to 20% compared to 38% respectively (104). Overexpression of ErbB1 is likely to be an early event in HNSCC development (a 30-fold elevation of ErbB1 mRNA can be detected in normal mucosa of HNSCC patients), contributing to oncogenesis and the concept of field cancerization (105). The overexpression of ErbB1 is generally not mediated by gene amplification, but rather due to mRNA overproduction (106, 107). Phosphorylated ErbB1 has also been detected in the nucleus of multiple tumour types, where it acts as a transcription factor that promotes the expression of proteins such as cyclin-D (90, 108). In addition to ErbB1 upregulation, an average 5-fold increase in mRNA encoding the ErbB1 ligand TGFα can be detected in HNSCC tumours. Levels of TGFα in the tumour tissue are mildly elevated during early carcinogenesis, but do not increase further as cells progress through to carcinomas, whereas ErbB1 expression increases progressively with the development of carcinomas (109, 110).

One of the most common altered forms of ErbB1 found in HNSCC and other solid tumours is the EGFRvIII deletion mutant. EGFRvIII is the result of an in-frame deletion of exons 2-7 of wild-type ErbB1. This causes the deletion of a large portion of the extracellular domain, and the insertion of a glycine at the fusion junction between exon 1 and 8. As a result the EGFRvIII has a distorted ligand-binding region, lacking the receptors dimerization arm. Consequently, the mutant receptor does not bind ligand and cannot assume the closed tethered structure, making it constitutively active (111, 112). Expression of EGFRvIII has been detected in 42% of HNSCC tumour tissue, but

was consistently co-expressed with normal ErbB1 (113). Expression of EGFRvIII leads to unregulated growth, improved survival, enhanced invasion and angiogenesis (114). It has been associated with increased tumour growth and metastasis formation, as well as an increased resistance to antitumor agents and survival (113, 115, 116).

1.2.3.2 ErbB2/3

ErbB2 and ErbB3 are mutually dependent receptors and function in a complementary manner (93). Neither the ErbB2 nor the ErbB3 receptor alone can be activated through ligands; however ErbB2/3 heterodimers are the most active signalling dimers of the family (117). In relation to cancer, the ErbB2/3 heterodimer is considered the most transforming and mitogenic of all dimers (91, 118, 119), increasing cell motility upon ligand stimulation (120).

Reports on the overexpression of ErbB2 in HNSCC have been very contradictory, ranging from very few to all tested samples (121-125). In cases where overexpression was seen, it has been significantly associated with positive lymph node status as well as advanced disease (126-128). However, overexpression of ErbB2 could not be correlated with clinicopathological factors (122, 123, 129). Therefore the use of ErbB2 as a prognostic factor remains to be elucidated. The discrepancies seen between studies may be contributed to the lack of a standardised method for the analysis of ErbB2 overexpression.

In 77.5% of primary HNSCC samples, expression of ErbB3 can predominantly be detected in the cytoplasm, and less frequently (8.8%) on the tumour cell membrane. However the membranous overexpression significantly increases to 30.0% in metastatic tissue (93). Membranous overexpression of ErbB3 is significantly correlated with worsened patient survival (93). Patients with ErbB2 positive and ErbB3 negative tumours have a significantly prolonged survival (93).

1.2.3.3 ErbB4

No significant levels of overexpression of ErbB4 have been detected in HNSCC tissue. In laryngeal carcinomas, overexpression of ErbB4 was detected in 25% of cases, compared to a 9% overexpression in benign lesions. Additionally, ErbB4 overexpression could not be associated with clinical and pathological characteristics of disease (130).

1.2.4 ErbB-Targeted Treatment for HNSCC

The role of the ErbB receptor family in oncogenesis and their overexpression in a wide range of solid tumours make them appealing candidates to develop targeted therapies against. Targeted therapies include the use of small molecules, antibodies, immunotoxins and cellular therapies. Currently the only Food and Drug Administration (FDA) and European Medicines Agency (EMA) approved ErbB-targeted therapy for HNSCC is Cetuximab (131, 132). Cetuximab is a high-affinity humanized monoclonal antibody (mAb) that binds with the extracellular domain of EGFR (133, 134). The binding affinity of Cetuximab and the natural ligands of ErbB1 are similar. However, Cetuximab is a receptor antagonist. Consequently, upon binding to EGFR, Cetuximab prevents the activation of downstream signalling pathways, induces antibody-dependent cellular cytotoxicity, inhibits nuclear ErbB1 transport and suppresses the DNA-dependent protein kinase (135-137). Additionally it induces receptor dimerization and downregulation of EGFR, preventing future activation resulting from binding of the receptor's natural ligands (138, 139). In pre-clinical studies, Cetuximab was shown to decrease tumour cell proliferation and survival *in vitro* as well as reducing tumour growth *in vivo* (137, 140, 141).

Besides affecting the signalling of ErbB1, the immunoglobulin (Ig)G1 framework of Cetuximab means that cells to which the antibody has bound become targets for antibody-dependent cell cytotoxicity (ADCC). Despite activity of this mechanism against HNSCC cells *in vitro*, the efficacy seems to be dependent on the polymorphic status of the Fc receptors expressed by the reacting immune cells (142-144). Similar ADCC *in vitro* has also been reported with the ErbB-2 targeting mAb, Trastuzumab (145).

1.2.4.1 Efficacy of Cetuximab Treatment

The FDA and EMA have approved clinical use of Cetuximab as a component in several treatment regimens for HNSCC. Cetuximab is licensed as a primary treatment for locally advanced disease, in combination with radiotherapy (146). The combination of radiotherapy with Cetuximab significantly improves the median duration of locoregional control (from 14.9 months for 24.4 months), median overall survival (OS) (from 29 to 49 months) and reduces the risk of mortality by 26% compared to radiotherapy alone (146, 147). The five-year survival rate increased from 36.4% to 45.6% after the addition of Cetuximab to high-dose radiotherapy (148). Combination of the two treatments did not increase the occurrence of grade 3 or 4 toxicity. Besides infusion-related reactions, interstitial lung disease, acneiform rash and hypomagnesaemia, the treatment regimen was well tolerated (146).

Cetuximab is also approved for first-line treatment of metastatic or recurrent HNSCC in combination with platinum-based chemotherapy. Patients treated with Cisplatin in combination with Cetuximab exhibited a significantly higher objective response rate when compared to patients treated with Cisplatin in combination with a placebo (26% and 10% respectively) (35, 36). The benefit of this combination was also evident in patients with disease progression after Cisplatin treatment alone (149, 150). After failure of platinum-based chemotherapy, Cetuximab may be used as a single agent. Administration of Cetuximab to patients who had disease progression after platinum-based chemotherapy resulted in a 13% overall response rate (151).

1.2.4.2 Toxicities Related to Cetuximab Treatment

Common toxicities observed at the recommended treatment dose of Cetuximab are limited to hypersensitivity reactions and acneiform rash (neutrophilic folliculitis) (152-155). In patients with metastatic colorectal cancer (CRC), the occurrence of Cetuximab-induced skin toxicity (Cet-ST) correlates with a better treatment response and longer survival times, and can be used as an early predictor of treatment efficacy (156). This correlation is not unique for Cetuximab. Similar relationships between skin toxicity and efficacy have been reported in patients treated with the ErbB-targeting tyrosine kinase inhibitors Erlotinib or Gefitinib (157-159). In the treatment of HNSCC, Cet-ST has been reported in up to 77% of patients (35). Increased Cet-ST and a trend toward reduced risk of tumour progression in response to Cetuximab have been correlated to the EGFR-R521K genotype (a point substitution from G to A which results in an amino acid substitution). This might be due to a difference in binding affinity. However, no correlation with overall survival was detected (160). A significant association between the development of skin rash (of at least grade 2) and overall survival of HNSCC patients has been reported in relation to Erlotinib treatment (161).

More severe side effects were seen in a phase II trial where Cetuximab was combined with radiotherapy and Cisplatin. Five severe adverse events (SAEs) were seen, including two deaths (one pneumonia and one unknown cause), one (non-fatal) myocardial infarction, one bacteraemia and one episode of atrial fibrillation (162). However, the occurrence of these SAEs could not be conclusively attributed to the addition of Cetuximab.

Other antibodies currently being investigated for the treatment of HNSCC including the previously mentioned Trastuzumab (a humanized IgG-1κ mAb targeted against ErbB2) (163), as well as Panitumamab (a humanized IgG-2 anti-EGFR mAb which prevents binding of endogenous ligands to ErbB1) (164) and Zalutumumab (a human IgG1 mAb which blocks ErbB1 signalling) (165). In addition to monoclonal antibodies, there are several tyrosine kinase inhibitors under investigation such as the previously mentioned Gefitinib (166, 167) and Erlotinib (168, 169), as well as Lapatinib (170).

1.2.5 Tumour Resistance against ErbB Targeted Therapies

Development of resistance against ErbB1 blockade may be contributed to by several mechanisms. First, this may result from aberrant activation of downstream signalling pathways, especially the activation of ERK1/2 due to KRAS, BRAF and NRAS mutations (171-173). A second mechanism involves the overexpression of other ErbB receptors. This has been shown to correlate with a worsened clinical outcome compared to tumours in which ErbB1 alone is overexpressed. Consequently, a (combined) treatment targeting several ErbB receptors at the same time might provide a possible strategy to overcome tumour resistance (128, 174). The combination of ErbB1 and ErbB2 inhibition using a dual kinase-targeting agents could overcome Cetuximab resistance in an *in vitro* and *in vivo* model of bladder cancer (175). In studies performed in non-small cell lung cancer (NSCLC) and CRC cell lines, increased activation of ErbB2 signalling (either through ErbB2 amplification or Heregulin upregulation) leads to persistent ERK1/2 signalling downstream of ErbB2 and consequently to Cetuximab resistance (176). In CRC patients, aberrant ErbB2 signalling is a mediator for both *de novo* and acquired Cetuximab resistance. Similarly, activation of ErbB1 signalling induces resistance to the ErbB2-targeted mAb Trastuzumab in both *in vitro* and *in vivo* breast cancer models (177). Resistance to Gefitinib was correlated to high protein levels of phosphorylated ErbB2 and total ErbB3 (178). However, ErbB2 overexpression does not lead to Gefitinib resistance, potentially because in contrast to Cetuximab, Gefitinib can also inhibit ErbB2 signalling (179). Combined inhibition of ErbB1 and ErbB2 with Cetuximab and Trastuzumab or a dual-tyrosine kinase inhibitor was able to restore sensitivity to Cetuximab (176). Afatinib and Dacomitinib are two ErbB receptor family targeting, small-molecule, irreversible inhibitors targeting ErbB1, ErbB2 and ErbB4 simultaneously and which are currently under investigation. In a phase II trial, Afatinib has shown a HNSCC control rate of 38.9% in patients where disease progression or toxicity was seen after Cetuximab treatment. Patients who received Cetuximab after Afatinib treatment only showed 18.8% disease control (174). Dacomitinib as a first-line treatment in metastatic/recurrent HNSCC showed a partial response in 11% and stable disease in 63% of patients. Treatment was associated with grade 3 adverse events including diarrhoea, fatigue, acneiform dermatitis and hand-foot skin reaction (174).

Other mechanisms of resistance include the failure to inhibit PI3K/Akt signalling which can be mediated at the level of substrate ErbB3, driven by ErbB2 kinase activity (180). Additionally overexpression of the proto-oncogene Mesenchymal-epithelial transition factor (MET) has been shown to cause Gefitinib resistance through ErbB3 dependent activation of PI3K. Drug sensitivity could be restored after inhibition of MET signalling (181, 182). Upregulation of vascular endothelial growth factor (VEGF) is induced through ErbB1 activation and has been shown to induce tumour growth, metastasis formation and treatment resistance (183, 184). Combined anti-ErbB1 and anti-VEGF treatment suggests a synergistic effect and more robust response than single-agent treatment (185). Expression of EGFRvIII has been correlated with higher expression levels of phospho-STAT3, which treatment with Cetuximab was able to decrease but unable to abrogate (116).

Tumour resistance against ErbB1 targeted therapies can be overcome through the simultaneous targeting of multiple ErbB receptors simultaneously. This provides a rationale for the development of a single treatment in which the extended ErbB receptor family is targeted. Tumour resistance against such a treatment should be reduced compared to the targeting of a single ErbB receptor.

1.3 Immunotherapy

Immunotherapy aims for targeted tumour cell killing using immune system's cytotoxic mechanisms. Multiple different approaches of immunotherapy exist, including both the humoral and cellular components of the immune system. Here the focus will be on adoptive cell therapies.

1.3.1 T-lymphocytes

T-lymphocytes are defined by the surface expression of a T-cell receptor (TCR), a transmembrane heterodimer consisting of either and alpha and beta chain (αβ T-cells), or a gamma and delta chain (γδ T-cells). The vast majority (95%) of peripheral circulating T-lymphocytes are αβ T-cells. T-cells are produced in the bone marrow and then migrate as immature pre-T-cells to the thymus where they undergo maturation. Immature progenitor cells are also referred to as pro- T-cells, or double-negative T-cells due to the lack of CD4 or CD8 expression. Within the thymus some pro-T-cells undergo TCR β-gene recombination. When successful, a β-chain is synthesized and is co-expressed with pre-Tα to form the pre-TCR complex on the pre-T-cell. Expression of the pre-TCR complex stimulates TCR α-gene recombination for completion of the TCR. At this point cells express both CD4 and CD8 and are referred to as double-positive T-cells. Thereafter, the T-cells undergo positive and negative selection. During positive selection, T-cells that do not recognize and MHC molecule in the thymus undergo apoptosis. During positive selection, T-cells that recognize MHC class-I preserve the expression of CD8 and lose expression of CD4, whereas T-cells that recognize MHC class-II preserve CD4 expression. Thus, positive selection results in single-positive T-cells that are either MHC class-I or MHC class-II restricted. During negative selection, immature, double-positive T-cells that interact strongly with MHC-peptide complexes within the thymus undergo apoptosis or are directed towards a $CD4^+$ regulatory T-cell lineage (186-188).

For T-lymphocytes to be fully activated, to proliferate and secrete cytokines antigen recognition and co-stimulation is required. The TCR interacts with the major histocompatibility complex (MHC) on the surface of cells. For stable and prolonged interaction, co-localisation of CD4 with MHC-class II or CD8 with MHC-class I in the TCR-complex is required. Additionally, co-localisation of the four chains of CD3 (δ, ε, γ and ζ) with the TCR is required. MHC class-I is expressed by virtually all nucleated cells I

the body. Peptide expression upon MHC class-I enables selective elimination of infected nucleated cells. Expression of MHC class-II is largely restricted to antigen presenting cells (APCs). These cells are able to phagocytose, process and present pathogens to T-cells. Co-stimulatory signals are required to ensure full activation. The co-stimulatory molecule CD28, the best understood co-stimulatory molecule, is constitutively expressed on human T-lymphocytes (189, 190). Other co-stimulatory molecules include OX40, 4-1BB and CD27 (191, 192). Their expression is more transient than CD28, with peaks ranging from hours-days after T-cells encounter antigen.

1.3.2 Immunological Tolerance

Immunological tolerance is the capacity of the immune system to respond to a wide range of microbes, but not to self-antigen. Tolerance can be divided into central tolerance and peripheral tolerance. Central tolerance is a mechanism based on tolerance to self antigens that are present in the generative lymphoid organs (bone marrow and thymus). In immature T-lymphocytes that strongly interact with self-antigen in the thymus, apoptosis is triggered before the cell can complete maturation (negative selection). Alternatively, self-antigen recognising $CD4^+$ lymphocytes can develop into regulatory T-cells, which can contribute to peripheral tolerance (193, 194). Peripheral tolerance occurs when mature lymphocytes recognize self-antigen in peripheral tissue. Several mechanisms contribute to peripheral tolerance. First, lymphocytes can go into anergy, due to the lack of sufficient co-stimulatory signalling. Second, regulatory T-cells can block the activation of potentially harmful lymphocytes through cytokines (such as IL-10 and TGF-β) or cell-cell interaction. Third, activation-induced cell death through the production of apoptotic proteins or the upregulation of death receptors and their ligands (such as Fas and FasL) (186). Because tumour antigens are aberrant forms of, or aberrantly expressed self-antigens, recognition by lymphocytes results in tolerance rather than activation. However, some cancers have shown to be moderately immunogenic. The suggestion of interplay between tumours and the immune system resulted in the theory of 'immunoediting'.

1.3.3 Tumour Immunoediting

The concept of an interaction between tumours and the immune system dates back to Ehrlich in 1909. He suggested that transformed cells continuously arise in the body, which the immune system recognises and destroys before they can become a clinically detectable tumour (195). The concept that tumour cells could be recognised and targeted by the immune system was later demonstrated *in vivo*. Mice could be immunised against syngeneic tumour transplants, establishing the presence of tumour-specific antigens (TSA) (196, 197). In 1957 the concept of 'cancer immunosurveillance' was hypothesised by Burnet and Thomas. They stated that '*small accumulations of tumour cells may develop and because of their possession of new antigenic potentialities provoke an effective immunological reaction with regression of the tumour and no clinical hint of its existence*' (198, 199). This hypothesis is supported by follow-up studies showing an increased incidence of (viral) tumours in patients who were immunosuppressed after organ transplantation compared to the general population (200-203). Additionally, a positive correlation was found between the presence of tumour infiltrating lymphocytes (TILs) and increased patient survival. In a study amongst melanoma patients, the level of TILs was divided into three categories ('brisk' – present throughout the tumour and infiltrated across the entire base, 'non-brisk' – present in one or more foci, and 'absent') (204). Patients with brisk TILs showed up to three times longer survival than patients in the absent group, while patients in the non-brisk group had intermediate survival times (204, 205). Similar observations have been made in other solid tumours such as breast (206), ovary (207), bladder (208), colon (209), prostate (210) and rectum (211).

Further studies into the interaction between tumour cells and the immune system suggest that the presence of immune cells has an effect on the immunogenicity of the tumour. Tumours formed in the absence of an intact immune system are generally more immunogenic than tumours that arise in an immunecompetent environment (212). Tumours are 'imprinted' by their immunologic environment, resulting in tumours that are better enabled to overcome the tumour-suppressive functions of the immune system (213, 214). This suggests that the immune system has a bilateral function in oncogenesis, host-protection as well as tumour-sculpting. To incorporate these two functions of the immune system, Dunn et al., introduced the concept of immunoediting in 2002*. 'We envisage the scope of this process to be very*

broad such that it can promote complete elimination of some tumours, generate a non-protective immune state to others or favour the development of immunologic anergy, tolerance or indifference' (215).

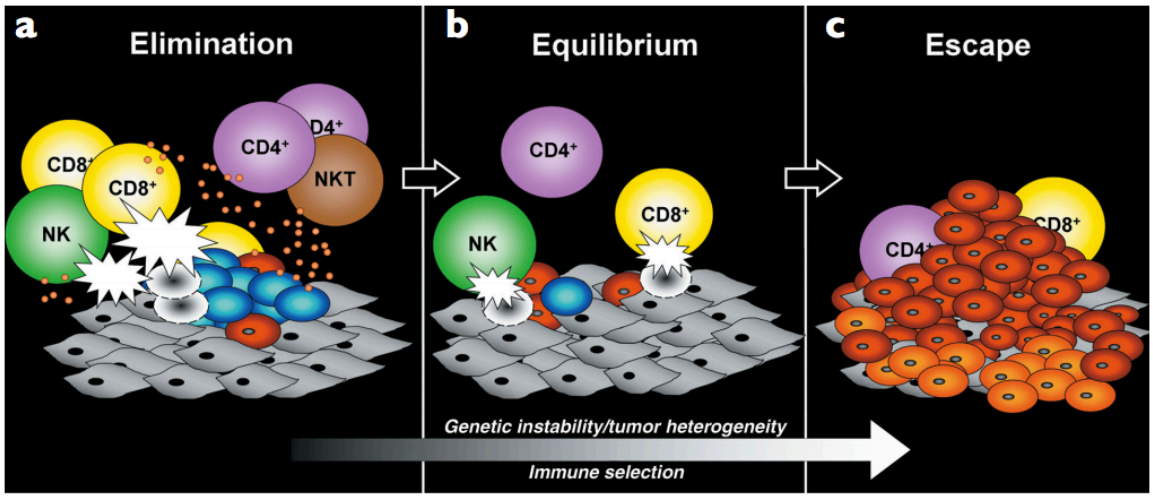

Figure 1-4 Tumour immunoediting
Schematic representation of the three phases of tumour immunoediting, elimination (**a**), equilibrium (**b**) and escape (**c**) Reprinted by permission form Macmillan Publishers Ltd: Nature Immunology (215), copyright (2002)

Tumour immunoediting would be a process of three stages: elimination, equilibrium and escape (Figure 1-4). The elimination phase encompasses the original concept of immunosurveillance. In the cases where tumour cells are successfully eradicated, there will be no progression to the second or third phase. The elimination phase itself can be broken down into four different stages (Figure 1-5). A first response in which natural killer (NK) cells, NK T-cells (NKT) and γδ T-cells accumulate at the tumour site and interferon (IFN)y is produced. The IFNy induces a second response through the induction of additional cytokines, anti-proliferative effects and the activation of cytocidal activity in macrophages and NK-cells. In the third response, tumour growth is controlled through the cytocidal activity of the macrophages and NK-cells. The final response is the expansion of tumour specific $CD4^+$ and $CD8^+$ T-cells. In the equilibrium phase, the immune system and remaining tumour cell variants enter a dynamic equilibrium. Intra-tumoural lymphocytes and cytokines exert a selective pressure on the tumour cells, allowing the persistence of a genetically unstable and rapidly mutating tumour. During the escape phase, tumour cells that have become insensitive to immunologic detection and/or elimination expand uncontrollably, resulting in clinical disease (215).

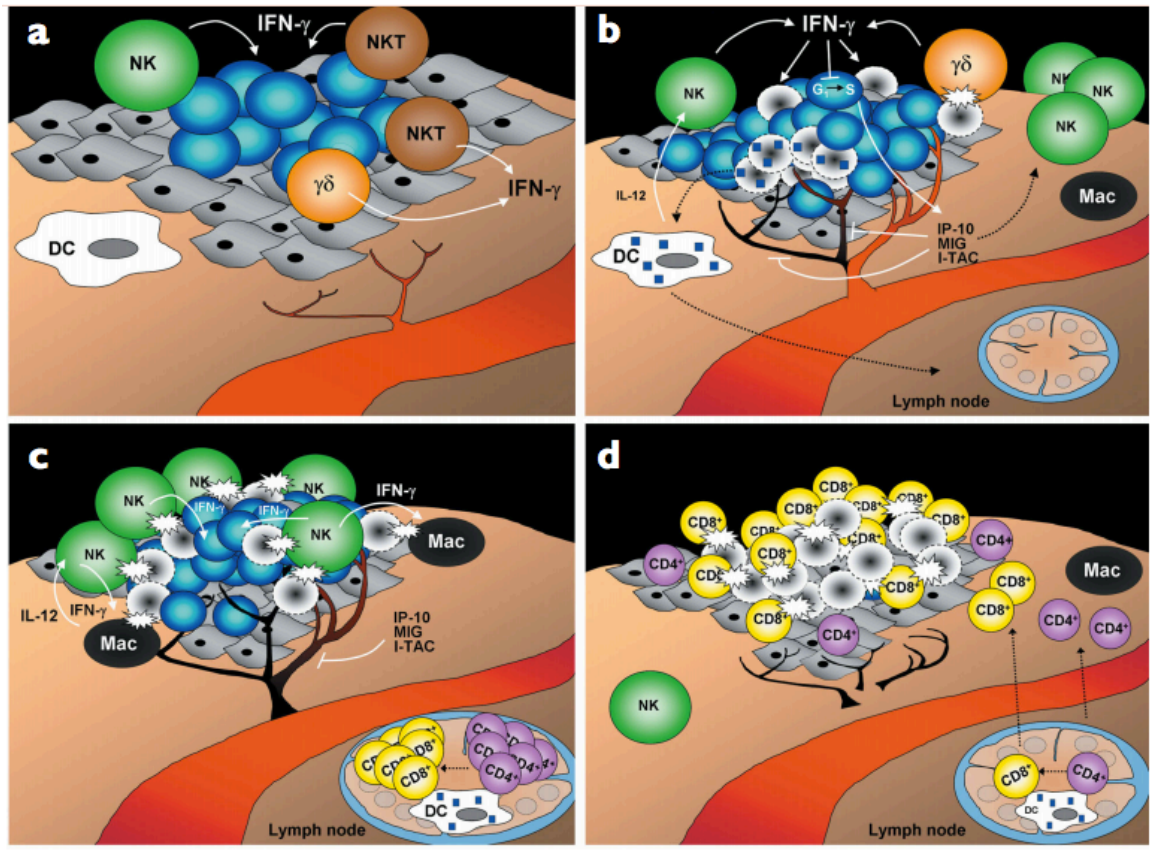

Figure 1-5 The four stages of the elimination phase
Immune cells accumulate at the tumour site and secrete IFNγ (**a**) which initiates an innate immune response including chemokine production, the recruitment of further immune cells, direct anti-proliferative action of IFNγ and the activation of cytolytic activity of immune cells (**b**). Tumour growth is kept under control while antigen specific lymphocytes develop (**c**) Tumour-specific lymphocytes migrate to the tumour and induce their cytotoxic effects (**d**). Reprinted by permission form Macmillan Publishers Ltd: Nature Immunology (215) copyright (2002).

Immunotherapy aims to tip the balance in favour of the immune system during tumour immunosurveillance through the enhancement or redirection of anti-tumour responses (216). To effectively enhance the anti-tumour response, an understanding of the mechanism for immune evasion is vital. Tumours have several strategies to silence immune responses. Tumours express self-antigens, to which lymphocyte responses are tolerized. Additionally, expression of tumour antigens can be reduced through the downregulation or loss of major histocompatibility complex (MHC) class-I presentation. Antigen presentation by MHC molecules is crucial during the T-cell priming as well as the effector phase. Antigen presentation can be altered through structural alterations in the MHC protein and through mutations and/or dysregulation of genes involved in antigen processing (217, 218).

1.3.4 Immunoediting in HNSCC

The occurrence of immunoediting has also been identified in HNSCC. Downregulation of human leukocyte antigen (HLA) class-I expression is seen in about 50% of cases (219). Additionally, downregulation of IFN-inducible components impair recognition by cytotoxic lymphocytes. This downregulation has been linked to a poorer prognosis (220). The microenvironment within the oral, nasal and laryngeal mucosa is rich in immune cells and immunomodulatory factors (221). Tumours are generally well infiltrated with T-cells and dendritic cells (DCs) (221, 222). Although tumour-infiltrating lymphocytes (TILs) are activated, they are functionally compromised at multiple levels in comparison to circulating lymphocytes of healthy controls. The expression of the ζ-chain and ZAP-70 (zeta-chain associated protein 70) is low or absent in TIL cells (223, 224). Furthermore, TIL cells show decreased proliferation in response to mitogens or IL-2 and are unable to destroy tumour target cells *in vitro* (221). There is an imbalance in their cytokine profile, with an absence of IL-2 production (225). Finally, DNA fragmentation has been observed in a proportion of TILs (224). The abnormal functionality of T-cells does not seem to be limited to the tumour microenvironment. Circulating T-cells from untreated HNSCC patients or patients who only underwent surgery also exhibit below normal activity (226). Finally, apoptosis of $CD8^+$ lymphocytes at the tumour site and depletion of reactive lymphocytes in the circulation have been reported (227). However, TILs showed a greater spectrum of defects than seen in circulating T-cells from HNSCC patients.

The level of ζ-chain expression in TIL cells proved to be a significant, independent predictor of poor survival of patients with advanced disease. The 5-year survival rate of patients with stage III/IV disease whose TILs did not express the ζ-chain is significantly shorter compared to patients with normal ζ-chain expression (223). Additional to TIL characteristics, numbers of intra-tumoural DCs have also been related to survival. A low number of infiltrating $S100^+$ DCs (mature monocyte-derived DCs) correlates with poor overall survival, disease-free survival and time to recurrence. The relationship between ζ-chain expression and level of DC infiltration is not exclusive to advanced disease, but proved also to be prognostically significant in early (stage I/II) disease (221).

Ex vivo, HNSCC cells can induce signalling defects and apoptosis of activated T-cell (226). Additionally, circulating T-cells of HNSCC patients undergo spontaneous

apoptosis *ex vivo* (227). The expression of Fas and Fas ligand (FasL) on tumour cells has been implicated as a cause for T-cell apoptosis (228). Nearly all T-cells of HNSCC patients express Fas (226). Apoptosis of tumour cells is disabled through impaired Fas function due to an overexpression of inhibitory proteins including FAP-1, cFLIP, IAP and Bcl2 (229). Additionally, FasL is difficult to detect on tumour cells, suggesting that it might be actively cleaved. This may render FasL levels insufficient to induce tumour cell apoptosis. The Fas/FasL interaction is therefore in favour of tumour cells and at a disadvantage for the T-cell population (226).

Head and neck tumours are generally well infiltrated and presence of functional immune cells is associated with improved prognosis. These two parameters suggest that the chances of patient survival could be improved through maintaining and improving the immune cell functionality.

1.3.5 Advantages and Disadvantages of different Immunotherapies

Immunotherapy can be broadly categorised into 3 different groups.

i) Specific, if the response of a certain aspect of the immune system is enhanced against a TAA. This can be achieved for example through the use of monoclonal antibodies or antibody-dependent cell-mediated cytotoxicity.

ii) Non-specific, when a broader, more general immune activation is elicited such as the activation of NK-cells, macrophages and granulocytes.

iii) Adoptive cell therapy (ACT), where autologous immune-cells are activated, enhanced and potentially selected or modified *in vitro* and then re-infused. Immune cells used for ACT include lymphokine activated killer (LAK) cells, tumour infiltrating lymphocytes (TILs), dendritic cells (DCs) and T-cell receptor (TCR) or chimeric antigen receptor (CAR) transduced T-cells (230).

There are several different immunotherapeutical approaches which are being investigated in order to enhance the cytotoxicity of the immune system against tumour cells and overcome tolerance. Each of these approaches have their advantages and disadvantages.

Vaccination is an attractive method of active immunization, which has several approaches. Vaccination strategies include tumour cell vaccines, antigen vaccines, DNA

vaccines, dendritic cell vaccines and virus targeted vaccines. There are currently two approved vaccination treatments. Cervarix, a virus-targeted vaccine aimed to prevent HPV-related cancers and Provenge, a dendritic cell vaccine using prostatic-acid phosphatase (PAP) pulsed DCs to treat prostate cancer. Advantages of vaccination are that they are easily administered, can be aimed not just to treat but also to prevent cancers. Additionally, vaccines do not have to be patient specific and can be applied without significant side effects. Disadvantages include that irradiated tumour cells or antigens used for vaccination can be destroyed by the patient's immunesystem after which it can return to a pre-vaccinated state. Also, there might be a psychological barrier for patients to be treated with irradiated tumour cells or tumour antigen. Additionally, vaccination does not overcome tolerance and relies on the ability of T-cells to be sufficiently activated and infiltrate tumour *in vivo* (231).

The *ex vivo* expansion of T-cells is an alternative approach to enhance immune efficacy. Lymphokine activated killer cells (LAKs) are *in vitro* IL-2 stimulated PBMCs (232). Clinical results have been achieved with LAK cells in colorectal carcinoma, metastatic renal cancer, melanoma and other cancers (233-235). A major general advantage to the use of T-cells population is the development of specific memory T-cells Other advantages of the LAK approach include that the treatment is autologous, and therefore patient specific. Additionally, PBMCs can be obtained relatively easily.. However disadvantages include that there is no selection of tumour-specific lymphocytes and the approach relies on the natural presence of tumour-specific T-cells and can therefore only be applied when targeting a naturally immunogenic tumour.

A more specific approach is the use of tumour infiltrating lymphocytes (TILs). TIL-based therapy has achieved good clinical responses in metastatic melanoma (236). An advantage of TILs compared to LAKs is that they are a more tumour-specific population. However, TILs are more difficult to obtain and expand to required numbers *ex vivo.* Similarly to LAKs, the approach relies on the natural immunogenicity of the tumour. Both LAK and TIL based approaches do not overcome tolerance, but they rely on efficacy based on a higher frequency and more activated tumour-specific T-cells. The lack of overcoming tolerance limits efficacy, however it is also advantageous in respect that it limits the risk of side effects due to targeting of healthy tissue.

A more specific approach is the use of tumour infiltrating lymphocytes (TILs). TIL-based therapy has achieved good clinical responses in metastatic melanoma (236, 237). An

advantage of TILs compared to LAKs is that they are a more tumour-specific population. However, TILs are more difficult to obtain and expand to required numbers *ex vivo* (238). Similarly to LAKs, the approach relies on the natural immunogenicity of the tumour. Both LAK and TIL based approaches do not overcome tolerance, but they rely on efficacy based on a higher frequency and more activated tumour-specific T-cells. The lack of overcoming tolerance limits efficacy, however it is also advantageous in respect that it limits the risk of side effects due to targeting of healthy tissue.

The proportion of tumour-specific T-cells can be enhanced through the introduction of a tumour antigen-specific TCR into a polyclonal T-cell population. This approach does not rely on the natural immunogenicity of the tumour and allows for the expansion of a large tumour-specific T-cell population. The use of a TCR to re-direct T-cells against the tumour allows both extracellular and intracellular tumour antigens to be targeted. However, the approach is HLA dependent, meaning that cells remain susceptible to immune evasion. Additionally, the HLA-restriction means that the HLA haplotype of the patient might restrict applicability. Currently most TCR transfers have focussed on the most common HLA-A2 haplotype, thereby excluding patients with different haplotypes. Introduction of a TCR circumvents central tolerance, however T-cells are still susceptible to peripheral tolerance. Finally, unpredictable toxicity can occur due to mis-pairing with the endogenous TCR (239).

An alternative method to re-direct T-cells is the use of Chimeric Antigen Receptors (CARs). Similar to TCR-based treatment this approach allows for the rapid expansion of a tumour antigen-specific population from an originally polyclonal T-cell population. In contrast to TCRs, CARs do not rely on HLA-based target recognition and are therefore applicable to a wider range of patients. However, this does exclude intracellular antigen to be targeted by this approach. Due to the flexibility of CAR design and the incorporation of co-stimulatory domains, full T-cell activation can be achieved upon target recognition. Introduction of a CAR into a polyclonal T-cell populations circumvents tolerance, however this also increases the risk of toxicity due to activation by target antigen expressed on healthy tissue (240, 241). An additional disadvantage of using a CAR is that an anti-CAR immune response can develop against for example murine elements in the binding moiety (242).

1.3.6 Adoptive Cell Therapy

Here, the focus will lie on ACT, specifically the use of T-cells for ACT. Consequently, the history of this approach is reviewed briefly. In early studies, it was observed that the *in vitro* stimulation of peripheral blood lymphocytes with IL-2 created so-called 'lymphokine-activated killer cells' (LAK cells) (232). These cells were shown to be effective in several pre-clinical tumour models and highlighted the importance of dose, adjuvant IL-2 treatment and host lymphodepletion through total body irradiation (TBI) (243-245). Additionally, it was shown that LAK cells cytotoxicity is induced in an MHC-independent manner and that efficacy is independent of the hosts natural T-lymphocytes (246, 247). Adoptive immunotherapy using LAK cells and adjuvant IL-2 have achieved partial and complete remission in colorectal carcinoma (233), metastatic renal cancer (234), melanoma (235), colon cancer, renal-cell cancer, lung adenocarcinoma (248) and glioblastoma (249, 250). However, in a direct comparison of LAK cells in combination with high-dose IL-2 versus high-dose IL-2 alone, no significant difference in outcome was seen between the two treatment regimens (251).

The most common side effects observed in these studies included hypotension, weight gain, fluid retention, 'capillary leak syndrome' anaemia and elevated serum creatinine and liver enzymes (233, 234). The majority of these side effects resolved after the administration of IL-2 was stopped (248). Less frequent but more severe side effects included cardiac events such as myocardial infarctions (235, 250).

A more tumour-specific adoptive T-cell immunotherapy approach involves the activation of tumour-infiltrating lymphocytes (TILs). Tumour-infiltrating lymphocytes are isolated from resected tumour and subsequently activated and expanded *in vitro* prior to reinfusion. TILs proved to have 50-100 times more therapeutic potency compared to LAKs (252). In pre-clinical models, a combination of cyclophosphamide, TILs and IL-2 administration proved highly successful in pre-clinical models of metastatic adenocarcinoma (252). It was also demonstrated that TILs could be successfully expanded *ex vivo* (253). Objective response rates of 20-40% were seen in clinical trials treating malignant melanoma and renal cell carcinoma (RCC) (254-256). In RCC, similar response rates were seen with IL-2 treatment alone, however that was associated with a significant risk of life threatening toxicity (257-259). For the treatment of metastatic melanoma, TIL treatment in combination with IL-2 has achieved a clinical response rate of 50-70% and prolongued progression-free survival

(236, 237, 260, 261). A higher proportion of $CD8^+$ T-cells and a more differentiated effector phenotype of $CD8^+$ T-cells and level of IFNγ production in response to autologous tumour have been indicated as significant factors associated with objective tumour regression (262, 263). However, enrichment of $CD8^+$ T-cells in culture did not improve response rate, but suggested a preference for 'young' TILs (231, 263). TIL therapy has its limitations, it can be difficult to obtain adequate cell expansion *ex vivo* within the required timeframe. Additionally, *ex vivo* TIL outgrowth is achieved in only approximately 60% of patients and previous systemic therapies have a negative impact on the achievement of outgrowth (238). Similarly, due to the low immunogenicity of solid tumours, TIL therapy is less effective.

1.3.7 Adoptive Cell Therapy in HNSCC

Several adoptive cell therapies for HNSCC using DCs or T-cells have been tested in Phase-I clinical trials. Dendritic cell based vaccines involve the use of autologous DCs loaded with tumour peptide, tumour lysates or tumour DNA to elicit tumour antigen-specific immunity *in vivo.* The use of antigen-pulsed DCs allows for the induction of a heterogeneous T-cell population, targeting multiple tumour associated antigens or peptides. In one trial, autologous DCs were pulsed through co-cultivation with autologous irradiated tumour cells. The resulting cytokine-matured DCs were administered intra-nodally to four patients (after surgical resection of the tumour). Immune responses were observed and little toxicity was reported. However, less than 10% of screened patients were eligible for treatment due to various reasons, including the requirement for sufficient numbers of DCs and tumour products, and a psychological resistance of the patients to having tumour products injected. (55). An alternative to the use of irradiated tumour cells is transfection of autologous tumour DNA into the patient's DCs, however this still requires sufficient numbers of resected tumour cells. A third approach is a multivalent p53 loaded DC vaccine. The p53 protein is commonly overexpressed by tumour cells. Treatment of patients with various stages of HNSCC has shown low toxicity. Vaccines were injected intra-nodally as adjuvant therapy and immunologic responses have been observed in several patients (55).

Besides DC vaccines, the potential of T-cell based immunotherapies has also been explored. The efficacy of three different patient-derived T-cell populations have been compared *in vitro*, namely PBMC-derived LAKs, IL-2 stimulated TILs (isolated from

surgically resected tumour tissue) and mixed-lymphocyte tumour cell culture (MLTC) cells. The cytotoxic activity against autologous tumour cells of TILs proved twice as high as LAKs. However, the strongest cytotoxicity was seen by MLTCs, which was three times as high as LAKs (264). These *in vitro* results are encouraging for the application of T-cell based therapy in HNSCC patients.

In 1993, Kubota et al reported on the use of allogeneic spleen cells (265) and autologous PBMCs (266) for loco-regional treatment of HNSCC. Allogeneic spleen cells were derived from splenectomies performed on patients with gastric cancer. Cells were activated using OK-432 (multiple cytokine inducer derived from the low-virulence SU strain of *Streptococcus pyogenes*) for 48 hours prior to injection. Two patients with a large tumour mass with necrosis were treated by intra-tumoural injection. The necrotic centre of the tumour formed a cavity, into which the allogeneic cells were injected to avoid the onset of a graft versus host-response (GvHR). Patients received OK-432 followed by 17.4 x 10^6 (patient 2) or 35.8 x 10^6 (patient 1) OK-SC (OK-432 activated spleen cells). Immunotherapy was given as adjuvant therapy in addition to chemotherapy (patient 1) or chemotherapy and radiotherapy (patient 2) as a part of pre-operative treatment. A minor response was obtained in patient 1 and a partial response in patient 2. Treatment was not associated with any toxic side effects, suggesting that adoptive cell therapy can be safely administered pre-operatively (265). In a similar trial, patients were treated with autologous OK-432 activated PBMCs by injection into the superficial temporal artery or directly into the tumour, as part of their pre-operative treatment (266). Nineteen patients were treated with doses ranging from 3.1 – 112.3 x 10^6 OK-MCs (OK-432 activated PBMCs). Complete remission was achieved in 35% of patients and partial remission in 53% of patients (with a combination of immuno-, chemo- and radiotherapy). A minor response was observed in two of three patients treated with OK-MCs alone. In one of these patients, focal necrosis of the tumour was observed at the site of injection as well as dense infiltration of mononuclear cells around viable or degenerated cancer cells (266). These results suggest functionality of adoptive T-cell transfer through loco-regional administration, both as a single treatment as well as a part of combination treatment.

Yasumura et al. showed that autologous tumour specific cytotoxic T-lymphocytes (CTL) could be expanded *in vitro* and retain MHC class-I dependent autologous tumour cell destruction (267, 268). In a phase I trial described by To et al.,

an alternative method for the development of autologous tumour specific CTL was used. Irradiated autologous tumour cells were injected intradermally and, after 10 days, the draining lymph nodes were removed and lymphocytes isolated. After *ex vivo* expansion, autologous lymphocytes were infused intravenously (IV) together with IL-2. Limited toxic effects were seen (fever, chills and emesis), all at grades 1 or 2. However no significant effect on survival duration was observed (269).

In an alternative approach, molecular targeting and adoptive cell therapy were combined. Catuxomab is a trifunctional bispecific antibody that binds one arm to epithelial cell adhesion molecule (EpCAM) positive cells, and the other arm to $CD3^+$ T-cells. This antibody has an intact Fc domain that can recruit several accessory cell types. Complete remission was seen in 1 out of 4 patients treated intravenously (IV) with peripheral blood mononuclear cells (PBMCs) after *ex vivo* opsonisation by Catuxomab (270).

Together, these findings indicate that adoptive cell therapy is a feasible and non-toxic approach for treatment of HNSCC, but with limited efficacy. This emphasises the fact that further development of adoptive cell therapy is required.

1.3.8 Retargeting of T-cells using T-Cell Receptors

To overcome the limitations of TIL therapy, genetic manipulation was introduced to rapidly redirect large polyclonal T-cell populations to a tumour-associated antigen (TAA). There are two such approaches in common use whereby T-cells can be redirected through the introduction of either a novel αβ TCR or a chimeric T-cell receptor (cTCR). In 1986, Dembic et al. demonstrated the feasibility of TCR engraftment in a mouse model. The genes for the α and β chains of a murine TCR were isolated from a cytotoxic T-cell clone and transferred into a clone with a different specificity. This successfully transferred the original T-cell specificity through α/β pairing of the ectopic TCR subunits (271). These results introduced the concept of retargeting T-cells against TAA through the introduction of a new TCR. T-cells have been successfully retargeted against several antigens, including melanoma-associated antigen recognized by T-cells (MART)-1 (272), NY-ESO-1 (273), p53 (274, 275), Wilm's Tumour antigen (WT)-1 (276, 277), glycoprotein-100 (gp100) (278), mouse double minute-2 (MDM2) (279), tyrosinase (280, 281) and CEA (282, 283). In clinical trials, objective response rates have been seen in 12-30% of melanoma patients (282, 284).

Interestingly, it was also revealed that selection of TCRs with supra-physiological affinity for HLA, $CD4^+$ T-cells were retargeted against HLA-class I epitopes. Cytotoxicity of $CD4^+$ T-cells was comparable to that of $CD8^+$ cells, bypassing the need for CD8 co-receptor binding (282, 285). Retargeting with the use of TCRs has its limitations. HLA-restriction limits the number of patients for whom this treatment is available and efficacy is dependent on sufficient HLA and co-stimulatory receptor expression on tumour cells. A major concern is the occurrence of autoimmunity due to cross-pairing with endogenous αβ TCR chains. Bendle et al. showed that such mis-pairing could lead to lethal autoimmunity in mice. Mis-pairing could be reduced through several mechanisms. Transduction of a monoclonal T-cell population, addition of a disulphide bond to promote improved dimerisation and the replacement of the internal ribosome entry site (IRES) with a *Porcine Tescho* virus-1 2A (P2A) sequence all significantly reduced the occurence of autoimmunity (239). Autoimmunity due to mis-pairing has also been reported in human studies (286). Additionally, cardiac toxicities have been reported due to peptide cross-recognition (287). Another concern involving the use of high affinity TCR is the risk of auto-immunity. Normally, T-cells with high-affinity for self-antigens are removed by negative selection in the thymus (288).

1.3.9 Retargeting of T-cells using Chimeric Antigen Receptors

In 1987, Kuwana et al. aimed to study the difference between T-cell and B-cell antigen recognition by replacing the structural variable (V)-regions of TCRs with that of Immunoglobulin (Ig)-derived V-regions. T-cells expressing two transgenes, V_HC_α and V_LC_β could be activated by antigen expressing target cells (289). This discovery was the first step in the development of CAR technology. Two years later, Gross et al. showed IL-2 production and cytotoxic activity in T-cells redirected against 2,4,6-trinitrophenyl (TNP) as well as heterodimerisation with endogenous TCRα/β chains and CD3. These results made them realise the clinical potential of redirecting cytotoxic T-cells to kill tumour or virally infected cells (290, 291). One of the first challenges that had to be overcome to allow for a broader application of the chimeric receptor technology was the fact that it required the transduction of one cell with two separate vectors (one containing V_L and a second containing V_H). Eshhar et al. developed a single-chain approach with the use of a single chain variable fragment (scFv) coupled to CD3ζ. In an scFv, the V_H and V_L are joined with a flexible linker, while retaining the antibody's

specificity and affinity (292, 293). This technique only required the transduction and expression of one transgene. Because of the combination of the antibody-like antigen recognition with T-cell activation, the technique was initially named 'T-body'. Since then, it has also been referred to as 'artificial T-cell receptor', 'chimeric T-cell receptor' (cTCR), 'chimeric immune receptor' (CIR) and the most widely used, 'chimeric antigen receptor' (CAR).

The general structure of CARs consists of four elements, the binding moiety, the hinge or spacer region, the transmembrane domain and the intracellular domain (see Figure 1-6). Details and function of the different elements are discussed below.

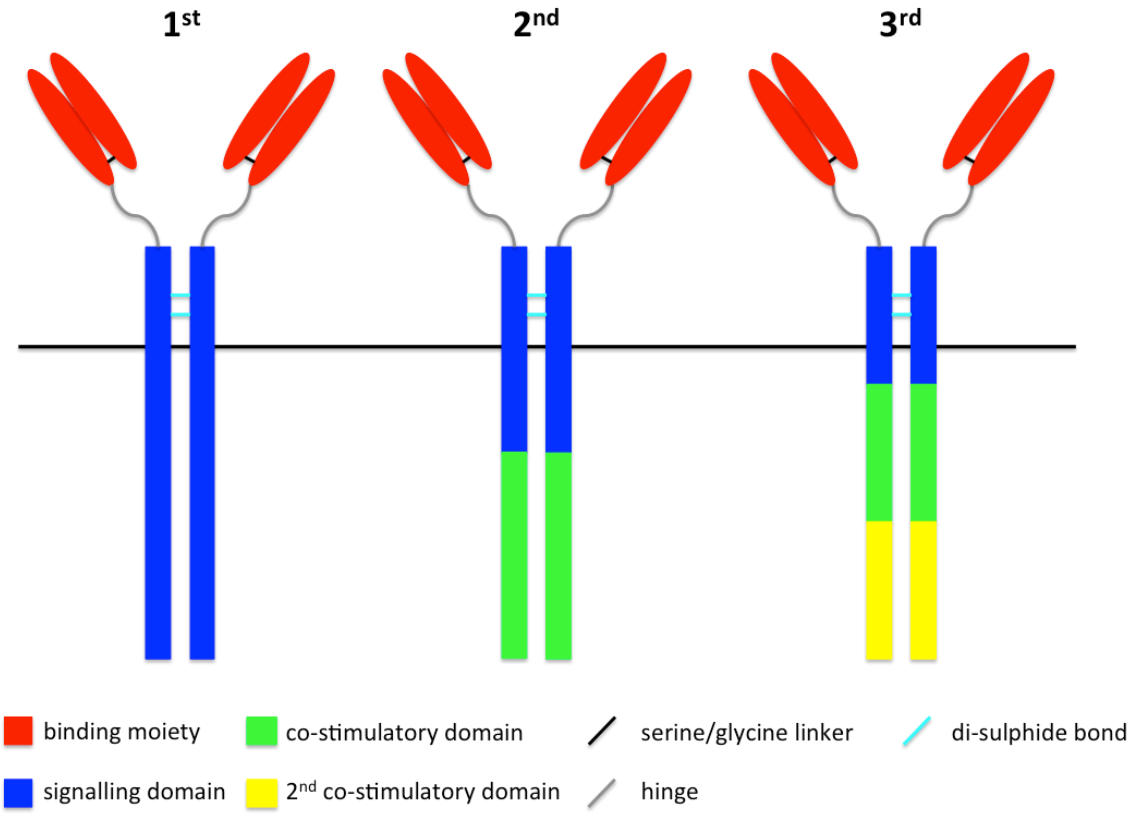

Figure 1-6 Schematic representation of CAR structures
General structure of 1st, 2nd and 3rd generation CARs. Serine/glycine linker is present when an scFv is used as the binding moiety. The inclusion of a hinge is optional in all generations. Receptors form dimers at the cell surface through disulphide bonds. *Note: size of the elements in the images does not correspond with the actual sizes.*

1.3.9.1 The Binding Moiety

Chimeric antigen receptors have been developed against a wide array of targets, as summarized in Table 1-3. The specificity of the CAR is determined by the binding moiety, it allows the CAR to recognize native cell-surface antigen, independent of HLA presentation and therefore also independent of the recipients' HLA haplotype. HLA-

independent recognition is an important advantage over TCR-HLA based activation due to the downregulation of HLA expression commonly seen on tumour cells (294). Additionally, it makes treatment available to all patients, regardless of their HLA-haplotype. Antibody single chain variable fragments are most commonly used to allow for target recognition and binding (295). Alternatively, ligands (296, 297), peptides (298), chimeric ligands (299), receptor derivatives (300) and single domain antibodies (301) can also function as the binding moiety. These binding moieties target specific tumour associated antigen. Recently, a more universal CAR design has been published, using monomeric avidin as a targeting moiety. This CAR can be used in combination with biotinylated antigen-specific molecules (mAbs, scFv or tumour-specific ligands), increasing the flexibility in T-cell targeted antigen specificity (302).

The choice of binding moiety is influenced by several factors. Antigen binding by CARs generally involves a high-affinity interaction. However, if the affinity is too high, healthy tissue expressing low levels of the antigen may also be targeted, increasing the risk of toxicity (303). The use of murine scFv sequences in the binding moiety can induce immunogenicity. The formation of blocking antibodies has been reported, compromising CAR effectiveness (242, 304). The use of humanized or fully human scFv sequences can eliminate this problem. The nature of the antigen can also complicate targeting. Molecular heterogeneity due to aberrant glycosylation as seen in Muc1 for example, can affect the binding affinity of the CAR to the different glycoforms (305).

Table 1-3 Tumour-associated antigen targeted by CAR$^+$ T-cells

Target Antigen	Malignancies	Development stage	Reference(s)
B7-H3	Various	Pre-clinical (*in vivo*)	(306)
B7-H6	Various	Pre-clinical (*in vivo*)	(300)
CAIX	RCC	*In vitro*	(307)
CD19	B-cell	Phase-I clinical trial	(308-323)
CD20	B-cell	Phase-I clinical trial	(322, 324-327)
CD22	B-cell	Pre-clinical (*in vivo*)	(328, 329)
CD23	Leukaemia	Pre-clinical (*in vivo*)	(330)
CD24	PAC	Pre-clinical (*in vivo*)	(331)
CD30	(N)HL	Phase-I clinical trial	(332-334)
CD33	Myeloid	Pre-clinical (*in vivo*)	(335-337)
CD38	B-cell NHL	Pre-clinical (*in vivo*)	(323, 338-340)
CD44v6	Various	Pre-clinical (*in vivo*)	(341)
CD44v7/8	Cervical	Pre-clinical (*in vivo*)	(342)

CD70	Various	Pre-clinical (*in vivo*)	(343)
CD123 (IL-3Rα)	Myeloid	*In vitro*	(344)
CEA	Various	Phase-I clinical trial	(345-350)
EGFRvIII	Various	Phase-I clinical trial	(351-353)
Target Antigen	**Malignancies**	**Development stage**	**Reference(s)**
EGP-2/EpCAM	Various	Pre-clinical (*in vivo*)	(354-356)
EGP-40	Colon	*In vitro*	(357)
ErbB1/2/3/4	Various	Phase-I clinical trial	(299, 358)
ErbB2	Various	Phase-I clinical trial	(240, 331, 349, 359-364)
ErbB3/4	HNSCC, Breast	*In vitro*	(296, 297)
FAR	Rhabdomyosarcoma	*In vitro*	(365)
G250/CAIX	Renal cell carcinoma	Phase-I clinical trial	(241, 366-369)
GD2	Neuroblastoma	Phase-I clinical trial	(327, 370-373)
GD3	Melanoma	Pre-clinical (*in vivo*)	(374, 375)
HLA-A1/MAGE1	Melanoma	*In vitro*	(376)
HLA-A2/NY-ESO-1	Various	Pre-clinical (*in vivo*)	(377)
HMW-MAA	Melanoma	*In vitro*	(378)
IL-13Rα2	Various	Phase-I clinical trial	(379-381)
Lewis Y	Lung, ovarian	Pre-clinical (*in vivo*)	(382-386)
Mesothelin	Various	Phase-I clinical trial	(387-389)
Muc1	Breast, ovarian, prostate	Pre-clinical (*in vivo*)	(305, 363, 390-392)
Muc16	Ovarian	Pre-clinical (*in vivo*)	(393)
NCAM	Neuroblastoma	Phase-I clinical trial	(394-396)
NKG2D ligands	Various	Pre-clinical (*in vivo*)	(397, 398)
PSCA	Prostate, pancreatic	Pre-clinical (*in vivo*)	(399-401)
PSMA	Prostate, tumour vasculature	Phase-I clinical trial	(369, 400, 402-404)
ROR1	B-cell	Pre-clinical (*in vivo*)	(405)
Tag72	Gastrointestinal	Phase-I clinical trial	(301, 406-409)
VEGF receptors KDR/Flk-1	Various	Pre-clinical (*in vivo*)	(410, 411)
αFR/FBP	Ovarian	Phase-I clinical trial	(304, 412-415)
$\alpha_v\beta_6$ integrin	Various	*In vitro*	(298)
κ -Light chain	B-cell malignancies	Phase-I clinical trial	(416)
5T4/TPBG	Various	Pre-clinical (*in vivo*)	(417)
Universal (biotin)	Various	*In vitro*	(302)

CAIX: carbonic anhydrase IX, CD44v6: CD44 exon v6, CEA: carcinoembryonic antigen, EGFRvIII: epidermal growth factor variant III, EpCAM: epithelial cell adhesion molecule. EPG: epithelial glycoprotein, FAR: foetal acetylcholine receptor, FBP: folate binding protein, G250: Renal cell carcinoma-associated antigen 250, HMW-MAA: high molecular weight melanoma-associated antigen, HNSCC: head and neck squamous cell carcinoma, IL-13Rα2: IL-13 receptor alpha 2, MAGE-1: melanoma antigen, Muc 1/16: mucin 1/16, NCAM: neural cell adhesion molecule, NHL: non-Hodgkin's lymphoma, NY-ESO-1: New York Oesophageal antigen-1, PAC: pancreatic adenocarcinoma, PSCA: prostate specific cell antigen, PSMA: prostate specific membrane antigen, RCC: renal cell carcinoma, ROR1: receptor orphan tyrosine kinase receptor 1, Tag72: tumour associated glycoprotein 72, TPBG: trophoblast glycoprotein, VEGF: vascular endothelial growth factor, αFR: alpha folate receptor.

1.3.9.2 The Hinge

Many CARs include a hinge or spacer region between the binding moiety and signalling domain. The hinge provides a separation between the binding moiety and the T-cell membrane (418). Examples of spacer regions include immunoglobulin domains such as the Fc region of IgG or the immunoglobulin-like extracellular regions of CD4 and CD8 (419). The importance of a spacer region with regards to the activation potential of CARs is dependent on the target antigen. Guest et al. showed that while CARs targeting 5T4 or neural cell adhesion molecule (NCAM) required an extracellular Fc domain spacer region to generate maximal cytotoxicity and IFNγ release, in CARs targeting CD19 and CEA the addition of a spacer region reduced IFNγ release, but cytotoxicity remained the same (419). A first-generation ErbB2-targeting CAR was only functional with the inclusion of a hinge-like CD8α segment (420). The influence of the spacer region was also shown in other models, shortening of the spacer region (12AA vs 229AA) in the ROR1-CAR was associated with superior cytokine secretion and proliferation in response to tumour cell recognition (421). The same long and short spacer regions were compared in an *in vivo* model with a CD19-specific CAR. Only cells transduced with the CAR containing the short spacer region were able to eradicate xenograft tumours. T-cells expressing the CAR containing the longer spacer region did not show any efficacy, which could not be compensated through higher dosing or a combination of CD28 and 4-1BB costimulatory domains. A high rate of activation induced cell death was seen in cells expressing the large spacer CAR (422). In an human immunodeficiency virus $(HIV)_{env}$-specific CAR, the choice of hinge showed to also be influential on the level of expression and turnover rate of the receptor (423). The inclusion of an Fc spacer domain in a CD30 targeting CAR increased the CAR's avidity to soluble ligand, but the equivalent receptor lacking the spacer region showed higher activation upon binding to antigen-positive cells. This suggested that the increased avidity in the presence of soluble ligand may impair the binding to membrane-bound antigen (424).

The necessity and size of a hinge for optimal CAR functionality is dependent on several factors. First, there is an optimal distance between T-cell and target cells. Membrane-distal epitopes would not require a hinge, whereas when targeting membrane-proximal epitopes the absence of a spacer region would result in sub-

optimal activation (328). It was suggested that as the size of the CAR:ligand pair increases, the efficiency of target lysis was decreased because of an enlarged effector:target intermembrane distance, which would permit phosphatases to enter the formed microclusters and dephosphorylate activated molecules of the signalling cascade (328). Additionally, Lymphocyte function adhesion molecule (LFA)-1: intracellular adhesion molecule (ICAM)-1 interference could occur, resulting in a defect in granule polarization and targeting (328). Although a size-dependent component was shown, this is not true for all target antigens. The inclusion of a hinge was required for effective targeting of Muc1 (305). Additionally, no difference in activation could be seen when comparing the targeting of full CEA with a truncated version of CEA (containing the target epitope). This suggests that it is not the size of the antigen, but rather the accessibility of the epitope that is important. Added flexibility through a spacer region might allow for better access of relatively inaccessible epitopes, where as in case of an easily accessible epitope it might reduce binding (419).

Besides influencing CAR functionality, the hinge can also affect the interaction with other elements of the immune system (425). The IgG1 Fc spacer can mediate cross-activation of IgG Fc receptor (FcγR) expressing immune cells (such as monocytes and NK-cells) and CAR^+ T-cells. This cross-activation can result in both an unintended innate immune response as well as a reduced anti-tumour efficacy because of activation induced cell death (AICD) induced by the 'off-target' activation of the CAR^+ T-cells. Fortunately, mutations in IgG Fc spacer can eliminate this cross-activation (425).

Cytotoxicity and cytokine production are dependent on the level of antigen expression on the target cell, level of receptor expression on the effector cell and the strength of the CAR-mediated signal (426, 427). Therefore, inclusion of a spacer region is not a requirement for optimal T-cell activation but should be investigated and optimised for each individual construct.

1.3.9.3 The Transmembrane Domain

The transmembrane domain is considered to mainly have a structural function. It is often derived from natural T-cell molecules such as CD3, CD4, CD8 and CD28. However, recently it has been shown that the transmembrane domain might also have an influence on receptor function. The CD3ζ transmembrane domain was shown to

play a vital role in the interaction between the CAR and endogenous CD3. The CD3ζ transmembrane domain induced upregulation of cell surface CD3ε, allowed for heterodimerisation with endogenous TCR and led to increased cytokine production (428).

1.3.9.4 The Intracellular Signalling Domain

T-cell activation in response to target recognition is achieved with the use of the intracellular signalling domain. It is the most extensively adapted element of the CAR, aiming to optimise T-cell activation. Generically, its evolution is often described in three generations (see Figure 1-6).

In physiological T-cell activation, TCRs co-localize with CD3, which induces the so-called 'signal 1' activation stimulus. The CD3 complex consists of dimers comprising four subunits, namely ζ, δ, ε and γ (429-431). In chimeric receptor constructs, it was revealed that CD3ζ alone is able to induce early and late activation signals identical to normal TCR/CD3 signalling (431, 432). Alternatively, the γ-subunit of the high affinity receptor for IgE, FcεR1 is also capable of inducing 'signal 1'. In a direct comparison between the two signalling components, CD3ζ was able to induce greater cytokine production and cytotoxicity *in vitro*, as well as better tumour growth control *in vivo* (433). This made CD3ζ the preferred element for CAR signalling in so-called 'first generation' constructs. However, CD3ζ signalling has also been implicated in the high levels of AICD in CAR^+ T-cells. The occurrence of this problem was reduced greatly by the insertion of inactivating mutations in two of the immunoreceptor tyrosine-based activation motif (ITAM) domains of CD3ζ, but this finding does spark debate as to whether complete CD3ζ is the best inducer of signal 1 (364).

The low immunogenicity of tumours is not just due to the downregulation of HLA, but also to the lack of the expression of costimulatory molecules that provide T-cells with activation 'signal 2'. This is illustrated by the fact that naïve T-cells expressing a first generation CARs could not be activated *in vivo*, whereas they could be activated *in vitro* in the presence of high-levels of IL-2 (420). Krause et al. demonstrated the value of enhancing costimulatory signalling in T-cells. Expression of a chimeric molecule, which coupled an antigen-specific scFv to the signal transduction domain of CD28, enhanced cell survival and selective expansion of transduced cells (434). Co-expression of scFv-CD28 and scFv-ζ chimeric receptors enabled the induction of

maximal levels of IL-2 production in response to antigen recognition (435). Finney et al. were the first to incorporate CD3ζ and CD28 signalling within one CAR, generating the first 'second generation' construct. The inclusion of CD28 led to a substantial increase in IL-2 production (an indicator for signal 2 delivery) compared to CD3ζ alone (436). Hombach et al. and Maher et al. showed that incorporation of CD28 signalling was also valuable in pre-activated T-cells. Second generation constructs targeting CEA or PSMA improved cytokine production (IL-2 as well as IFNγ), and proliferation compared to first generation constructs (403, 437). The orientation of both signalling domains has also been proven to be of importance. Optimal T-cell activation seems to be achieved with CD28 in the transmembrane/juxtamembranous and CD3ζ in the distal position (403, 436). Additionally, the presence of CD28 within the construct can protect CAR^+ T-cells from suppression mediated by regulatory T-cells (Tregs) (313). Alternatively, the high levels of IL-2 produced by T-cells with CD28-CD3ζ CARs may promote the infiltration of Tregs, leading to poorer anti-tumour response (438).

Second generation CARs may also be constructed using alternative co-stimulatory molecules, in addition to CD28. Constructs have been designed including inducible costimulatory (ICOS) (439), OX40 (308, 439, 440), 4-1BB (308, 439, 441), CD27 (442), DNAX-activation protein-10 (DAP10) (308) or 2B4 (443). All second generation CARs improve T-cell function compared to constructs containing CD3ζ alone; however there are differences depending on which co-stimulatory element is used. Incorporation of CD28 generally results in the highest IL-2 production levels (308), whereas 4-1BB seems to result in the highest multifunctionality of cytokine production (387). In a comparative study ICOS induced the greatest cytotoxicity. ICOS might also promote the persistence of Th_{17}-type CAR^+ T-cells (439). *In vivo*, second generation CARs containing CD28, CD27 or 4-1BB elements showed improved survival compared to first generation constructs, both in mouse (387, 442, 444) and in man (320, 445, 446). A reduction in AICD and improved T-cell survival might be the cause for these observations.

The beneficial effect of including a costimulatory domain initiated further studies investigating whether a combination of costimulatory domains could further enhance functionality. With the combination of two costimulatory domains within one construct, the 'third generation' CAR was born. Third generation CARs combining p56lck and CD28 (447); OX-40 and CD28 (305, 440, 448) or 4-1BB and CD28 (305, 326,

387, 404) have been described. However, the results obtained using combinations of multiple co-stimulatory elements are inconsistent. One study reported that the combination of CD28 and OX-40 enhanced cytotoxicity, expansion and proliferation (440), whereas another only measured a reduction in IL-10 production but no change in the production of other cytokines, cytotoxicity or expansion (448). The combination of CD28 with 4-1BB shows a more consistent improvement in (multifunctional) cytokine release, and increased persistence and cytotoxicity both *in vitro* and *in vivo* (326, 387, 404). Although increase T-cell functionality is desirable with regards to anti-tumour effects, it also raises concern of increased toxicity.

There is no universally applicable 'optimal CAR design'. Optimal functionality is dependent on multiple factors and therefore design optimisation of all elements is required for each individual target.

1.3.10 Limitations of CARs

The major advantage that CAR-mediated T-cell activation has over TCR-activation is the HLA-independent antigen recognition as well as the recognition of non-protein antigen. This circumvents the need for HLA-matched gene transfer, allowing for the use of one construct for all patients. Additionally, there is no risk of toxicity due to mispairing with endogenous TCR (239, 449). However, there are also limitations to CAR-mediated therapy.

First, unlike TCRs, CARs are only able to recognise antigen expressed on the cell surface, thereby excluding TAA such as p53, MDM2 and tyrosinase as targets. Second, use of the CAR approach circumvents central (thymic) tolerance. This is not just a concern for the CAR approach but also for TCR-mediated therapy. Tumour antigen expression is rarely exclusive to tumour cells, but more often results from expression of higher levels or an aberrant form of a protein that is also found in healthy tissue. The introduction of TCR or CAR transgenes circumvents central tolerance in order to improve tumour targeting, but thereby also increases the risk of targeting healthy tissue. Side-effects due to antigen expression on healthy tissue (so-called 'on-target'-toxicity) have been reported in studies targeting carbonic anhydrase IX (CAIX) (366), ErbB2 (240) and CD19 (450). Third, peripheral tolerance is unaffected by ACT and remains a potent factor by which efficacy can be reduced.

Recent clinical trials using CAR T-cells have achieved remarkable preliminary results in acute lymphoblastic and chronic lymphocytic leukaemia (317, 321), but this efficacy was associated with severe toxicity. Unfortunately, the majority of clinical trials involving solid tumours in particular have not achieved such results. Issues such as cell longevity, survival, homing, resistance to suppression and specificity still have to be overcome to allow for a more reliable treatment.

1.3.11 T4 Immunotherapy

T4 immunotherapy is an ErbB targeted adoptive T-cell immunotherapy using cells that have been transduced with two chimeric receptors. Respectively, these are a second-generation CAR named T28ζ (299) and a chimeric cytokine receptor named 4αβ (391).

1.3.11.1 The T28ζ Chimeric Antigen Receptor

T28ζ is a second generation CAR, containing CD28 and CD3ζ signalling domains (see Figure 1-7). Targeting of not just ErbB1 receptor type but of the extended ErbB receptor family is enabled through the use of the T1E-peptide as the binding moiety of the receptor (451). The signalling domain of T28ζ consists of the partial extracellular, transmembrane and intracellular domain of CD28 and the intracellular domain of the CD3ζ chain (please refer to paragraph 2.1.1.1 for details). To maximize the probability of signal cleavage at the junction with the TGFα N-terminus, the leader sequence of macrophage colony-stimulating factor receptor (FMS) was placed upstream of the T1E sequence (299).

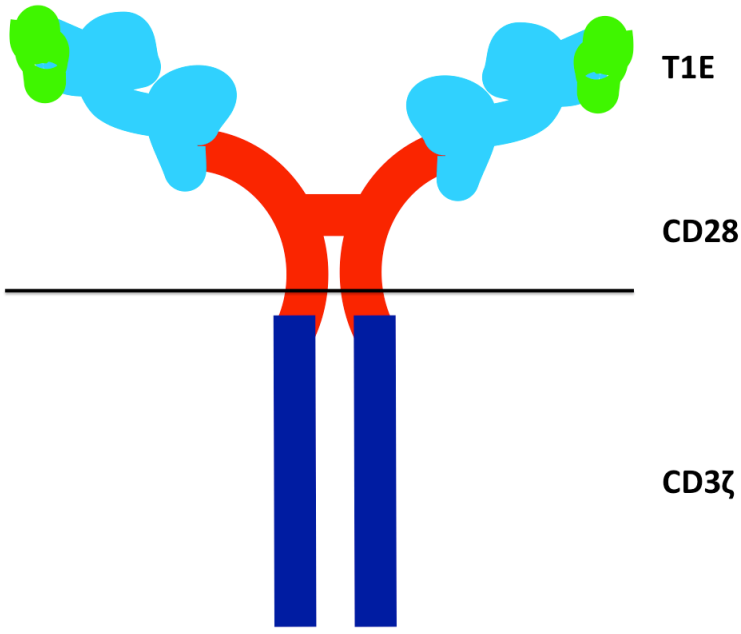

Figure 1-7 Schematic representation of T28ζ
T28ζ is a second generation CAR. The binding moiety consists of the chimeric peptides, coupled to the CD28 hinge and transmembrane domain and the CD3ζ intracellular signalling domain. The receptor forms dimers through disulphide bonds upon membrane expression.

The T1E peptide is an epidermal growth factor (EGF)/ transforming growth factor alpha (TGFα) chimera (see Figure 1-8). Ligand-ErbB receptor binding specificity depends on the interaction between specific residues in the ligands with the extracellular domains of the ErbB receptors. All ErbB growth factors share an EGF-like

domain, which is defined by three disulphide bridges, creating the A-, B-, and C-loop regions and additional linear N- and C-termini (451). Specific residues within the C-loop of EGF and TGFα are thought to be directly involved in binding to ErbB1 (452, 453). Residues in the N-terminus of TGFα also have direct contact with receptor domain I, which is not the case for EGF (68, 69). For Neuregulin (NRG)-1 binding to ErbB3, residues in the N-terminus and B-loop have been indicated to be of primary importance. In the T1E peptide, the N-terminal linear region of EGF is replaced with that from TGFα. The chimera maintained high affinity for ErbB1 and additionally gained the ability to bind to ErbB2/3 heterodimers with a nearly identical affinity as NRG-1. The combination of the His^{4} and Phe^{5} residues in the N-terminus of TGFα with the Leu^{28} residue in the B-loop of EGF was identified to be essential for the high affinity of the T1E chimera for the ErbB2/3 heterodimers (454). Binding of T1E to ErbB3 alone is weak, suggesting that heterodimerization with ErbB2 is required to stabilise the low affinity binding with ErbB3. The weak binding to ErbB3 alone has been attributed to sub-optimal sequences in the linear N-terminus (455-457). The use of the T1E peptide as binding moiety, allows for targeting of the extended ErbB receptor family. As mentioned previously, in paragraph 1.2.5, targeting of multiple ErbB receptors can reduce chances of tumour resistance and increase tumour control.

T1E	**VVSHFNDCPLSHDGYCLHDGVCMYIEALDKYACNCVVGYIGERCQYRDLKWWEL**
TGFα	**VVSHFNDCPDSHTQFCFH-GTCRFLVQEDKPACVCHSGYVGARCEHADLLA**
EGF	**--NSDSECPLSHDGYCLHDGVCMYIEALDKYACNCVVGYIGERCQYRDLKWWELR**

Figure 1-8 Amino acid sequence of the T1E peptide

The specificity of T28ζ for all possible ErbB dimers was tested using the ErbB-negative haematopoietic cell line 32D. Cells were engineered to express ErbB1-4 alone and in all possible heterodimerisation combinations. Co-cultivation of $T28\zeta^{+}$ T-cells with the transduced 32D cells revealed that T-cell activation and subsequent production of IL-2 and IFNγ was induced by all ErbB1 containing homo- and heterodimers, as well as the ErbB2/3 heterodimer, but not ErbB2 or ErbB3 alone. The ErbB1/2 heterodimer consistently achieved most efficient activation. Weak targeting of ErbB4 and ErbB4-containing dimers was also seen (299). These results are consistent with the reported binding properties of the T1E peptide (454). *In vitro*, $T28\zeta^{+}$

T-cells successfully destroyed a wide panel of ErbB$^+$ HNSCC cell lines, which was accompanied by cytokine production (IFNγ), proliferation and enrichment. This was dependent on the presence of both an ErbB$^+$ target as well as a signalling-competent CAR (299). *In vivo*, T28ζ$^+$ cells showed efficacy in several xenograft models, including the slowly progressive, ErbB1/2$^+$ HN3 tumour xenograft and the highly aggressive, ErbB2/3$^+$ MDA-MB-435-ErbB2 (MDA-MB-435 transduced with ErbB2) tumour model (299).

1.3.11.2 The 4αβ Chimeric Cytokine Receptor

Survival and expansion of T-cells following infusion is one of the challenges to successful adoptive cell therapy. These properties are highly dependent on cytokine stimulation, with IL-2 and IL-15 being the most potent stimulators. To stimulate *in vivo* survival and expansion of T-cells, ACT is often combined with a preceding lymphodepleting regimen and high-dose IL-2 administration after T-cells infusion. However, high-dose IL-2 does not selectively stimulate the transferred T-cells but stimulates all lymphocytes and is associated with profound toxicity (458). To allow for selective stimulation of transferred cells without profound toxicity, Wilkie et al. developed a chimeric cytokine receptor (named 4αβ) in which the ectodomain of the IL-4-Rα is coupled to the endodomain of the IL-2/IL-15-Rβ (see Figure 1-9) (391). Co-expression of 4αβ with any CAR (or other transgene) of interest allows for selective expansion and enrichment of transduced cells through stimulation with IL-4. Co-expression of both receptors was achieved through the use of an intervening *Thosea asigna* virus 2A (T2A) peptide downstream of a furin cleavage site (391).

Interleukin-4 was chosen as a selective stimulus for two major reasons. First, endogenous IL-4 plays a role in several tumour types. Second, IL-4 administration has been tested as a therapeutic option for metastatic cancer in man. Cancer cells as well as tumour infiltrating lymphocytes can produce endogenous IL-4. Interleukin-4 is a Th_2 lymphocyte-derived differentiation and growth factor, which can also be produced by mast cells and basophils (459). Interleukin-4 naturally interacts with two heterodimeric receptors. The receptors have a mutual high affinity α-subunit (IL-4Rα), which upon cytokine binding dimerizes with either γ_c (receptor type I), or with IL-13Rα1 (receptor type II). Receptor type I is expressed by activated T-cells, allowing for survival support and limited proliferation through IL-4 stimulation. Fusion of the IL-4Rα ectodomain to

the endodomain of the IL-2/15 β-chain (β_c), allows for the delivery of a much more potent mitogenic signal in T-cells in response to IL-4 binding to 4αβ (391).

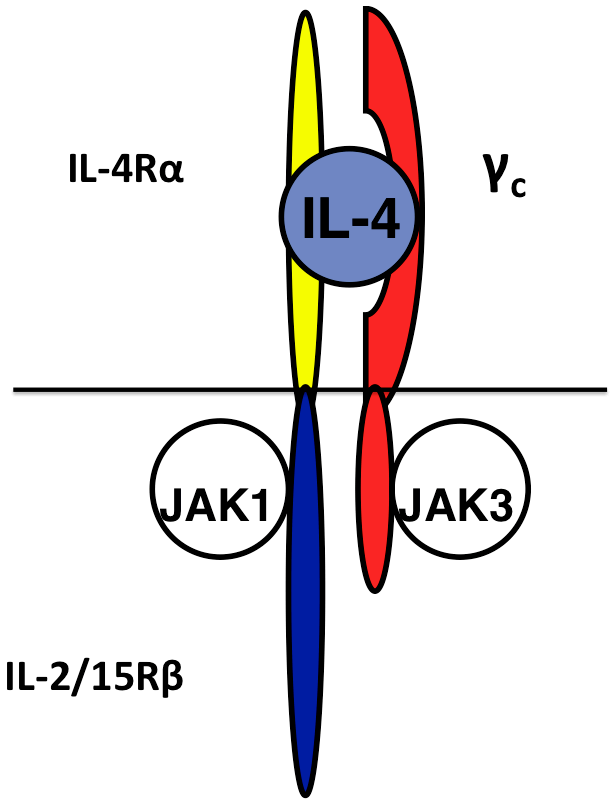

Figure 1-9 Schematic representation of the chimeric cytokine receptor 4αβ
The chimeric cytokine receptor 4αβ is a combination of the IL-4Rα ectodomain coupled to the IL-2/15Rβ endodomain. Upon binding with IL-4, the receptor dimerizes with γ_c and signalling is induced through JAK phosphorylation.

Functionality of 4αβ was proven using the mouse $CD8^+$ T-cell cell line CTLL-2. These cells are highly dependent on IL-2/15 but are unresponsive to human IL-4. However, both human IL-2 and IL-4 elicited a dose-dependent expansion of $4\alpha\beta^+$ CTLL-2 cells (391). Enrichment and expansion of $4\alpha\beta^+$ human primary T-cells was seen consistently, regardless of which CAR it was co-expressed with (the Muc1 targeting HOX, prostate specific membrane antigen (PSMA) targeting P28ζ, or T28ζ) (299, 391, 460). Analysis of signal transducer and activator of transcription (STAT)-phosphorylation (STAT3, 5 and 6) in $4\alpha\beta^+$ cells revealed that IL-4 elicits both IL-4-type (STAT-6) and an IL-2/15-type (STAT3/5) signalling (391). Cells do not show a polarisation toward a Th_2 phenotype, possibly because cells are not exposed to IL-4 prior to activation in combination with the signals delivered through 4αβ. Culture supplementation with IL-4 revealed to be superior in $4\alpha\beta^+$ T-cell expansion over IL-2. This is probably due to an enhanced signalling potency delivered via $4\alpha\beta/\gamma_c$ compared to IL-2/15 β_c/γ_c. This was confirmed by higher STAT3 phosphorylation in response to IL-

4 compared to IL-2 supplementation. Reasons for this can be the high affinity of the IL-4Rα for IL-4 as well as the constitutive expression of 4αβ in combination with the up-regulation of γ_c in activated T-cells. Co-expression of CARs with 4αβ and the subsequent culture in IL-4 does not impair T-cell cytotoxicity or the levels of cytokine production (391).

The role of IL-4 in tumour development and immunotherapy is a 'double-edged sword'. Iinterleukin-4 can inhibit cell growth and invasion through several mechanisms such as the induction of apoptosis, inhibition of angiogenesis, downregulation of matrix metalloproteinases (MMPs) or the induction of higher expression of adhesion molecules (461-464). However, in malignant neoplastic cells IL-4 can induce growth through paracrine mechanisms (465). Additionally, it can inhibit cell-mediated immunity by antagonizing the effect of IFNγ (466). Serum levels of IL-4 are consistently elevated in HNSCC patients, independent of tumour stage (467-469). Production of IL-4 is attributed to TILs and other inflammatory cells in the invasive front of tumours (465, 470). Supernatants of short-term primary HNSCC cell cultures or tumour-derived cell lines showed no, or baseline levels, of IL-4 production (471, 472). However, this could be significantly enhanced through the supplementation of exogenous IL-1 (472). Interleukin-4 is considered to have a stimulatory effect on tumour growth. Primary tumours express variable levels of IL-4 receptor, in comparison to no IL-4R expression in benign lesions (465, 473). *In vitro*, exogenous IL-4 showed to have a growth stimulating effect on 6 out of 13 HNSCC-derived tumour cell lines (465). *In vivo*, a single nucleotide polymorphism (SNP) in the promoter-region of the IL-4 gene, affecting transcriptional activity, was associated with a higher risk for oral squamous cell carcinoma (OSCC) (474). Additionally, in a phase I/II trial intra-tumoural administration of recombinant human IL-4 did not have any clinical benefit, but disease progression was seen in one case (475). However, in OSCC IL-4 can also exert an inhibitory effect through the down-regulation of MMPs (461). The differences in levels and effects of IL-4 could be due to the specific kinetics, metabolism or binding protein modulation parameters of each individual tumour (476).

The use of IL-4 to expand T-cells *in vitro* will not affect the tumour microenvironment after T-cell administration, therefore there is no risk of stimulating tumour growth. However, the IL-4 naturally present in the tumour microenvironment may stimulate survival and expansion of $4\alpha\beta^+$ T-cells.

1.3.11.3 T4 – Combined Expression of T28ζ and 4αβ

T4 immunotherapy is the combined expression of T28ζ and 4αβ in gene-modified T-cells. As previously mentioned, co-expression of both transgenes is achieved through the use of an intervening T2A peptide downstream of a furin cleavage site. $T4^+$ T-cells are activated by a similar spectrum of ErbB combinations (all dimers containing ErbB1 and ErbB2/3 heterodimer) and ErbB expressing tumour cell lines (299). Marked enrichment of $T4^+$ T-cells was achieved *ex vivo* in cultures supplemented with IL-4. After enrichment, co-cultivation of $T4^+$ T-cells with target tumour monolayers resulted in monolayer destruction at an effector:target ratio <1 (299). Activated cells produce IFNγ and IL-2, but small amounts of IL-4. Production of IFNγ is enhanced by exogenous IL-4 addition (299).

Patients are often immuno-deprived, which could make transduction and expansion of T-cells more challenging. Reassuringly however, PBMCs from epithelial ovarian cancer patients were successfully transduced and expanded and showed efficacy against both ovarian cancer cell lines as well as autologous tumour spheres (358).

In vivo, 7.5 x 10^6 $T4^+$ T-cells proved to be equally effective against an established (highly $ErbB1^+$) HN3 tumour as a dose of 20 x 10^6 $T4^+$ T-cells. $T4^+$ T-cells were also highly effective against the aggressive $ErbB2/3^+$ tumour cell line MDA-MB-435-ErbB2 (299). Combination of $T4^+$ T-cells with adjuvant IL-4 slightly increased efficacy. This could be due to an additive effect of both treatments (IL-4 alone also had an anti-tumour effect). Alternatively, IL-4 could have improved *in vivo* persistence of $T4^+$ T-cells (299). In an IP xenograft models with the ovarian cancer cell line SKOV-3, treatment with $T4^+$ T-cells resulted in rapid tumour regression, followed by disease progression. Repeated T-cell administration resulted in improved tumour control compared to a single treatment, but still resulted in tumour progression. Pre-treatment with the chemotherapeutic agent carboplatin lead to a significant enhancement of anti-tumour activity, which was further increased by a metronomic carboplatin and T-cell treatment regimen, using a relatively low dose of 2.5 x 10^6 T-cells. However, complete tumour eradication was not achieved in any of the models. Mild and reversible weight loss was the only toxicity observed (358).

1.4 Clinical Trials of CAR-based Immunotherapy – the balance between Efficacy and Toxicity

Pre-clinical data suggests that CAR-mediated adoptive T-cell therapy has potential as an immunotherapy for the treatment of a wide range of tumours. Multiple Phase-I clinical trials have been conducted in order to explore the safety and efficacy of this therapy in man. Initial clinical trials showed little toxicity but also limited efficacy. In order to improve efficacy, several adaptations were investigated to enhance co-stimulatory signalling and circumvent the 'cytokine sinks'. However, in the process to improve efficacy, increased toxicity was also encountered. Here, the advances made in Phase-I clinical trials are described, including their implications for both efficacy and toxicity.

1.4.1 Efficacy – T-cell Expansion and Persistence

The first Phase-I clinical trial results involve the use of CAR-engineered T-cells were published by Kershaw et al. in 2006 (304). Patients with ovarian cancer were treated in an intra-patient dose escalation study with a first-generation CAR targeting folate receptor-α. No evidence of anti-tumour response was seen. Reasons for the lack of efficacy included poor trafficking of T-cells to the tumour site and limited persistence of transfused cells. After transfusion, cells initially accumulated in the lungs and subsequently migrated to the liver and spleen. Despite adjuvant IL-2 administration, CAR^+ T-cells were barely detectable 3 weeks after infusion (304). The lack of an anti-tumour response was linked to the lack of homing to the tumour as well as limited cytotoxicity and persistence of the transfused T-cells. Several techniques were investigated to improve these elements in various clinical trials, as summarised in Table 1-4. The best clinical responses so far have been reported in the treatment of chronic lymphocytic leukaemia (CLL) and acute lymphoblastic leukaemia (ALL) with CD19 re-targeted T-cells (317, 477).

Table 1-4 Phase-I Clinical Trial results published to date

CAR	Malignancy	IL-2	Lymphodepl	Efficacy	Reference
aFR 1st Gen	Ovarian Cancer	Yes	No	No OR	(304)
aCAIX 1st Gen	RCC	Yes	No	No OR	(242, 366)
aCD20 1st Gen	Lymphoma	Yes/No	No	Limited efficacy	(478)
aCD20 2nd Gen	Lymphoma	Yes	Yes	PR, PF	(327)
aGD2 1st Gen	Neuroblastoma	No	No	Prolonged TTP CR	(370, 372)
L1-CAM 1st Gen	Neuroblastoma	No	No	SD, PR, CR	(394)
aCD19 1st Gen	FL	Yes	Yes	No OR	(322)
aCD20 1st Gen	DLCL	No	Yes	CR (combined with HSCT)	(322)
aCD19 2nd Gen	Lymphoma	Yes	Yes	OR, PR	(312, 319)
aErbB2 3rd Gen	Colon Cancer	No	Yes	SAE	(240)
aCD19 2nd Gen	CLL/ALL	No	Yes/No	PR, SD, SAE	(450, 479)
aCD19 1st & 2nd Gen	NHL	No	No	Transient SD	(446)
aCD19 2nd Gen	ALL	No	Yes	MRD^-, CR	(317)
aCD19 3rd Gen	CLL	No	Yes	PR, CR	(320, 445)
aCD19 3rd Gen	ALL	No	Yes	CR	(477)

Lymphodepl: lymphodepletion, Gen: generation, FR: Folate Receptor-α, CAIX: carbonic anhydrase IX, RCC: renal cell carcinoma: FL: follicular lymphoma, DLCL: diffuse large cell lymphoma, NHL: non-Hodgkin's lymphoma, CLL: chronic lymphocytic leukaemia, ALL: acute lymphoblastic leukaemia, OR: objective response, PR: partial response, PF: progression free, TTP: time to progression, CR: complete response, SD: stable disease, SAE: serious adverse event, HSCT: hematopoietic stem cell transplant, MRD: minimal residual disease.

1.4.1.1 Enhanced Co-Stimulatory Signalling

A possible reason for the limited persistence and cytotoxicity of transfused T-cells is the absence of sufficient co-stimulatory signals when using first-generation constructs. In order to improve the co-stimulation, Pule et al. compared Epstein-Barr Virus (EBV)-specific and non-specific T-cells, which had both been re-targeted against GD2. Transduced EBV-specific T-cells were expected to be superior in survival and function. Co-stimulation can be provided to these cells *ex vivo* by co-culture with EBV^+ B-cells and *in vivo* by encounter with (latent) viral antigens (370). Neuroblastoma patients with EBV-specific IgGs were treated with a single injection containing an equal amount of CAR^+ EBV-specific (C-EST) and CAR^+ non-specific (C-NST) T-cells, thereby acting as a 'self-control'. Prior to injection both cell populations were of similar phenotypes and equivalent cytotoxicity against $GD2^+$ neuroblastoma cell lines. As early as 24 hours after T-cell injection, higher levels of C-EST were detected compared to C-NST and which persisted for a period of up to 6 weeks after injection. Transfused C-NST were detectable up to 3 weeks. Additionally, C-EST retained their cytotoxicity better than C-NST (370). However, in contrast to short-term persistence, long-term persistence of C-NST at low levels was more sustained compared to C-EST (192 weeks and 96 weeks respectively). Persistence of either CAR^+ cell population was associated with a significantly longer TTP in patients with active disease, due to a true difference in PFS (372). Rather than EBV-specificity, prolonged T-cell persistence was shown to be positively correlated with the number of $CD4^+$ T-cells and central memory $CD8^+$ T-cells within the administered cell population (372). Similarly, in a trial targeting CLL with CD19 re-targeted T-cells the influence of cell phenotype on persistence was noted. The persisting $CD8^+$ CAR^+ T-cell population differentiated *in vivo* from a mainly effector memory phenotype, to a mixed effector and central memory phenotype. The *in vivo* persisting $CD4^+$ CAR^+ T-cells were mainly of the central memory phenotype (320).

An alternative method to induce sufficient co-stimulation to the administered T-cells, is the use of second generation CARs rather than first generation CARs. Savoldo et al. compared the expansion and persistence *in vivo* of T-cells transduced with a first (CD3ζ alone) or second (CD28 and CD3ζ) generation CD19-targeting CAR (446). Patients with relapsed or refractory NHL were treated with both CD19ζ and CD19-28ζ transduced T-cells. Both cell populations were similar phenotypically and were detectable in peripheral blood as early as 3 hours after injection. However, in contrast

to CD19ζ transduced cells, CD19-28ζ transduced cells were able to expand *in vivo*. Both the $CD4^+$ and $CD8^+$ T-cell populations were shown to contribute to the *in vivo* expansion. Additionally, CD19-$28\zeta^+$ T-cells were able to infiltrate cutaneous tumour lesions in contrast to $CD19\zeta^+$ T-cells (446).

1.4.1.2 Enhanced Cytokine Stimulation

Besides co-stimulatory signalling, cytokine stimulation is also important for the functionality of T-cells. Increasing the cytokine stimulation to transfused T-cells has been pursued through the administration of adjuvant IL-2 or lymphodepletion prior to T-cell administration. Lymphodepletion removes the so-called 'cytokine sinks', making the cytokines more available to the transferred T-cells because they are not consumed by circulating lymphocytes. Additionally, lymphodepletion increases the production of homeostatic cytokines and removes Tregs (480). Till et al. showed that adjuvant IL-2 administration prolonged the persistence of their CD20 re-targeted T-cells (using a first generation CAR) from 5-21 days (without IL-2) to 5-9 weeks (with IL-2) in patients with NHL. However no anti-tumour response was seen (478). In a second trial by the same group, T-cells engineered to express a third generation CD20-targeted CAR were administered following lymphodepletion. The infused cells migrated to malignant lymph nodes within 24-48 hours, were detectable in bone marrow 1 month after transfusion and persisted for 9-12 months (327). Treatment resulted in 1 partial response and 2 patients remained progression free for 12 months (327). Comparison of the results of these two trials suggests that improved co-stimulatory signalling and lymphodepletion both may have contributed to an increase in efficacy. The positive effect of lymphodepletion upon efficacy of CD19-targeted T-cells was confirmed by Brentjens et al. In this trial, patients were treated with a CD19-targeted second generation CAR, with or without prior cyclophosphamide treatment. Lymphodepletion increased CAR^+ T-cell persistence, infiltration into tumour beds, allowed for migration to the bone marrow and improved efficacy. Combined therapy led to a reduction of peripheral lymphadenopathy and stable disease, whereas no objective disease response was seen when patients were not lymphodepleted (479).

1.4.1.3 Trafficking to Bone Marrow

In B-cell targeted treatments, CAR^+ T-cell migration to the bone marrow could also be beneficial for T-cell persistence. Kalos et al. reported persistence of CD19 re-targeted T-cells for at least 6 months (the maximum period of reported follow-up) as well as CAR^+ T-cell trafficking to the bone marrow. Importantly, in this study the CAR endodomain comprised a fusion of 4-1BB followed by CD3ζ. In the bone marrow, CAR^+ T-cells could be repeatedly activated by encounter with emerging progenitor B-cells, resulting in prolonged persistence (320).

1.4.1.4 Immune Response against CARs

The efficacy and persistence of CAR^+ T-cells can also be limited due to the induction of an immune response against the administered T-cells. Multiple CAR constructs use scFv derived from mouse-anti human antibodies. The presence of mouse elements within the expressed construct can elicit an immune response against the CAR. Lamers et al. treated patients with metastatic RCC with CAIX re-targeted T-cells. The binding moiety of the CAR used consisted of an scFv of the anti-CAIX mouse mAb G250. No objective clinical response was seen in the patients, however 'on-target' hepatotoxicity was observed (described in paragraph 1.4.2.2), suggesting functionality of the transfused T-cells *in vivo* (242, 366). A human antibody response to G250 (human anti-CAR antibodies; HACA) became detectable after the second CAR^+ T-cell treatment cycle. *In vitro*, HACA was shown to inhibit CAR-mediated cytolysis in a concentration-dependent manner (242). In addition to an antibody-mediated response, a cell-mediated immune response against CAR^+ T-cells was also detected. The cell-mediated response was also initiated after the second treatment, but occurred before detectable HACA levels could be measured (242). Whether an immune response is elicited against the mouse scFv domain used in the CAR is dependent its immunogenicity. In keeping with this, Till et al. used a mouse anti-human CD20 scFv as a binding moiety and no immune response against the CAR was detected (327, 478). However, mouse scFv is not the only element that can induce an immune response. Lamers et al. also reported on the induction of an immune response against viral-vector immunogenic epitopes in two of their patients (242).

1.4.2 Toxicity – Common to Serious Adverse Events

The severity of adverse events recorded in Phase-I clinical trials is generally graded using a scale developed by the National Cancer Institute (NCI). The 'common terminology for adverse events' (CTCAE)(481) distinguishes 5 grades of toxicity. Table 1-5 gives a brief definition of each grade as summarized by the NCI (481).

Table 1-5 Severity grades for adverse events as described in CTCAE version 4.03

Grade 1	**Mild**; asymptomatic or mild symptoms; clinical or diagnostic observations only; intervention not indicated.
Grade 2	**Moderate**; minimal, local or non-invasive intervention indicated; limiting age-appropriate instrumental ADL.
Grade 3	**Severe or medically significant but not immediately life-threatening**; hospitalization or prolongation of hospitalization indicated; disabling; limiting self care ADL.
Grade 4	**Life-threatening consequences**; urgent intervention indicated.
Grade 5	**Death related to adverse event**.

A semi-colon indicates 'or' within the description of the grade. ADL = Activities of Daily Living

1.4.2.1 Common Adverse Events

The most common adverse events reported in CAR-mediated Phase-I clinical trials include fatigue, nausea, hypotension, rigors, diarrhoea, fevers, injection site reactions, mental status changes, hepatic toxicity, renal failure and respiratory distress (304, 322, 327, 394, 478, 479). The severity of adverse effects can range from grade 1-4. In CAR-based trials in which IL-2 was also administered, most side effects resolved once the IL-2 treatment was stopped (304, 327, 478). When caused by T-cell transfusion, steroid treatment could ameliorate most symptoms (317). In several cases, no treatment was required and side-effects resolved spontaneously overnight (327).

Hypogammaglobulinemia and cytopenia are common side effects due to lymphodepleting chemotherapy and CD19 or CD20 targeting treatments (311, 319, 322, 394). The occurrence of these adverse events required Immunoglobulin replacement therapy. The occurrence of bacteremia and pneumonitis has also been reported in patients suffering from cytopenia (394).

1.4.2.2 'On-target '-Toxicity

'On-target'-toxicity occurs when the target antigen expressed on healthy tissue activates redirected T-cells. Lamers et al. reported the occurrence of 'on-target'-toxicity in a Phase-I clinical trial in which patients with metastatic renal cell carcinoma were treated with T-cells retargeted against CAIX. Immunohistochemistry showed T-cell infiltration around $CAIX^+$ bile duct epithelial cells, suggesting a specific attack by CAR^+ cells which resulted in clinical grade 3-4 hepatotoxicity (366). To mitigate against this toxicity, low-dose anti-CAIX mAb cG250 (chimeric G250; humanized mouse G250 in which the constant regions of the heavy and light chains have been substituted by their human analogues) treatment was administered prior to infusion of the T-cells. By this means, it was possible to avert the occurrence of high-grade liver toxicity. At a low dose, cG250 blocks CAIX in the liver cells but leaves it accessible at RCC tumour sites, owing to higher expression at the tumour site (242). This 'on-target'-toxicity does not always occur when targeting antigens that are also expressed on healthy tissue. For example, Park et al. reported no toxicity against L1-CAM expressing healthy tissues in a CAR study targeting neuroblastoma with a first-generation CAR, despite the expression of L1-CAM on healthy tissue including the central nervous system, adrenal medulla and sympathetic ganglia (394).

1.4.2.3 Cytokine Release Syndrome

An important side effect that may complicate immune-modulating therapies is the occurrence of cytokine release syndrome (CRS). Clinical symptoms of CRS include hypothermia or fevers, rigors, hypotension, rash, dyspnea and occasionally bronchospasm, rash, nausea and diarrhoea. More severe symptoms include pulmonary oedema, hepatitis and multi-organ failure (482). Severe CRS is also referred to as a cytokine storm, cytokine cascade or hypercytokinemia. For a more detailed description of the kinetics of a cytokine storm, please refer to Chapter 4.1. The most common side effects registered in CAR-mediated therapy are consistent with the occurrence of CRS. Cytokines most commonly upregulated include TNF, IFNγ, IL-6 and IL-10 (319, 320, 327, 445). The increases in serum cytokine levels have been connected to both the occurrence of adverse events as well as anti-tumour efficacy. Kochenderfer et al. showed that an elevation in serum IFNγ and TNF levels correlated with more severe toxicity (319). The severity of toxicity was measured over a period of 10 days and

quantified with the 'sequential organ failure assessment' (SOFA) score. The SOFA score is based on the measurements of blood pressure, respiratory function, renal function, and the blood platelet count (483, 484). Patients with elevated cytokine levels had a significantly higher SOFA score (mean 105.0) compared to patients without an increase in cytokine levels (mean 61.5) (319). The SOFA score for each patient was correlated to the level of IFNγ and TNF measured over time (319). The increased cytokine levels were probably not caused by exogenous IL-2, because new elevations and severe toxicity also occurred several days after the last IL-2 administration (319).

The relationship between T-cell induced cytokine production, toxicity and efficacy, is illustrated in a case report by Porter et al. (445). A patient with CLL received a dose of 3 x 10^8 total T-cells (5% transduced) after lymphodepletion without any additional cytokine administration. Side effects started fourteen days after transfusion and progressed during the following week. Tumour lysis syndrome was diagnosed at day 22. At the same time, the peak level (20%) of CAR^+ T-cells in the blood were measured as well as peak levels of IFNγ and IL-6 (160 fold higher than base level). At day 23, there was no detectable CLL found in the bone marrow and no lymphadenopathy evident on the CT scan at day 31. At the time of publication, the patient has sustained remission for 10 months (445). This relationship between efficacy and CRS was confirmed in three additional patients (320). There is a delicate balance between efficacy and toxicity related to cytokine production as illustrated by the serious adverse events described in paragraph 1.4.2.4. Timely treatment to reduce the toxicity induced by a cytokine storm is required. Grupp et al. described rapid effects after anti-cytokine therapy in a 7-year old patient with acute lymphoblastic leukaemia. The patient developed severe CRS five days after T-cell transfusion, including elevated levels of IFNγ and IL-6. The patient developed severe respiratory and cardiovascular compromise. Within hours after anticytokine therapy, consisting of Etanercept (a TNF inhibitor) and Tocilizumab (anti-IL-6Rα mAb), the fever lowered and the acute respiratory distress syndrome was resolved (477).

Brentjens et al. reported a positive correlation between tumour burden at the time of T-cell administration and the level of cytokine production. Additionally, tumour burden was also correlated to the amount of circulating CAR^+ T-cells and the expansion of CAR^+ T-cells (317). Patients received steroid treatment to ameliorate cytokine toxicities, however this also led to a reduction of CAR^+ T-cells (317).

1.4.2.4 Serious Adverse Events

To date, the occurrence of two serious adverse events (SAE) in Phase-I trials of CAR T-cells have been reported. Brentjens et al. reported an SAE in their trial treating CLL with a CD19-targeting second generation CAR (containing CD28 and CD3ζ signalling domains) (450). The patient underwent lymphodepleting chemotherapy and was subsequently treated with a dose of 1.2-3.0 x 10^7 CAR^+ T-cells/kg. Three prior patients had been treated with the same CAR^+ T-cell dose, without prior lymphodepletion. In these patients, toxicity was limited to rigors, chills and a transient fever within the first 24 hours after T-cell injection. However, in the first patient who received additional lymphodepletion, the fever persisted and was associated with hypotension, as well as respiratory distress. Additionally, the patient suffered from acute renal failure and eventually died 44 hours after T-cell infusion. Despite the occurrence of this SAE shortly after T-cell infusion, it is suggested that CAR^+ T-cells were not the cause of this toxicity. Post-mortem pathology did not show any signs of tumour-lysis syndrome. Serum cytokine levels (IL-2, IL-7, IL-15 and IL-12) were increased after lymphodepletion, TNF and IFNγ levels remained unchanged prior to and after T-cell infusion. These data suggest that the patient developed a sepsis-like syndrome induced by a prior sub-acute infection, which was aggravated by the lymphodepletion. In response to the SAE, the administered T-cell dose was lowered and administered in split infusions over three days. Patients treated with the modified protocol did not show any signs of a 'cytokine storm' in response to lymphodepletion, or any notable toxicity after T-cell treatment (450, 479).

The second SAE was reported by Morgan et al. who treated a patient with metastatic colon cancer with an ErbB2-targeted third generation CAR (containing CD28, 4-1BB and CD3ζ signalling domains) (240). The patient was treated with a dose of 1 x 10^{10} cells (79% CAR^+) after administration of a lymphodepleting regimen (cyclophosphamide and flurodarabine). Within 15 minutes after T-cell administration, the patient developed respiratory distress caused by pulmonary oedema. The patient then developed hypotension and underwent two cardiac arrests. Five days after treatment, progressive hypotension, bradycardia and gastrointestinal bleeding resulted in a final cardiac arrest. Post-mortem pathology revealed that the patient had multiple organ failure secondary to systemic microangiopathic injury. Transduced cells were detected predominantly in the lung and abdominal/mediastinal lymph nodes but

had not homed to tumour sites. Serum cytokine levels showed a rapid increase in IFNγ, GM-CSF, TNF, IL-6 and IL-10. All cytokines except IL-10 peaked at 4 hours after infusion and decreased over the following 3 days. Interleukin-10 levels remained high for the entire study duration. An increase in IL-2 levels was also detected at 4 hours, however this was likely to be the result of the IL-2 present in the T-cell infusion product. Morgan et al. postulated that the highly-active anti-ErbB2 redirected T-cells recognized ErbB2 expressed by healthy lung tissue, inducing the release of inflammatory cytokines. This resulted in pulmonary toxicity and oedema, followed by a cascading cytokine storm and resulting in multiple organ failure (240).

The results achieved in Phase-I clinical trials have shown the potency of CAR-mediated adoptive T-cell therapy against a range of target antigen and tumours. However, the occurrence of high-grade toxicity has also indicated limitations to the application of this therapy. More detailed investigation into the parameters influencing both efficacy and toxicity of CAR-mediated therapy is essential for the progression and wider application of this therapy.

1.5 Aims of this Thesis

The work performed by Dr DM Davies prior to the commencement of this PhD has detailed the functionality, specificity and efficacy of T28ζ and T4, both *in vitro* and *in vivo* (299). The work performed in this PhD aims to determine the safety of T4 immunotherapy, in pre-clinical *in vitro* and *in vivo* models, as well as prepare for first-in-man toxicity testing in a phase-I clinical trial.

The specific aims of this PhD project include:

1. Determine the suitability of a SCID/Beige immunodeficient mouse model for pre-clinical toxicity testing.
2. Determine the longevity and migration pattern of human transduced T-cells after intravenous and subcutaneous injection.
3. Determine the risk of 'on-target'-toxicity *in vitro* and *in vivo.*
4. Determine the risk of cytokine release syndrome in response to T4 immunotherapy.
5. Determine the functionality of T4 immunotherapy through intra-tumoural administration.
6. Development of a GMP-compliant production process for a phase-I clinical trial.

CHAPTER 3 details the experiments investigating the suitability of the SCID/Beige pre-clinical model and the experiment undertaken to investigate the risk of 'on-target off-target'-toxicity. CHAPTER 4 details the investigation into the onset of cytokine release syndrome after intra-peritoneal T4 immunotherapy administrations and the factors influential to the onset of this. The use of a GMP-compliant production process for the application in a phase-I clinical trial of T4 immunotherapy is described in CHAPTER 5.

CHAPTER 2

MATERIALS AND METHODS

2.1 Molecular Biology Techniques

2.1.1 Generation of CAR Constructs

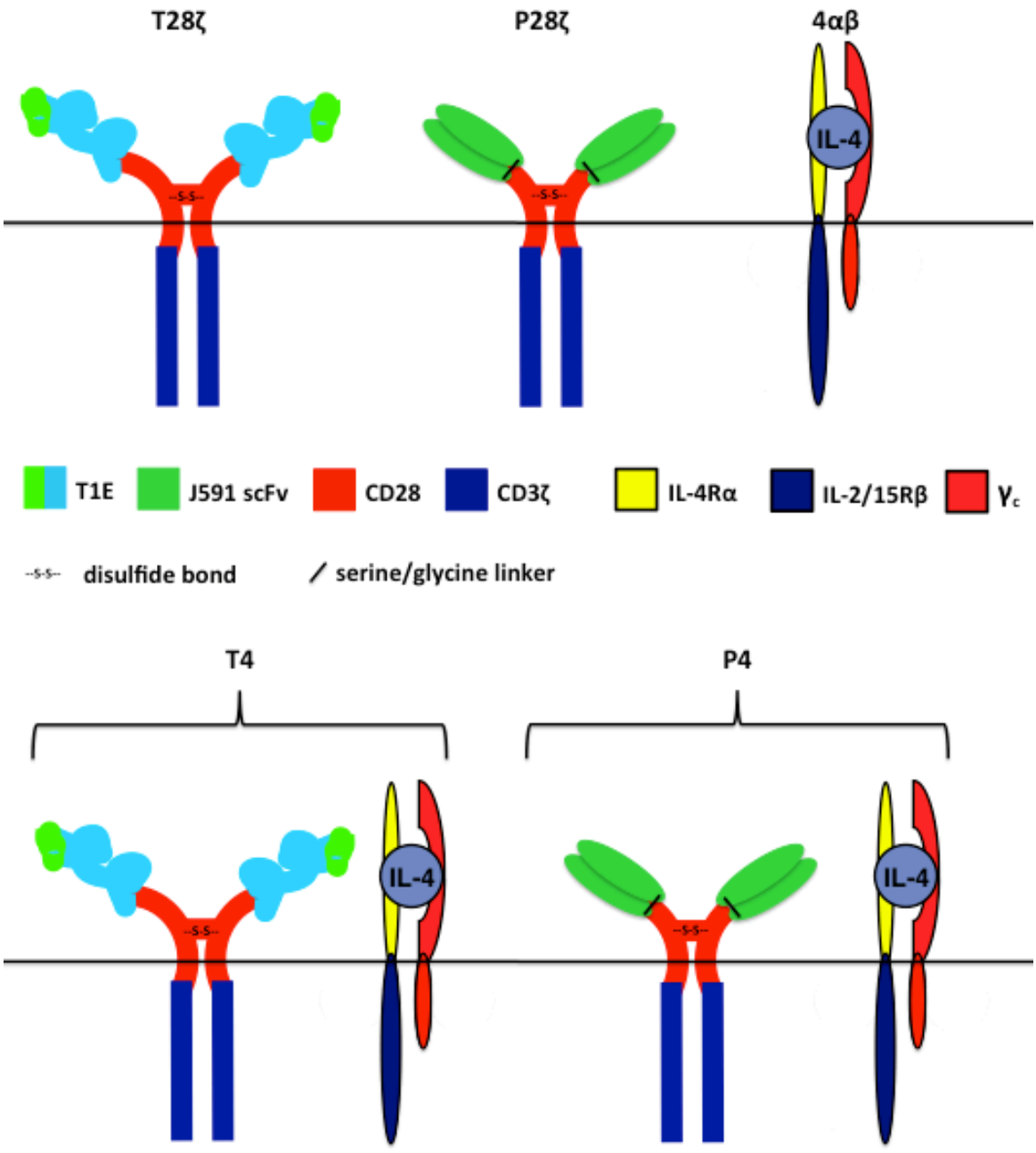

Figure 2-1 Schematic overview of the ErbB- and PSMA-targeting CARs
IL-4Rα: Interleukin-4 Receptor α; IL-2/15Rβ: Interleukin-2/15 Receptorβ; γ_c: common γ-chain.

2.1.1.1 T28ζ

The ErbB-targeting T28ζ chimeric antigen receptor (CAR, Figure 2-1) was produced and cloned into SFG prior to the commencement of this PhD (299). The construct comprises a human fusion gene encoding the macrophage colony stimulating factor receptor (FMS) leader sequence, the T1E peptide (for a detailed description please refer to paragraph 1.3.11.1) (451, 457), the partial extracellular, transmembrane and intracellular domain of CD28 (from amino acid 114 to 220) and the intracellular domain of the CD3 zeta (CD3ζ) chain (amino acids 52-164). The T1E peptide is a chimeric fusion protein composed of the entire processed human EGF protein, excluding the five most N-terminal amino acids, which have been replaced by the seven most N-terminal amino aids of the mature human TGF-α protein. The cDNA was cloned as an *NcoI/XhoI* fragment into pre-digested SFG-P28ζ (403). The SFG retroviral vector backbone (a kind gift from Dr M. Sadelain, Memorial Sloan-Kettering Cancer Center, New York) contains a 5' long terminal repeat (LTR) as a promoter and a packaging signal flanked by splice donor and acceptor sites (please refer to paragraph 2.2.3.1).

2.1.1.2 P28ζ

The prostate specific membrane antigen (PSMA)-targeting P28ζ CAR (see Figure 2-1) is a second-generation CAR that was constructed by Dr J. Maher prior to the commencement of this PhD (403). The CAR was expressed using the SFG retroviral expression vector. The binding moiety of P28ζ comprises of an scFv derived from the J591 hybridoma (485), joining the V_H and V_L fragments through a serine/glycine linker. The transmembrane and intracellular domain of P28ζ comprises of CD28 and CD3ζ fragments, as described in paragraph 2.1.1.1 for T28ζ. Adequate expression on the cell membrane is enabled through the addition of the CD8α leader sequence upstream of the P28ζ sequence (in contrast to the FMS leader sequence which is used in T28ζ).

2.1.1.3 4αβ

The chimeric cytokine receptor 4αβ (see Figure 2-1) is a fusion of the IL-4Rα ectodomain (amino acids 1-233) to the shared IL-2/15Rβ transmembrane and endodomain (amino acids 241-551) (391). The construct was design by Dr SE Papa and Dr S Wilkie prior to the commencement of this PhD. The 4αβ sequence was designed

as a *NcoI/NcoI* fragment to allow for cloning upstream of any selected CAR. The 4αβ sequence was followed by an optimised furin cleavage site (RRKR)(486), a serine glycine linker, and a T2A sequence (detailed in paragraph 2.1.1.4). The stop codon form the 4αβ gene sequence is omitted prior to the T2A sequence to ensure full expression of the 3' gene.

2.1.1.4 T4

The T4 (T28ζ + 4αβ) vector construct (see Figure 2-1) was produced prior to the commencement of this PhD by Dr Davies (299). The construct is defined by the co-expression of the T28ζ CAR with the chimeric cytokine receptor 4αβ (391). Dual expression of both proteins using the same promoter was achieved by the inclusion of a self-cleaving 2A peptide sequence between the 4αβ and T28ζ coding regions. This peptide, derived from the insect virus *Thosea asigna* (and therefore referred as a T2A sequence (487, 488) permits dual polypeptide expression from the same mRNA molecule by inducing a ribosomal 'skip', in which a peptide bond between the two constructs is 'missed' (489). To ensure full expression, the stop codon at the 3' end of the 4αβ sequence has been removed. Furthermore, to reduce the inclusion of the T2A sequence at the C-terminal end of the 4αβ construct, a furin cleavage site was introduced 5' of the T2A sequence (see Figure 2-2) Construction of T4 into SFG was achieved through the insertion of the *NcoI*-flanked 4αβ and T2A sequence at the *NcoI* site upstream of T28ζ.

2.1.1.5 P4

The P4 (P28ζ and 4αβ) vector construct (see Figure 2-1) was produced by Dr Papa prior to the commencement of this PhD. The P28ζ CAR has a naturally occurring *NcoI* restriction site within the J591 scFV, making it impractical to insert the 4αβ-furin-T2A cassette upstream of P28ζ as an *NcoI* fragment. Consequently, an alternative cloning strategy was devised. Both the HOX (a Muc-1 targeting third generation receptor)(305) CAR and P28ζ have a CD8α leader sequence at their 5' end. There is an *SphI* restriction site within the CD8α leader, which is not replicated in either SFG-P28ζ or H4 (HOX co-expressed with 4αβ) (391). Consequently, SFG-P28ζ was digested with *SphI/XhoI* and the smaller (CAR-encoding) cDNA fragment was substituted for the corresponding sequence in SFG-H4, thereby generating SFG-P4 (see Figure 2-2).

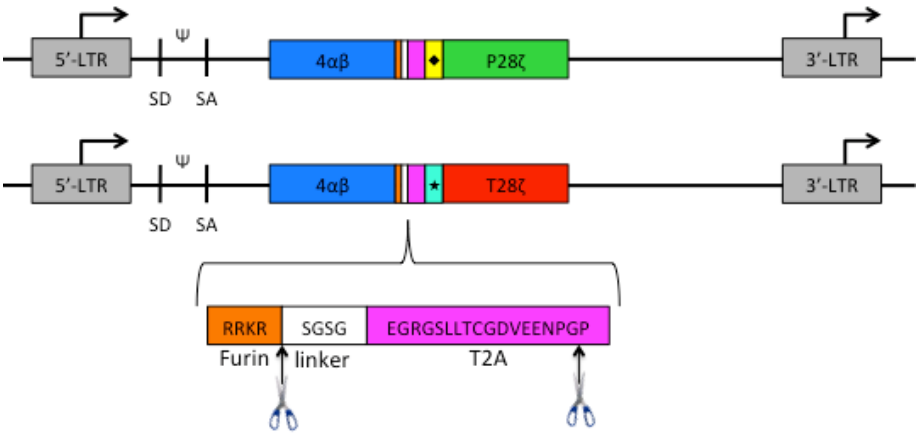

Figure 2-2 Schematic representation of P4 and T4 within SFG

Within the P4 and T4 combinations, the coding sequences are separated by the T2A peptide derived from the *Thosea asigna* plant virus, which induces a ribosomal 'skip' and therefore misses a peptide bond between the flucine and proline (as indicated by the right scissors). Expression of the T2A peptide sequence at the C-terminus of the mature 4αβ protein is prevented by the presence of a furin cleavage site (as indicated by the left scissors). The Furin cleavage site is linked to the T2A peptide by a serine-glycine linker. LTR: long terminal repeat; SD: splice donor; ψ: packaging signal; SA: splice acceptor; ★: FMS leader sequence; ◆: CD8α leader sequence. *Note: size of the blocks is not representative of the sizes of the individual elements.*

2.1.1.6 T4luc

The T4luc (T28ζ + 4αβ + fireflyLuciferase) construct is defined by the co-expression of the T4 construct with the gene encoding for the firefly Luciferase (ffLuc) enzyme. Expression of all three elements is achieved with the insertion of a second T2A peptide and furin cleavage site, separating the T28ζ protein from the ffLuc enzyme. To avoid the introduction of a large direct repeat, that would promote proviral instability, the DNA sequence of the second T2A sequence was made as different as possible from the first T2A sequence. The ffLuc sequence was cloned into the SFG-T4 retroviral vector by means of a four-piece ligation (see Figure 2-3). The SFG-T4 plasmid was digested with *NotI/XhoI* to isolate the SFG backbone and the majority of the T4 sequence. The pBabe-puro-ffLuc plasmid was digested with *NcoI/AgeI*, isolating the majority of the ffLuc sequence (base 53-1186). Two linker peptides were designed by Dr Papa, and synthesized by GenScript (Piscataway, New Jersey) to replace the removed bases from T4 and ffLuc. The pUC47-ffLuc plasmid was digested with two separate digestions, *NotI/NcoI* and *AgeI/XhoI*, isolating the two linker-peptides.

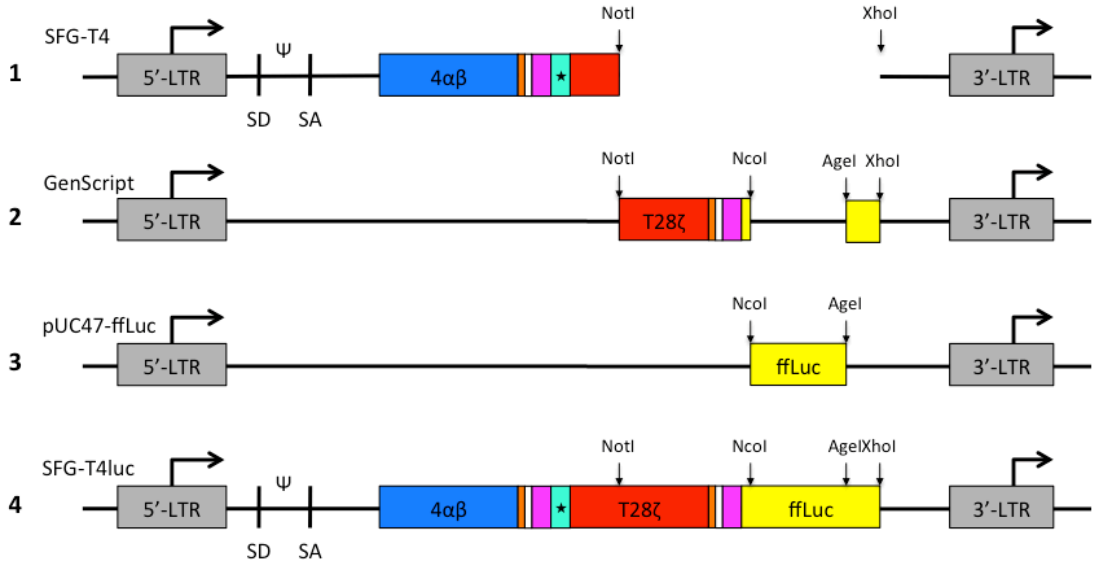

Figure 2-3 Schematic representation of cloning strategy of SFG-T4luc

The T4luc construct was cloned by means of a four-piece ligation. (**1**) The partial T28ζ sequence was removed from the SFG-T4 vector through *NotI/XhoI* digestion. (**2**) The removed partial T28ζ sequence combined with a second T2A sequence and furine cleavage site, flanked by *NotI/NcoI* was generated by GenScript as well as a 3' sequence element of ffLuc, flanked by *AgeI/XhoI*. (**3**) The partial ffLuc sequence was removed from pUC47-ffLuc by means of *NcoI/AgeI digestion.* (**4**) The four elements resulting from the digestions performed in 1-3 are ligated together to form SFG-T4luc. *Note: size of the blocks is not representative of the sizes of the individual elements.*

2.1.2 Production of New Vectors and Constructs using Restriction Enzyme Digestion

The production of the CAR constructs required DNA digestion with restriction enzymes. Additionally, restriction patterns were used to accurately verify plasmid inserts. Digestion was performed in the presence of buffers designed to optimize enzyme efficiency.

2.1.2.1 Materials, Reagents and Equipment

- Restriction enzymes — New England Biolabs (NEB)
- 10x Enzyme buffer — NEB
- 100x Bovine Serum Albumin (BSA) where required — NEB
- Nuclease Free H_2O — BioLine
- DNA Template
- Eppendorf Mastercycler Gradient PCR Machine — Eppendorf
- Ice

2.1.2.2 Protocol

1. A 20µL reaction mixture, as detailed below for a double digest, was produced. All components were kept at 4°C throughout
    a. XµL (0.5-1.0µg) DNA Template
    b. XµL Nuclease Free H_2O
    c. 2µL NEB Buffer
    d. 10-20U Enzyme 1
    e. 10-20U Enzyme 2
    f. 1µL 1 in 10 diluted BSA

    NOTE: in reactions requiring a single enzyme, the 20µL reaction volume was achieved using additional ultrapure water. For sequential digests, a 20µL reaction containing the first enzyme only was produced. The second enzyme (1.2µL) and buffer (3µL) were added after completion of the first incubation. When performing these sequential digests, the enzyme requiring the buffer containing a lower salt concentration was used in the first reaction. For very dilute DNA samples, 50µL reaction volumes were used, with the volume of individual components altered accordingly.

2. Reaction mixtures were incubated for one hour in a PCR machine at the temperature required for optimal enzyme activity. For sequential digests using enzymes with differing optimal temperatures, the reaction mixture was cooled on ice prior to incubation at the second temperature.
3. Once completed, an 18µL aliquot of each reaction was mixed with 3µL DNA loading buffer (*Buffers and solutions* paragraph 2.1.3.1) and separated by electrophoresis on an agarose gel (please refer to paragraph 2.1.3).

2.1.3 Isolation of DNA Fragments using Agarose Gel Electrophoresis

Separation of DNA fragments was achieved using agarose gel electrophoresis. The constant mass to charge ratio of DNA molecules means that separation is determined by fragment size. Migration rates are therefore influenced by the pore size of the gel, which in turn is determined by the agarose concentration (see Table 2-1). Consequently, careful selection of the percentage of agarose used ensured optimal resolution of the fragments of interest.

Table 2-1 Agarose concentrations required to achieve separation of specific DNA fragments

Agarose (% w/v)	Range of Separation (kb)
0.5	0.7-25
0.8	0.5-15
1.0	0.25-12
1.2	0.15-6
1.5	0.08-4

Adapted from Table 5-2, page 5.6 reference (490).

2.1.3.1 Materials, Reagents and Equipment

▪ Electrophoresis grade Agarose	MP Biomedicals
▪ TBE Buffer	(please see below)
▪ Ethidium Bromide	Sigma-Aldrich
▪ DNA Loading Buffer	(please see below)
▪ 1kb DNA Ladder	Invitrogen
▪ Gel Mould	Biorad
▪ Gel Comb	Biorad
▪ Balance	Mettler Toledo
▪ Gel Tank	Life Technologies
▪ Power Pack	Kingshill
▪ Microwave Oven	Proline
▪ UV Transilluminator	UVI Tech
▪ TV Zoom Lens	Avenir
▪ P90 Thermal Monochrome Printer	Mitsubishi

Buffers and solutions:

10x TBE = 108g Tris-base, 55g boric acid, 9.3g EDTA in 1L deionised water

6x DNA Loading Buffer = Distilled water, 40% (w/v) sucrose, 0.25% (w/v) bromophenol blue, 0.25% (w/v) xylene cyanol.

2.1.3.2 Protocol

NOTE: The protocol described below is for the production of a 1% 100mL agarose gel. The weight of agarose used and the volume of TBE into which it was dissolved differed depending upon the size and percentage of the gel required.

1. One gram of agarose was mixed with 100mL 1x TBE and heated in a microwave oven (with regular agitation) until completely dissolved.
2. After cooling under cold running water to 37°C, 0.30µg/mL ethidium bromide was added and the mixture swirled vigorously to ensure even distribution without the introduction of air bubbles.
3. The gel was poured into a pre-cast mould, a comb inserted and left to set at room temperature.

4. Prior to loading, samples were mixed 5:1 with 6x DNA loading buffer. In addition to the samples, a 1kb DNA ladder was loaded to allow the size of migrating DNA fragments to be estimated.
5. Once loaded, the gel was run at 5-8V/cm until sufficient migration (as visualized by the loading dye) had occurred.
6. The DNA was visualized with UV light at 154nm using a UV transilluminator. Images were taken using a TV zoom lens and thermal monochrome printer.

NOTE: In instances when the DNA was required for further manipulation, the level of UV exposure was minimized to reduce the risk of mutagenesis.

2.1.4 Retrieval of DNA from Agarose Gel

DNA fragments are isolated from agarose gel to enable their insertion into a viral vector. Isolation of the DNA relies its ability to bind the silica membrane of a purification column in the presence of chaotropic salt. The DNA is subsequently eluted following the replenishment of the hydration gell upon the addition of water.

2.1.4.1 Materials, Reagents and Equipment

- Wizard SV Gel and PCR CleanUp System — Promega
- Water Bath
- Eppendorf 5415R Microcentrifuge — Eppendorf
- 1.5mL Eppendorfs — Greiner Bio-One
- Vortex — Rotormixer
- Scalpel — Swann Morton Ltd
- Balance — Mettler Toledo
- UV Transilluminator — UVI Tech

Buffers and Solutions:

Membrane Binding Solution (MBS) = 4.5M guanidine isothiocyanate, 0.5M potassium acetate (pH 5.0)

Membrane Wash Solution (MWS) = 10mM potassium acetate (pH 5.0), 80% ethanol, 16.7µM EDTA

2.1.4.2 Protocol

1. The location of the required DNA fragment was visualised with UV light at 254nm using a UV transilluminator.
2. The required DNA band was excised from the gel using a sterile scalpel and placed into a nuclease-free 1.5mL Eppendorf tube.
3. The gel fragment was weighed and submerged in the required volume of membrane binding solution (MBS, v/w 1µL/1mg) and incubated at 54°C with frequent vortexing until the gel had completely melted.
4. The resulting mixture was added to the silica membrane within a purification column and centrifuged at 10.700g for one minute in a microcentrifuge.
5. The eluate was discarded and the column washed with 700µL membrane wash solution prior to centrifugation for one minute at 10,700g.
6. The eluate was discarded, the column washed with 500µL membrane wash solution and subsequently centrifuged for five minutes at 10,700g.
7. Following an additional dry centrifugation step, the DNA bound to the membrane was eluted by the addition of nuclease-free water and centrifugation at 10,7000g. A one-minute incubation step at room temperature was performed prior to centrifugation to ensure complete dissociation of the DNA from the membrane.

2.1.5 Calf Intestinal Alkaline Phosphatase Treatment

Calf Instestinal Alkaline Phosphatase (CIP) catalyzes the removal of 5´ phosphate groups from DNA, RNA, ribo- and deoxyribonucleoside triphosphates. Since CIP-treated fragments lack the 5´phosphoryl termini required by ligases, they cannot self-ligate. This property can be used to decrease the vector background in cloning strategies (490).

2.1.5.1 Materials, Reagents and Equipment

- CIP (10,000U/mL) NEB
- DNA template NEB
- Nuclease Free H_2O BioLine
- Ice
- Techne Dri-block DB2A Techne

2.1.5.2 Protocol

NOTE: All steps of the procedure (except for the incubations) were performed on ice

1. The CIP was diluted 1/30 in nuclease free H_2O to a final concentration of 0.3U/µL
2. For each 1µg of DNA template (from a previously performed restriction digest), 0.5U CIP were added.
3. The mixture was incubated at 37°C for 45 minutes.
4. Optional: CIP was incompletely inactivated by incubating the sample for 30 minutes at 65°C. Because CIP cannot be completely heat inactivated, further processing of the sample was required immediately.
5. The appropriate amount of 6x loading buffer was added and the sample was run on an agarose gel.

2.1.6 Fragment Insertion using DNA Ligation

New DNA fragments were inserted into a linearised vector backbone using a ligation reaction.

2.1.6.1 Materials, Reagents and Equipment

- T4 DNA Ligase — NEB
- 10x T4 DNA Ligase Buffer — NEB
- Nuclease-Free Water — Promega
- Eppendorf mastercycler Gradient PCR Machine — Eppendorf
- 0.5mL Eppendorfs — Greiner Bio-One

2.1.6.2 Protocol

1. A 20µL ligation mixture, as detailed below, was produced. The example given is representative of a three-piece ligation.
    a. Xµg DNA Backbone
    b. Xµg Fragment 1
    c. Xµg Fragment 2
    d. 2µL 10x DNA Ligase Buffer
    e. 2µL (4000 cohesive end units) DNA Ligase
    f. XµL Nuclease free water

NOTE: For reactions requiring ligation of fewer or more fragments, the volume of nuclease free water was altered to ensure a final reaction volume of 20µL.

2. The reaction was incubated overnight at 15°C in the Eppendorf mastercycler Gradient PCR Machine.

2.1.7 Analysis of DNA Concentration

The concentration of DNA was measured using the Nanodrop ND-1000 system. The Nanodrop is a full-spectrum (220-750nm) spectrophotometer that can assay 1µL samples. The sample is pipetted onto the end of a fibre optic cable (the receiving fibre). A second fibre optic cable (the source fibre) is then brought into contact with the liquid sample causing the liquid to bridge the gap between the fibre optic ends. The gap is controlled to both 1mm and 0.2mm paths. A pulsed xenon flash lamp provides the light source and a spectrometer utilizing a linear CCD array is used to analyse the light after passing through the sample.

2.1.7.1 Materials, Reagents and Equipment

- Nuclease Free H_2O — BioLine
- Elution Buffer — Qiagen
- Nanodrop ND-1000 — Thermo Scientific

2.1.7.2 Protocol

1. The Nanodrop is equilibrated using 1µL nuclease free H_2O.
2. Blank measurement is made using 1µL of elution buffer.
3. 1µL of DNA is added to the Nanodrop.
4. The DNA concentration is directly calculated by the Nanodrop software and given in ng/µL, using the measured absorbance and the Beer-Lambert equation.
    a. Absorbance $= -\log(\text{intensity}_{sample}/\text{intensity}_{blank})$
    b. The Beer-Lambert equation is used to correlate the calculated absorbance with concentration:

        $A = E * b * c$

        A = the absorbance represented in absorbance units

E = the wavelength-dependent molar absorptivity coefficient with units of litre/mol-cm

b = path length in cm

c = analyte concentration in moles/litre or molarity

2.1.8 Production of Chemically Competent *Escherichia Coli* TOP10F'

Competent *Escherichia Coli* (*E. Coli*) TOP10F' are required for the replenishment of plasmid stocks and selection of newly produced vectors.

2.1.8.1 Materials, Reagents and Equipment

- TOP10F' *E. Coli* — Invitrogen
- Agar — Fisher Scientific
- Luria-Broth (L.Broth) — Fisher Scientific
- 100% Ethanol (EtOH) — Fisher Scientific
- 0.3M Potassium Acetate (CH_3CO_2K) — Sigma Aldrich
- 1M Rubidium Chloride (RbCl) — Sigma Aldrich
- 0.1M Calcium Chloride ($CaCl_2$) — Sigma Aldrich
- 0.5M Manganese Chloride ($MnCl_2$) — Sigma Aldrich
- 0.2M Acetic Acid ($C_2H_4O_2$) — Sigma Aldrich
- 1M 3-(N-Morpholino)-propanesulfonic acid (MOPS) — Sigma Aldrich
- 0.75M Calcium Chloride ($CaCl_2$) — Sigma Aldrich
- Potassium Hydroxide (KOH) — Sigma Aldrich
- Distilled water
- Glycerol — Fisher Scientific
- Oven set at 37°C — GenLab Ltd
- Bunsen burner
- Sorvall RC 6+ centrifuge — Thermo Scientific
- 14mL snap-cap tubes — BD Pharmingen
- Excella E25 shake incubator — New Brunswick Scientific
- Spectrophotometer UVI mini 1240 — Shimadzu
- 0.22µM vacuum filtration system — TPP

- Corex tubes Kendro Laboratory Products
- Ice
- Dry ice

2.1.8.2 Protocol

NOTE: amounts mentioned are for 1 picked colony

1. Frozen TOP10F' *E. Coli* were streaked onto an agar plate in a zig-zag pattern and incubated overnight at 37°C.
2. A single colony was picked and inoculated in 5mL L.Broth and cultured overnight at 37°C at 225rpm (Excella E25 shake incubator).
3. The 5mL L.Broth culture was transferred to 100mL L.Broth and cultured at 37°C, 225rpm for 1-2 hours. The bacteria were allowed to grow to OD_{550} = 0.4-0.6 (preferably around 0.48)
4. Cells were chilled on ice for 5 minutes.
5. Cells were pelleted by centrifugation at 6000g for 5min at 4°C in pre-chilled corex tubes.
6. The pelleted cells were resuspended in 40mL TbfI buffer:

a. *TbfI buffer:*

    - 30mM potassium acetate
    - 100mM rubidium chloride
    - 10mM calcium chloride
    - 50mM manganese chloride
        - pH was adjusted to 5.8 using 0.2M acetic acid
        - Volume was made up to 85mL using distilled water
    - Buffer was filtered sterile prior to addition of 15mL sterile glycerol

7. Cells were chilled on ice for 15 minutes.
8. Cells were pelleted at 6000g for 5min at 4°C.
9. Cells were resuspended in 4mL TbFII buffer

b. *TbfII buffer:*

- 10mM MOPS
- 75mM calcium chloride
- 10mM rubidium chloride
    - pH was adjusted to 6.5 using KOH
    - Volume was made up to 85mL using distilled water
- Buffer was filtered sterile prior to addition of 15mL sterile glycerol

10. Cells were left on ice for 15 minutes.
11. Aliquots of 100µL were snap frozen on dry ice and stored at -80°C until further use.

2.1.9 Transformation of *Escherichia Coli* TOP10F'

Replenishment of plasmid stocks and selection of newly produced vectors was achieved by introducing the plasmid into chemically competent *E. Coli.* All steps followed common microbiological practice, using a Bunsen burner to provide the sterile vacuum.

2.1.9.1 Materials, Reagents and Equipment

- TOP10F' *E. Coli*
- Plasmid DNA
- Agar Plates
- Super Optimal broth with Catabolite repression (SOC) media — Invitrogen
- Glucose — BDH
- Water Bath
- Ice
- Oven set at 37°C — Genlab Ltd
- Bunsen Burner
- Excella E-25 shake incubator
- Eppendorf 5415R refrigerated Microcentrifuge — Eppendorf
- Glass spreaders
- 100% Ethanol — Fisher Scientific

Buffers and solutions:

1L SOC Media = 20g bacto tryptone, 5g bacto yeast extract, 10mM Sodium Chloride (NaCl), 2.5mM potassium Chloride (KCl), 10mM Magnesium Chloride ($MgCl_2$), 10mM Magnesium Sulphate ($MgSO_4$), 20mM Glucose.

2.1.9.2 Protocol

1. One vial of *E. Coli* was thawed on ice.
2. 1µg Plasmid DNA was added to the *E. Coli* and incubated for 30 minutes on ice.
3. Bacteria were heat shocked at 42°C for 90 seconds and subsequently incubated on ice for 5 minutes.
4. Following addition of 300µL SOC media, samples were shaken at 160rpm for one hour at 37°C.
5. Simultaneously, agar plates containing the required antibiotic were dried in an oven at 37°C (The antibiotic required was dependent upon the plasmid being amplified).
6. The *E. Coli* were subsequently centrifuged at 15,700g for 3 minutes and 150µL of supernatant removed.
7. Once resuspended in the remaining 150µL SOC media, bacteria were spread onto the pre-dried plate and incubated either at 37°C overnight, or at room temperature for 72 hours.

2.1.10 Production of Agar Plates

2.1.10.1 Materials, Reagents and Equipment

- LB-Agar — Novagen
- Ampicillin — Sigma
- Kanamycin — Sigma
- Microwave Oven
- Non-tissue culture treated 10cm petri-dishes — Falcon
- Bunsen burner

Buffers and solutions:

Agar = 5g yeast extract, 10g peptone from casein, 10g NaCl in 1L deionised water

2.1.10.2 Protocol

1. 500mL agar was melted in a microwave oven for 20min at 40% maximum power to obtain a molten solution
2. After cooling down, a selective antibiotic (50mg ampicillin or 50µg kanamycin) was added and mixed thoroughly
3. The solution was distributed evenly over 20 petri dishes and left to solidify at room temperature.
4. Petri dishes were stored at 4°C

2.1.11 Selection of Bacterial Clones

2.1.11.1 Materials, Reagents and Equipment

- L-Broth
- Antibiotic of choice
- 14mL Polystyrene round-bottom tubes
- 20µL pipette tips Star Lab
- Excella E-25 shake incubator

Buffers and solutions:

L-broth: 10g tryptone, 5g yeast extract, 0.5g NaCl

2.1.11.2 Protocol

1. 3mL of L-broth, containing 150ng - 150µg of the selected antibiotic was aliquotted into 14mL round-bottom tubes.
2. Single bacterial colonies were selected using a pipette tip and submerged in the L-broth.
3. The tubes were shaken at 160rpm for 16 hours at 37°C prior to being centrifuged at 1500g for 10 minutes to pellet the bacteria. The supernatant was discarded and the pellet subjected to plasmid isolation.

2.1.12 Isolation of Plasmid DNA – Miniprep

Retrieval of plasmid DNA was achieved using a QIAprep Spin Miniprep kit. This procedure is based on the rapid alkaline lysis procedure reported by Birnboim and Doly (491), in which bacterial lysis was achieved using sodium dodecyl sulphate (SDS) in the presence of 200mM sodium hydroxide (NaOH). The resulting denaturation of proteins and chromosomal DNA caused by the strongly alkaline environment ensured their co-precipitation with SDS upon neutralization of the solution and the conversion to high salt conditions by the addition of potassium acetate. The supercoiled conformation of the plasmid DNA prevented separation of the DNA strands, thereby ensuring that it remained in solution. Contaminating RNA was removed by both the addition of RNAse A to the intial resuspension buffer and precipitation in the high salt environment of the neutralization buffer. Removal of any remaining impurities was achieved by running the aqueous phase through a column containing a silica membrane. The presence of the chaotropic salt, guanidine hydrochloride, in the neutralization buffer induced dehydration of the plasmid DNA, allowing it to bind strongly to the silica membrane (492), whilst other contaminating factors were removed in the flow-through. Following to further wash steps with chaotropic salt and ethanol-containing buffers, the purified plasmid DNA was eluted from the column using a low salt buffer.

2.1.12.1 Materials, Reagents and Equipment

- QIAprep spin Miniprep kit — Qiagen
- Pelleted TOP10F' *E. Coli*
- 1.5mL Eppendorfs
- Eppendorf 5415R refrigerated Microcentrifuge — Eppendorf

Buffers and solutions:

Buffer P1 = 50mM Tris-Cl, 1mM EDTA, 100µg/mL RNAse A

Buffer P2 = 200mM NaOH, 1% SDS

Buffer EB = 10mM Tris-Cl (pH 8.5)

NOTE: Qiagen does not publish the full composition of the neutralizing N3 buffer, buffer PB or buffer PE. Buffer N3 is known to contain guanidine hydrochloride (as the source of chaotropic salt) and acetic acid (probably in the form of potassium acetate)

to neutralize the alkaline environment caused by the NaOH in buffer P2. Buffer PB also contains guanidine hydrochloride, along with isopropanol. No details regarding the composition of buffer PE have been released.

2.1.12.2 Protocol

1. Pelleted bacteria were resuspened in 250µL buffer P1.
2. An equal volume of buffer P2 was added and the sample was gently inverted approximately 10 times to ensure complete mixing.
3. After a five-minute incubation at room temperature, 350µL buffer N3 was added to each sample. Complete mixing was achieved through gentle inversion.
4. Centrifugation at 15,700g pelleted the white precipitate in each sample.
5. The aqueous phase was carefully transferred to a QIAprep spin column and the white precipitate discarded.
6. Following centrifugation at 15,700g, each column was washed with 500µL buffer PB and centrifuged at 15,700g, before discarding the eluate.
7. Each column was washed with 750µL buffer PE and centrifuged at 15,700g and the eluate was again discarded.
8. After an additional centrifugation at 15,700g to remove any residual ethanol, the DNA was eluted in 50µL buffer EB through centrifugation at 15,700g.
9. The concentration of the isolated DNA was determined and stored at -20°C.

2.1.13 Isolation of Plasmid DNA – Maxiprep

Maxipreps were used for the production of higher concentrated DNA preparations As with minipreps, the *E. Coli* were lysed under strong alkaline conditions, with proteins and chromosomal DNA removed by precipitation upon neutralization and conversion to a high salt environment. As before, RNA impurities were removed through the addition of RNAse A in the initial resuspension buffer. Once insoluble contaminants had been removed via filtration, the eluate (containing the plasmid DNA was subjected to anion-exchanged chromatography. Plasmid DNA is able to bind strongly to the positively charged diethylaminoethyl (DEAE) resin beads, until eluted using a high-salt containing buffer. Intermediate washes with buffers of increasing salt concentrations ensured the removal of remaining contaminants. Once eluted, the DNA was

precipitated and desalted using a series of alcohol washes before being dissolved in EB buffer.

2.1.13.1 Materials, Reagents and Equipment

- 500mL TOP10F' *E. Coli* containing plasmid of interest
- QIAgen Plasmid Maxi Kit — Qiagen
- 50mL Falcon tubes — SLS
- 1.5mL Eppendorfs
- Oak ridge polypropylene copolymer centrifuge tubes — Nalgene
- Sorvall RC +6 Centrifuge — Sorvall
- Vacuum filtration system 0.22µM PES membrane — TPP
- 70% Ethanol — Fisher Scientific
- Isopropanol — Fisher Scientific
- Excella E-25 shake incubator

Buffers and solutions:

Buffer P1 = 50mM Tris-Cl (pH 8.0), 10mM EDTA, 100µg/mL RNAse A, lyse blue (optional)

Buffer P2 = 200mM NaOH, 1% (w/v) SDS

Buffer P3 = 3M Potassium Acetate

Buffer QBT = 750mM NaCl, 50mM 3-(N-Morpholino)-propanesulfonic acid (MOPS), 15% (v/v) isopropanol, 0.15% (v/v) Triton X-100

Buffer QC = 1M NaCl, 50mM MOPS, 15% (v/v) isopropanol

Buffer QF = 1.25M NaCl, 50mM Tris-Cl (pH 8.5), 15% (v/v) isopropanol

2.1.13.2 Protocol

NOTE: The plasmids were treated as low-copy plasmids to ensure maximum possible yield.

Before starting:

i. The provided RNase A and Lyse Blue were added to buffer P1.
ii. Buffer P2 was checked for SDS precipitation due to low storage temperatures. If necessary, the SDS was dissolved by warming to 37°C.
iii. Buffer P3 was pre-chilled to 4°C.

1. A single colony was picked from a freshly streaked selective plate and inoculated of a starter culture of 2-5mL L-Broth media containing the appropriate selective antibiotic.
2. The culture was incubated for 8 hours at 37°C with vigorous shaking (300rpm).
3. The started culture was diluted 1/1000 into selective L-Broth medium. For low-copy plasmids, 500µL of starter culture was added to 500mL L-Broth medium and incubated overnight at 37°C with vigorous shaking (300rpm).
4. The bacteria were pelleted through centrifugation at 3500g for 10 minutes at 4°C.
5. The bacterial cell pellet was resuspended vigorously in 10mL buffer P1 until no cell clumps remained.
6. An equal volume of buffer P2 was added, and the sealed tube inverted 4-6 times and incubated at room temperature for 5 minutes. Complete lysis of the bacterial pellet is confirmed by the cell suspension turning blue.
7. An equal volume of buffer P3 is added and the suspension was mixed vigorously by inverting the sealed tube 4-6 times and incubated on ice for 20 minutes. Complete protein precipitation is confirmed by the suspension becoming colourless.
8. The suspension is filtered through a 0.22µM PES membrane vacuum filter.
9. During filtration of the suspension, a QIAgen-tip 500 was equilibrated with 10mL buffer QBT. The column was allowed to empty by gravity flow.
10. The eluate from step 8 was added to the QIAgen-tip and allowed to enter the resin by gravity flow.
11. The tip was washed twice using 30mL buffer QC before the plasmid was eluted into a polypropylene copolymer centrifuge tube using 15mL buffer QF.

12. The DNA was precipitated by adding 10.5mL isopropanol and pelleted by centrifugation for 30 minutes at 15,000g and 4°C.
13. The pellet was washed with 5mL 70% ethanol to remove the salt and the DNA was again pelleted by centrifugation at 15,000g for 10 minutes.
14. After removal of the supernatant the DNA pellet was air-dried at room temperature for 15 minutes and resuspended in 200µL of EB buffer.
15. The concentration of the DNA was determined using the Nanodrop ND-1000 and was stored at -20°C.

2.1.14 Analysis of DNA Sequences

The ability to quickly and precisely determine DNA sequences has been an invaluable tool to verify the correct production of new constructs and investigate successful insertion of sequences into plasmids and viral vectors. The technique used was based on the chain termination method originally described by Sanger *et al.* (493) and utilised Big Dye Terminator chemistry. In this method, the dideoxynucleotides (ddNTP) responsible for chain termination are fluorescently labelled with a different fluorophore for each base, thereby enabling their incorporation into DNA fragments that can easily be distinguished. Sequencing of the DNA was achieved using capillary zone electrophoresis and was kindly performed by Cancer Research UK (London Research Institute, Lincoln's Inn Fields), using an Applied Biosystems 3730 DNA Analyzer.

2.1.14.1 Materials, Reagents and Equipment

- Primers (see Appendix 1)
- DNA Template
- Big Dye Terminator (BDT) reaction mix — Applied Biosystems
- Distilled water
- Eppendorf Mastercycler Gradient PCR Machine — Eppendorf
- DyeEx 2.0 spin kit — Qiagen
- PCR tubes — Bio-Rad

2.1.14.2 Protocol

1. A reaction mixture as detailed below was produced:
    a. 8µL BDT
    b. 1.5µL Template DNA
    c. 1µL (3.2pmol) Primer
    d. 9.5µL dH_2O
2. Samples were incubated using the following PCR program:

a. Denaturation	96°C	1 minute	
b. Denaturation	96°C	10 seconds *	
c. Annealing	58°C	5 seconds *	* = 25 cycles
d. Elongation	60°C	4 minutes *	
e. Hold	6°C	HOLD	

3. Excess unbound nucleotides were removed by running the reaction mixture through a size exclusion column (DyeEx 2.0 spin kit) according to the manufacturer's protocol.
4. The resulting eluate was sent for sequence analysis via capillary zone electrophoresis (CRUK London Research Institute, Lincoln's Inn Fields).
5. Obtained sequences were analysed using 4Peaks 1.7.1 and Serial Cloner 2.5.0, allowing for rapid identification of restriction sites and open reading frames.

2.2 Cell Culture

All cells were incubated at 37°C, 97% O_2 / 5% CO_2

2.2.1 Media and Common Solutions

2.2.1.1 Media

D10	=	500mL Dulbecco's Modified Eagle Medium (DMEM) + 4.5g/L glucose	Lonza
		50mL Foetal Bovine Serum	Sigma
		200mM GlutaMAX	Gibco
		50,000U Penicillin	Lonza
		50mg Streptomycin	Lonza
		125µg Amphotericin B	Lonza

D5	=	500mL Dulbecco's Modified Eagle Medium (DMEM) + 4.5g/L glucose	
		25mL Foetal Bovine Serum	
		200mM GlutaMAX	
		50,000U Penicillin	
		50mg Streptomycin	
		125µg Amphotericin B	

R10	=	500mL Roswell Park Memorial Institute (RPMI) 1640 Medium without L-Glutamine	
		50mL Human Male AB Serum	Sigma-Aldrich
		200mM GlutaMAX	
		50,000U Penicillin	
		50mg Streptomycin	
		125µg Amphotericin B	

mR10 = 500mL Roswell Park Memorial Institute (RPMI) 1640 Medium without L-Glutamine
50mL Foetal Bovine Serum
200mM GlutaMAX
50,000U Penicillin
50mg Streptomycin — Sigma-Aldrich
125µg Amphotericin B
50µM β2-mercapto-ethanol

2.2.1.2 Common Solutions

Trypsin = 0.25% Trypsin-EDTA — Gibco

CDB = Cell Dissociation Buffer — Invitrogen Life Tech
Enzyme free aqueous formulation of salts, chelating agents, and cell-conditioning agents in either Ca^{2+} and Mg^{2+} free PBS

PBS = Phosphate Buffered Saline — Biochrom AG

2.2.2 Primary Cells and Cell Lines

Primary cell lines were used for *in vitro* examination of the targetability of human and mouse $ErbB^{+}$ healthy tissue by $T4^{+}$ T-cells.

2.2.2.1 Materials, Reagents and Equipment

- D10 media — Please refer to paragraph 2.2.1.1
- D5 media — Please refer to paragraph 2.2.1.1
- R10 media — Please refer to paragraph 2.2.1.1
- Endothelial Cell Basal Medium MV — PromoCell
- Endothelial Cell Growth Medium MV2 SupplementMix — PromoCell
- Myocyte Basal Medium — PromoCell
- Myocyte Growth Medium SupplementMix — PromoCell

- Mouse Endothelial Cell Medium — CellBiologics
- Mouse Endothelial Cell Medium Supplement Kit — CellBiologics
- Gelatin-based coating solution — CellBiologics
- Interleukin-2 (IL-2, Aldesleukin) (rhIL-2) — Novartis
- Recombinant human Interleukin-4 (rhIL-4) — Gentaur
- Tetracycline — Calbiochem
- Puromycin — Merck
- 6-well tissue culture-treated plates — Greiner Bio-one
- T25 tissue culture flasks — NUNC
- T75 tissue culture flasks — NUNC
- T175 tissue culture flasks — NUNC

2.2.2.2 Human T-cells

Human T-cells were cultured in R10 media supplemented with 100U/mL IL-2 (or 30ng/mL hIL-4 for $T4^+$ T-cells). Fresh media and cytokine were supplied when required.

2.2.2.3 Primary Cell (Lines)

Primary Human Pulmonary Microvascular Endothelial Cells (HPMEC) and Human Cardiac Myocytes (HCM) were obtained from Promocell (Heidelberg, Germany). Primary Balb/C mouse Pulmonary Microvascular Endothelial Cells (MPMEC) were obtained from CellBiologics (Chicago, Illinois, USA).

The HPMEC originate from the capillary walls and were cyropreserved at passage 2. The cells were cultured at a density of 10,000-20,000 cells/cm^2 in the Endothelial Cell Growth Medium MV2 (494). The HCM are derived from normal human ventricular tissue of the adult heart. The cells were cyropreserved at passage 2 (495). The cells were cultured at a density of 10,000-15,000 cells/cm^2 in the Myocyte Growth Medium. The MPMEC are isolated from tissue of pathogen-free laboratory mice. Cells are cultured in T25 flasks pre-coated with a gelatin-based coating solution for 30 minutes. Medium was changed when cell density >60%, cells were passaged 1:2 when cells reached 100% confluency (496).

2.2.2.4 Tumour Cell Lines

Immortalized tumour cell lines were acquired from multiple sources (see Table 2-2). All tumour cell lines were grown as serially diluted cultures in D10 media and monolayers were passaged when appropriate. The HN3luc cell line was produced prior to the commencement of this PhD by transducing HNSCC HN3 cells with the pBabe puro retroviral vector (497)(please refer to paragraph 2.2.3.2) containing the gene for firefly luciferase (ffLuc). The cell line PLP was produced prior to the commencement of this PhD by the transduction of the prostate cancer cell line PC3-LN3 with the pBabe puro retroviral vector containing prostate-specific membrane antigen (PSMA). In order to ensure retention of the luciferase or PSMA gene, the cell lines were periodically grown in the presence of 1.5mg/mL Puromycin.

Table 2-2 Sources of acquired tumour cell lines

Tumour Cell Line	Origin	Source
HN3 (HN3luc)	Human (HNSCC)	Dr Sue Eccles, Institute for Cancer Research, Sutton, UK
SKOV3luc	Human (Ovarian)	Caliper Lifesciences
PC3-LN3 (PLP)	Human (Prostate)	Dr Sue Eccles, Institute for Cancer Research, Sutton, UK
MDA-MB-435	Human (Breast)	Cancer Research UK
B7E3	Mouse (HNSCC)	Dr Carter van Waes, National Institute of Health, Bethesda, Maryland, USA

2.2.2.5 Retroviral Packaging Cell Lines

The majority of gene transfer undertaken during this PhD was achieved using engineered retroviruses. The genome of every retrovirus (a dimer of two RNA copies) encodes at least four specific genes (498), all of which are crucial for completion of the retroviral life cycle (see Figure 2-4). The binding of a mature retroviral particle to a target cell is mediated by interactions between glycoproteins expressed in the viral envelope and a specific receptor or molecule on the surface of the host cell. These glycoproteins are encoded by the retroviral *env* gene and are therefore responsible for the tropism of the viruses (i.e. the target cells with which it can interact) (498). Following fusion of the retroviral envelope with the host cell membrane, the RNA

genome is extruded into the cytoplasm of the host cell, where it is converted to a double stranded DNA copy by reverse transcriptase. This is subsequently integrated into the host cell genome by an integrase enzyme, to give a 'provirus' (498, 499). Both of these enzymes are encoded by the *pol* gene in the retroviral genome and are contained within the packaged virus, before being released into the host cell cytoplasm upon viral fusion. The transcription and translation of the viral genome by the host cell RNA polymerase results in production of the proteins encoded by the *gag* gene, as well as the production of new reverse transcriptase and integrase enzymes. Although expressed as a single polypeptide until the late stages of viral budding, the *gag* gene codes for a number of separate proteins. Taking the Moloney murine leukaemia virus (MoMLV) as an example, the matrix (MA, p15), p12, capsid (CA, p30) and nucleocapsid (NC, p10) structural proteins are all present within the *gag* polypeptide (498). The N-terminal end of the polypeptide (the N-terminus of the MA protein) is myristylated, thus anchoring it in the host cell membrane and providing a focal point at which a new viral particle can be formed. Indeed, inhibition of myristylation can interfere with viral assembly (500). At the C-terminal end of the *gag*-encoded polypeptide, the NC protein interacts with the viral genome an is responsible for ensuring its packaging into the new retroviral particle (501). The reverse transcriptase and integrase enzymes are incorporated into the new viral particle, along with a viral protease, which is the product of the *pro* gene found between the *gag* and the *pol* genes. During and following budding this protease is responsible for cleaving the *gag*-encoded polypeptide into its four constituent proteins. The importance of this polypeptide processing is highlighted by the fact that mutations in the cleavage site between the p12 and CA proteins are sufficient to inhibit the formation of infectious MoMLV viral particles (502). This cleavage event is part of the maturation process, during which retroviruses gain the ability to infect target cells and begin another round of replication.

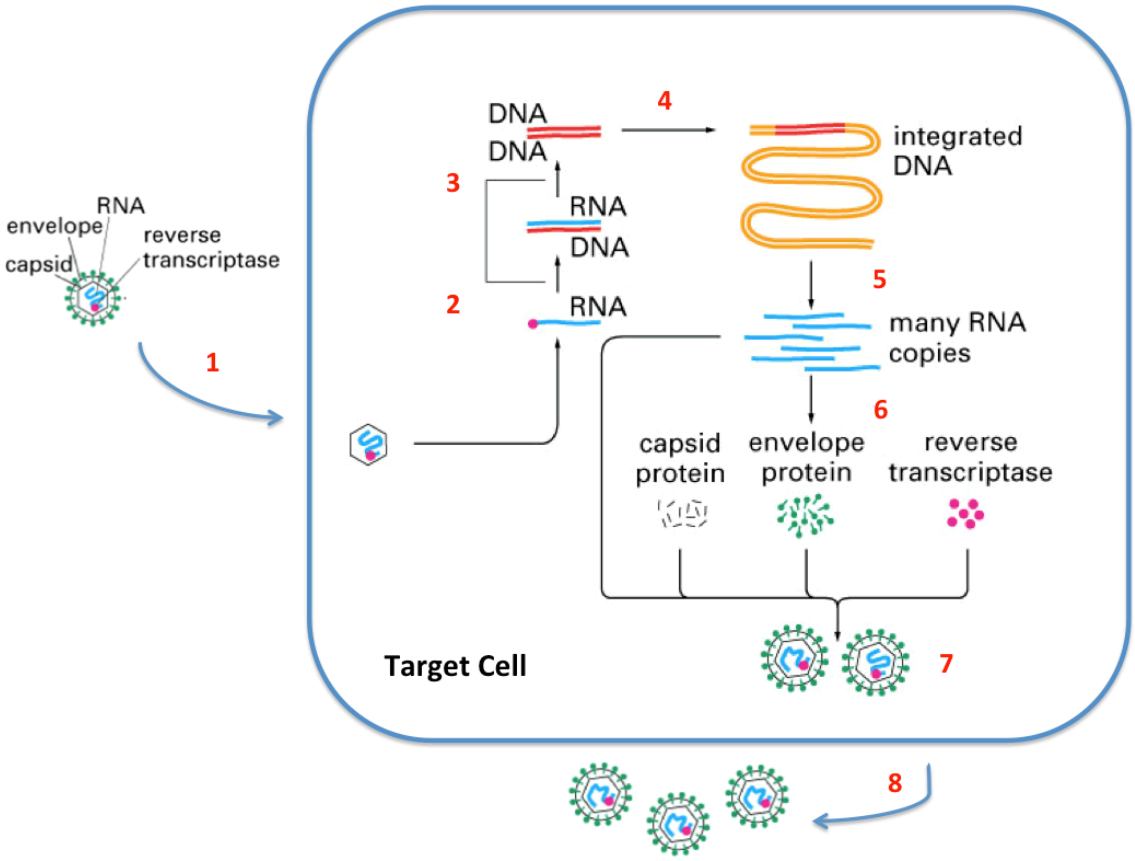

Figure 2-4 Retroviral Life Cycle

Image is adapted from Figure 6-39, Essential Cell Biology, 3rd Edition (503). Following fusion of the viral particle with the target cell (step 1), the envelope and capsid are disassembled, releasing the viral genome and proteins into the cytoplasm. The reverse transcriptase from the disassembled viral particle binds to a transfer RNA (tRNA) primer bound the LTR at the 5' end of the viral genome and synthesises a complementary DNA strand (step 2). The degradation of the RNA strand by the RNase H subunit of the reverse transcriptase enzyme enables synthesis of a second DNA strand (step 3). The double stranded DNA (dsDNA) is integrated into the host genome by the viral integrase enzyme (step 4). Amplification of the viral genome by the host RNA polymerase produces large quantities of the viral RNA (step 5). Following export from the nucleus, the majority of this is transcribed to give the *gag*, *pol*, and *env* proteins (step 6). These proteins, along with two copies of untranslated viral RNA are incorporated into a new viral particle (step 7), which subsequently buds from the target cell (step 8).

The ability of retroviruses to integrate their genome into that of a host cell provides an attractive way of achieving stable expression of a transgene within a specific target cell population. In the majority of cases, however, the continued replication of the virus following infection of the target cell population is undesirable. One way of preventing the production of so-called replication-competent retrovirus (RCR) within the target cell is to replace the *gag, pro, pol* and *env* genes with that of the transgene of interest. However, as detailed above, the proteins encoded by these four genes are essential for the production and function of viable virions. The use of retroviral packaging cell lines offers a way of producing viable viral particles that are unable to replicate following infection of the target cell, and of the required proteins are available for viral

assembly. The retroviral genomic sequence (containing the desired gene) is subsequently packaged into these viruses, which are then capable of infecting the target cell of choice. However, as these viruses do not contain any of the genes required for the formation of fresh viral particles, further replication is prevented. In order to minimize the risk of producing RCR, the *gag-pol* and *env* genes are expressed on separate plasmids within the packaging cells. Consequently, three separate recombination events would need to occur before all of these genes could be expressed *in cis*. The *pol* gene is always expressed on the same plasmid as *gag* due to the fact that the *gag-pro-pol* genes are transcribed as a single mRNA transcript. The presence of a stop codon at the end of the *gag* coding sequence means that, in 95% of cases, translation results in expression of the *gag* polypeptide alone. Occasionally, however, translational readthrough (caused by the misreading of the stop codon) results in the production of a *gag-pro-pol* polypeptide (504).

Two different types of retroviral packaging cell lines were used throughout this PhD, depending on the required type of transfection.

2.2.2.5.1 H29D

The H29D retroviral packaging cell line (293GPG in (505)) is based on the human embryonic kidney adenoviral 5-transformed cell line (HEK293, ref (506)). This packaging cell line expresses the MoMLV *gag-pol* genes under the control of the cytomegalovirus (CMV) immediately early (IE)(505). Expression of the vesicular stomatitis virus-G (VSV-G) *env* proteins results in the production of viral particles displaying a brad tropism ('pantropic'). As constitutive expression of the VSV-G envelope protein is toxic, controlled expression was achieved by placing the VSV-G coding sequence under the control of a tetracycline-repressed promoter (505). Originally described by Gossen and Bujard (507), activation of transcription from this promoter is depedent upon the binding of a tetracycline-transactivator (tTa) molecule. In the presence of tetracycline, however, the binding of the tTa molecule to the promoter is inhibited and thereby prevents subsequent gene expression. Consequently, to prevent constitutive expression of the VSV-G *env* protein, these cells were maintained in D10 media supplemented with 2µg/mL tetracycline. Fresh media and tetracycline were provided every three days and the cells were passaged when

confluent. As detailed in paragraph 2.2.5.2, removal of the tetracycline was required for the production of VSV-pseudotyped virus and the toxicity of this envelope protein meant that fresh H29D transductions were required for each preparation of fresh virus.

2.2.2.5.2 PG13

The PG13 retroviral packaging cell line is derived from the NIH 3T3 murine fibroblast cell line (508). As with H29D cell, PG13 cells express the MoMLV *gag-pol* genes. In contrast, however, PG13 viral particles are pseudotyped with the gibbon-ape leukaemia virus (GaLV) envelope protein. As with the VSV-G psuedotyped virus, the PG13 GaLV pseudotyped viral particles are capable of infecting human cells. However, as the GaLV is not toxic to the PG13 cells, stably expressing clones can be produced. The PG13 packaging cells were grown in D10 media in serially diluted cultures and were passaged when confluent.

2.2.3 Retroviral Vectors

Retroviral vectors constitute the backbone of the virus an tend to include necessary elements, such as the promoter regions required for transcription of the inserted gene(s) and the packaging signal (Ψ) required for packaging of the mRNA transcript into new viral particles. Two different retroviral vectors were used during this study.

2.2.3.1 SFG

The SFG retroviral vector is based on the MFG vector (509), in which gene expression is driven by the MoMLV long terminal repeats (LTRs). The presence of the MoMLV Ψ packaging signal ensures efficient packaging of the RNA into the virus. The presence of the splice donor and splice acceptor sites allow the production of the subgenomic RNA transcripts usually required for the translation of the *env* gene (504). The gene of interest is inserted at a naturally occurring *NcoI* site, ensuring that its start codon is in the precise location previously occupied by the deleted *env* gene. This vector does not contain a eukaryotic cell-compatible selectable marker gene. It does contain an ampicillin resistance gene for selection following transformation of competent bacteria.

2.2.3.2 pBabe puro

The pBabe puro retroviral vector uses the LTRs of the murine leukaemia virus (MLV) to drive transcription of the transgene. An improved vector, as described by Zhao *et al*. (510), was used in which a constitutive transport element (CTE) from the Mason-Pfizer monkey virus (MPMV) is included to increase titre, by increasing nuclear export of the RNA. This vector also has an improved safety profile as the partial *gag* gene in the parental vector has been removed to reduce potential areas of homology that may favour recombination. Prior to the commencement of this PhD, the firefly luciferase (ffLuc) was cloned into pBabe puro using a *BamHI, BglII* digest from the commercially available pGL3-Basic Vector (Promega). Antibiotic selection of pBabe puro transduced cells is possible due to the presence of the puromycin resistance gene.

2.2.4 PBMC Isolation and Activation

Peripheral blood mononuclear cells (PBMCs) were isolated from healthy donor or patient blood samples using Ficoll-Paque gradient. Recruitment of healthy volunteer donors for this purpose was approved by the Guy's Hospital Research Ethics Committee (09/H0804/92; Use of Donor Blood Samples for Pre-Clinical Development of Active and Passive Immunotherapy for Cancer). Recruitment of patient donors was approved by the Guy's Hospital Research Ethics Committee (09/H0707/086; Generation of clinical grade T-cells for adoptive cell therapy)

2.2.4.1 Materials, Reagents and Equipment

- Fresh Blood
- Citrate-Dextrose solution (ACD) — Sigma
- 50mL Syringe — BD Biosciences
- 21G Butterfly Needle — Greiner Bio-One
- 50mL Falcon tubes — SLS
- Ficoll-Paque Plus — GE Healthcare
- Eppendorf 5804 Centrifuge — Eppendorf
- Pasteur Pipettes — SLS
- Phytohaemagglutinin/Leucoagglutinin (L-PHA) — Sigma-Aldrich
- Anti-CD3/Anti-CD28 Dynabeads — Invitrogen
- R10 Medium

2.2.4.2 Protocol

Note: All steps of the procedure and all reagents used are at room temperature for optimal cell recovery.

1. 15mL Ficoll-Paque was aliquotted into two separate 50mL Falcon tubes.
2. Fresh Blood (25mL) (anticoagulated with 1x citrate-dextrose solution) was slowly layered onto the Ficoll-Paque and were centrifuged at 1150g for 25 minutes (acceleration = 0, deceleration = 0).
3. The PBMC layer, present at the interface between the Ficoll-Paque and the plasma, was transferred into fresh 50mL Falcon tubes using a Pasteur pipette and diluted to a final volume of 50mL in pre-warmed PBS and centrifuged for 15 minutes at 550g.
4. The cell pellet was re-suspended in 50mL pre-warmed PBS and centrifuged for 10 minutes at 400g.
5. Following aspiration of the supernatant, the cell pellet was resuspended in 10mL R10 media and cells were counted.
6. Cells were resuspended in R10 media at a concentration of 3 x 10^6 cells/mL and activated with 5µg/mL phytohaemagglutinin (PHA) or with anti-CD3, anti-CD28 paramagnetic Dynabeads at a 1:1 cell:bead ratio.

2.2.5 Production of retroviral packaging cell lines

For the transduction of human T-cells stable PG13-retroviral packaging cell lines were produced using H29D viral supernatant as an intermediate for PG13 transduction.

2.2.5.1 Materials, Reagents and Equipment

- CalPhos mammalian transfection kit — CloneTech
- Vortex
- Polyethylenimine (PEI) — Sigma-Aldrich
- Plasmid DNA
- H29D cells
- PG13 cells
- H29D retroviral supernatant

Components of the CalPhos Calcium Phosphate transfection kit:

- 2M Calcium Solution ($CaCl_2$)
- 2x HEPES-buffered saline (HBS)
- Sterile H_2O

2.2.5.2 Calcium-Phosphate transfection (H29D)

Preparation of H29D cells

1. H29D cells were transduced in 6-well culture plates.
2. Cells were split at least 2 days prior to transfection day so they would reach 80-90% confluence on the day of transfection in 3mL D10 media supplemented with tetracycline.
3. The tetracycline was removed from the H29D cells a minimum of 2 hours prior to transfection by replacing the tetracycline-containing D10 with fresh D10 only.

Preparation of Transfection Mixture

1. Solution A was prepared and left to incubate at room temperature for 5 minutes;
   Solution A:
   - 12.4µL 2M Calcium Solution ($CaCl_2$)
   - 1-3µg retroviral vector
   - Sterile H_2O to a final volume of 100µL
2. Solution A was added dropwise to 100µL 2X HBS whilst vortexing.
3. The mixture was incubated at room temperature for 20 minutes to ensure the formation of precipitate, before being added dropwise to the target cells.
4. After gentle rocking ensured complete mixing of the transfection mixture, the cells were incubated for 24 hours after which the media was replaced.
5. Supernatants were harvested daily from day 3-7 post transfection and directly used for infection of target cells (PG13).

2.2.5.3 PEI-mediated transfection (H29D)

1. H29D packaging cell lines were prepared as described in paragraph 2.2.5.2.
2. Transfection mixture was prepared and left to incubate at room temperature for 20 minutes.
    - 400µL serum free DMEM
    - 5µg plasmid DNA
    - 1µl 1mM PEI
3. Transfection mixture was dropwise added to the target cells.
4. The cells were incubated for 3-4 hours after which the media was replaced with fresh D10 media.
5. Media was again refreshed 24 hours prior to the (first) harvest of retroviral supernatant.
6. Supernatants were harvested daily from day 3-7 post transfection and directly used for target cell infection (PG13).

2.2.5.4 PG13 Transduction

1. The media was removed from empty PG13 packaging cells and replaced with 3mL H29D supernatant containing the VSV-pseudotyped virions.
2. 8µg/mL polybrene was added and mixed thoroughly to facilitate retroviral uptake.
3. The PG13 were subsequently incubated for 72 hours prior to analysis for transgene expression using flow cytometry.
4. PG13 population in which >90% of the cells were expressing the virus of interest were used as stable packaging cell lines.

2.2.6 Production of RetroNectin coated plates/bags

In order to improve T-cell transduction rates, the plates used were pre-treated with RetroNectin (RN). RetroNectin is a fragment of the extracellular matrix protein fibronectin that binds the target T-cell through a CS-1 domain and a cell-binding domain (CBD), which interacts with the VLA-4 and VLA-5 integrin receptors respectively. Attachment of the virus to the heparin binding domain present in RN between the CS-1 and CBD causes co-localisation of the target cell and the virus, thus greatly improving gene transfer efficiency (511, 512). Amounts less than 20 x 10^6 T-cells were transduced in 6-well plates; quantities larger than 20 x 10^6 T-cells were

transduced in 197-adherent culture (AC) VueLife fluorinated ethylene propylene (FEP) bags.

2.2.6.1 Materials, Reagents and Equipment

- RetroNectin — TaKaRa
- Non-tissue culture treated 6-well plates — Falcon
- 197-AC VueLife FEP bags — American Fluoroseal Corporation
- PBS
- Pasteur pipettes
- 50mL syringe

2.2.6.2 Protocol – 6 well plates

1. 200µg of RN was resuspended in 12mL PBS/plate
2. 2mL of the resulting solution was transferred using a Pasteur pipette into each well of a non-tissue culture treated 6-well plate, thereby giving coverage of approximately 3.5µg/cm^2
3. Plates were incubated for a minimum of 2 hours at room temperature or 24 hours at 4°C prior to use.
4. When the plate was to be used, unbound RN was transferred to a new plate using a Pasteur pipette. Retronectin was used for a maximum of two transductions.

2.2.6.3 Protocol – 197-AC VueLife FEP Bags

1. One vial (2.5mg) of RN was diluted in 150mL PBS and transferred into a 197-AC VueLife FEP bag, using a 50mL syringe, to give coverage of approximately 6µg/cm^2.
2. The bag was incubated at 4°C overnight.
3. When the bag was to be used, the unbound RN was removed prior to retroviral supernatant and transferred into non-tissue culture plates or a 197-AC VueLife FEP bag.

2.2.7 Retroviral-Mediated Human T-cell Transduction

To introduce the CAR constructs into T-cells, they were subjected to retroviral-mediated transduction. This ensured integration of the inserted coding DNA into the host T-cell genome, thereby permitting stable CAR expression.

2.2.7.1 Materials, Reagents and Equipment

- Activated T-cells
- Retroviral packaging cell lines
- Centrifuge
- Retronectin-coated plate/bag
- Pasteur pipettes
- Interleukin-2 (Aldesleukin) Novartis

2.2.7.2 Protocol – 6 well plate

1. After the unbound RN had been transferred to a fresh plate using a Pasteur pipette, each well was coated with 3mL of retrovirus-containing supernatant from the desired packaging cell line.
2. Activated T-cells were counted using trypan-blue exclusion and 1 x 10^6 viable cells added to each well.
3. Each well was supplemented with 100U/mL of IL-2.
4. Plates were centrifuged for one hour at 50g, at room temperature.
5. Cells were subsequently incubated for 96 hours, after which the transduction rate was determined using flow cytometry.

2.2.7.3 Protocol – 197-AC VueLife FEP bag

1. The unbound retronectin was removed from the FEP bag and coated with 60mL of retrovirus-containing supernatant from the desired packaging cell line.
2. Activated T-cells were counted using trypan-blue exclusion and 20-40 x 10^6 viable cells were added.
3. The bag was supplemented with 100U/mL of IL-2.
4. Cells were incubated for 96 hours, after which the transduction rate was determined using flow cytometry.

2.2.8 Determination of the Anti-Tumour Potential of CAR$^+$ T-cells

In order to demonstrate the ability of CAR$^+$ T-cells to recognise and destroy ErbB-expressing targets, they were co-cultured with a variety of human and murine ErbB$^+$ tumour cell lines. Target recognition was monitored by measuring cytokine release, whilst anti-tumour activity was quantitated using an MTT (3-[4,5-dimethylthiazol-2-yl]-2,5- diphenyltetrazolium bromide; thiazolyl blue) assay (please refer to paragraph 2.2.9) and visualized with crystal violet staining (please refer to paragraph 2.2.10).

2.2.8.1 Materials, Reagents and Equipment

- Transduced T-cells
- Tumour cells
- R10 media
- Interleukin-2 (Aldesleukin)
- rhIL-4 Gentaur
- 24-well cell culture plate

2.2.8.2 Protocol

1. Tumour cells were seeded into a 24-well cell culture plate and allowed to reach confluence.
2. T-cells were counted using trypan-blue exclusion and re-suspended in R10 media at a concentration of 1 x 10^6 cells/mL and gently pipetted onto the surface of the confluent tumour monolayer.
3. After 24 hours of incubation, 500µL supernatant was removed for analysis of cytokine (IL-2 and IFNγ) secretion.
4. T-cells were supplied with fresh R10 media containing 100U/mL rhIL-2 or 30ng/mL IL-4 at 2-3 day intervals until the desired monolayer destruction was achieved.

2.2.9 Quantification of Tumour-Cell Destruction

Anti-tumour activity of CAR$^+$ T-cells was quantified using an MTT (3-[4,5-dimethylthiazol-2-yl]-2,5- diphenyltetrazolium bromide; thiazolyl blue) assay. MTT is a water soluble tetrazolium salt yielding a yellowing solution when prepared in media or salt solutions lacking phenol red. Mitochondrial dehydrogenases of viable cells cleave the tetrazolium ring in dissolved MTT, yielding purple formazan crystals which are

insoluble in aqueous solutions. The crystals are dissolved in acidified isopropanol. The resulting purple solution is detected optimally at a wavelength of 570nm using a spectrophotometer. Dead cells do not cause this change. An increase or decrease in viable cell number results in a concomitant change in the amount of formazan formed, indicating the degree of cytotoxicity caused (513).

2.2.9.1 Materials, Reagents and Equipment

- MTT — Sigma
- MTT solubilisation solution — Sigma
- PBS
- DMSO — VWR
- FLUOstar Omega — BMT Labtech
- Omega Software (version 1.20) — BMT Labtech
- MARS data analysis software (version 1.20 R2) — BMT Labtech

MTT Solubilisation Solution: 10% Triton X-100 plus 0.1 N HCl anhydrous isopropanol

2.2.9.2 Protocol

1. MTT assays were performed in 24-well cell culture treated plates.
2. MTT stock solution was reconstituted at a concentration of 5mg/mL in MTT solubilisation solution. Stock solution is stored at -20°C.
3. Medium was aspirated from the co-culture and wells were washed with 500µL PBS to remove residual T-cells.
4. MTT stock solution was diluted 1/10 (to a concentration of 500µg/mL) in D10 media and 500µL (250µg) was added to each well.
5. Cell cultures were incubated for 2-4 hours at 37°C and 5% CO_2.
6. The supernatant was aspirated and the formed formazan crystals were resuspended in 300µL DMSO.
7. Absorbance was measured spectrophotometrically at 570nm.
8. Relative cell viability was calculated using the following equation:
   Viability = (absorbance of test well/ average absorbance of untreated tumour monolayer)x100

2.2.10 Visualisation of Tumour Cells using Crystal Violet Staining

Visualisation of tumour-cell destruction by CAR-transduced T-cells may be effectively achieved by staining the remaining target cells with crystal violet. Crystal violet is commonly used as a stain for identifying Gram-positive bacteria due to it becoming trapped within the peptidoglycan layer upon ethanol-induced dehydration. When supplied with a mordant (methanol), it is also capable of staining human cells.

2.2.10.1 Materials, Reagents and Equipment

- Crystal Violet — Sigma-Aldrich
- PBS
- Methanol — Fisher Scientific
- Inverted light microscope — Nikon TMS
- AxioVision HR camera — AxioVision
- Axiovert S100 software — AxioVision

2.2.10.2 Protocol

1. Media was carefully aspirated from the plate of interest.
2. The wells were gently washed with 500µL PBS before being treated with 500µL of ice-cold methanol and fixed at -20°C for a minimum of ten minutes.
3. After aspiration of the methanol, each well was submerged in crystal violet dye and incubated at room temperature for five minutes.
4. Following removal of the crystal violet, the plates were washed by gentle submersion in water to remove excess dye.
5. Plates were dried at room temperature overnight.
6. Images were captured under light microscopy on an inverted microscope with an AxioVision HR camera. Images were analysed and scale determined using Zeiss Axiovert S100 software.

2.2.11 Analysis of firefly Luciferase Expression

Bioluminescent imaging (BLI) was used to monitor tumour growth and T-cell migration and longevity *in vivo*. This was achieved by expression of a firefly luciferase (ffLuc) enzyme within the transplanted cells. Stable expression of the luciferase enzyme by the various tumour cell lines was achieved using the retroviral vector pBabe puro

(details of this vector are given in paragraph 2.2.3.2). Expression of the firefly enzyme in T-cells was achieved using the retroviral vector SFG, containing 4αβ, T28ζ and ffLuc (details of the vector are given in paragraph 2.1.1.6). Prior to transfer of the luciferase-tagged cells *in vivo*, it was important to ensure the continued expression and functionality of the enzyme. Firefly luciferase catalyses the conversion of a molecule of D-luciferin to an electronically 'excited' molecule of oxyluciferin when in the presence of magnesium, ATP and oxygen. The subsequent relaxation of this oxyluciferin molecule to a lower energy state results in the release of a single photon, which can be detected by a super-cooled 'charged-coupled device' (CCD) and a camera or luminometer (514-516).

2.2.11.1 Materials, Reagents and Equipment

- Luciferase assay substrate — Promega
- Luciferase assay buffer — Promega
- 5x Reporter Lysis buffer — Promega
- Cell Lysate
- White 96-well plate — Nunc
- FLUOstar Omega Plate Reader — BMT Labtech
- Omega Software (version 1.20) — BMT Labtech
- MARS data analysis software (version 1.20 R2) — BMT Labtech

2.2.11.2 Protocol

1. The 5x Reporter Lysis buffer was diluted in dH_2O to give a 1x solution, which was equilibrated to room temperature prior to use.
2. Viable cells were counted based on trypan-blue based exclusion and 0.5 x 10^6 cells were resuspended in 500µL 1x Reporter Lysis buffer.
3. Lysed Cells were transferred into a 1.5mL Eppendorf and snap-frozen on dry ice.
4. Cell lysate was centrifuged for 15 seconds at 10,400g.
5. 20µL of cell lysate was mixed with 100µL luciferase assay substrate in one well of a white 96-well plate.
6. The luminescence was read using the FLUOstar Omega luminometer.
7. Luminescence values were compared with negative control lysates gained from matched luciferase-negative cells.

2.3 *In vivo* models

All in vivo experiments were performed strictly adhering to the UK Home Office guidelines as stated in the project license (license number 70/7603) and personal license (license number 70/23089) that governed this work.

2.3.1 Tumour Inoculation

Tumour cells were inoculated by either subcutaneous (SC) or intra-peritoneal (IP) injection.

2.3.1.1 Materials, Reagents and Equipment

- 1mL Syringe — BD Plastipak
- 25 G Needle — BD Biosciences
- BD Matrigel Basement Membrane Matrix Growth Factor Reduced, Phenol Red-free — BD Biosciences
- PBS

2.3.1.2 Protocol

The amount of tumour cells and injection volumes used are specified in the individual experiments.

Intra-peritoneal (IP) tumour inoculation

1. Mice were randomised into the required number of groups.
2. The specified number of tumour cells were resuspended in 400µL PBS and injected into the intra-peritoneal cavity using a 25G needle connected to a 1mL syringe.
3. Tumour growth was monitored using BLI (please refer to paragraph 2.3.4).

Subcutaneous (SC) tumour inoculation

1. Mice were randomised into the required number of groups.
2. Mice were anaesthethised with 3-4% gaseous isofluorane.
3. The specified number of tumour cells were resuspended in 200µL PBS or Matrigel and injected subcutaneously into the left flank using a 25G needle connected to a 1mL syringe.

4. Tumour growth was monitored using BLI (please refer to paragraph 2.3.4) and caliper measurements (please refer to paragraph 2.3.5) where appropriate.

2.3.2 T-cell Administration

To determine *in vivo* efficacy and toxicity of T-cell immunotherapy, mice were treated with different doses of CAR^+ or control T-cells, administered using the SC, IP or intravenous (IV) routes of injection.

2.3.2.1 Materials, Reagents and Equipment

- 1mL insulin syringes (29G) Terumo
- PBS

2.3.2.2 Protocol

The amount of T-cells and route of administration used is specified in the individual experiment descriptions in the results chapters.

Intra-peritoneal T-cell injection

1. The required number of T-cells was resuspended in 500µL PBS and injected intra-peritoneally using a 1mL insulin syringe.

Intra-tumoural (IT)/ peri-tumoural (PT) T-cell injection

1. The mice were anaesthethised with 3-4% gaseous isofluorane.
2. The required amount of T-cells were resuspended in 50µL PBS and injected into the subcutaneous tumour using a 1mL insulin syringe.
3. If SC tumours were too small to allow for IT injection, T-cells were injected PT.

Intravenous T-cell injection

1. Mice were restrained and better visualization of the tail vein was achieved using a heat lamp.
2. The required number of T-cells were resuspended in 200µL PBS and injected into the tail vein using a Terumo 1mL insulin syringe.

2.3.3 Body Weight Measurement

One of the hallmarks by which toxicity can be quantified is the change in body weight of the mouse. Body weights were measured at regular intervals during the studies

2.3.3.1 Materials, Reagents and Equipment

- Balance — Mettler Toledo

2.3.3.2 Protocol

1. Mice were individually transferred from their cage to the balance
2. Weight was monitored at regular timepoints during the study

2.3.4 Bioluminescent Imaging

Bioluminescent Imaging (BLI) is a sensitive, non-invasive technique, which allows semi-quantitative monitoring of tumour growth and T-cell migration *in vivo*. After administration of the D-luciferin substrate, the luciferase-tagged cells can be visualized *in situ* whilst the mice are under anaesthetic.

2.3.4.1 Materials, Reagents and Equipment

- D-Luciferin — Caliper Lifesciences
- Isofluorane — Baxter
- IVIS Lumina II imaging platform — Caliper Lifesciences
- 1mL insulin syringes (29G)

2.3.4.2 Protocol

1. Mice were injected with 3mg (400µL) D-luciferin intra-peritoneally and placed back into the cage for five minutes
2. Mice were anaesthethised with 3-4% gaseous isofluorane and transferred to the IVIS Lumina II imaging platform
3. A total of nine images of increasing duration (1s, 2s, 5s, 10s, 30s, 45s, 60s, 120s, 180s) were taken using small (for tumours) or large (for T-cells) binning. Throughout the imaging the mice were kept under 1.5% isofluorane anaesthesia.
4. After completion of the imaging, the mice were returned to their cages and monitored until they regained consciousness.

2.3.5 Caliper Measurements

Caliper measurements are a non-invasive way to monitor subcutaneous tumour growth. The length and width of a subcutaneous tumour is measured using an electronic caliper, which allows the calculation of the tumour volume using the formula indicated below.

2.3.5.1 Materials, Reagents and Equipment

- Golden A5 animal clipper — Oster
- Electronic Caliper — SiTE

2.3.5.2 Protocol

1. The area of the subcutaneous is shaved using an electronic shaver
2. The length and width of the tumour is measured using an electronic caliper
3. The volume of the tumour is calculated using the formula:
   Volume = (length x width^2)/2

2.3.6 Blood Sampling from Tail Vein

To determine serum cytokine levels after T-cell administration, blood samples were taken from the tail vein at suitable time-points during the study.

2.3.6.1 Materials, Reagents and Equipment

- Isofluorane — Baxter
- Scissors
- Microvette CB300 tubes — Sarstedt
- 1.5mL Eppendorf tubes — Eppendorf

2.3.6.2 Protocol

1. Prior to the first blood sample, mice were anaesthetised with 3-4% gaseous isofluorane.
2. The tip of the tail vein is clipped off and 100µL of blood is collected in the Microvette CB300 tube.

3. Blood samples are taken at multiple timepoints after T-cell injection during the study:
    a. 4 hours
    b. 24 hours
    c. 48 hours
4. To isolate the serum, blood was allowed to clot within the Microvette CB300 tubes and were centrifuged for 5 minutes at 10,000g. The serum was transferred to 1.5mL Eppendorf tubes and stored at -20°C.

2.3.7 Liposomal Clodronate and Liposomal PBS treatment

Liposomal Clodronate (LC) and Liposomal PBS (LP) were obtained from Dr N. van Rooijen, Foundation Clodronate Liposomes, Haarlem, the Netherlands. Mice received two doses of LC/LP, one four days prior to T-cell administration, and a second one day prior to T-cell administration.

2.3.7.1 Materials, Reagents and Equipment

- Liposomal Clodronate (10mg/mL) — Foundation Clodronate Liposomes
- Liposomal PBS (10mg/mL) — Foundation Clodronate Liposomes
- 1mL syringe
- 23G Needle — BD
- Balance

2.3.7.2 Protocol

1. Mice were transferred individually from the cage to the balance
2. Weight of the mice was recorded
3. Mice were injected ip with the required dose of LC/LP
    a. Dose 1: 1mg/10g body weight
    b. Dose 2: 0.5mg/10g body weight

2.3.8 Peritoneal Lavage

To determine the content of macrophages in the peritoneal cavity after treatment with LC or LP, ip lavages were performed to remove all cell-content and macrophage content was determined by flow cytometry.

2.3.8.1 Materials, Reagents and Equipment

- Ice-cold PBS
- 5mL syringe — BD Plastipak
- 19 G Needle — BD
- 50mL Falcon tube — BD
- Scissors
- Tweezers
- Ice

2.3.8.2 Protocol

1. Prior to ip lavage, mice were culled by dislocation of the neck
2. 5mL ice-cold PBS was injected into the intra-peritoneal cavity.
3. The body of the mouse was massaged to ensure optimal distribution of the PBS
4. The skin was opened, leaving the peritoneum in tact.
5. A small hole was made in the peritoneum, allowing the PBS to flow out into a 50mL falcon tube that was placed on ice.
6. The macrophage content was determined by flow cytometry (please refer to paragraph 2.4.1.10).

2.3.9 Homogenisation of Mouse Organs

Organs were harvested from untreated healthy SCID/Beige mice to analyse ErbB expression using flow cytometry.

2.3.9.1 Materials, Reagents and Equipment

- Organs from SCID/Beige mice
- 2mL syringe — BD Plastipak
- 100µM Nylon filter — BD
- Red Blood Cell Lysis buffer — Miltenyi
- PBS
- mR10 — Please refer to paragraph 2.2.1.1

2.3.9.2 Protocol

1. Organs were harvested and directly submerged into sterile PBS.
2. Single organs were passed through a 100µm nylon filter with the aid of the plunger of a 2mL syringe.
3. Cells were washed in mR10 and red blood cells were lysed using red blood cell lysis buffer.
4. For flow cytometry analysis: cells were washed in excess mR10 after which the pellet was resuspended in 1-10mL mR10 (depending on the organ size) and immediately used for flow cytometry analysis.

2.4 Flow Cytometry

Flow cytometry was used to probe for protein expression either at the cell surface or intracellularly. Determination of protein expression at the cell surface was important for showing the expression of the CAR by the T-cells and packaging cell lines as well as for investigation of the levels of ErbB expression on tumour cells and healthy tissue.

2.4.1 Cell Surface Staining

2.4.1.1 Materials, Reagents and Equipment

Antibodies	(please see below)
FACS Calibur Flow Cytometer	Becton Dickinson
5mL polystyrene round-bottom flow cytometry tubes	BD Falcon
Normal Rabbit Serum	DAKO
Cell Dissociation Buffer	Gibco
Ice	
Methanol	Fisher Chemical
Trypsin/EDTA	Gibco
Intracellular (IC) staining buffer	(please see below)
38% Paraformaldehyde	Fisher Scientific

Buffers and common solutions:

IC staining buffer = 4 parts D10 + 6 parts PBS

2.4.1.2 Antibodies

Staining for T28ζ

Mouse IgG_1 anti-human EGF (clone 10825)	R&D Systems
Polyclonal $F(ab')_2$ Goat anti-mouse PE-conjugated	DAKO
Affinity purified Goat IgG hEGF biotinylated	R&D Systems
Streptavidin PE-conjugated	Invitrogen

Staining for P28ζ

Goat anti-mouse IgG PE-conjugated	DAKO

Staining for 4αβ

Mouse IgG_1 anti-human CD124 PE-conjugated	BD Pharmingen

Staining for CD4 and CD8

Mouse IgG PC5-conjugated	Beckman Coulter
Mouse IgG anti-human CD8 PC5-conjugated	Beckman Coulter
Mouse IgG FITC-conjugated	MACS
Mouse IgG anti-human CD4 FITC-conjugated	MACS

Staining for human ErbBs

Rat anti-human ErbB1 (ICR62)	ICR
Purified rat monoclonal IgG_{2A} (clone 54447)	R&D Systems
Rat anti-human ErbB2 (ICR12)	ICR
Purified rat monoclonal IgG_{2B} (clone 441045)	R&D Systems
Mouse anti-human ErbB3 (clone H3.105.5)	Neomarkers
Mouse anti-human ErbB4 (clone H4.77.16)	Neomarkers
Goat anti-rat IgG PE-conjugated	Invitrogen
Goat anti-mouse IgG PE-conjugated	DAKO
Rat IgG_{2A} anti-human ErbB1 FITC-conjugated	R&D Systems
Mouse IgG_{2B} anti-human ErbB2 APC-conjugated	R&D Systems
Mouse IgG_1 anti-human ErbB3 PerCP-conjugated	R&D Systems
Mouse IgG_{2A} anti-human ErbB4 APC-conjugated	R&D Systems
Rat IgG_{2A} FITC-conjugated	R&D Systems
Mouse IgG_1 APC-conjugated	R&D Systems
Mouse IgG_1 PerCP-conjugated	R&D Systems

Staining for murine ErbBs

Polyclonal Rabbit IgG anti-EGFR (1005, sc-03)	SantaCruz Biotech
Polyclonal Rabbit IgG anti-Neu (c-18)	SantaCruz Biotech
Polyclonal Rabbit IgG anti-ErbB3 (c-17)	SantaCruz Biotech
Polyclonal Rabbit IgG anti-ErbB4 (c-18)	SantaCruz Biotech
Swine $F(ab')_2$ anti-rabbit IgG FITC-conjugated	DAKO

Staining for PSMA

Mouse anti-human PSMA (clone K0142-3)	MBL International
Goat anti-mouse IgG PE-conjugated	DAKO

Staining for mouse macrophages

Anti-mouse CD16/CD32 (Fc receptor block)	eBioscience
Anti-mouse CD45 PerCP-Cy5.5-conjugated	eBioscience
Anti-mouse IgG PerCP-Cy5.5-conjugated	eBioscience
Anti-mouse F4/80 FITC-conjugated	eBioscience
Anti-mouse IgG FITC-conjugated	eBioscience

2.4.1.3 Analysis of T28ζ Expression

1. A pre-determined number of T-cells ($1 \times 10^5 - 1 \times 10^6$) were placed in a flow-cytometry tube and incubated with 400ng primary antibody for 30 minutes on ice.
2. Samples were washed using 2mL PBS, and each sample was incubated with 3µg secondary antibody for 30 minutes on ice in the dark.
3. Samples were again washed with PBS, centrifuged and subsequently resuspended in 200µL PBS immediately prior to analysis. Samples were kept in the dark and on ice until analysed.
4. Results were compared against untransduced T-cells stained using the same protocol.

2.4.1.4 Analysis of P28ζ Expression

1. A pre-determined number of T-cells ($1 \times 10^5 - 1 \times 10^6$) were placed in a flow-cytometry tube and incubated with 400ng antibody for 30 minutes on ice
2. Samples were washed using 2mL PBS, and resuspended in 200µL PBS immediately prior to analysis. Samples were kept in the dark and on ice until analysed.
3. Results were compared against untransduced T-cells stained using the same protocol.

2.4.1.5 Analysis of 4αβ Expression

NOTE: $4\alpha\beta^+$ T-cells were transferred to media supplemented with rhIL-2 at least 24 hours prior to analysis of 4αβ expression.

1. A pre-determined number of T-cells ($1 \times 10^5 - 1 \times 10^6$) were placed in a flow-cytometry tube and incubated with 400ng of the directly-conjugated antibody for 20 minutes at room temperature in the dark.
2. Samples were washed with PBS, centrifuged and subsequently resuspended in 200µL PBS immediately prior to analysis. Samples were kept in the dark and on ice until analysed.
3. Results were compared to untransduced cells stained using the same protocol.

2.4.1.6 Analysis of CD4 and CD8 content

CD4 and CD8 content in the total population was determined, not on the CAR^+ population specifically.

1. A pre-determined number of T-cells ($1 \times 10^5 - 1 \times 10^6$) were placed in a flow-cytometry tube and incubated with 400ng of the directly-conjugated antibody for 20 minutes at room temperature in the dark.
2. Samples were washed with PBS, centrifuged and subsequently resuspended in 200µL PBS immediately prior to analysis. Samples were kept in the dark and on ice until analysed.
3. Results were compared to untransduced cells stained using the same protocol.

2.4.1.7 Analysis of Receptor Expression on Viral Packaging Cells

In order to determine the quality of the retroviral packaging cells, cells were regularly tested for CAR expression.

1. Viral packaging cells were removed using Cell Dissociation buffer and washed in PBS
2. Cells were stained using the same protocol of step 1-4 of paragraphs 0 - 2.4.1.5.

2.4.1.8 Extracellular ErbB Receptor Detection

Expression of ErbB receptors was analysed using either unconjugated antibodies or directly-conjugated antibodies.

1. Adherent cells were harvested using Cell Dissociation Buffer and a pre-determined number (1×10^5-1×10^6) was transferred to a flow-cytometry tube.
2. Prior to staining cells were washed in 2mL PBS and the cell pellet was resuspended in the remainder of the PBS at the bottom of the tube.

Directly conjugated antibodies

3. 500ng of the directly conjugated antibody was added and the cells were incubated for 20 minutes in the dark, at room temperature.
4. Cells were washed and resuspended in 200µL PBS prior to analysis.
5. Results were compared to cells stained with the appropriate isotype control.

Unconjugated antibodies

3. 400ng of the primary antibody was added to the cells and were incubated for 30 minutes on ice.
4. Cells were washed in 2mL PBS and subsequently incubated with 3-7µg of the appropriate secondary antibody. Cells were incubated for 30 minutes on ice, in the dark.
5. Cells were washed and resuspended in 200µL PBS prior to analysis.
6. Results were compared to cells stained with the secondary conjugated antibody alone.

NOTE: Staining for PSMA was performed using the same protocol as staining for ErbB receptors using unconjugated antibodies.

2.4.1.9 Intracellular ErbB Receptor Detection

1. Adherent cells were trypsinised to harvest and a pre-determined number (1×10^5-1×10^6) was transferred to a flow-cytometry tube.
2. Cells were washed in D10 and resuspended in 1mL D10 with addition of 52µL 38% paraformaldehyde and fixed at 37°C for 10 minutes.

3. For permeabilisation, 2mL ice-cold methanol was added and cells were incubated on ice for at least 30 minutes.
4. Cells were centrifuged for 5 minutes at 200g and subsequently washed in 2mL IC staining buffer.
5. The supernatant was removed and 30µL of a 1/50 dilution of rabbit serum was added, as well as 5µL (1µg) of the primary antibody. Cells were incubated at room temperature for 20 minutes and washed again in 2mL IC staining buffer.
6. 500ng of secondary antibody was added and the cells were incubated for 20 minutes at room temperature, in the dark.
7. After a final wash in 2mL IC staining buffer, the cells were resuspended in 200µL PBS and analysed.
8. Results were compared to cells stained with rabbit serum and the secondary conjugated antibody alone.

2.4.1.10 Staining for Mouse Macrophages

To determine the macrophage content in the intra-peritoneal cavity of mice treated with LC or LP cells were stained using anti-mouse CD45 and anti-mouse F4/80.

1. IP lavage content was washed and resuspended in 3mL red blood cell lysis buffer
2. Cells were incubated on ice for 10 minutes
3. Cells were washed and resuspended in 2mL PBS
4. Total cell count was enumerated using trypan-blue exclusion
5. A pre-determined number of cells (approximately 1 x 10^5) cells were transferred to a flow-cytometry tube
6. 1µL of Fc receptor block was added and cells were incubated for 30' in the dark, on ice.
7. Cells were washed in PBS and resuspended in 200µL PBS.
8. 500ng of both anti-mouse CD45 and anti-mouse F4/80 were added, and cells were incubated for 30', in the dark, on ice.
9. Cells were washed, resuspended in 200µL PBS and analysed.
10. Results were compared to cells stained with the appropriate isotype control.

2.4.1.11 Gating strategy for FACS analysis

To determine the level of expression of the receptor of interest, fluorescence on the stained cells of interest was compared to the level of fluorescence on the appropriate control population. Figure 2-5 shows the gating strategy for the analysis of ErbB1 expression on HN3 cells.

1. Live cells were gated based on their position in the forward/side scatter plot. Live gate was adjusted to the appropriate location for each separate analysis (see Figure 2-5 1).
2. A total of 100,000 cells were recorded.
3. Fluorescence of cells within the live gate was visualised in dot plots and histograms of the right FL channel (see Figure 2-5 2 and 3).
4. Gates and markers were set to indicate negative or background staining. Gates and markers remained in the same position between each control and test sample pair (see Figure 2-5 2 and 3).
5. MFI indicates the mean fluorescence intensity of the entire population within the live gate.
6. Percentage of cells (within the live gate) positive for the receptor of interest is calculated based on:

   % test population within M1 - % control population within M1 = % test population expressing the receptor of interest.

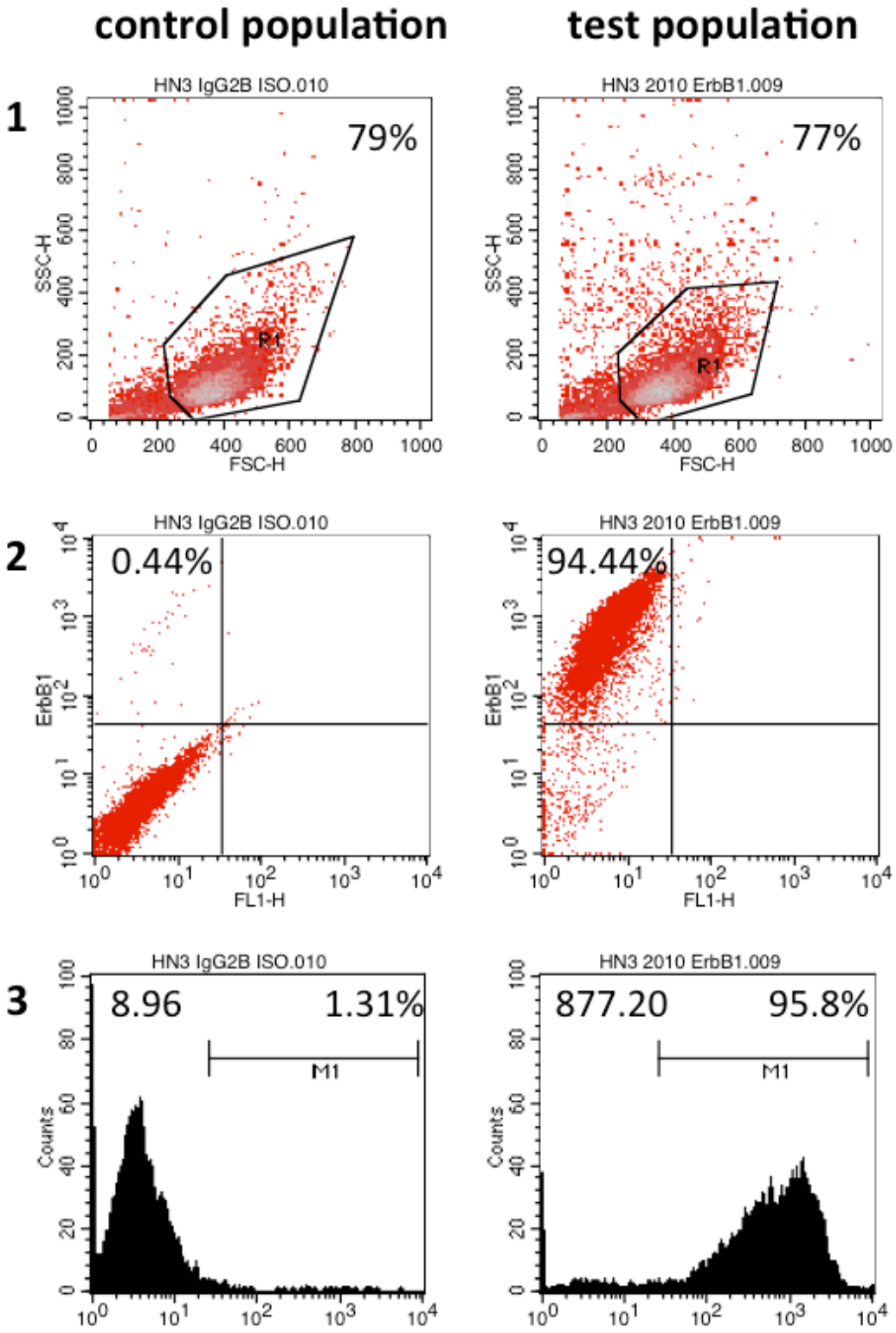

Figure 2-5 FACS gating strategy

Analysis of ErbB1 expression on HN3 cells. HN3 cells are stained with rat IgG_{2A} and goat-anti-rat PE-conjugated (control population) or rat anti-human ErbB1 and goat-anti-rat IgG PE-conjugated (test population) (**1**) Live gate R1 is set to analysis only the live cell population, based on their location within the forward/side scatter plot. Percentage indicates amount of cells within the live gate. (**2**) Fluorescence of the live cell population within the channel of interest (in this case FL2) and quadrants are placed to indicate level of background signal on control population. Percentage indicates the percentage of cells within the upper left quadrant. (**3**) Histograms indicating the fluorescence of the live cell population in the channel of interest. Marker is set to indicate level of background fluorescence based on control population. Value in the upper left corner indicates MFI, value in upper right corner indicates the amount of cells within M1.

2.5 Detection of Cytokine Release

2.5.1 Enzyme-Linked Immunosorbent Assay (ELISA)

Cytokine release in cell culture supernatants was detected using a sandwich Enzyme Linked Immunosorbent Assay (ELISA), tailored to the cytokine of interest (human IL-2 or human IFNγ). Measuring the release of specific cytokines by CAR-transduced T-cells, during co-culture with targets provided a quantitative technique for investigating T-cell activation. Plates were pre-coated with a 'capture' antibody specific for the cytokine of interest thereby immobilizing cytokine present within the samples. Bound cytokine was detected using a biotin-labelled antibody and subsequently with avidin-labelled horseradish peroxidase (HRP). Visualisation was achieved using a 3,5,3',5'-tetramethylbenzadine (TMB)/hydrogen peroxide solution. Oxidation of the colourless TMB reagent to a blue solution (an equilibrium between the TMB cation radical and the diamine-diimine charge transfer complex (517)) highlighted assay progression. Following a reasonable development time (as determined by development of the standard curve), the reaction was stopped using 1M sulphuric acid. The reduction in pH induced by the addition of sulphuric acid results in the formation of the yellow diimine product and prevented further development by denaturation of the HRP. Plates were subsequently read at 450nm and the concentrations of each sample were calculated with respect to the known concentrations of the standard curve.

2.5.1.1 Materials, Reagents and Equipment

- Human IFNγ Ready-SET-Go! ELISA — eBioscience
- Human IL-2 Ready-SET-Go! ELISA — eBioscience
- Mouse IL-6 Ready-SET-Go! ELISA — eBioscience
- Corning Costar 9018 96-well flat-bottom plates — Costar
- FLUOstar Omega plate reader — BMT Labtech
- Omega Software (version 1.20) — BMT Labtech
- MARS data analysis software (version 1.20 R2) — BMT Labtech

Contents of Ready-SET-Go! ELISA kits:

- Capture antibody
- Detection antibody
- Standard
- 10x Coating buffer
- 5x Assay diluent
- Avidin-HRP
- Substrate solution

Buffers and solutions:

Wash buffer = PBS + 0.05% Tween-20

2.5.1.2 Protocol

1. The capture antibody was diluted 1/250 in coating buffer. Subsequently the 96-well ELISA plate was coated with 100µl/well of capture antibody.
2. Plates were covered and incubated overnight at 4°C
3. All the wells were aspirated and washed 5 times with >250µL/well wash buffer. The wash buffer was allowed to soak for 1 minute during each step for increased effectiveness of the washes.
4. One part 5x concentrated assay diluent was diluted in 4 parts distilled water.
5. All wells were blocked with 200µL/well of 1x assay diluent for the duration of 1 hour at room temperature.
6. Plates were washed as described in step 3.
7. Standard curve samples were serially diluted two-fold in assay diluent to give a seven point standard curve ranging from an initial concentration of 500pg/mL to 3.9pg/mL and were plated in duplicate. Background absorbance was measured by plating assay diluent alone. Samples of co-cultivation were diluted between 1:2 and 1:20 in assay diluent prior to plating in triplicate. Serum samples were diluted 1:20 and plated single.
8. Plates were covered and incubated overnight at 4°C
9. Plates were washed as described in step 3.
10. Detection antibodies were diluted 1/250 in assay diluent, and 100µL/well was added.

11. Plates were covered and incubated for 1 hour at room temperature
12. Plates were washed as described in step 3.
13. Avidin-HRP was diluted 1/250 in assay diluent, and 100µL/well was added.
14. Plates were covered and incubated for 30 minutes at room temperature.
15. Plates were washed as described in step 3. On this occasion, plates were washed a total of 7, allowing 1-2 minutes of soaking between washings.
16. 100µL/well of TMB substrate solution was added to each well.
17. Plates were incubated for 15 minutes at room temperature.
18. 50µL of stop solution (1M H_2SO_4) was added to each well.
19. Absorbance was read at 450nm using the FLUOStar Omega plate reader and Omega Software (version 1.20).
20. Standard curves and cytokine concentrations were calculated using the MARS data analysis software (version 1.20 R2).

2.5.2 BD Cytometric Bead Array (CBA)

To deterime the cytokine levels in murine blood serum samples, the BD Cytometric Bead Array was used. The BD CBA assays provide a method of capturing a soluble analyte or set of analytes using beads of known size and fluorescence, making it possible to detect analytes using flow cytometry. Each capture bead in a BD CBA kit has been conjugated with a specific antibody. The detection reagent provided in the kit is a mixture of phycoerythrin (PE)-conjugated antibodies, which provides a fluorescent signal in proportion of the amount of bound analyte. When the capture beads and detector reagent are incubated with an unknown sample containing recognized analytes, sandwich complexes (capture bead + analyte + detection reagent) are formed. These complexes can be measured using flow cytometry to identify particles with fluorescence characteristics of both the bead and the detector.

The Human Th1/Th2/Th17 Cytokine Kit can be used to measure IL-2, IL-4, IL-6, IL-10, TNF, IFNγ, and IL-17A protein levels in a single sample. The mouse Th1/Th2/Th17 Cytokine Kit measures the equivalent mouse cytokines. Seven bead populations with distinct fluorescence intensities have been coated with capture antibodies specific for one of each of the cytokines. The seven bead populations are mixed together to form the bead array, which is resolved in a red channel of a flow cytometer.

2.5.2.1 Materials, Reagents and Equipment

- BD Cytometric Bead Array (CBA)
  Human Th1/Th2/Th17 Cytokine Kit — BD Biosciences
- BD Cytometric Bead Array (CBA)
  Mouse Th1/Th2/Th17 Cytokine Kit — BD Biosciences
- FACS Calibur Flow Cytometer — Becton Dickinson
- FCS Filter Software — Soft Flow Inc
- FCAP Array Software — BD Biosciences

2.5.2.2 Protocol

1. The number of assay tubes (including standards and controls) required for the experiment was determined.
2. Each Capture Bead suspension was vigorously vortexed for 3 to 5 seconds before mixing.
3. For each assay and standard tube to be analysed, a 10µL aliquot of each Capture Bead was added to a single tube labelled 'mixed Capture Beads'.
4. The bead mixture was mixed thoroughly and centrifuged for 5 minutes at 200g.
5. Supernatant was carefully aspirated and discarded.
6. The mixed Capture Beads pellet was resuspended in Serum Enhancement Buffer (an equal volume as was removed in step 5) and vortexed thoroughly.
7. The mixed Capture Beads were incubated for 30 minutes at room temperatre, protected from light.
8. Serum samples were diluted 1:5 using the appropriate volume of Assay Diluent and samples were mixed thoroughly.
9. One vial of lyophilized Human (or Mouse) Th1/Th2/Th17 Standards was opened. The spheres were transferred to a 15mL conical, polypropylene tube, creating the Top Standard.
10. Standards were reconstituted using 2mL of Assay Diluent and equilibrated for at least 15 minutes at room temperature.
11. Reconstituted protein was gently mixed by pipetting.
12. The Top Standard was serially diluted to create an 8-point standard curve, ranging from 5,000pg/mL to 20pg/mL.

13. One tube containing only Assay Diluent was prepared to serve as the 0pg/mL negative control.
14. The mixed Capture Beads were vortexed, and 50µL was added to all assay tubes as well as the standard curve tubes.
15. 50µL of each unknown sample or standard curve sample was added to the appropriately labelled tube.
16. 50µL of the Human (or Mouse) Th1/Th2/Th17 PE Detection Reagent was added to all tubes.
17. The tubes were incubated for 3 hours at room temperature, protected from light.
18. 1mL of Wash Buffer was added to each assay tube and centrifuged at 200g for 5 minutes.
19. The supernatant was carefully aspirated and discarded from each tube.
20. The bead pellet was resuspended in 300µL of Wash Buffer.

The FACS Calibur Flow Cytometer was set up as follows:

21. 50µL of Cytometer Setup Beads were added to three cytometer setup tubes labelled A, B, and C.
22. 50µL of FITC Positive Control Detector was added to tube B.
23. 50µL of PE Positive Control Detector was added to tube C.
24. Tubes A, B, and C were incubated at room temperature for 30 minutes, protected from light.
25. 450µL of Wash Buffer was added to tube A, and 400µL of Wash Buffer was added to tubes B and C.
26. Tubes A, B and C were used to set up the instrument settings on the flow cytometer to allow for optimal detection.

Cytokine Content in serum samples was determined as follows:

27. All samples were analysed using the optimised instrument settings.
28. The raw data acquired with BD CellQuest could not be analysed directly by the FCAP software due to debris, which is detected by the system and disturbs the data analysis. For this reason, data had to be “cleaned” by FCS Filter Software prior to analysis.
29. Cleaned data is analysed using FCAP Array Software.

2.6 Statistical Analysis

To investigate statistical significance, values were subjected to a student's t-test, equal variances assumed. p-values < 0.05 were taken as significant. Data was analysed using GraphPad Prism software (version 5.0d), and Microsoft Excel (version 14.3.5).

CHAPTER 3

‘ON-TARGET’-TOXICITY OF T4 IMMUNOTHERAPY

3.1 Introduction

'On-target'-toxicity is the toxicity induced by recognition of the target antigen on healthy tissue. The ErbB-receptor family is overexpressed on tumour cells, but is also expressed on healthy tissue. Therefore, ErbB-targeted therapies have been associated with 'on-target'-toxicities. Here, the risks of 'on-target'-toxicity in response to the targeting of the extended ErbB-family with T4 immunotherapy are described.

3.1.1 T4 Immunotherapy

T4 immunotherapy uses ErbB re-targeted T-cells to induce cytotoxicity against ErbB$^+$ tumour cells. T-cells are transduced to express two transgenes, the chimeric antigen receptor T28ζ and the chimeric cytokine receptor 4αβ. The composition and functionality of both receptor and the combined expression is detailed in chapter 1.3.11.

T28ζ is a second generation CAR (see Figure 3-1). The binding moiety consists of the chimeric T1E peptide, which is coupled to the CD28 hinge, transmembrane domain and partial intracellular domain. In turn, CD28 is coupled to the intracellular domain of CD3ζ (299). The T1E peptide is a chimeric peptide resulting from the replacement of the first five amino acids of EGF with the first seven amino acids of TGFα. Epidermal growth factor and TGFα are both exclusive ligands for ErbB1. However, the combination of the His^4 and Phe^5 residues of TGFα with the Leu^{28} residue in EGF enables the T1E peptide to also bind the ErbB2/3 heterodimer with high affinity (451, 457). The use of the T1E peptide as the binding moiety, allows for the targeting of the extended ErbB-receptor family. Targeting of multiple ErbB receptors may reduce tumour resistance and increase tumour control compared to the targeting of a single ErbB receptor. *In vitro*, T28ζ$^+$ T-cell activation can be achieved by all ErbB1-containing homo- and heterodimers, as well as the ErbB2/3 heterodimer, but not ErbB2 or ErbB3 alone (299). Additionally, weak activation can be induced by ErbB4 containing dimers. *In vivo*, T28ζ$^+$ cells were shown to be able to control tumour growth of the ErbB1/2$^+$ HN3 xenograft model, the ErbB2/3$^+$ MDA-MB-435-ErbB2 xenograft model (299) and the SKOV-3 ovarian tumour xenograft (358).

4αβ is a chimeric cytokine receptor, which consists of the IL4-Rα ectodomain coupled to the shared IL-2/-15Rβ endodomain (see Figure 3-1). Upon binding of IL-4 to the receptor, it dimerizes with the common γ-chain and an IL-2 like signal is induced.

Co-expression of 4αβ with any CAR allows for the selective expansion of the transgene$^+$ T-cell population through the culture in media supplemented with IL-4 rather than IL-2. Culture in IL-4 induces both IL-4 and IL-2 like signalling. However, cells do not polarize towards a Th_2 phenotype (391).

The combined expression of T28ζ and 4αβ is referred to as 'T4'. The expression of two transgenes using one retroviral vector is achieved with the insertion of a T2A peptide sequence. The T2A peptide induces a ribosomal 'skip' in which a peptide bond between the two constructs is 'missed' (488, 489). To enable this, the stop codon at the 3' end of 4αβ has been removed. A furin cleavage sequence was introduced upstream of the T2A-sequence to ensure that most of the residual T2A peptide is removed from the C-terminus of 4αβ.

In vivo, T4$^+$ T-cells showed functionality against the HN3 and MDA-MB-435-ErbB2 xenograft models as well as the SKOV3 xenograft model. In the SKOV3 model it was shown that repeated T-cell administration resulted in better tumour control compared to a single treatment dose. Additionally, combined treatment with carboplatin further increased the anti-tumour activity (358).

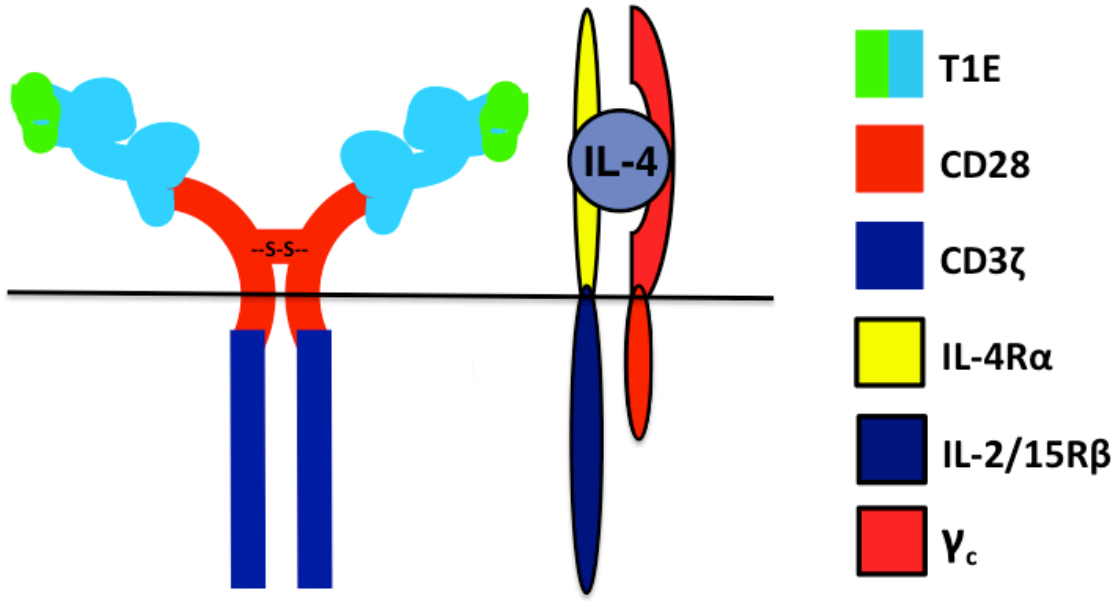

Figure 3-1 Schematic representation of T4
The combined expression of the T28ζ chimeric antigen receptor and the 4αβ chimeric cytokine receptor is referred to as 'T4'. T28ζ comprises of the T1E peptide (shown in green/turquoise) as a binding moiety, the CD28 hinge and transmembrane domain (shown in red), coupled to the CD3ζ intracellular domain (shown in dark blue). The receptor is expressed on the cell surface as a dimer, coupled by a disulphide bond. 4αβ comprises of the IL-4Rα ectodomain (shown in lined yellow) coupled to the IL-2/15Rβ endodomain (shown in lined blue). Upon binding with IL-4 the receptor dimerizes with the common γ-chain (γ_c)(shown in lined red).

3.1.2 'On-Target'-Toxicities in ErbB Targeted Therapies

Members of the ErbB-receptor family are commonly upregulated on tumour cells. However, ErbB expression is not exclusive to tumour cells. Healthy tissues expressing ErbB receptors are also at risk of being affected by ErbB-targeted treatment. The occurrence of such 'on-target'-toxicities have been reported in the treatment with the ErbB-targeting monoclonal antibodies Cetuximab and Herceptin.

Cetuximab is a monoclonal antibody targeted against ErbB1. It is a receptor antagonist, which prevents downstream signalling and nuclear translocation upon receptor binding. Additionally it induces antibody-dependent cellular cytotoxicity (ADCC) as well as downregulation of receptor expression (135-137). The most common toxicities reported are skin toxicities such as acneiform rash (152-155). However, the occurrence of Cetuximab-induced skin toxicities (Cet-ST) has been correlated to treatment outcome, and can be used as an early indicator for treatment efficacy (156). Skin toxicities are not exclusive to Cetuximab, similar results have been obtained with the use of Erlotinib and Gefitinib (small tyrosine kinase inhibitors) (157-159). More severe side effects were seen in a trial in which Cetuximab was combined with chemo-radiotherapy. Side effects included two deaths (one myocardial infarction and one unknown cause). However, these side effects could not conclusively be attributed to Cetuximab (162).

Herceptin is a monoclonal antibody targeted against ErbB2. Similar to Cetuximab, Herceptin is a receptor antagonist. Upon binding to the receptor, Herceptin induces cell cycle arrest, thereby reducing cell proliferation (518). Additionally, it can also induce ADCC and it has been indicated to have an anti-angiogenic effect (519). One major side effect of Herceptin is cardiac toxicity, including congestive heart failure and a lower left ventricular ejection fraction (520, 521). Alcohol intake during treatment (≥10 drinks per week) and the ErbB2 Ile/Val single nucleotide polymorphism are associated with a significantly higher risk of developing cardiac toxicity (522, 523). However, the cardiac toxicity induced by Herceptin seems to be reversible (524). Patients recovered after drug withdrawal (525, 526). Recently, a case report on the occurrence of severe neutropenia (grade 3) and oral stomatitis (grade 4) has been described in the treatment of breast cancer with Herceptin (527).

3.1.3 'On-Target'-Toxicities in CAR-mediated Adoptive Cell Therapies

Three reports of 'on-target'-toxicity have been published so far due to CAR-mediated ACT. First, Lamers et al. reported 'on-target'-hepatotoxicity in a trial using CAIX re-targeted T-cells to treat metastatic renal cell carcinoma (242, 366). Carbonic Anhydrase IX is overexpressed in RCC, however most healthy tissues also express low levels of CAIX (528). A total of eleven patients were treated, with and inpatient dose-escalation scheme ranging from 2 x 10^7 to 2 x 10^9 cells IV in combination with subcutaneous IL-2 administration. Four patients developed grade 3-4 hepatotoxicity, leading to cessation of the treatment (366). A liver biopsy of one of the patients revealed discrete cholangitis with T-cell infiltration around the bile ducts. Expression of CAIX on the bile duct epithelial cells was also detected. Although CAR expression in the infiltrated T-cells could not be verified, these data suggest that the toxicity seen was caused by a specific cytotoxicity of CAR^+ T-cells against the $CAIX^+$ bile duct epithelial cells (366). The occurrence of this toxicity in subsequent patients could be prevented by pre-treatment with a low dose (5mg) of the anti-CAIX antibody cG250. A single low dose results in a saturated uptake by the liver cells, protecting them from CAR^+ T-cells. However, it leaves the CAIX expressed on tumour cells available for CAR-mediated cytotoxicity (529, 530). Three patients who received this pre-treatment with cG250 did not develop hepatotoxicity after T-cell treatment (242).

Second, Morgan et al. reported a severe adverse event in response to treatment with ErbB2 re-targeted T-cells. A patient with metastatic colon cancer was treated with a single dose of 1 x 10^{10} cells (79% CAR^+) IV, after lymphodepletion. Within 15 minutes after T-cell administration the patient developed respiratory distress. Chest X-ray revealed pulmonary oedema. The patients received vasopressors and ventilator support but eventually succumbed to a cardiac arrest. At post mortem examination, high levels of CAR^+ T-cells were detected in the lung and abdominal/mediastinal lymph nodes. It was suggested that the CAR^+ T-cells recognized ErbB2 expressed by healthy lung tissue/ endothelium, inducing cytokine release, which resulted in a fatal cytokine storm (240). *In vitro*, IFNγ production by CAR^+ T-cells could be induced by a wide range of healthy human cells, including fibroblasts, umbilical vein endothelial cells (HUVEC), bronchial/tracheal epithelial cells (NHBE), prostate epithelial cells (PrEC), skeletal muscle myoblasts (HSMM), keratinocytes, mammary epithelial cells (HMEC) and renal epithelial cells (HRE). However, these *in vitro* analyses were not

performed until after the occurrence of the SAE. Prior to the start of the trial, safety considerations were based on the use of Herceptin, the lack of toxicity seen in studies immunizing against epitopes of ErbB2 as well as the lack of toxicity seen in the use of autologous anti-ErbB2 T-cell clones in breast cancer treatment (240).

Finally, 'on-target'-toxicity is common with the use of CD19 re-targeted T-cells. Normal human plasma cells also express CD19, and antigen-specific eradication of normal B-cells has been reported in several trials (311, 317, 319, 320, 445, 477, 479). Eradication of the B-cell lineage has been reported to last up to 7 months (latest time-point of follow-up) (319). This eradication results in decreased serum immunoglobulin levels (320). Hypogammaglobulinemia can be treated with IV infusions of IgGs, making B-cell depletion a manageable form of 'on-target'-toxicity (319). Recovery of normal B-cell clones and normal B-cell lymphophoiesis have been reported, alongside restoration of normal hematopoiesis (317). Restoration of normal B-cell clones without recurrence of disease is thought to be due to waning persistence of CAR^+ T-cells (317).

3.1.4 Risk of 'On-Target' Toxicity of T4 Immunotherapy

The previously discussed toxicities which have been reported in response to ErbB-targeted and CAR-mediated therapies raise the concern of which toxicities could be induced by T4 immunotherapy. The combination of two circumstances is required for organs to be at risk of T4-mediated toxicity. First, $T4^+$ T-cells need to migrate into the organ, and second, the organ in question must express one or more ErbB receptors at levels that are amenable to recognition by the T28ζ chimeric antigen receptor. All four ErbB receptors are widely expressed in several major organs (531-536). After intravenous (IV) injection, $T4^+$ T-cell can migrate throughout the whole body via the circulation. Imaging studies have shown that IV injected T-cells initially reside in the lungs and then migrate to the liver, spleen and lymph nodes, gaining access to these sites within the first 24 hours after injection (460). Lung and liver are sites that have previously been affected by profound toxicity in studies of CAR-mediated immunotherapy (240, 242). The experience with ErbB2 re-targeted T-cells also emphasized the importance of adequate pre-clinical safety testing in order to assess the level of potential side effects. In this chapter, experiments investigating the potential occurrence of 'on-target'-toxicity in response to T4 immunotherapy are described. The toxicity is assessed using a SCID/Beige mouse model. There are four

reasons as to why this model was chosen for pre-clinical toxicity assessment. First, the regulatory authorities require safety testing of the therapeutic product (in this case human $T4^+$ T-cells). Second, it is anticipated that the T28ζ CAR will be able to activate human T-cells upon engagement with mouse ErbB receptors. Third, activated human T-cells are able to elicit severe toxicity in mice (537). Finally, trafficking of T-cells after IV administration is similar in mouse and man (460).

3.2 Results

3.2.1 Functionality of the T4 construct

Expression of T4 in T-cells is achieved by transduction using the SFG retroviral vector, which is derived from the MFG vector. Gene expression is driven by the promoter activity of the Moloney murine leukaemia virus (MoMLV) long terminal repeat (LTR) (Figure 3-1). Efficient packaging of SFG-based T4 viral particles is ensured by the presence of the MoMLV packaging signal.

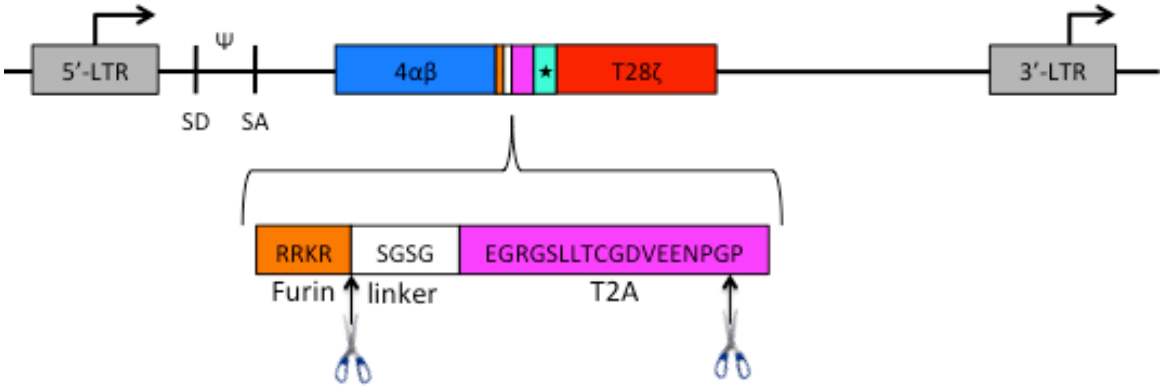

Figure 3-2 Schematic representation of the SFG retroviral vector containing the T4 construct

Schematic representation of the T4 construct in SFG. Co-expression of both 4αβ and T28ζ transgenes under the control of the long terminal repeat (LTR) promoter is achieved using an intervening T2A peptide sequence, which induces a ribosomal 'skip' and therefore misses a peptide bond between the glycine and proline (as indicated by the right scissors). Expression of the T2A peptide sequence at the C-terminus of the mature 4αβ protein is prevented by the presence of a furin cleavage site (as indicated by the left scissors). SD = splice donor site; Ψ = packaging signal; SA = splice acceptor site; ★ = macrophage colony stimulating factor receptor (FMS) leader sequence. *Note: size of the blocks is not representative of the sizes of the individual elements.*

Retroviral transduction of primary human T-cells was achieved using virus produced by the packaging cell line, PG13. Expression of both transgenes was detected on the surface of PG13 cells by flow cytometry, indicating stable gene insertion and protein expression (Figure 3-3). Following retroviral-mediated gene transfer, T-cells were cultured in media supplemented with 30ng/mL IL-4 to allow for selective expansion of the transduced population, acting through the cytokine receptor 4αβ (391). As shown in Figure 3-3 B, selective IL-4-driven expansion of transduced T-cells resulted in the enrichment of an initially small CAR^+ population (day 7) so that it later became dominant within the culture (day 14). Expression of both transgenes was detected on the T-cell surface by flow cytometry (Figure 3-3 B and C). A decrease in the level of CAR

expression was observed over time (as indicated by a decrease in MFI). The LTR promotor within SFG exhibits a low basal transcriptional activity in unstimulated cells. During the *in vitro* expansion, cells are not stimulated, and therefore a downregulation of transgene expression is observed. Besides enrichment of the transduced cell population, expansion of the total cell population was also recorded (see Figure 3-3 D). Viability of the total cell population remained high throughout culture (see Figure 3-3 E).

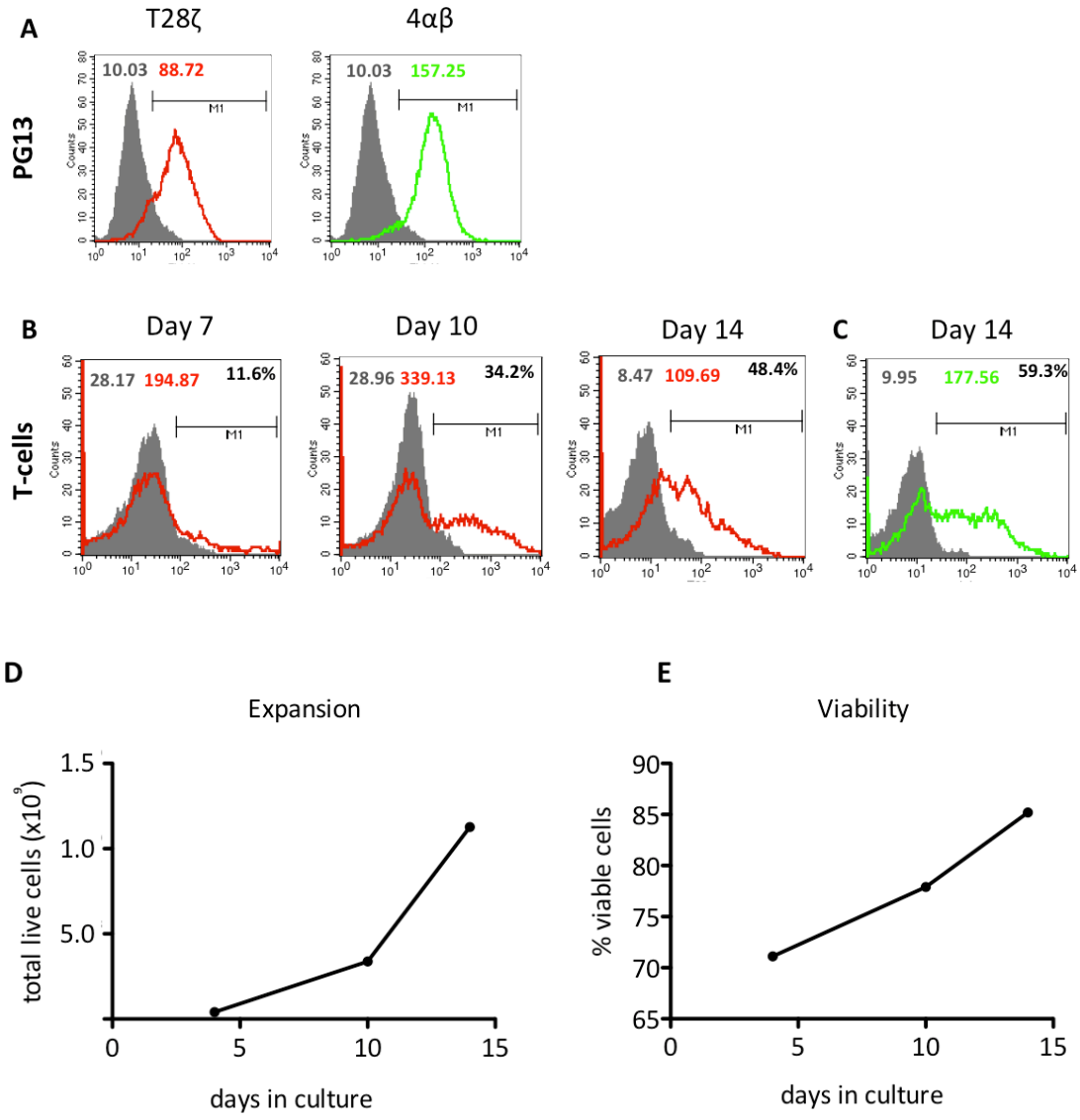

Figure 3-3 T4 expression in PG13 packaging cells and T-cells

A: Expression of T28ζ (open red histogram) and 4αβ (open green histogram) was detected on the surface of PG13 packaging cells using flow cytometry Filled histograms show untransduced PG13 stained with the same protocol. Light grey number represents MFI background staining, coloured number represents MFI receptor stained population. **B:** Expression of T28ζ was detected on the surface of T4-transduced primary human T-cells using flow cytometry (open red histograms). Cells were analysed at multiple days after transduction to determine enrichment of the transduced population in cultured media supplemented with IL-4. Filled histograms show untransduced T-cells stained with the same protocol. Light grey number represents MFI background staining, red number represents MFI T28ζ stained population, black number indicates percentage T28ζ positive cells. **C:** Expression of 4αβ (open

green histogram) on T-cells transduced with T4. To determine expression of 4αβ on day 14 cells were cultured in media supplemented with IL-2 24 hours prior to analysis. Filled histogram shows untransduced T-cells stained with the same protocol. Light grey number represents MFI background staining, red number represents MFI 4αβ stained population, black number indicates percentage 4αβ positive cells. **D**: Expansion of total cell population, live cells were counted on day 4, 10 and 14 during cultured based on trypan blue exclusion of dead cells. **E**: Viability of cells during culture based on live/dead gating on day 4, 10 and 14. Data show one of three similar experiments.

Functionality of $T4^+$ T-cells was investigated by co-cultivation of 1 x 10^6 transduced T-cells with a confluent monolayer of the human head and neck cancer cell line HN3(luc). HN3 cells express high levels of both ErbB1 as well as ErbB2, with low expression of ErbB3 and ErbB4 (Figure 3-4 A), making it a theoretically suitable target for recognition by the T28ζ CAR. Additionally $T4^+$ was co-cultivated with confluent monolayers of the $ErbB^{LO}$ human breast cancer cell line MDA-MB-435 (hereafter referred to as 435), which expresses low levels of ErbB2 and ErbB3 but is negative for ErbB1 and ErbB4 (see Figure 3-4 A). Both cell lines were also co-cultivated with 1 x 10^6 $P4^+$ (the PSMA targeting CAR P28ζ (403) combined with 4αβ) T-cells, or untransduced (UT) T-cells to determine whether tumour monolayer destruction was specific for T28ζ-expressing T-cells. Expression of P4 on PG13 packaging cells as well as expression and expansion of P4 on T-cells is shown in Supplementary Figure 1 in Appendix 2. The HN3 cell line is negative for PSMA and 435 expressed very low levels of PSMA (see Supplementary Figure 2 in Appendix 2), allowing for $P4^+$ T-cells to function as a negative control for $T4^+$ T-cells. Functionality of $P4^+$ T-cells was confirmed by co-cultivation with the $PSMA^+$ human prostate cancer cell line PLP (see Supplementary Figure 3 in Appendix 2).

After 24 hours of co-cultivation, monolayer destruction was quantified using an MTT assay (see Figure 3-4 B). Alternatively, residual tumour cells were visualised by staining with crystal violet (see Figure 3-4 C). This showed that tumour monolayer destruction was specific for the combination of $T28ζ^+$ T-cells co-cultivated with $ErbB^+$ tumour monolayer. Levels of IL-2 and IFNγ in the supernatant were also measured after 24 hours co-cultivation. The presence of increased levels of these cytokines confirm that the interaction between T28ζ and ErbB receptors caused T-cell activation. This finding is consistent with the results of monolayer destruction assay (see Figure 3-4 D). Low levels of IFNγ production in response to co-cultivation with $ErbB^{LO}$ tumour cell line 435 is most likely due to recognition of low expression levels of the ErbB2/3 heterodimer. Production of IFNγ was also detected in co-cultivations of $P4^+$ T-cells with 435, which can be attributed to the low level of target (PSMA) expression.

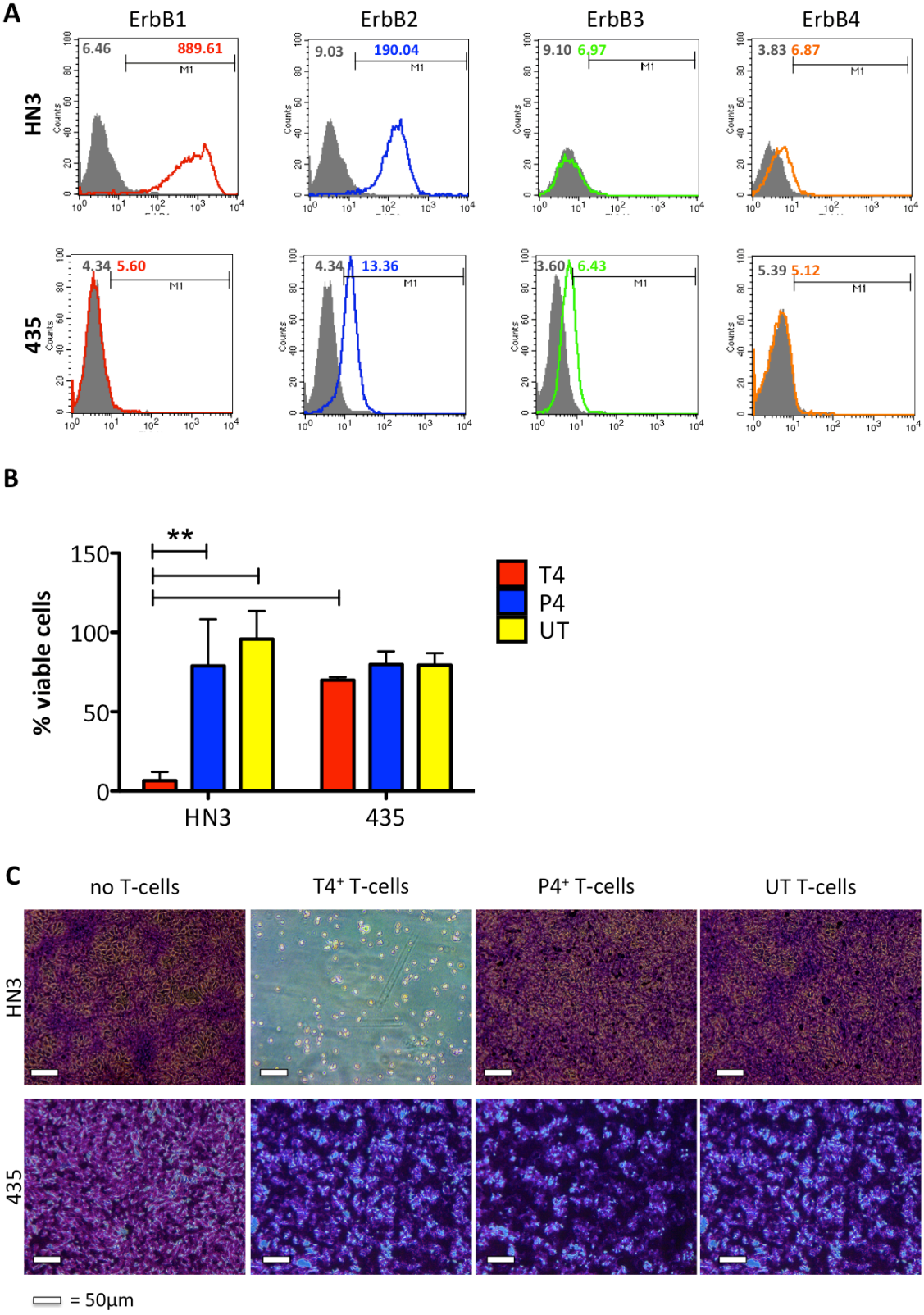
A
ErbB1
ErbB2
ErbB3
ErbB4
HN3
435
6.46
889.61
9.03
190.04
9.10
6.97
3.83
6.87
4.34
5.60
4.34
13.36
3.60
6.43
5.39
5.12
M1
Counts
B
% viable cells
150
100
50
0
**
HN3
435
T4
P4
UT
C
no T-cells
T4+ T-cells
P4+ T-cells
UT T-cells
HN3
435
= 50µm

D

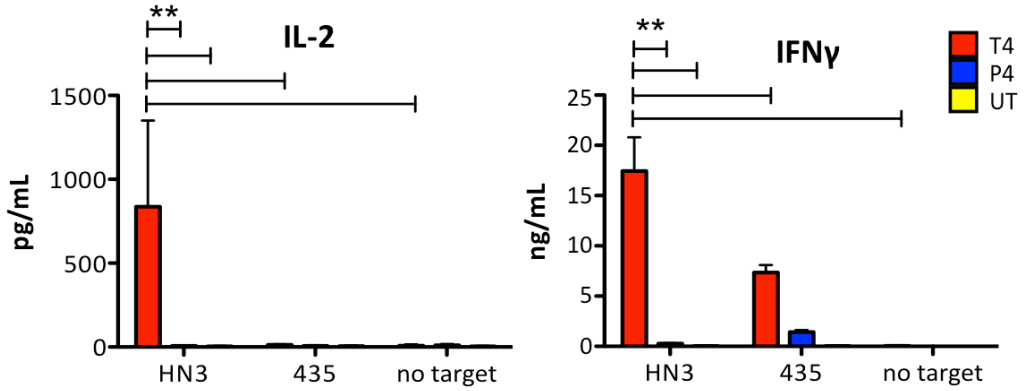

Figure 3-4 T-cell activation through interaction of T28ζ and ErbB receptors

A: ErbB expression on HN3 and MDA-MB-435 tumour cell as determined by flow cytometry. Cells were stained using ICR12 (ErbB1), ICR62 (ErbB2) followed by anti-rat-PE, ErbB3-PerCP (ErbB3) or ErbB4-APC (ErbB4) (open coloured histograms) MFI indicated by coloured number. Expression levels are compared to isotype control stained cells (filled histograms) MFI indicated by grey umber. **B:** MTT assay performed after 24 hours of co-cultivation of 1 x 10^6 $T4^+$ (red bar), $P4^+$ (blue bar) or UT (yellow bar) T-cells. Values were corrected for background level of T-cell cultured without a target monolayer, % viable cells was calculated in comparison to a confluent monolayer, which had not been co-cultivated with T-cells. ** = $p<0.01$ n=3 data show mean ± SD. **C**: Crystal violet staining of remaining monolayers after 24 hour co-cultivation of the indicated tumour monolayer and T-cell population as described in B. **D:** IFNγ and IL-2 production by 1 x 10^6 $T4^+$ T-cells (red bars), $P4^+$ T-cells (blue bars) or UT T-cells (yellow bars) after 24 hours co-cultivation with HN3 or 435 confluent tumour monolayers or without a target monolayer. ** = $p<0.01$ n=6 data show mean ± SD one of 3 similar experiments

3.2.2 Evaluation of Toxicity Risk on Healthy Primary Cells

Primary human cardiac myocytes (HCM) and primary human pulmonary endothelial cells (HPMEC) were examined for expression of the four ErbB receptors using flow cytometry. Both the HCM and HPMEC showed clear expression of ErbB1 and ErbB2, low expression of ErbB3 and no expression of ErbB4 (see Figure 3-5 A).

Based on the ErbB expression profiles of both of these cultured cell types, it was expected that $T4^+$ T-cells would be capable of targeting these cells. To confirm this, HCM and HPMEC were co-cultivated with 1 x 10^6 $T4^+$ or 1 x 10^6 UT T-cells. Crystal violet staining (see Figure 3-5 B) showed that both HCM and HPMEC were destroyed by $T4^+$ T-cells, whereas there was no monolayer destruction when target cells were co-cultivated with UT T-cells. These results suggest that $T4^+$ T-cells were activated through CAR-target interaction, unlike UT T-cells. Activation of $T4^+$ T-cells in these co-cultures was confirmed by measurement of IL-2 and IFNγ in supernatant collected after 24 hours of co-cultivation (see Figure 3-5 C). Remarkable is the higher level of IL-2 production by $T4^+$ T-cells in response to co-cultivation with healthy primary cells compared to tumour cell lines. Various reasons could attribute to this. First, ErbB expression levels are not static and can change during prolonged culture. Downregulation of ErbB receptors by HN3 has been observed during prolonged culture (data not shown), this downregulation can affect the level of T-cell activation and cytokine production. Second, the affinity of the T28ζ CAR is dependent of the formed ErbB dimers. Dimerisation patterns have not been determined in the cell lines, but differences in the expression of ErbB1 homo- and heterodimers and the ErbB2/3 heterodimer can contribute to the level of T-cell activation. Third, endothelial cells have been reported to support the induction of mitogen-induced T-cell activation *in vitro (538)*. Expression of accessory molecules on HPMEC could have attributed to a stronger T-cell activation.

The ErbB expression levels detected on healthy primary cells (Figure 3-5 A), is lower than the expression levels on the tumour cell line HN3luc (Figure 3-4 A). Higher ErbB expression levels on tumour tissue could give the $T4^+$ T-cells a higher activation stimulus, and increase affinity for tumour tissue compared to healthy tissue.

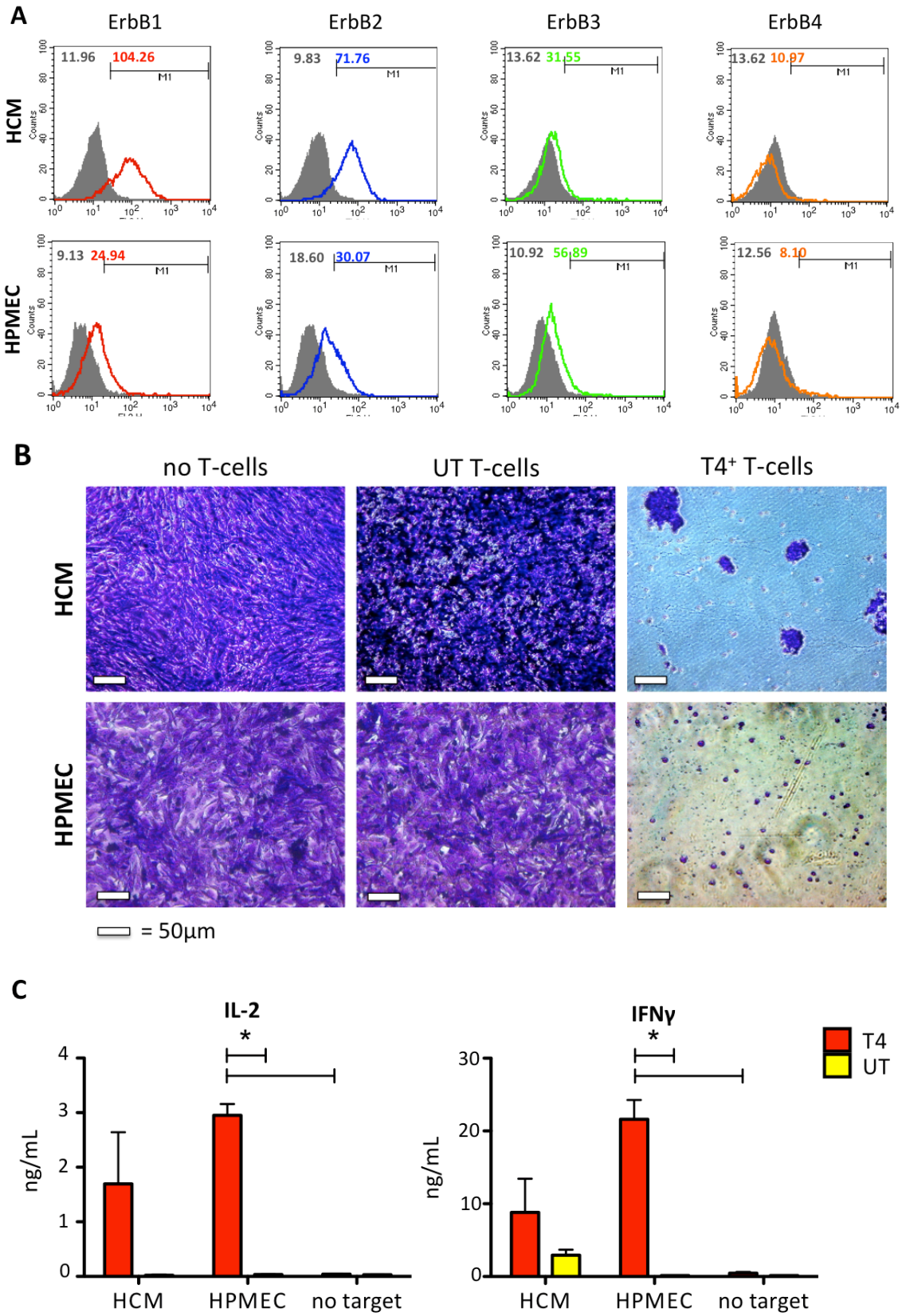
A
ErbB1
ErbB2
ErbB3
ErbB4
HCM
HPMEC
11.96 104.26
9.83 71.76
13.62 31.55
13.62 10.87
9.13 24.94
18.60 30.07
10.92 56.89
12.56 8.10
M1
Counts
B
no T-cells
UT T-cells
T4+ T-cells
HCM
HPMEC
= 50µm
C
IL-2
IFNγ
*
ng/mL
T4
UT
HCM
HPMEC
no target

Figure 3-5 $T4^+$ T-cell activation by HCM and HPMEC

A: ErbB expression (open coloured histograms, MFI indicated by coloured number) by HCM and HPMEC was determined using flow cytometry. Expression is compared to cells stained with isotype control (closed grey histograms, MFI indicated by grey number). Cells were stained as described in Figure 3-4 A. **B:** A confluent monolayer of the indicated cell lines (24 well dish) were co-cultivated for 24 hours with 1 x 10^6 $T4^+$ T-cells, a similar number of UT T-cells or without T-cells as control. Medium and non-adherent cells were then removed and residual monolayers fixed and stained using crystal violet. **C:** IFNγ and IL-2 production by 1 x 10^6 $T4^+$ (red bars) or UT (yellow bars) T-cells after co-cultivation as described in B. Data shows mean ± SD of 3 replicates. * = $p<0.001$ compared to T-cells without a target and compared to UT T-cells on the same target (HPMEC).

3.2.3 *In Vivo* Subcutaneous Growth of HN3luc

In order to develop an *in vivo* model to test T4 immunotherapy, the ability of the human tumour cell line HN3luc to grow subcutaneously in SCID Beige mice was determined. Subcutaneous tumour growth would allow for testing of efficacy and safety of T4 immunotherapy, delivered using the intra-tumoural or alternative routes.

Animals were injected with 5 x 10^6 HN3luc tumour cells in Matrigel in the left flank. Matrigel is a reconstituted basement membrane extract, which is reported to enhance tumour growth (539, 540). Tumours were grown over a period of 56 days and size was measured at regular intervals. Additionally, the weight and clinical status of the animals was monitored to eliminate the possibility that tumour progression resulted in significant distress to the animals. As shown in Figure 3-6 A, the weight of the animals remained stable throughout the entire study, suggesting that subcutaneous tumour growth is not detrimental to overall health over this time period. Tumour growth was monitored using caliper measurements (Figure 3-6 B) and BLI (Figure 3-6 C). Tumours showed exponential growth over time. However, substantial variability between animals was observed.

To determine whether HN3luc cells retain their ErbB expression during subcutaneous growth, tumours were harvested and homogenised. ErbB expression was analysed using flow cytometry (Figure 3-6 D). Cells were stained using ICR12 (ErbB1), ICR62 (ErbB2) followed by anti-rat-PE, ErbB3-PerCP (ErbB3) or ErbB4-APC (ErbB4). Expression levels were compared to isotype control stained cells. Tumours retained expression of ErbB receptors when grown as subcutaneous xenografts. Expression of ErbB1 and ErbB2 was still present, although levels were decreased compared to *in vitro* culture. ErbB3 expression remained negative and ErbB4 expression remained low. The demonstration that HN3luc cells exhibit *in vivo* growth

with retention of ErbB expression suggested that subcutaneous HN3luc tumours can be used to test intra-tumoural T4 immunotherapy treatment in mice.

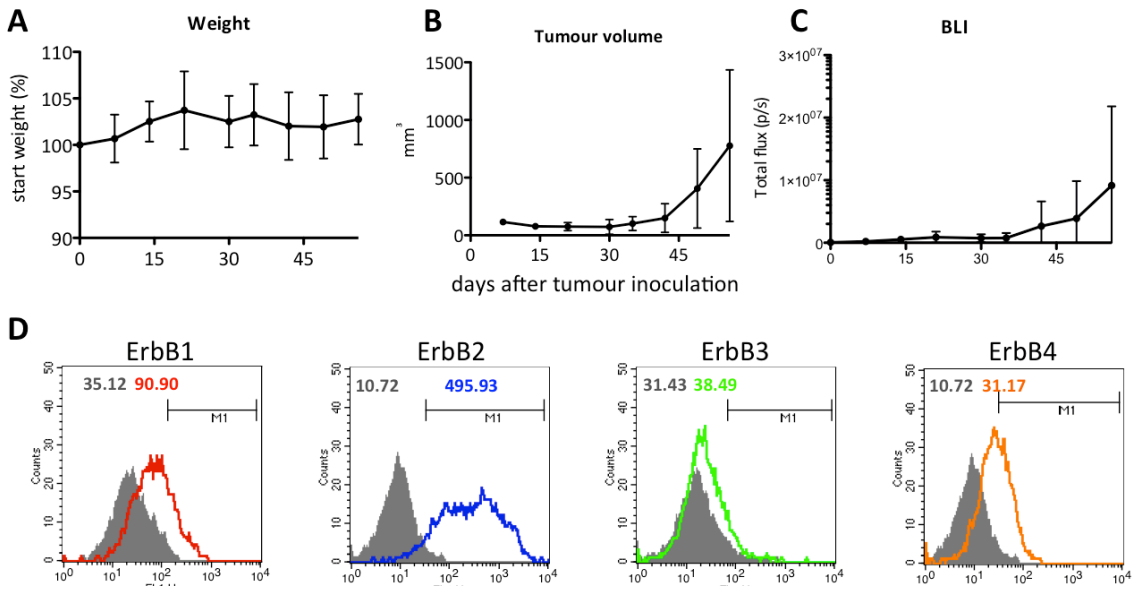

Figure 3-6 HN3luc growth subcutaneous in SCID/Beige mice

Animals were injected subcutaneously in the left flank with 5 x 10^6 HN3luc tumour cells in 200µL matrigel. **A:** Sequential weight measurements over the duration of *in vivo* tumour growth. Weight change is expressed as relative change compared to start of the study (start weight equals 100%) **B:** Tumour volume based on sequential caliper measurements. Volume is calculated based on: volume = (length x width^2)/2. **C:** Tumour growth based on sequential bioluminescent imaging (total flux). Data in panels A to C show mean ± SD of 10 mice. **D:** ErbB expression (open coloured histograms, MFI indicated by coloured number) as determined by flow cytometry of resected subcutaneous tumour. Filled histograms show isotype control stained cells, MFI indicated by grey number. Samples were stained as described in Figure 3-4. Data are representative of three separate tumours, all of which yielded similar results.

3.2.4 Activation of $T4^+$ T-cells by Mouse ErbB Receptors

The results shown in Figure 3-5 raise concerns that cardiac- and pulmonary endothelial toxicity may be elicited by T4 immunotherapy. However, there are substantial differences between the conditions *in vitro* and *in vivo*. This possible toxicity can only be induced if the T-cells migrate into these organs to interact with the ErbB receptors expressed on the cell surface. An animal model is required to determine whether this migration and interaction occurs. To decide whether a mouse model would be suitable for this purpose, it has to be shown that human T-cells expressing human T4 can be activated by mouse ErbB receptors. To test this, the mouse HNSCC tumour cell line B7E3 was selected. The ErbB expression profile of B7E3 was tested using flow cytometry (Figure 3-7). B7E3 showed intermediate expression of ErbB1, no ErbB2 expression and low expression of ErbB3 and 4 (see Figure 3-7). If the human T-cells expressing human T28ζ can be activated by mouse ErbB receptors, exposure of human $T4^+$ T-cells to these mouse tumour cell lines should induce T-cell activation, tumour cell destruction and cytokine production.

To allow for a comparison of the ErbB expression levels on mouse tumours with the human tumour cell line HN3, HN3 was stained using the same intracellular staining protocol. The levels of ErbB1, ErbB2 and ErbB3 expression are higher on HN3 compared to B7E3, both in regard to the increase in measured MFI compared to control stained cells, as well as the proportion of cells positive for the receptors. The level of ErbB4 expression is higher on B7E3. However, because T28ζ has very low affinity for ErbB4, differences in expression level of this receptor are very unlikely to contribute to differences in efficacy (Figure 3-7). Both cell lines are negative for PSMA (Supplementary Figure 2 in Appendix 2).

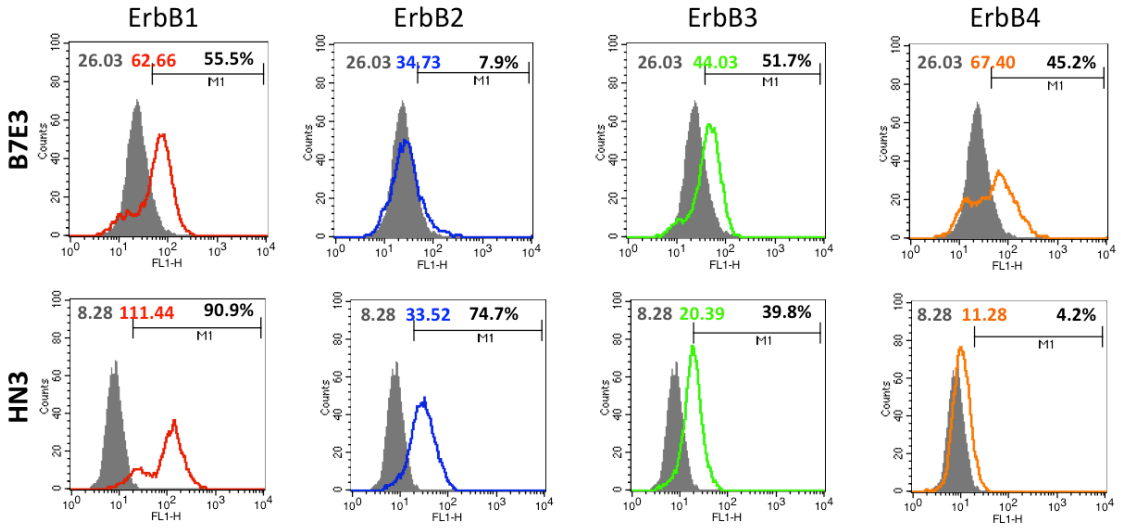

Figure 3-7 ErbB expression profiles mouse and human tumour cell lines

ErbB expression on the mouse tumour cell line B7E3 and the human tumour cell line HN3luc, was detected by flow cytometry after intracellular staining using the same rabbit polyclonal ErbB-specific antibodies followed by sheep anti-rabbit-FITC (coloured open histograms), MFI represented in coloured number. Grey solid histograms represent background staining (rabbit serum followed by sheep anti-rabbit-FITC) MFI represented in grey number. Black number indicates percentage of cells positive for the ErbB receptor of interest. Data are representative of n=5 (B7E3) and n=2 (HN3) independent experiments.

Co-cultivation of 1 x 10^6 human $T4^+$, $P4^+$ or UT T-cells with confluent B7E3 monolayers resulted in T28ζ-specific monolayer destruction (see Figure 3-8 A and B). Consistent with monolayer destruction, cytokine production (IL-2 and IFNγ) were also only produced in co-cultivation of $T4^+$ T-cells with B7E3 (see Figure 3-8 C). The level of IL-2 produced in response to B7E3 is similar as to the level produced in response to exposure to HN3 (see Figure 3-4 D). However, the level of IFNγ produced is significantly higher ($p<0.001$) in response to HN3 compared to B7E3. This lower level of IFNγ production could indicate a lower level of activation in response to mouse ErbB receptors compared to human ErbB receptors, perhaps because the T1E peptide has a higher affinity for the human ErbB receptors than the mouse ErbB receptors. Alternatively this may reflect differences in interactions between accessory molecules on human T-cells, interacting with human compared to mouse target cells.

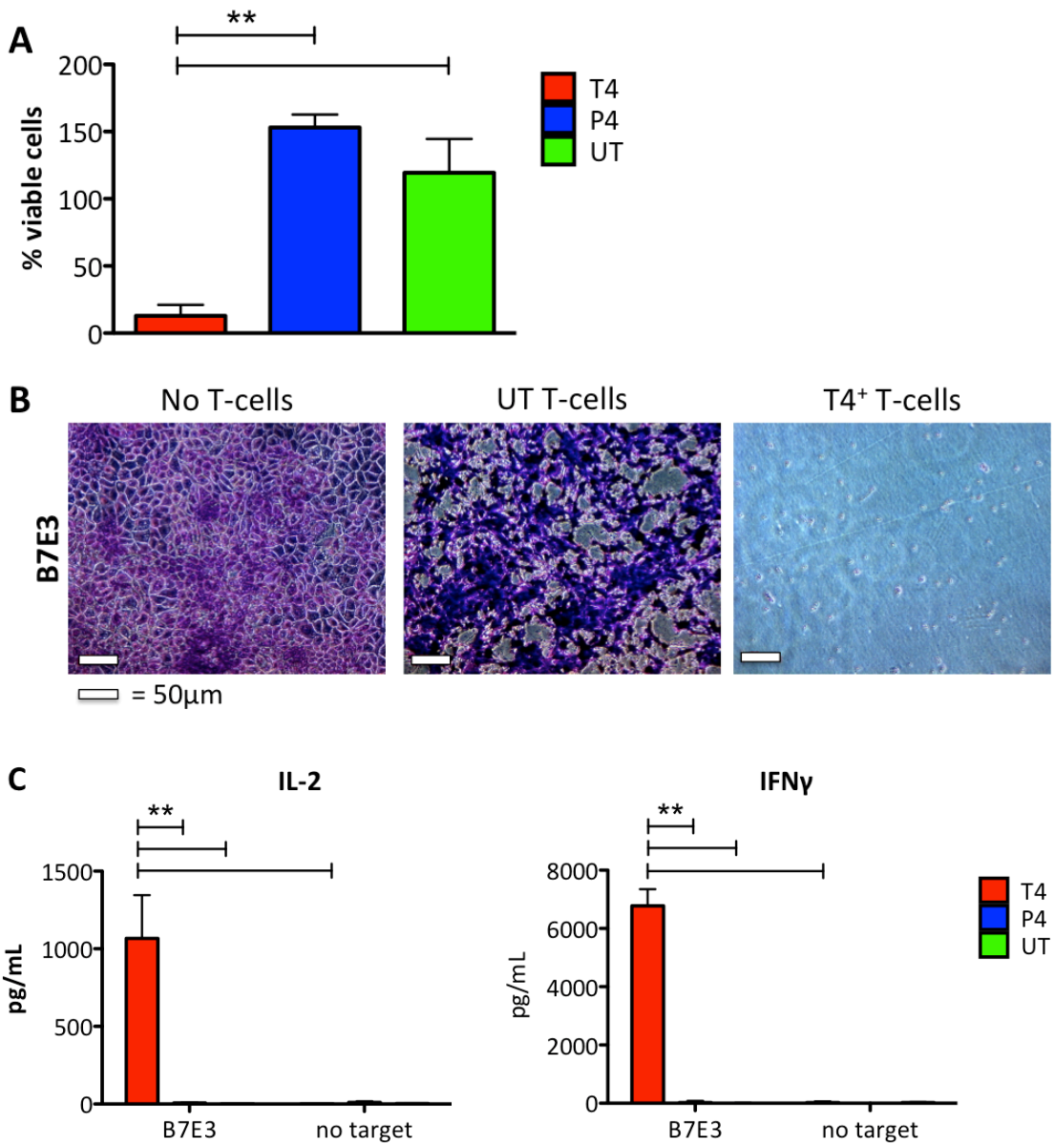

Figure 3-8 Activation of human T4$^+$ T-cells by mouse HNSCC tumour cell line B7E3

T4$^+$, P4$^+$ or UT T-cells (1 x 10^6) were co-cultivated with a confluent monolayer of B7E3 tumour cells (24 well plate) for 24 hours. **A:** The degree of tumour monolayer destruction was quantified with an MTT assay. Results are expressed as % viable cells compared to a confluent monolayer without T-cells. Data represents mean ± SD (n=6). ** = p<0.001 **B:** Residual tumour monolayers were fixed and visualised using crystal violet after 24 hours of co-culture with indicated T-cell population **C:** IL-2 and IFNγ production were measured in the supernatant after 24 hours of co-cultivation. Data shown mean ± SD (n=9). ** = p<0.001.

3.2.5 ErbB Expression in Healthy Mouse Organ Tissue

As described in paragraph 3.2.2, cardiac and endothelial tissue could be at risk to be targeted by $T4^+$ T-cells. To determine which specific organs might be susceptible to T4-mediated toxicity *in vivo*, mouse organs were harvested and tested for ErbB expression using flow cytometry (see Figure 3-9). Organs were harvested from healthy, tumour-free SCID/Beige mice and homogenized. The level of ErbB expression was determined by intracellular staining with rabbit serum and the appropriate polyclonal anti-ErbB1/2/3/4 rabbit IgG, followed by Sheep anti-Rabbit FITC-conjugated secondary antibody. Expression levels were compared to cells stained with rabbit serum alone followed by the Sheep anti-Rabbit FITC-conjugated secondary antibody. ErbB expression was only determined within the live cell population, based on their position within the FFSC/SSC scatter plot. The organs tested for ErbB expression include brain, heart, kidney, liver, lung and intestines.

The strongest T-cell activation through T28ζ can be elicited by ErbB1-containing dimers and the ErbB2/3 heterodimer. Therefore, high expression levels of all these three receptors would place an organ at risk for potential 'on-target' toxicity. Heart, Kidney and Lung tissue all show expression of ErbB1, 2 and 3 in which expression is most pronounced in Heart tissue (see Figure 3-9). Intestinal tissue shows expression of ErbB1 and 2 but is negative for ErbB3 expression. Brain and Liver show low to no expression of ErbB 1, 2 and 3, placing them at a reduced risk for toxicity compared to the other organs. Expression of ErbB4 is detected in all organ tissue, except for Liver tissue. However, because T28ζ has a low affinity for ErbB4 it is unlikely to be of significant influence to the risk of toxicity. Due to different antibody staining protocols, a reliable comparison between ErbB expression on mouse organ tissue and their human equivalents (Figure 3-5) cannot be made.

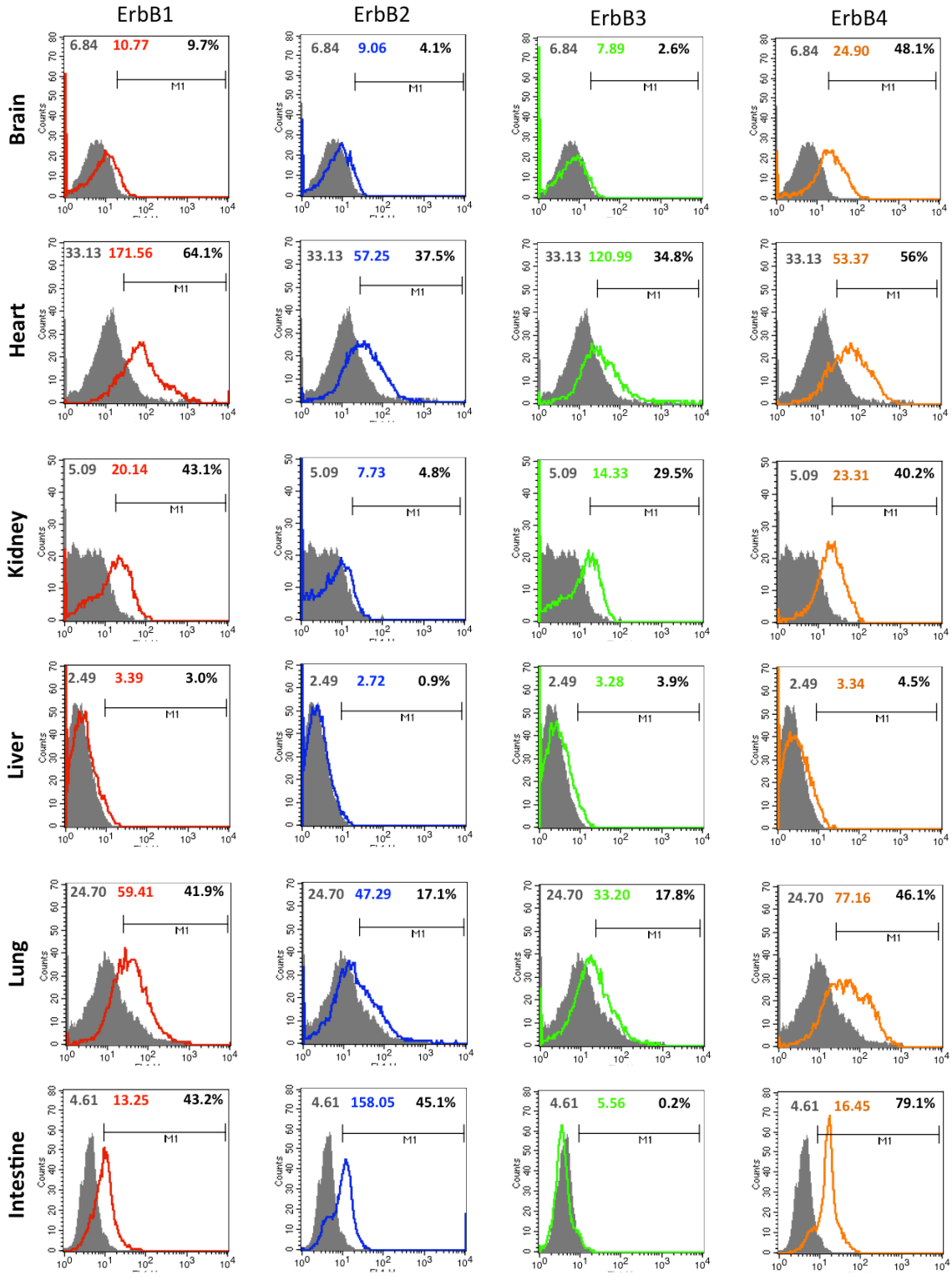

Figure 3-9 ErbB expression in mouse organs

Organs were harvested and homogenised using a cell strainer or electronic homogenizer. ErbB expression profile was tested using intracellular staining and flow cytometry analysis. Coloured open histograms represent ErbB expression (rabbit serum + polyclonal anti-ErbB1/2/3/4 rabbit IgG followed by sheep anti-rabbit-FITC). Grey solid histograms represent background staining (rabbit serum followed by sheep anti-rabbit-FITC). Grey numbers indicate background MFI, coloured numbers indicate MFI or receptor of interest. Percentage of positive cells is indicated in top right corner. Data show one of four similar experiments (except intestine where n=1).

3.2.6 Activation of Human $T4^+$ T-cells by Primary Mouse Pulmonary Endothelial Cells

To determine whether the ErbB expression levels on mouse primary healthy tissue is also sufficient to induce activation of human $T4^+$ T-cells, 1 x 10^6 $T4^+$ (or control T-cells) were co-cultivated with confluent monolayers of primary mouse pulmonary endothelial cells (MPMEC). The MPMEC express intermediate levels of ErbB1 and ErbB2, low levels of ErbB3 and high levels of ErbB4 (see Figure 3-10 A). This expression pattern is similar to that detected in fresh mouse lung tissue (see Figure 3-9). ErbB expression levels are also similar as on HPMEC, except for the high expression of ErbB4 on MPMEC compared to no expression of ErbB4 on HPMEC (see Figure 3-5 A). Co-cultivation of confluent MPMEC monolayers with 1 x 10^6 $T4^+$, $P4^+$ or UT T-cells resulted in T28ζ-dependent monolayer destruction (see Figure 3-10 B) and cytokine production (see Figure 3-10 C).

These results indicate that the human T1E peptide can cross the species barrier and consequently that human $T4^+$ T-cells can be activated by mouse ErbB receptors. These data support the use of a mouse model to determine the *in vivo* toxicity of T4 immunotherapy, satisfying the requirement of the Medicines and Healthcare products Regulatory Agency (MHRA) for direct testing of the therapeutic product.

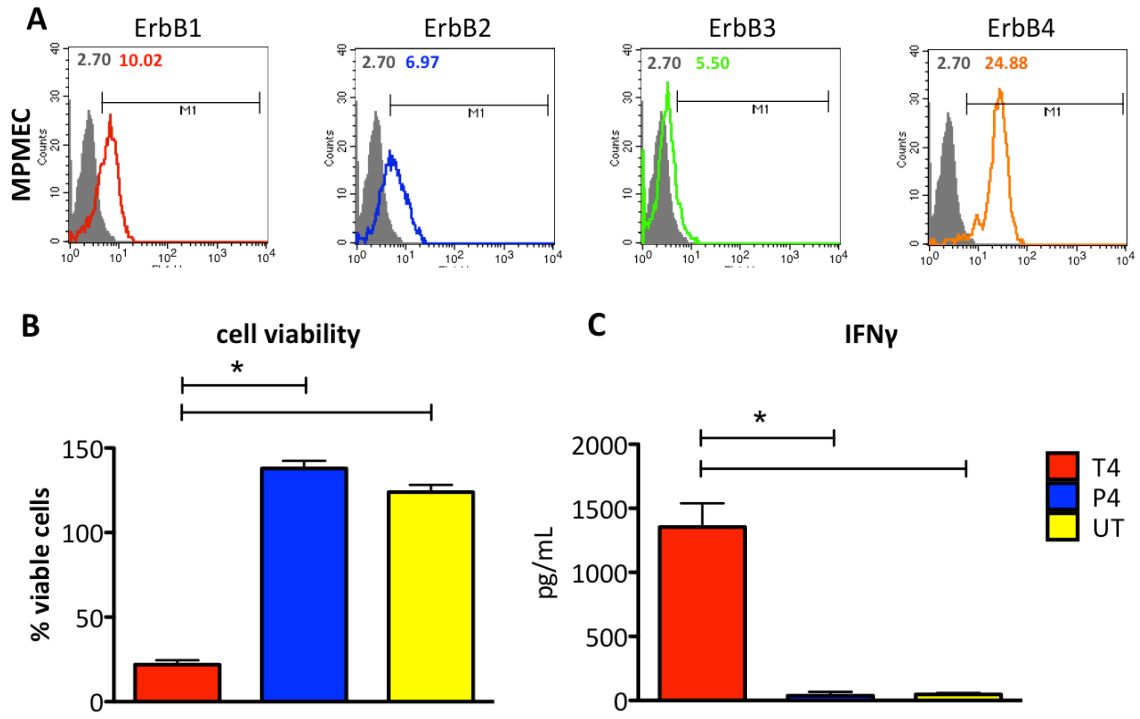

Figure 3-10 Human $T4^+$ T-cell activation by mouse pulmonary microvascular endothelial cells

A: ErbB expression in the mouse pulmonary microvascular endothelial cells was determined by flow cytometry (as described in Figure 3-7) Open coloured histograms represent ErbB expression, coloured number represent MFI stained population, filled histograms represent isotype control staining, grey number represents MFI isotype control population. **B:** 1 x 10^6 $T4^+$, $P4^+$ or UT T-cells were co-cultivated with confluent MPMEC monolayers. After 24 hours monolayer destruction was quantified using an MTT assay. % viable cells were calculated compared to a confluent monolayer without T-cells. Data represents mean ± SD (n=3). *=p<0.001. **C:** IFNγ levels in the supernatant after 24 hours of co-cultivation as described in B. Data represents mean ± SD (n=6). * = p<0.001.

3.2.7 Functionality of T4luc

Toxicity due to the expression of ErbB receptors by healthy tissue (so-called 'on-target toxicity) is a risk for as long as viable $T4^+$ T-cells remain in the body. For this reason, the MHRA directed that *in vivo* toxicity testing of the proposed therapeutic product (eg human $T4^+$ T-cells) should be performed at the time-point when viable $T4^+$ T-cells could no longer be detected *in vivo*. The rationale behind this time-point for toxicity assessment is that toxicity can only occur as long as the medicinal product (in this case the $T4^+$ T-cells) is present in the body, and therefore the experiment can only be terminated when there are no viable $T4^+$ T-cells present anymore. However, assessment of the toxicity at this single timepoint also assumes that any toxicity occurring prior to that endpoint will still be detectable at the pre-determined endpoint. Any mild, reversible, clinically undetectable toxicity will not be detected with this methodology. If any clinically visible toxicity were to occur prior to the endpoint, the experiment would be terminated for human reasons.

To determine the longevity of human $T4^+$ T-cells in a SCID/Beige mouse model, a long-term imaging study was required. To perform this study, a new construct named T4luc was designed (see Figure 3-11). In this construct, T4 is co-expressed with firefly luciferase, allowing for *in vivo* T-cell tracking using bioluminescent imaging. It was assumed that when no luciferase activity could be detected, significant numbers of viable $T4luc^+$ T-cells were no longer present. Consequently, toxicity testing could be performed shortly after this time point, in compliance with MHRA directions. In addition to determining the longevity of the engrafted cells, BLI also allows the investigator to monitor the migration pattern of the cells. Migration patterns could indicate which organs are at risk for toxicity following T-cell delivery using different routes of administration.

Figure 3-11 Schematic representation of the SFG γ-retroviral vector containing the T4luc construct

All three transgenes are expressed under the control of the long terminal repeat (LTR) promoter. This is achieved using two intervening T2A peptide sequences (each placed downstream of a furin cleavage site). Though encoding an identical protein sequence, the DNA sequence of the second furin cleavage and T2A peptide (✤) has been maximally altered from the first through codon "wobbling", in order to minimise the risk of vector instability. SD: splice donor site; Ψ: packaging signal; SA: splice acceptor site; ★: macrophage colony stimulating factor receptor (FMS) leader sequence; ✤: altered T2A peptide sequence. *Note: size of the blocks is not representative of the sizes of the separate elements.*

The T4luc construct was cloned into the SFG γ-retroviral vector. The expression of three separate transgenes under the control of a single promoter was facilitated through the incorporation of two intervening T2A sequences/ furin cleavage sites (Figure 3-11). T-cells were transduced using GALV-enveloped virions produced using the packaging cell line PG13. Validation of PG13 packaging cells prior to T-cell transduction was determined by analysis of transgene expression. Expression of both T28ζ and 4αβ was demonstrated by flow cytometry, while firefly luciferase expression was confirmed using an *in vitro* luciferase assay (Figure 3-12 A and D). Following transduction with the T4luc vector, T-cells were cultured in media supplemented with IL-4. By this means, the $T28\zeta^+$ population could be increased from 4.01% to 47.5% over 8 days, thereby confirming the function of T4luc-encoded 4αβ (Figure 3-12 B). At the end of the 14 day culture period, $CD4^+$ and $CD8^+$ T-cells both contributed to about half of the total population (Figure 3-10 C). Transduced cells did not only expand in proportion within the entire population, but total cell count also increased during culture (Figure 3-10 E). Cell viability decreased between day 10 and 14 of culture (Figure 3-10 F) this is most likely due to the selective pressure of culture in IL-4. The large proportion of dead cells is most likely untransduced T-cells. Firefly luciferase function in T4luc-transduced T-cells was confirmed using an *in vitro* luciferase assay (Figure 3-10 D).

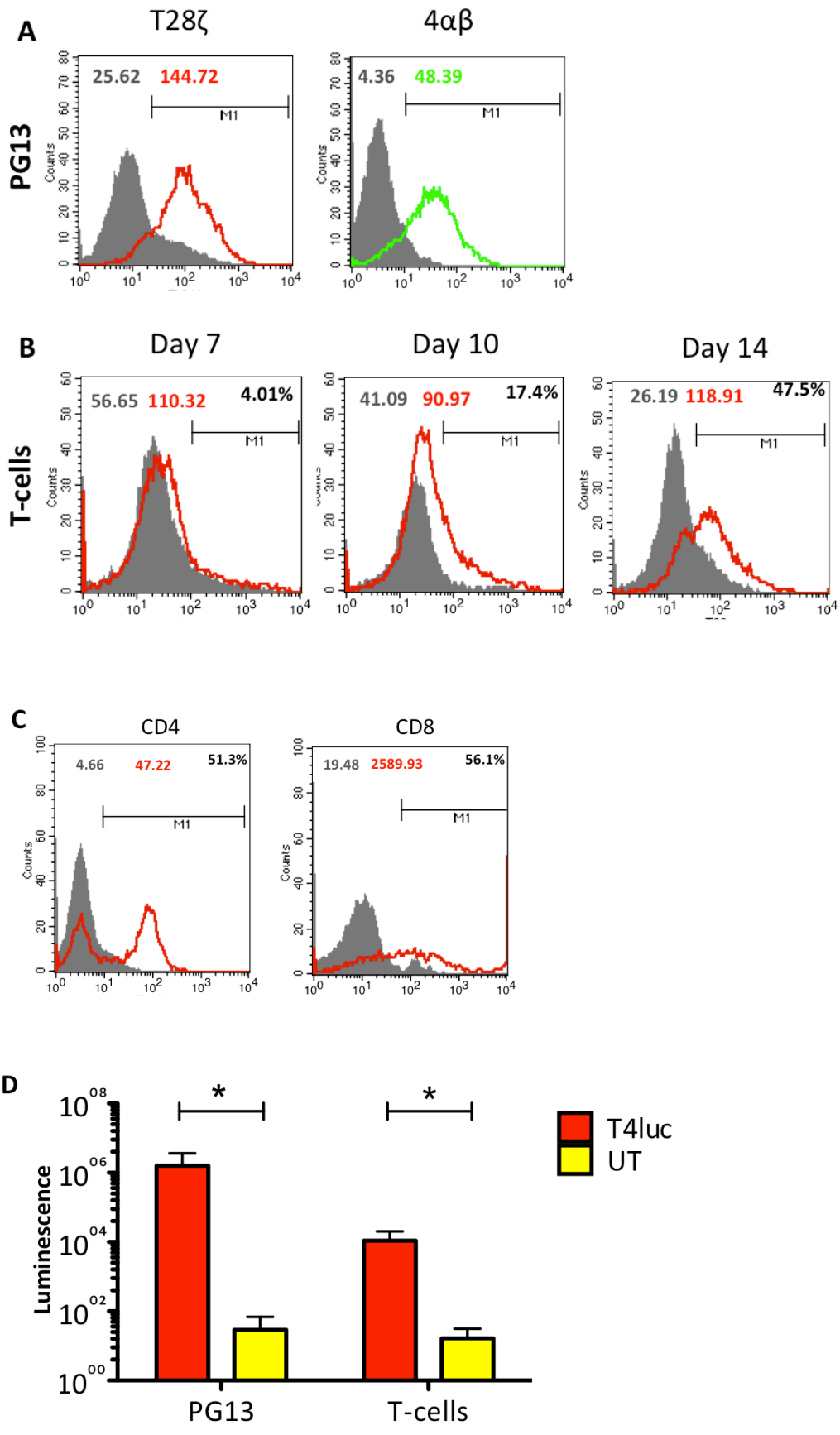
A
T28ζ
4αβ
PG13
25.62
144.72
4.36
48.39
M1
Counts
B
Day 7
Day 10
Day 14
T-cells
56.65
110.32
4.01%
41.09
90.97
17.4%
26.19
118.91
47.5%
C
CD4
CD8
4.66
47.22
51.3%
19.48
2589.93
56.1%
D
Luminescence
T4luc
UT
PG13
T-cells

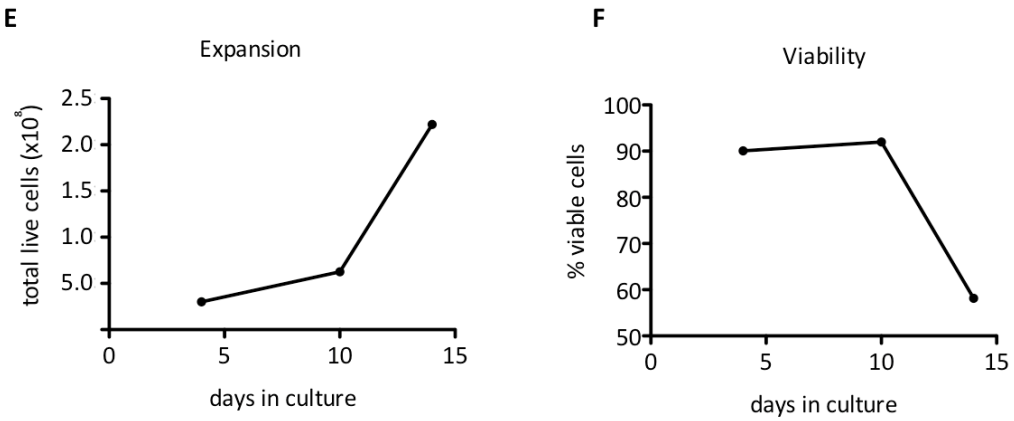

Figure 3-12 T4luc expression in PG13 and T-cells

A: Expression of T28ζ (open red histogram, MFI indicated by red number) and 4αβ (open green histogram, MFI indicated by green number) on the cell surface of PG13 packaging cells using flow cytometry. Expression is compared to untransduced PG13 stained with the same protocol (closed grey histograms, MFI indicated by grey number) **B:** Expression of T28ζ (open red histograms, MFI indicated by red number) on the cell surface of primary human T-cells using flow cytometry. Expression is compared to untransduced cells stained with the same protocol (closed grey histograms, MFI indicated by grey number). Cells were analysed at multiple days after transduction to test for enrichment of the transduced population in media supplemented with IL-4. Proportion of CAR^+ cells indicated by percentage in upper right corner **C:** Proportion of $CD4^+$ and $CD8^+$ T-cells within the entire T-cell population on day 14 of culture. **D:** Activity of firefly luciferase was determined using an *in vitro* luciferase assay. A total of 0.5 x 10^6 cells (T4luc transduced or untransduced cells as control) were lysed and luciferase activity was determined using the FLUOStar Omega plate reader (mean $\pm$ SD of n=3). * = $p < 0.05$ of T4luc transduced cells compared to matched untransduced cells. **E**: Expansion of total cell population, live cells were counted on day 4, 10 and 14 during cultured based on trypan blue exclusion of dead cells. **F**: Viability of cells during culture based on live/dead gating on day 4, 10 and 14.

Functionality of T28ζ in T4luc was confirmed by co-cultivation of 1 x 10^6 $T4luc^+$ T-cells with human (HN3 and 435) and mouse (B7E3) tumour monolayers. Monolayer destruction and cytokine production were both monitored. $T4luc^+$ T-cells destroyed both $ErbB^+$ human (HN3) and $ErbB^+$ mouse (B7E3) monolayers, but left the $ErbB^{LO}$ human monolayer 435 intact (see Figure 3-13 A). Untransduced T-cells did not affect any of the monolayers, as predicted. Cytokine production (see Figure 3-13 B) by activated $T4luc^+$ T-cells was consistently low. Interleukin-2 production was not significantly higher in co-cultivations of $T4luc^+$ T-cells with $ErbB^+$ monolayers compared to any of the controls. Interferon-γ levels were significantly higher in co-cultivations of $T4luc^+$ T-cells with HN3 compared to co-cultivation with other targets (see Figure 3-13 B).

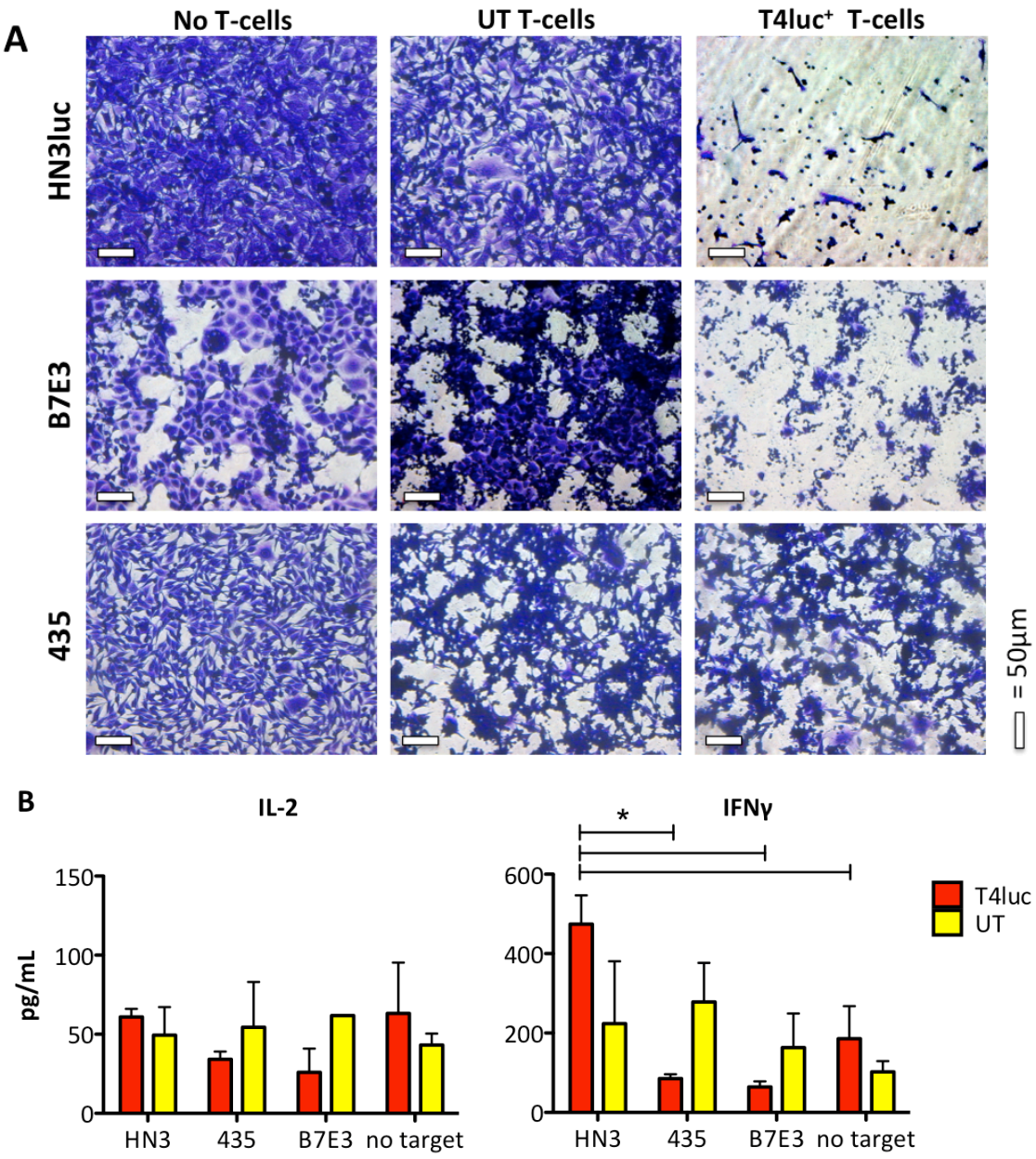

Figure 3-13 T4luc functionality *in vitro*

A: 1 x 10^6 T4luc$^+$ T-cells or UT T-cells were co-cultivated with confluent monolayers of the ErbB$^+$ human tumour cell line HN3luc, the ErbB$^+$ mouse tumour cell line B7E3 or the ErbB^{LO} human tumour cell line 435 for 24 hours. Residual tumour monolayer was visualised using crystal violet staining.), **B:** IL-2 and IFNγ was measured in supernatants collected from the indicated T-cell / tumour cell monolayer co-cultivations after 24 hours of co-cultivation. Data shows mean ± SD (n=3) from one of two similar experiments. * = $p<0.05$.

Collectively, these *in vitro* data confirm the functionality of all three transgenes encoded by T4luc. However, transduction efficiency, rates of CAR positivity, IL-4-mediated enrichment of the CAR^+ population and CAR functionality were consistently lower in cells transduced with T4luc compared to T4. Expression of all three transgenes by a single LTR driven promoter is likely to account for the decrease in expression level and functionality of each of the transgenes. However, the main purpose of the T4luc construct was to permit serial *in vivo* imaging of T-cells that co-express the T28ζ and 4αβ transgenes. Consequently, such experiments were undertaken in tumour-bearing mice.

3.2.8 *In Vivo* Imaging of $T4luc^+$ T-cells in Mice bearing HN3 Tumour Xenografts

To determine the longevity of transduced human T-cells *in vivo*, SCID/Beige mice bearing subcutaneous HN3 head and neck tumours were treated with T4luc transduced T-cells. Tumours were included in the experimental design to account for the possible effect of ErbB-T28ζ interaction on T-cell proliferation as well as to determine whether the T-cells migrated towards the tumour. An imaging gene was not included in HN3 cells since the resultant tumours could be visualised directly, allowing for imaging of $T4luc^+$ T-cells using BLI. Both male and female mice were included in the experiment to account for possible gender differences.

T-cells were activated using CD3/CD28-coated paramagnetic beads and, following transduction, were expanded in IL-4 for a period of 11 days. Expanded $T4luc^+$ T-cells were administered using either the intravenous or peri-tumoural (PT) routes (in proximity to the tumour site), as summarised in Table 3-1. Control mice received no T-cells. Thereafter, animals were analysed by BLI on days 1, 2, 5, 7, 9 and 12 in order to monitor T-cell distribution and longevity *in vivo*.

Table 3-1 Design of 'T4luc *in vivo* imaging study'

Number Mice	HN3 Tumour cells SC	$T4luc^+$ T-cells IV	$T4luc^+$ T-cells PT
2 male **1 female**	-	-	-
2 male **1 female**	5×10^6	-	-
3 male **3 female**	5×10^6	20×10^6	-
3 male **3 female**	5×10^6	-	20×10^6

Figure 3-14 A and B show serial images obtained from one representative animal of each gender, following IV or PT administration of T4luc$^+$ T-cells. Pooled data from all animals are shown in Figure 3-14 C. These data demonstrate that infused T4luc$^+$ T-cells became undetectable after day 5, with no secondary rebound observed over the ensuing 7 days. The small residual signal seen in animals following IV treatment was similar to that seen in untreated animals, indicating that it is non-specific in nature (Figure 3-14 C).

When looking at the T-cell migration patterns, clear differences can be seen between the two injection routes. Directly after IV injection (Figure 3-14 A), T-cells can be detected throughout the entire body, with the highest signal detected in the area of the lungs. After 24 hours (day 1) the signal has clearly decreased, and focuses on the liver/intestine area and around the site of injection in the tail vein. After 48 hours (day 2) the detectable signal and pattern have reduced similar to the signal detected in untreated animals. No clear homing towards the SC tumour site could be detected. No difference was seen between male and female animals.

Animals treated PT (Figure 3-14 B) show a completely different migration pattern compared to the IV treated animals. T-cells were injected SC in close proximity to the tumour site, and imaged at the same time-points as the IV treated animals. Imaging revealed that the PT injected T4luc$^+$ T-cells resided at the site of injection and did not migrate throughout the rest of the body. Similarly as seen in the IV treated animals, the signal decreased over time and had reduced to background level five days after T-cell injection.

The weight of the animals was monitored throughout the entire duration of the experiment (Figure 3-14 D). Animals in all groups showed no changes in weight in response to tumour inoculation, nor in response to T-cell injection.

The T-cell migration patterns seen with the bioluminescence imaging correspond with results previously reported by our group using 111-indium-labelled T4$^+$ T-cells, which were imaged using single photon emission computed tomography (SPECT)-CT (460).

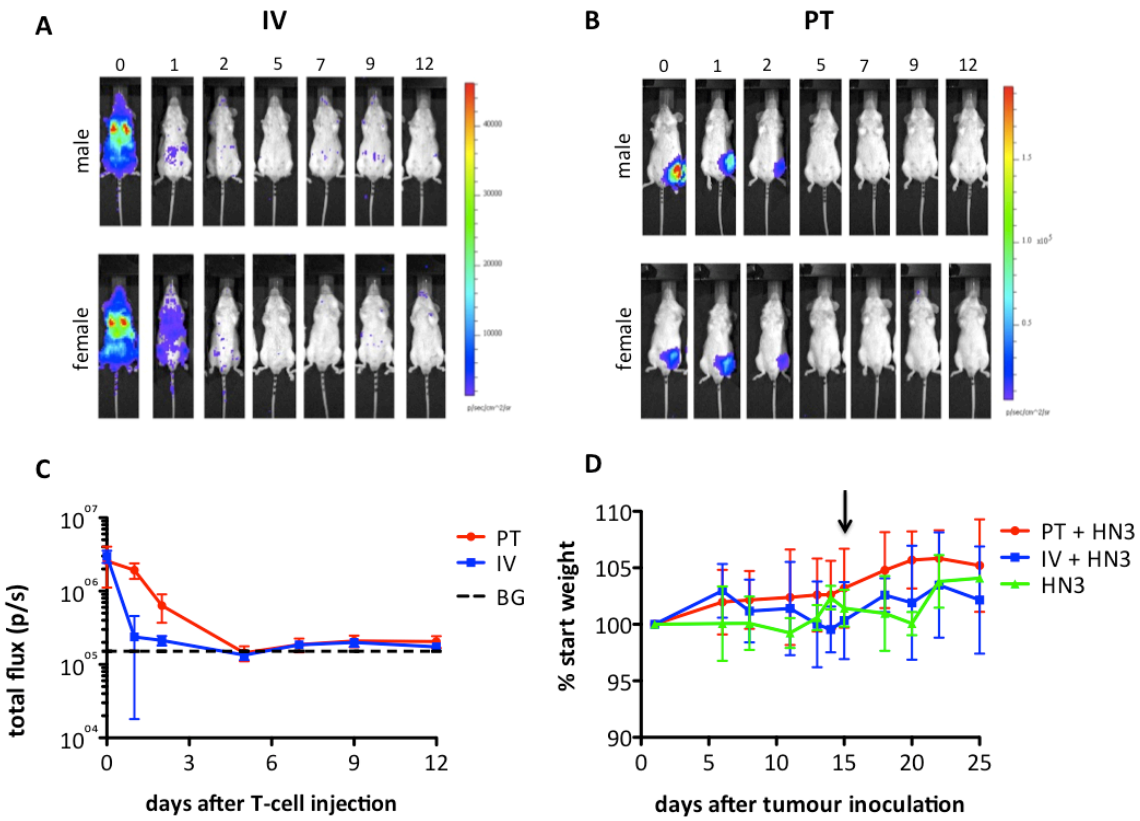

Figure 3-14 *In vivo* bioluminescence imaging of T4luc$^+$ T-cells
Animals received 5 x 10^6 HN3 tumour cells SC in 200µL PBS and tumours were allowed to grow over a time period of two weeks prior to T-cell administration. **A:** Bioluminescent imaging of 20 x 10^6 T4luc$^+$ T-cells after IV administration. One representative animal of three per gender is shown. (exposure time = 3min, field of view = 20, binning = 4) **B:** BLI imaging of 20 x 10^6 T4luc$^+$ T-cells injected PT. One representative animal of three per gender is shown. (exposure time = 3min, field of view = 20, binning = 4) **C**: Quantification of BLI signal, black dotted line represents background (BG) seen in untreated animal. Data shown mean ± SD for n=6 (except for BG where n=3). **D:** weight as monitored over the entire duration of the study, black arrow indicates the timepoint of T-cell injection. Data shown mean ± SD for n=6 (except for HN3 alone where n=3)

3.2.9 Pre-Clinical Toxicity Study *(in vitro)*

The MHRA required pre-clinical toxicity assessment using the exact product described in the investigational medicinal product dossier (IMPD). To address this, a study was planned in which human T4$^+$ T-cells were evaluated for safety in an immunodeficient (SCID/Beige) mouse model. The use of an immunodeficient mouse model was considered appropriate for three major reasons. First, human T-cells are able to elicit severe xenogeneic graft-versus-host toxicity in mice (537). Second, as previously described, human T28ζ$^+$ T-cells can engage with mouse ErbB receptors, resulting in cytokine production and monolayer destruction. ErbB expression levels on both healthy and tumour mouse tissue can elicit T-cell activation (see Figure 3-8 and Figure 3-10). Third, after IV injection, human T-cells migrate similarly in mouse and in man

(460). The capacity of human T-cells to traffic appropriately in SCID/Beige mice provides reassurance concerning the validity of the model for pre-clinical toxicity testing. In particular, the capacity of the cells to accumulate in the lung and liver is important because of previously reported toxicities in these areas (240, 366, 450). The cells were transduced using the GMP-grade vector produced by EUFETS GmbH (batch VR-0042-R-1711). Cells were transduced and cultured according to the most recent clinical batch manufacturing protocol (as described in CHAPTER 5) available. For detailed information regarding the risk of toxicity, the MHRA required extensive histological assessment of the major organs of the mice. The organs required for testing were listed in Annex I of the EMA guideline of repeated dose toxicity (CPMP/SWP/1042/99) (see Figure 3-15).

Imaging studies described in paragraphs 3.2.7 and 3.2.8 indicated that T4luc$^+$ T-cells persisted *in vivo* following IV or peri-tumoural injection for a maximum of five days. As indicated above, MHRA dictated that toxicity induced by T4$^+$ T-cells should be tested at the end of their lifespan *in vivo*. To accommodate for potential batch-variances and low sensitivity of the ffLuc imaging, it was decided to undertake this safety study in organs harvested from mice seven days after T4$^+$ T-cell injection.

In our planned Phase-I clinical trial, we intend to inject T4 immunotherapy using the intra-tumoural route. However, tumour sizes in the mouse model are substantially smaller than in humans, making IT injections challenging. If an IT injection was not feasible, T-cells were injected in a peri-tumoural (PT) distribution to mimic an IT injection as closely as possible. Intravenous injections were also included in the safety study to provide a worst-case scenario of toxicity induced by T4$^+$ T-cells

The T4$^+$ T-cell dose level with which the animals were treated was 20 x 10^6 total T-cells (51% transduced), mimicking a dose level of 5 x 10^9 total cells (2.5 x 10^9 transduced) in humans (for calculation details please refer to Appendix 3). This makes the chosen dose for the toxicity study two fold higher than the dose that would be administered to the patients within the highest dose cohort (1 x 10^9 T4$^+$ T-cells).

To determine the possible toxicity, the general behaviour and body weight of the animals was monitored throughout the study. After termination of the study, all organs were harvested for independent histopathological studies performed by Abbey Vet Services (Newton Abbot, Devon, United Kingdom).

LIST OF TISSUES TO BE STUDIED HISTOLOGICALLY IN A REPEATED DOSE TOXICITY STUDY[a]

Adrenal gland	Pancreas
Aorta	Parathyroid gland
Bone with bone marrow[b]	Peripheral nerve
Brain	Pituitary
Cecum	Prostate
Colon	Salivary gland
Duodenum	Seminal vesicle
Epididymis	Skeletal muscle
Esophagus	Skin
Eye	Spinal cord
Gallbladder	Spleen
Harderian gland	Stomach
Heart	Testis
Ileum	Thymus
Jejunum	Thyroid gland
Kidney	Trachea
Liver	Urinary bladder
Lung	Uterus
Lymph node(s)	Vagina
Mammary gland[c]	Other organs or tissues with gross lesions
Ovary	Tissue masses

a) This tissue list is intended to be a minimum core list that can be used for all types of repeat-dose toxicity and carcinogenicity studies, regardless of route of administration, species or strain of mammalian laboratory animal, duration of study, or class of drug to be tested. It is recommended that the route of administration be considered at the time of study design and that tissues relevant to the route of administration be added to this core list. For example, the addition of nasal cavity and turbinates, larynx, and tracheobronchial lymph nodes may be considered for inclusion in the tissue list for inhalation studies. Likewise, depending upon the species or strain of laboratory animal, the addition of organs or tissues unique to or characteristic of that species or strain may be selected, as appropriate. It is also recommended that additional tissues that are known to be targets of the test article or those of its class be added to this core tissue list.
b) For nonrodents, either rib or sternum. For rodents, femur including articular cartilage.
c) Females only.

Figure 3-15 Annex I of EMA guideline CPMP/SWP/1042/99 'Guideline on repeated dose toxicity'

To perform the toxicity study, blood was derived from a healthy volunteer donor. T-cells were activated using CD3/CD28 beads and cultured over a period of 72 hours prior to transduction. A total of 80 x 10^6 cells were transduced in a Retronectin-coated (5µg/cm^2) 197-AC VueLife Bag, using clinical-grade virus produced by EUFETS (Batch VR-0042-R-1711). After transduction, cultures were propagated based on the GMP-manufacturing process described in CHAPTER 5.

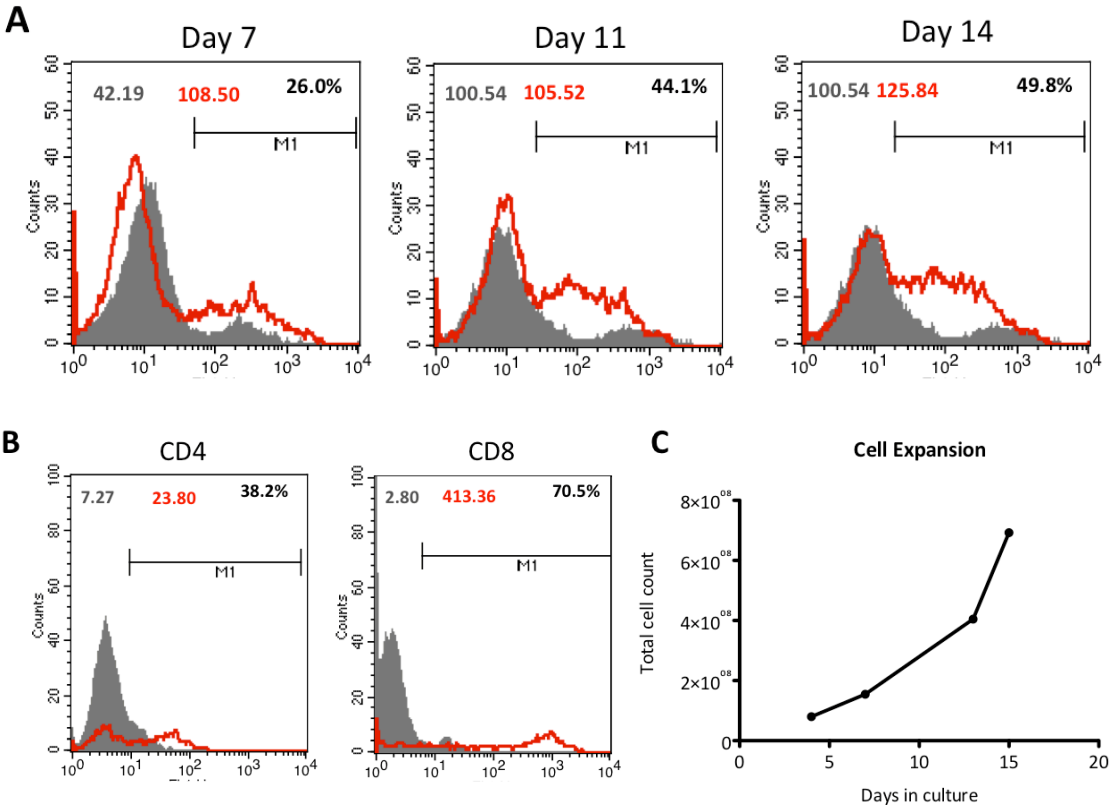
A
Day 7
42.19
108.50
26.0%
M1
Day 11
100.54
105.52
44.1%
M1
Day 14
100.54
125.84
49.8%
M1
Counts
B
CD4
7.27
23.80
38.2%
M1
CD8
2.80
413.36
70.5%
M1
C
Cell Expansion
Total cell count
Days in culture

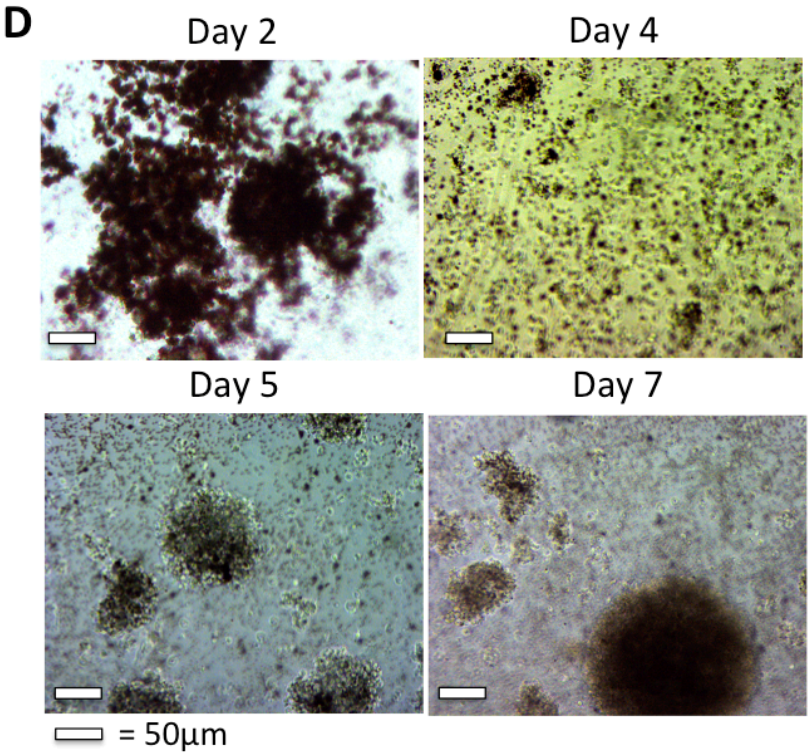
D
Day 2
Day 4
Day 5
Day 7
= 50µm

Figure 3-16 $T4^+$ T-cell enrichment and expansion

A: Enrichment of $T4^+$ population during culture in media supplemented with IL-4, as determined by flow cytometry. Day 7 equals three days after transduction (performed on day 4). Open red histograms shown $T28\zeta^+$ cells, filled histograms represent untransduced cells stained with the same protocol. Grey number indicates background MFI, red number indicates MFI of CAR-stained population. **B:** CD4/CD8 content within the entire cell population on day 15 of culture. **C:** Expansion of total cell population in media supplemented with IL-4 from the day of transduction (day 4) to the final day of culture (day 15) **D:** Micrographs of T-cell during first week of culture, prior to transduction (day 2), at transduction (day 4) and after transduction (day 5 and day 7).

Over the 14 day culture period, the $T4^+$ T-cell population enriched from 26% to ~50% (Figure 3-16 A) and total cell number increased from 80 x 10^6 to 7 x 10^8. This represents a greater than 25 fold expansion of $T4^+$ T-cells (Figure 3-16 C). At the end of the 15 day culture period, CD4:CD8 ratio was approximately 1:2 (Figure 3-16 B). Figure 3-16 D shows micrographs of the T-cells prior to transduction (day 2), immediately after transduction (day 4) and on day 5 and day 7 of culture (the first and third day of IL-4 feeding regimen). Cells looked healthy and activated throughout the entire culture period.

To verify functionality of the $T4^+$ T-cells prior to the *in vivo* study, monolayer destruction and cytokine production were determined (see Figure 3-17). $T4^+$ T-cells were able to destroy HN3 monolayers *in vitro* (Figure 3-17 A). Increased levels of IFNγ production were detected in co-cultivations of $T4^+$ T-cells with HN3 compared to untransduced T-cells or $T4^+$ T-cells alone (Figure 3-17 B).

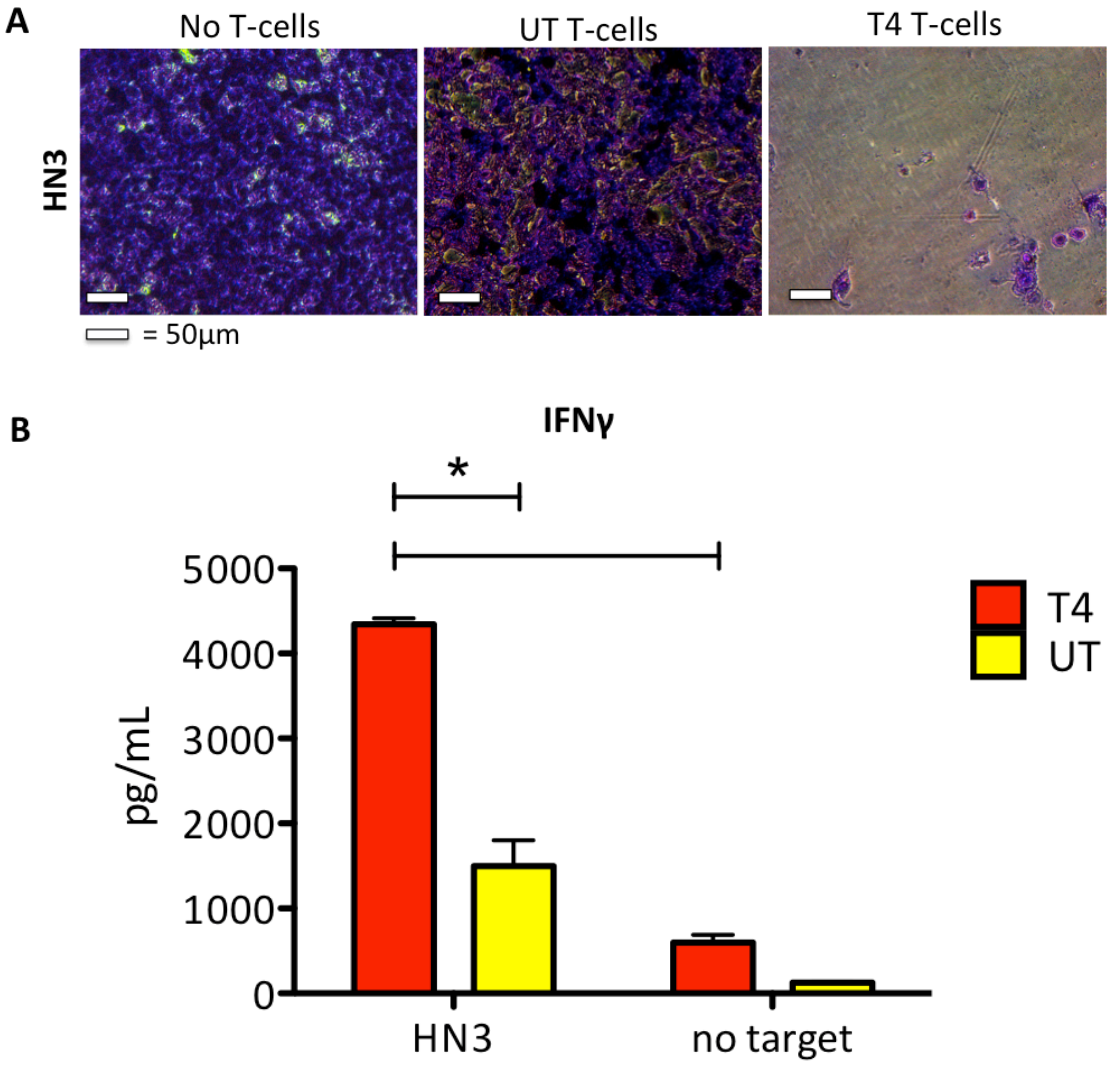

Figure 3-17 *in vitro* T4$^+$ T-cell functionality
A: 1 x 10^6 T4$^+$ or UT T-cells were co-cultivated with a confluent HN3 monolayer for 24 hours. Residual monolayer was visualised using crystal violet staining. **B:** IFNγ production measured after 24 hours of co-cultivation as described in A. Data show mean ± SD of n=3, * = p<0.01.

In the proposed clinical study in which T4 immunotherapy will be tested in patients with HNSCC (please refer to paragraph 5.1), release of the therapeutic cell product is dependent on satisfying several criteria (see Table 3-2). Consequently, where possible, the cells used for toxicity testing were tested for compliance with these release criteria. The final product passed all available release criteria and therefore met the quality requirements necessary for pre-clinical toxicity testing of the cell product.

Table 3-2 Testing of $T4^+$ toxicity cell production against release specifications*

Test	Test Method	Test Limits	T4 toxicity cell product	Comments
Viability	Flow cytometry (DAPI staining)	≥70% viable cells within the lymphocyte gate	84%	Based on live/dead gating**
Cell number	Flow cytometry using Trucount tube technology	≥1 x 10^7 cells.	7 x 10^8 cells - Pass	Trucount was not yet available, trypan blue count used.
Identity	% $T4^+$ cells – stained with appropriate antiserum	≥ 10% $T4^+$ transduced cells	40% - Pass	N/A
Transgene function	Cell count on day 15 divided by cell count on day 4.	At least doubling in cell number achieved in response to culture in IL-4.	8.75 fold increase - Pass	N/A
Sterility	BacT-ALERT & direct inoculation	No growth	Not performed	Test method was not yet in place.
Mycoplasma Culture	Ph. Eur (2.6.7)	No growth	Not performed	Test method was not yet in place.
Residual ClinExVivo bead number	Flow cytometry	<333,000 beads/mL in final product	Not performed	Beads were removed, test method was not yet in place.

* Release specifications were defined in version 2.1 of the Investigational Medicinal Product Dossier pertaining to first in man testing of T4 immunotherapy in patients with HNSCC.
** For gating strategy please refer to Supplementary Figure 4 in Appendix 2.

3.2.10 Pre-Clinical Toxicity Study *(in vivo)*

Mice with 15 day-established subcutaneous tumours were treated with a total of 20 x 10^6 T-cells (of which approximately 51% were $T4^+$). Cells were administered either by IV injection or by direct PT administration. For each route of administration, 3 males and 3 females were treated, as specified in Table 3-3.

Table 3-3 Design of 'T4 toxicity study'

Number Mice	HN3 Tumour cells SC	$T4luc^+$ T-cells IV	$T4luc^+$ T-cells PT
3 males 3 females	7.5 x 10^6	20 x 10^6	-
3 males 3 females	7.5 x 10^6	-	20 x 10^6

Mice were monitored for clinical parameters of toxicity, e.g alterations in behaviour, appearance or weight. No differences were seen between males and females, therefore the data was pooled per route of T-cell administration. No significant changes in behaviour or appearance were observed and mice continued to gain weight over the duration of the study (see Figure 3-18). These findings suggested that no severe toxicity had occurred.

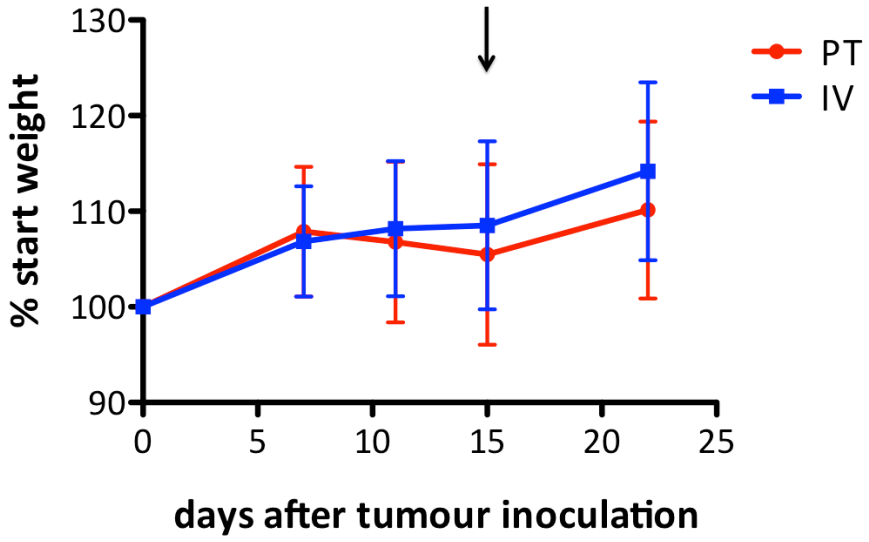

Figure 3-18 Serial weight measurements of PT and IV $T4^+$ treated mice
The weight of the mice was monitored at regular intervals as a primary indicator for toxicity. Mice with 15 day-established tumours were treated with 20 x 10^6 T-cells (as indicated by arrow), either through peri-tumoural (PT, red line) or intravenous (IV, blue line) administration. Data represent mean ± SD of 6 mice (3 male and 3 female). No difference was seen between males and females, data was therefore pooled per injection route.

Functionality of $T4^+$ T-cells is elementary to the ability to detect possible toxicity. To determine functionality *in vivo*, tumour size was monitored using caliper measurements (data not shown) as well as bioluminescent imaging (see Figure 3-19). Based on BLI data, in all animals a significant decrease in tumour size was detected, independent of gender or route of injection, suggesting *in vivo* functionality of the administrated $T4^+$ T-cells.

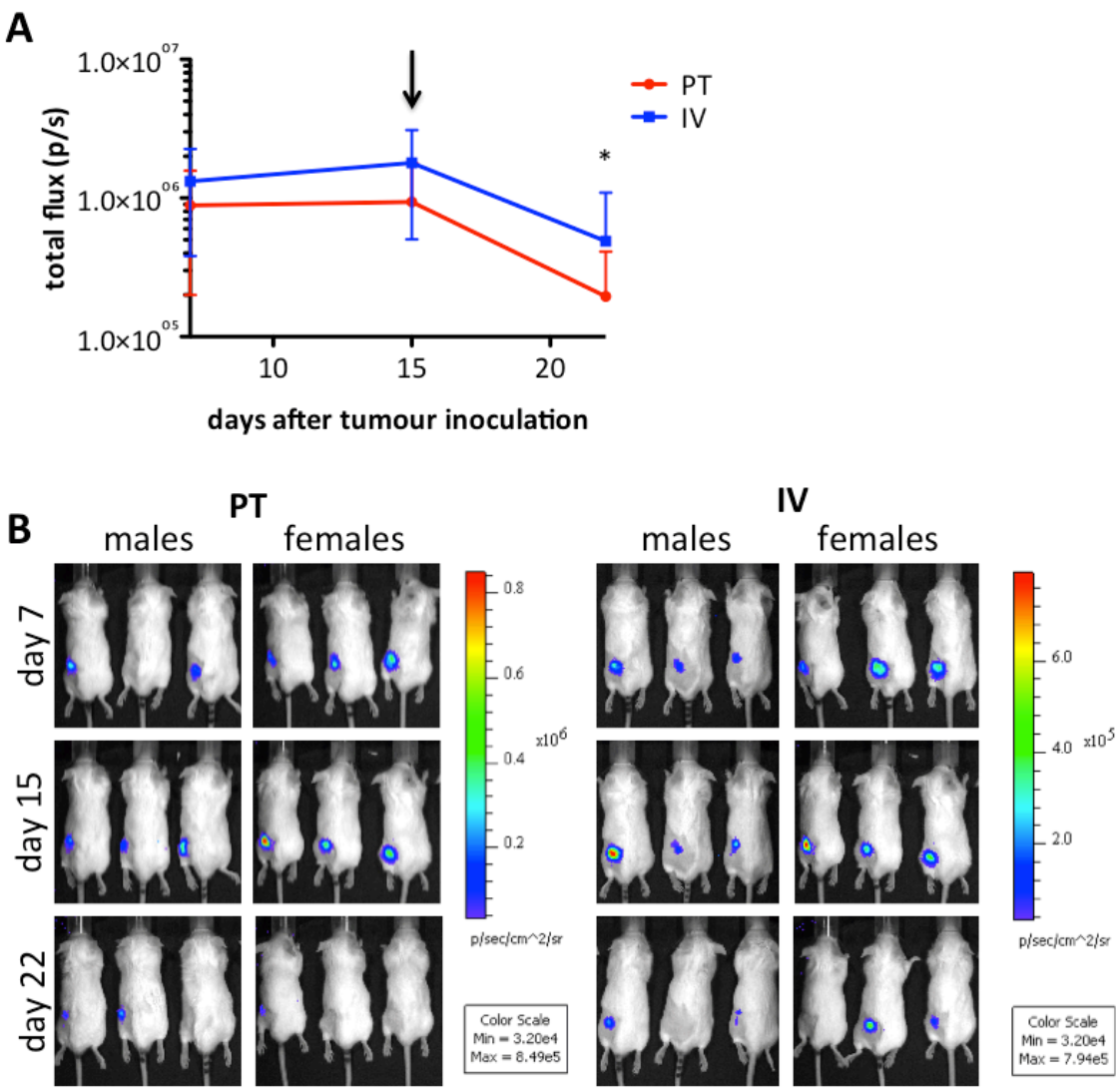

Figure 3-19 Tumour size

Mice received 7.5 x 10^6 HN3luc tumour cells SC in 200uL Matrigel. Mice were treated with 20 x 10^6 T4 transduced T-cells 14 days after tumour inoculation. T-cell administration was performed either via peri-tumoural (PT) or intravenous (IV) routes. **A:** Sequential BLI of tumour size (as total flux (p/s)) prior to (day 7 and day 15) and after (day 22) T-cell administration. T-cells were administered on day 15 as indicated by the arrow. Data represent mean ± SD of n=6 mice. * = $p<0.05$ comparing BLI signal on day 22 with day 15 after IV T-cell administration **B:** Images of all animals indicating tumour size one week prior to T-cell injection (day 7) on the day of T-cell injection (day 15) and a week after T-cell injection (day 22), prior to histopathological analysis.

As described in paragraph 3.2.8, the goal was to analyse toxicity at a timepoint at which there were no more viable T-cells detectable *in vivo.* The organs were harvested, embedded in 10% paraformaldehyde and sent to Abbey Veterinary Services for independent histopathological analysis. Results are summarised in Table 3-4, full reports can be found in Appendix 4. As shown in Table 3-4, no evidence of toxicity or residual T-cells was detected in any of the organs.

Table 3-4 Independent histopathological analysis of organs collected from mice treated with T4 immunotherapy

	IV		SC	
	Male	**Female**	**Male**	**Female**
Cerebellum	NAD*	NAD	NAD	NAD
Cerebrum	NAD	NAD	NAD	NAD
Spinal cord	NAD	NAD	NAD	NAD
Bone marrow	NAD	NAD	NAD	NAD
Cortical bone	NAD	NAD	NAD	NAD
Vertebral muscle	NAD	NAD	NAD	NAD
Heart	NAD	NAD	NAD	NAD
Lung	Mild collapse No inflammation	Moderate collapse No inflammation Moderate patchy thickening alveolar walls	Moderate collapse. Haemosiderophages within wall not in alveolar spaces	Mild collapse
Oesophagus	NAD	NAD	NAD	-
Ovary	-	NAD	-	NAD
Uterus	-	NAD	-	NAD
Salivary gland	NAD	NAD	NAD	NAD
Kidney	NAD	NAD	NAD	NAD
Liver	NAD	NAD	NAD	NAD
Pancreas	NAD	NAD	NAD	NAD
Small intestine	NAD	NAD	NAD	NAD
Large intestine	NAD	NAD	NAD	NAD
Spleen	NAD	NAD	Depleted lymphoid cells	NAD
Stomach	NAD	NAD	NAD	NAD
Lymph node	NAD	-	Severe depletion lymphocytes	NAD
Bronchial lymph node	-	NAD	-	NAD
Lacrimal gland	NAD	-	-	-
Eye	NAD	-	-	-
Testis	NAD	-	NAD	-
Adrenal	NAD	-	-	-

* NAD: No abnormality detected

3.3 Discussion

T4 immunotherapy is a form of adoptive cell therapy in which T-cells are re-targeted against the extended ErbB-receptor family using a chimeric antigen receptor. $T4^+$ T-cells have effectively controlled tumour growth in three separate xenograft tumour models (299, 358). However, ErbB receptor expression is not exclusive to tumour cells. Low level expression on healthy tissue can lead to so-called 'on-target'-toxicity. Toxicity induced by ErbB receptor recognition on healthy lung epithelial cells, and cardiac myocytes has been reported in relation to ErbB targeted therapies (240, 520, 521). A clinical trial using a third generation CAR re-targeting T-cells against ErbB2 has resulted in a serious adverse event, due to a cytokine storm induced by T-cell activation in response to ErbB2 expression in the pulmonary microvasculature and parenchyma (240). These results show the severity of the potential risks of ErbB re-targeted cell therapy and emphasize the need for extensive pre-clinical toxicity assessment. In this chapter the experiments performed to investigate potential 'on-target'-toxicity of T4 immunotherapy have been described.

$T4^+$ T-cells have been shown to be able to selectively enrich in culture supplemented with IL-4 (see Figure 3-3), and have selective cytotoxicity towards $ErbB^+$ tumour cells (HN3) and no activity against $ErbB^{LO}$ tumour cell lines (435) (see Figure 3-4). These results are all in agreement with previously reported extensive functionality assessment of T28ζ and T4 by Dr Davies (299). Targeting of healthy tissue was first determined *in vitro*. Expression of ErbB receptors by primary cardiac monocytes (HCM) and primary human pulmonary microvascular endothelial cells (HPMEC) was determined by flow cytometry. It has previously been reported that ErbB3 is no longer detectable in adult heart tissue, but ErbB1, 2 and 4 are expressed at detectable levels (532). Additionally, ErbB2 is reportedly not overexpressed in cardiomyocytes (541). Flow cytometry analysis of the primary cell lines derived from these tissues confirmed the expression of ErbB1 and 2 and the absence of ErbB3 on HCM. In contrast to earlier results, expression of ErbB4 was not detected by these cells. Expression of ErbB2 in the respiratory tract has also been previously reported (536). Primary HPMEC showed low expression of ErbB1, 2 and 3 but no expression of ErbB4. Co-cultivation of $T4^+$ T-cells with either primary cell type resulted in CAR-mediated monolayer destruction, T-cell activation and cytokine production (see Figure 3-5). These results suggest that T-cells could be activated by ErbB receptors expressed

in the pulmonary microvasculature, which could lead to destruction of the microvascular epithelial cells or the induction of a cytokine storm. Additionally, if T-cells are able to migrate into the heart, cardiotoxicity could be induced.

Intra-tumoural T-cell administration could reduce the risk of pulmonary and cardiac toxicity. We have previously reported that imaging studies showed that T-cell injected subcutaneously reside in the area of injection and do not migrate to the lungs and liver as seen after intravenous injection (460). Therefore, we decided to design a phase I clinical trial in which patients with locally recurrent HNSCC will be treated with escalating doses of $T4^+$ T-cells, delivered using the intra-tumoural route. The risk of 'on-target'-toxicity after intra-tumoural T-cell injection was determined in a pre-clinical mouse model. The human $ErbB^+$ HNSCC cell line HN3(luc) was shown to grow following subcutaneous inoculation in SCID/Beige mice. The resultant tumours retained ErbB expression *in vivo* (see Figure 3-6), providing a model to test intra-tumoural T4 immunotherapy. However, toxicity against healthy tissue can only be determined in mice if human $T4^+$ T-cells can also be activated by mouse ErbB-receptors. This cross-species recognition is expected to occur based on the fact that both human and mouse EGF exert an equimolar capacity to promote eyelid opening in newborn mice (542), augment cytokine production by mouse splenocytes (543), stimulate proliferation of mouse Balb/C 3T3 cells and can inhibit the binding of radiolabelled mouse EGF to mouse ErbB1 (544). Additionally, human TGFα is highly active in promoting bone resorption in mice (545) and is as active as mouse EGF in accelerating eyelid opening in newborn mice (542). Third, human NRG-1β exerts potent therapeutic activity in mouse model of Parkinson's disease and viral myocarditis (544, 546). Finally, human CAR^+ T-cells can undergo equally efficient activation by mouse and human target cells that express comparable levels of target antigen (403). To confirm whether the T1E peptide can indeed cross the species border, human $T4^+$ T-cells were co-cultivated with the mouse $ErbB^+$ HNSCC tumour cell line B7E3 (see Figure 3-7). Co-cultivation confirmed monolayer destruction and T-cell activation in response to interaction between T28ζ and mouse ErbB receptors (see Figure 3-8). Analysis of the ErbB expression levels in mouse healthy tissue confirmed expression in several major organs, including heart, kidney, lung and intestines (see Figure 3-9). To determine whether the expression level of ErbB receptors in healthy mouse tissue was also sufficient to elicit T-cell activation, $T4^+$ T-cells were co-cultivated with primary mouse pulmonary microvascular

endothelial cells (MPMEC). Similar as seen in HPMEC co-cultivations, $T4^+$ T-cells were activated and destroyed the $ErbB^+$ primary cells. These data suggest that the SCID/Beige mouse model should be able to indicate whether 'on-target'-toxicity can be induced by T4 immunotherapy.

The MHRA guidelines required extensive histopathological analysis for 'on-target'-toxicity at the timepoint at which no detectable levels of $T4^+$ T-cells were present. To determine the longevity and migration of human $T4^+$ T-cells *in vivo*, prolonged imaging is required. To enable this, T4 was co-expressed with firefly Luciferase (T4luc) (see Figure 3-11). The expression of three transgenes within one retroviral vector resulted in low expression of the three encoded proteins. $T4luc^+$ expanded *in vitro* when cultured in IL-4. However, expansion and enrichment of these cells was substantially lower compared to $T4^+$ T-cells. Cell surface expression levels of T28ζ and 4αβ were also low. $T4luc^+$ T-cells were able to destroy both human and mouse $ErbB^+$ monolayers. However $T4luc^+$ T-cells were not as effectively as $T4^+$ T-cells in this regard and the levels of cytokine production were barely detectable (see Figure 3-12 and Figure 3-13). However, most importantly, $T4luc^+$ T-cells had luciferase activity *in vitro* and could be visualised *in vivo* by bioluminescent imaging (see Figure 3-14). Migration and longevity of $T4luc^+$ T-cells was determined in both males and female mice after peri-tumoural or intravenous administration. Trafficking patterns seen after either route of administration were consistent with those previously reported using SPECT-CT imaging in mice and in humans (460, 547-550). Bioluminescent signals reduced to background levels as soon as five days after T-cell administration and remained low for the consecutive week. No differences could be seen between males and females. Since the expression level of the receptors and the luciferase activity of $T4luc^+$ T-cells was low, the sensitivity of bioluminescent imaging of $T4luc^+$ T-cells was suboptimal and high binning was required for T-cell visualisation. It has been previously reported that the ffLuc signal is lower in human T-cells compared to other haematopoietic cells or tumour cells (551, 552). Histopathological analysis of the organs retrieved in the toxicity study revealed no changes in any of the healthy tissue analysed, and no infiltrated T-cells, regardless of gender or route of administration (see Table 3-4). This suggests that despite the low expression of ffLuc by $T4luc^+$ T-cells, this was sufficient for adequate estimation of *in vivo* longevity. Additionally and most

importantly, these results show that T4 immunotherapy did not cause any 'on-target'-toxicity in the pre-clinical model.

The absence of detectable 'on-target'-toxicity attributable to T4 immunotherapy is remarkable considering the toxicities seen in response to ErbB2 re-targeted T-cells and both monoclonal antibodies and tyrosine kinase inhibitors targeting the ErbB receptor family (154, 157, 159, 521). Potential reasons for the discrepancy between the toxicity seen with ErbB2 re-targeted T-cells and T4 immunotherapy is the dose administered and the degree of T-cell activation (a third generation CAR versus a second generation CAR). *In vitro*, $T4^+$ T-cells produced approximately 15 fold higher cytokine levels in response to HPMEC compared to MPMEC, suggesting more efficient T-cell activation by the HPMEC. The dose of 20×10^6 T-cells administered in the pre-clinical toxicity study is equivalent to a clinical dose of 5×10^9 T-cells (of which 51% were CAR^+) in man. This is half the dose (1×10^{10} cells of which 79% CAR^+) that was administered in the ErbB2 re-targeting trial (240). The occurrence of toxicities has been related to the T-cell dose, and delayed toxicity has been observed after substantial expansion of the administered T-cells *in vivo* (319). This SCID/Beige pre-clinical model does not support *in vivo* expansion of $T4^+$ T-cells due to the absence of appropriate cytokine stimulation. Therefore, it cannot be determined whether T-cell expansion could lead to toxicity at a later time-point. Additionally, prolonged *in vivo* longevity could result in more extensive T-cell migration and infiltration into organs, which cannot be determined in this model.

In summary, the combination of the lack of T-cell migration after intra-tumoural injection, the ability of $T4^+$ T-cells to be activated by $ErbB^+$ healthy mouse tissues and previous reports that toxicity can be induced by human T-cells in a mouse model (537) would suggest that local treatment with $T4^+$ T-cells is not expected to induce severe 'on-target'-toxicity in patients. However, due to previously mentioned limitations of the used mouse model, this cannot be said with certainty. Prolonged T-cell longevity and/or altered T-cell migration patterns could induce 'on-target'-toxicity in patients which was not detected in the pre-clinical model.

CHAPTER 4

THE INDUCTION OF CYTOKINE RELEASE SYNDROME BY T4 IMMUNOTHERAPY

4.1 Introduction

In addition to 'on-target' chronic organ damage, a second major predicted risk of immunotherapy is 'cytokine release syndrome'. When clinically overwhelming, cytokine release syndrome is often referred to as a cytokine storm, cytokine cascade or hypercytokinemia. Cytokine storms have been reported to occur in response to infectious diseases such as cytomegalovirus (553), Epstein-Barr virus-associated hemophagocytic lymphohistiocytosis (554), severe acute respiratory syndrome (SARS) coronavirus (555) and avian H5N1 influenza virus infection (556). Additionally, cytokine storms may be induced by several forms of immunotherapy, including the administration of IL-2 (557), some monoclonal antibodies (558, 559) as well as CAR-engineered T-cells (240). To illustrate this, in approximately 50% of patients treated with Muromonab-CD3 (OKT3; an anti-CD3 monoclonal antibody used for the treatment of renal allograft rejection) severe CRS occurs if patients are not pre-treated with high-dose corticosteroids (560). High-dose corticosteroids are routinely applied as pre-medication before the first administration of mAbs to reduce the effects of CRS (561). In adoptive cell therapy, corticosteroids have been administered after T-cell administration to reduce the effects of CRS (240). Clinically significant cytokine release syndrome carries a high morbidity and fatality rate (562, 563). As described in paragraph 1.4.2.3, CRS has been implicated as the cause of a serious adverse event in a patient treated with ErbB2 re-targeted T-cells (240). However, the occurrence of CRS has also been related to treatment efficacy. Porter et al. have described a temporal relationship between the occurrence of CRS and *in vivo* expansion of CAR^+ T-cells, leading to the onset of tumour lysis syndrome (445). Additionally, Grupp et al. and Brentjens et al. have reported clinical efficacy using CD19 re-targeted T-cells which, in both cases, was related to patients showing signs of severe CRS (317, 321).

4.1.1 Components and consequence of severe cytokine release syndrome

There is no definition as to what exactly constitutes severe cytokine release syndrome, or a cytokine storm. Also, there remains a lack in knowledge concerning the molecular events that precipitate a cytokine storm and what contribution a cytokine storm makes to the pathogenesis of disease and functionality of treatments (564). A cytokine storm is comparable to sepsis, in which a local inflammation 'spills-over' into the systemic circulation, causing persistent hypotension, hyper- or hypothermia, leucocytosis or

leukopenia and often thrombocytopenia (565). Acute lung injury is a common consequence of a cytokine storm in the lung alveolar environment, associated with infections in the lungs and other organs. Acute lung injury is characterised by an acute mononuclear and neutrophilic inflammatory response followed by a chronic fibroproliferative phase marked by progressive collagen deposition in the lung (566). Patients with severe sepsis resulting from pulmonary infections show characteristic plasma cytokine profiles. Acute-response cytokines including TNF, IL-1β and the chemotactic cytokines IL-8 and monocyte chemoattractant protein (MCP)-1 (CCL2) appear in the early minutes to hours after infection, followed by a sustained increase in IL-6. Interleukin-6 production is stimulated by TNF and IL-1β and can therefore be used to assess the intensity of the cytokine response. The anti-inflammatory cytokine IL-10 can be detected later, as part of the counter-inflammatory response, also known as 'immunoparalysis'. Patients who initially recover from a cytokine storm but die later on may not have recovered from the 'immunoparalysis'-state, leading to uncontrolled infection (567). The occurrence of a cytokine storm in response to a dengue virus infection is associated with increased capillary permeability syndrome. Increased capillary permeability syndrome occurs between day four and six of illness, at which IL-10 and IFNγ are at their peak-levels. T-cells have been identified as potent contributors to cytokinaemia, which contributes to vasodilation during this stage of illness (568).

4.1.2 Unexpected severe CRS in TGN1412 Phase-I clinical trial

The significance of CRS as a key risk related to immunotherapy is strikingly illustrated by the events that took place during phase-I clinical testing of an immunotherapeutic monoclonal antibody named TGN1412. TGN1412 is a 'superagonist' of CD28, bypassing any required TCR-stimulation as well as co-stimulatory signals and resulting in direct T-cell activation upon binding to CD28 (569). In pre-clinical studies, TGN1412 was predicted to stimulate the release of anti-inflammatory cytokines and expand regulatory T-cells (Tregs) giving it a potential therapeutic application in autoimmune disease (569-571). In March 2006, six healthy, male volunteers were treated with 0.1mg/kg body weight of TGN1412 by IV administration. Two additional healthy male volunteers received a placebo control. Within 60 minutes after administration, all six test-volunteers were critically ill. Investigation at the time indicated the presence of pulmonary infiltrates, acute lung injury, acute renal failure followed by disseminated

intravascular coagulation. All six required intensive care therapy including cardiopulmonary support and dialysis. Two patients developed prolonged cardiovascular shock and acute respiratory distress, requiring intensive organ support for 8-16 days (558). Analysis of circulating cytokine levels revealed a dramatic increase in TNF levels within one hour after TGN1412 administration. This was followed by elevations of circulating IL-2, IL-6, IL-10 and IFNγ within the first four hours (558). The disastrous results of this clinical trial prompted two important questions. First, how was this cytokine storm induced and second, why had pre-clinical toxicity studies failed to predict the occurrence of these adverse events?

High levels of IL-2 production (in combination with TNF and IFNγ) were already reported in response to administration of the first clinically available mAb, OKT3 (Muromonab-CD3). These pro-inflammatory mediators cause *inter alia*, capillary leakage, leukocyte sequestration and flu-like symptoms (572). TGN1412 was shown to induce a 28.4-fold higher level of IL-2 compared to OKT3. The difference in levels of IL-2 production could be a driving force behind the severity of the induced CRS (573). This was because high-dose IL-2 administration for therapeutic purposes (eg in selected cancers) can induce similar toxicity (574). Increased levels of the soluble forms of adhesion molecules ICAM1, VCAM and E-selectin are found after IL-2 administration. These are suggested to play a role in the inflammatory reaction induced by IL-2 in addition to promoting blood vessel inflammation, vascular damage, leakage and hypotension (557). Increased circulating levels of metalloproteinases (MMP) 2, 3, 10 and 13 have also been detected after IL-2 administration. This finding may be responsible for the destruction of endothelial basement membranes, extravasation of mononuclear cells and the accumulation of toxic by-products in tissues (557).

4.1.3 Role of Macrophages in CRS

T-cells might not be the only source of cytokine release in CRS. Sandilands et al showed that the high levels of TNF seen as early as two hours after TGN1412 stimulation was most likely produced by monocytes. Monocytes were the only cell population that showed a significant upregulation of TNF mRNA, along with 11 other monocyte cytokines, including IL-1β, IL-2R, IL-6 and IL-17 (575). Macrophages have also been implicated in the induction of CRS in response to Blinatumomab treatment. Blinatumomab is a CD19/CD3-bispecific T cell receptor-engaging (BiTE) antibody, which

has shown efficacy in refractory B-precursor acute lymphoblastic leukaemia (B-ALL). However, Blinatumomab has been associated with considerable but manageable toxicity. Elevated circulating levels of IL-6, IL-10 and IFNγ are detected in all patients receiving Blinatumomab (576). Elevated levels of these three cytokines were also seen in patients receiving CD19-re-targeted CAR T-cells (317, 321). Because these cytokines are also elevated in 'macrophage activation syndrome', Teachey et al. suggested that severe toxicity might be due to abnormal macrophage activation, which is triggered by the release of cytokines by cytotoxic T-cells (577). This theory is supported by the fact that high levels of IL-6 and IL-10 would normally not be expected in a cytotoxic T-cell response alone. Interleukin-6 is principally released by macrophages and IL-10 is a negative regulator of macrophage function. Additionally, treatment with the IL-6R blocking-antibody Tocilizumab induces a rapid improvement in patients with clinically severe CRS (317, 321, 577), suggesting that IL-6 and perhaps macrophage activation plays an important role in CRS alongside cytotoxic T-cells.

4.1.4 Cytokine Release Syndrome in CAR-mediated adoptive T-cell therapy

Cases of cytokine storms in response to CAR-mediated adoptive T-cell therapy have been reported (240). In one such case, 1 x 10^{10} T-cells (79% gene-modified with a third generation ErbB2-specific CAR) were administered IV after the patient had received lymphodepleting chemotherapy. Within 15 minutes after T-cell transfusion, the patient developed respiratory distress and was transferred to intensive care. The patient finally succumbed to a cardiac arrest five days later. Serum cytokine analysis showed high levels of IFNγ, TNF, GM-CSF and IL-6, peaking at 4 hours after T-cell administration. Interleukin-10 levels also increased after infusion but remained stable thereafter (240). This case illustrates the rapid onset and severity of CAR T-cell induced cytokine release syndrome. Cytokine storms have also been reported with delayed onset in patients treated with CAR T-cells. Porter et al. described a case in which peak cytokine levels were not seen until 22 days after T-cell transfusion. However, in this case a lower CAR^+ T-cell dose was given (1.46 x 10^5 T-cells/kg of which 5% were CAR^+), separated over three days. The onset of the CRS coincided with the diagnosis of tumour lysis syndrome, suggesting that CRS could also be an indicator for treatment functionality (445). This suggestion is confirmed in two further clinical experiences described by Grupp et al. and Brentjens et al. In both cases patients suffered from

severe CRS, combined with treatment efficacy leading to complete remission in some cases. In both trials, CRS was successfully treated with Tocilizumab administration, implicating IL-6 mediated toxicity in this event (317, 321).

4.1.5 The importance of appropriate pre-clinical safety testing

An important question is why *in vivo* and *in vitro* pre-clinical studies had failed to indicate the risk of CRS in response to Immunotherapies? In the case of TGN1412, pre-clinical toxicity studies using the rat-equivalent of TGN1412, named JJ316, the antibody was shown to be well tolerated and not accompanied by a toxic cytokine storm. This was attributed to the release of counter-regulatory anti-inflammatory cytokines such as IL-10 by regulatory T-cells (569, 578). In humans, this mechanism failed most likely due to the fact that $CD4^+$ effector memory T-cells (the main source of cytokine production) are present in a higher abundance in adult humans compared to young rodents (579).

Pre-clinical testing using TGN1412 itself was performed in cynomolgus macaques. TGN1412 binds to macaque CD28 with the same affinity as to human CD28. Pre-clinical testing in cynomologus macaques, at doses of up to 50mg/kg/week was well tolerated with no signs of toxicity or systemic immune stimulation (579). The absence of a cytokine storm in TGN1412-treated cynomolgus macaques is most likely due to a specific species difference. Whereas all human $CD4^+$ memory T-cell subsets express high levels of CD28, the $CD4^+$ memory T-cell subsets of cynomolgus macaques (as well as rhesus macaques) do not express CD28 (579). The difference in the distribution of CD28 expression by human and macaque PBMCs is most likely to be the reason why TGN1412 did not induce a cytokine storm in cynomolgus macaques (580). *In vitro* studies showed that human $CD4^+CD45RO^+$ memory T-cells are predominantly responsible for the TNF, IFNγ and IL-2 production in response to stimulation with immobilised TGN1412 (579, 581). The immobilisation of TGN1412 in the *in vitro* assays promoted the formation of an immunological synapse (582), similar to that formed upon cell-to-cell contact. Aqueous-phase TGN1412 allows for CD28 engagement outside of the immunological synapse, which is known to impede T-cell activation (583, 584). However, immobilised TGN1412 fails to stimulate PBMCs from cynomolgus macaques *in vitro*. Römer et al. reported that cell density is another important factor contributing to the level of cytokine production in response to TGN1412. Pre-culture of

human PBMCs at ten-fold higher densities showed increased cytokine response to aqueous-phase TGN1412, possibly due to the increased cellular interaction, in response to which both monocytes and T-cells upregulated functional activity mediated (585, 586). The experience with TGN1412 emphasises the importance of performing pre-clinical toxicity studies using an appropriate model, which allow for the detection of potential adverse events.

This chapter discusses the risk of CRS in relation to T4 immunotherapy. I have investigated this question using an immunodeficient SCID/Beige mouse model. This model should allow for detection of CRS in response to T4 immunotherapy for two reasons. First, as shown in paragraph 3.2.4, T28ζ can induce T-cell activation in response to mouse ErbB receptors. Second, although SCID/Beige mice are deficient in T-cells, B-cells and NK-cells, they retain a normal macrophage population (587), which is the major source of the key toxic cytokine, IL-6.

4.2 Results

4.2.1 Transient Weight Loss Induced by $T4^+$ T-cells in Ovarian Cancer Xenograft Model

As described in paragraph 3.2.10, no toxicity such as weight loss was observed in the IV and PT HNSCC xenograft models, following treatment with T4 immunotherapy. By contrast, transient weight loss has been consistently reported in IP xenograft models of ovarian cancer performed by Dr AC Parente-Pereira and Dr LM Whilding following IP administration of $T4^+$ T-cells (Figure 4-1). In those studies, mice with 18 day established firefly luciferase-expressing SKOV3 (SKOV3luc) tumours were treated with 10 x 10^6 $T4^+$ T-cells, making comparison with control $P4^+$ T-cells or PBS. Mice treated with $T4^+$ T-cells consistently showed transient and mild weight loss, from which they recovered over a 14-day period. No weight loss was seen in control mice.

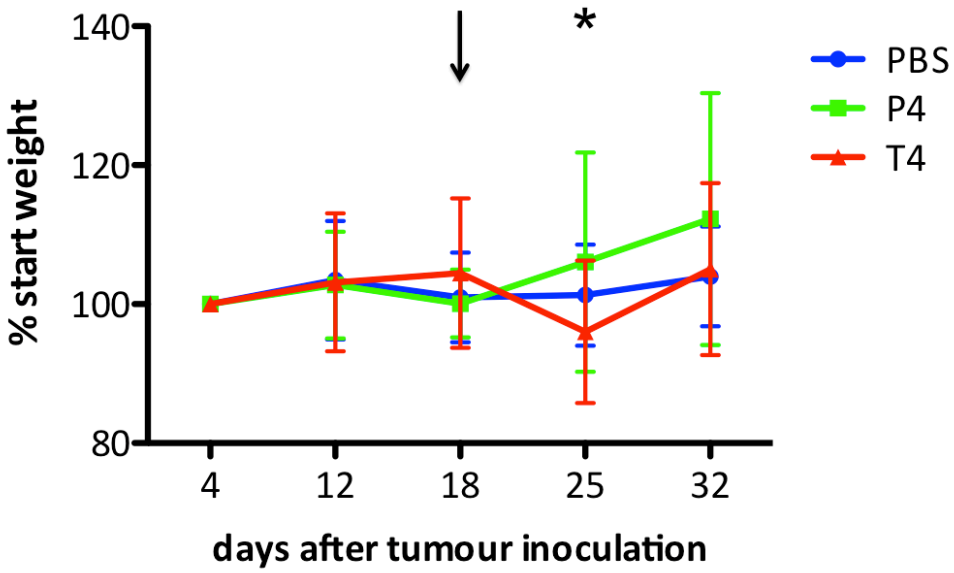

Figure 4-1 Transient weight loss in ovarian cancer xenograft model after T4 treatment

Serial weight measurement of SKOV3luc tumour-bearing mice following $T4^+$ or $P4^+$ T-cell, or PBS treatment (mean ± SD; number of replicates indicated below). The y-axis indicates weight change normalised to that at the start of the study (e.g. weight at day 0 = 100%). Mice were treated with engineered T-cells 18 days after tumour inoculation (as indicated by the arrow). Mice received 10 x 10^6 $T4^+$ T-cells, 10 x 10^6 $P4^+$ T-cells or PBS as control. PBS, n=15; P4, n=5; T4, n=14. Data are derived from three pooled experiments * = $p<0.01$ comparing weight of T4 treated mice on day 25 with the weight of T4 treated mice on day 18.

4.2.2 Serious Adverse Events in Ovarian Cancer Xenograft Model

In an additional experiment performed by Dr Parente-Pereira and Dr Whilding, female SCID/Beige mice with a high IP SKOV3luc-tumour burden (34 days established), were treated with 10 x 10^6 $T4^+$ T-cells IP, or PBS as a control. Within 72 hours after T-cell injection, 11 of 12 mice had died or had to be culled, whereas all control mice (PBS treated) remained healthy. The single-surviving mouse after T4 treatment showed a remarkable reduction in tumour burden. Control mice showed an increase in tumour levels (see Figure 4-2). At post-mortem examination of 5 of these T4 treated mice, no apparent cause of death could be determined and no residual tumour was detected. Signs of inflammation were detected in the abdomen (see Appendix 5). These finding suggested that $T4^+$ T-cells are able to induce severe toxicity of rapid onset when injected IP in the presence of tumour.

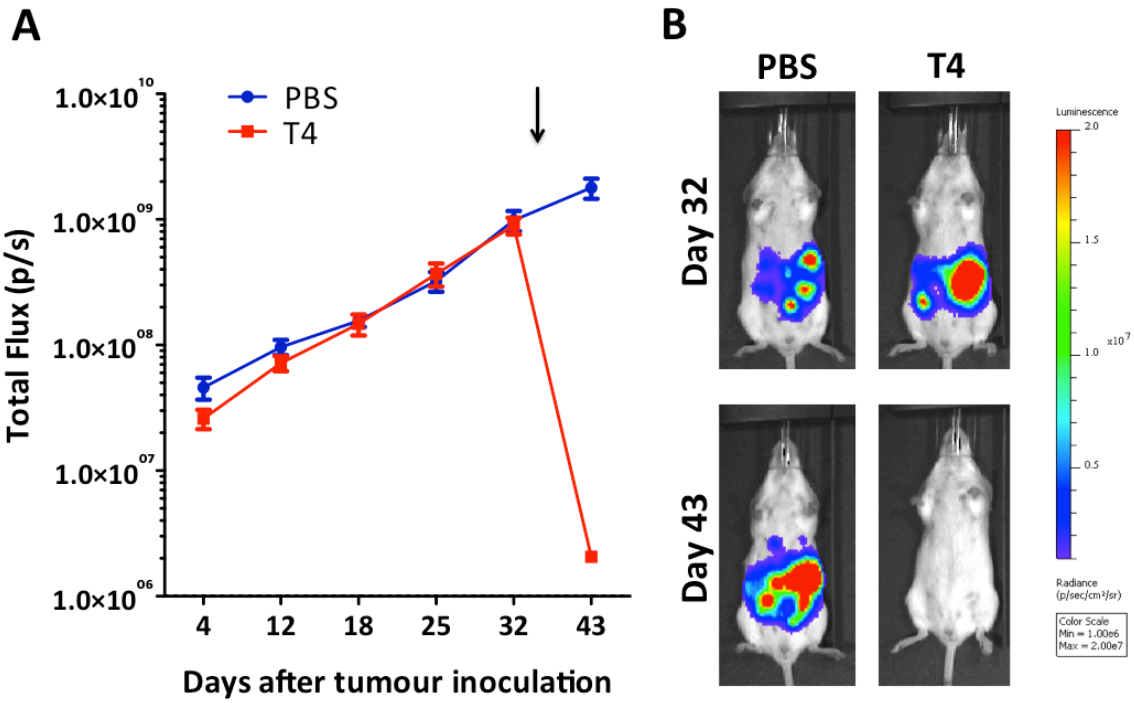

Figure 4-2 Severe Adverse Events in IP xenograft model of ovarian cancer

Twelve mice with advanced, 34 day-established SKOV3luc tumours were treated with 10 x 10^6 $T4^+$ T-cells (n=12) IP, control mice received 400µL PBS IP (n=9). **A:** Serial BLI indicating IP tumour growth (mean ± SD, n=12 for T4 or 9 for PBS). Arrow indicates timepoint of T-cell/PBS treatment. Lethal toxicity occurred in 11/12 mice treated with T4 immunotherapy within 72 hours after T-cell administration. The day 43 imaging in the T4 group is the single surviving mouse from the original group of 12 **B:** BLI of the surviving T4 treated mouse compared to one representative PBS-treated control. Day 32 represents tumour burden 2 days prior to treatment, day 43 represent tumour burden 9 days after treatment. Images are from the same mice, before and after treatment and shown on the same scale.

4.2.3 Transient Weight Loss induced by $T4^+$ T-cells in IP HNSCC Xenograft Model

The SKOV3luc xenograft model is a more aggressive and faster growing tumour model than the HN3luc xenograft model. In order to determine whether the toxicities seen were specifically related to the ovarian cancer model or a more general side effect of T4 immunotherapy, weight loss was measured in an IP model of HNSCC. Mice with 14-day established HN3luc tumours were treated with either 5 x 10^6 or 10 x 10^6 $T4^+$ T-cells or 10 x 10^6 UT T-cells as control (see Table 4-1). Due to the risk of inducing severe toxicity, only 2 mice were included for ethical reasons (as specified in the Project License governing this work). Additionally, non-tumour bearing mice were treated with either 5 x 10^6 or 10 x 10^6 $T4^+$ T-cells to determine whether the presence of tumour influenced the severity of toxicity. Functionality of *in vivo* administered $T4^+$ T-cells was confirmed by serial tumour burden measurement using BLI. A reduction of tumour burden was seen using both 5 x 10^6 and 10 x 10^6 $T4^+$ treatment doses (see Figure 4-3).

Table 4-1 Design of 'Efficacy of T4 immunotherapy after IP administration'-study

Number Mice	HN3 Tumour cells IP	T-cells IP
2 male	-	5 x 10^6 T4
2 male	-	10 x 10^6 T4
2 male	10 x 10^6	5 x 10^6 T4
2 male	10 x 10^6	10 x 10^6 T4
2 male	10 x 10^6	10 x 10^6 UT

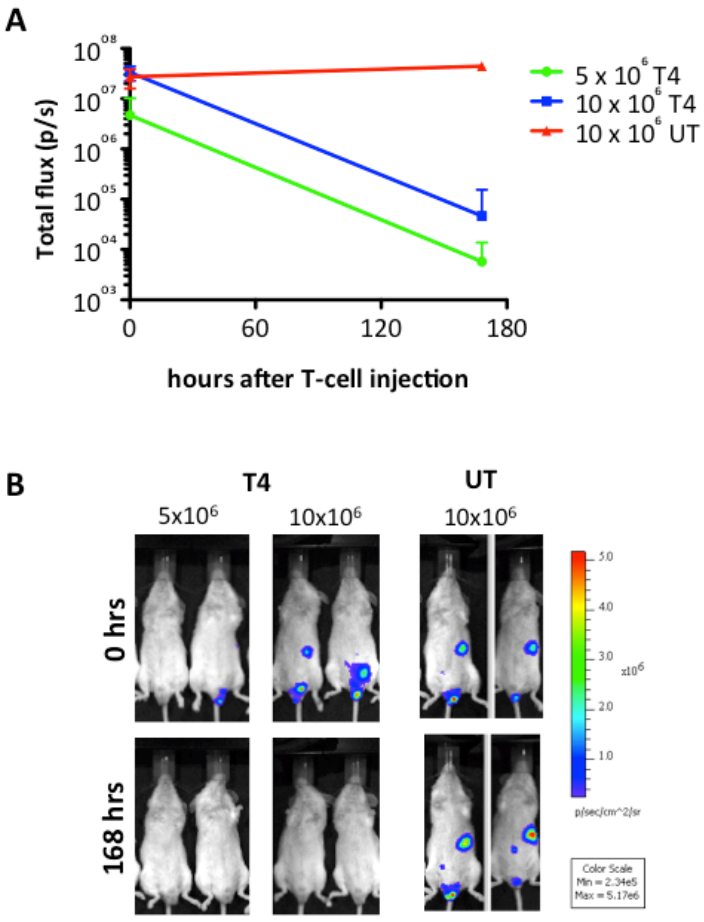

Figure 4-3 Efficacy of T4 immunotherapy after intra-peritoneal T-cell administration
Mice with 14 day-established HN3luc tumours were treated IP with 5 x 10^6 or 10 x 10^6 $T4^+$ T-cells (n=2). Control mice were treated with 10 x 10^6 UT T-cells (n=2). **A:** Serial BLI indicating tumour status directly prior to T-cell administration (0 hours) and 7 days (168 hours) after T-cell administration (mean ± SD). **B:** BLI images of all mice prior and after T-cell administration. All mice are shown on the same scale.

The weight of all mice was measured at regular intervals (0, 4, 24, 48, 72 and 168 hours after T-cell administration). Minor weight loss was seen in mice treated with 10 x 10^6 UT T-cells in the first 72 hours after T-cell administration (see Figure 4-4). More pronounced weight loss was seen in mice treated with $T4^+$ T-cells. Mice that received 10 x 10^6 $T4^+$ T-cells lost relatively more weight than mice treated with 5 x 10^6 $T4^+$ T-cells. The presence of tumour did not influence the degree of weight loss in both treatment dose levels (see Figure 4-4). These results suggest that the adverse events observed are dose-dependent toxicities of T4 immunotherapy, independent of the tumour type treated.

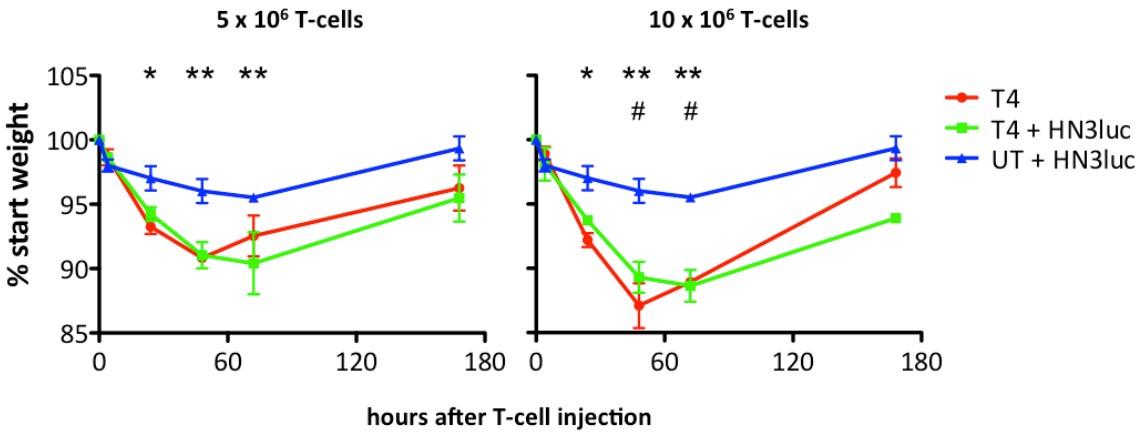

Figure 4-4 Serial weight monitoring of mice following T4 immunotherapy in absence or presence of tumour burden

Serial weight measurements in tumour-bearing (shown in green) or tumour-free (shown in red) mice treated with 5 x 10^6 (left graph) or 10 x 10^6 (right graph) $T4^+$ T-cells (mean ± SD). Weight loss in both graphs is compared to control tumour-bearing mice that received 10x10^6 UT T-cells (shown in blue). (n=2). Weights of tumour-bearing and tumour-free mice following treatment with either dose of $T4^+$ T-cells are not significantly different. * = $p<0.05$; ** = $p<0.01$ comparing $T4^+$ T-cells with UT T-cells; # = $p<0.05$ comparing the effect of 5 x 10^6 with 10 x 10^6 $T4^+$ T-cells in tumour-free mice. The latter difference is not significant in tumour-bearing mice.

4.2.4 Induction of Cytokine Release Syndrome by T4 immunotherapy in Tumour-Free Mice

The rapid onset of the toxicities recorded, and the absence of any major organ pathology, suggested that a cytokine storm might be the cause for these adverse events. As mentioned previously, complications due to cytokine release syndrome (CRS) have been reported in clinical studies involving CAR-engineered T-cells. To determine whether the toxicities seen in the SCID/Beige xenograft models could be due to CRS, non-tumour bearing mice were treated IP with escalating doses (3 x 10^6, 10 x 10^6 and 30 x 10^6) of $T4^+$ T-cells or the same dose of $P4^+$ or UT T-cells as a control (see Table 4-2). Serial weight measurements performed in mice treated with $T4^+$ T-cells were consistent with a dose-dependent induction of toxicity (see Figure 4-5). Mice treated with the lowest dose (3 x 10^6 $T4^+$ T-cells) did not show any weight change. Minor weight loss was recorded in mice treated with 10 x 10^6 $T4^+$ T-cells. Mice treated with 30 x 10^6 $T4^+$ T-cells had significant weight loss within 24 hours and died within 30 hours after T-cell administration (see Figure 4-5). Mice treated with 30 x 10^6 $T4^+$ T-cells showed additional clinical signs including piloerection, subdued behaviour and reduced mobility. Control mice treated with the same doses of $P4^+$ T-cells or UT T-cells did not

have any significant weight loss in response to treatment, nor did they show any clinical signs of toxicity (see Figure 4-6). The absence of weight loss in mice treated with $P4^+$ T-cells, suggest that the induced toxicity is specific for the ErbB-targeting CAR T28ζ, present within the T4 combination.

Table 4-2 Design of 'Cytokine Release Syndrome'-study

Number Mice	$T4^+$ T-cells IP	$P4^+$ T-cells IP	UT^+ T-cells IP
2 male	3×10^6	3×10^6	3×10^6
2 male	10×10^6	10×10^6	10×10^6
2 male	30×10^6	30×10^6	30×10^6

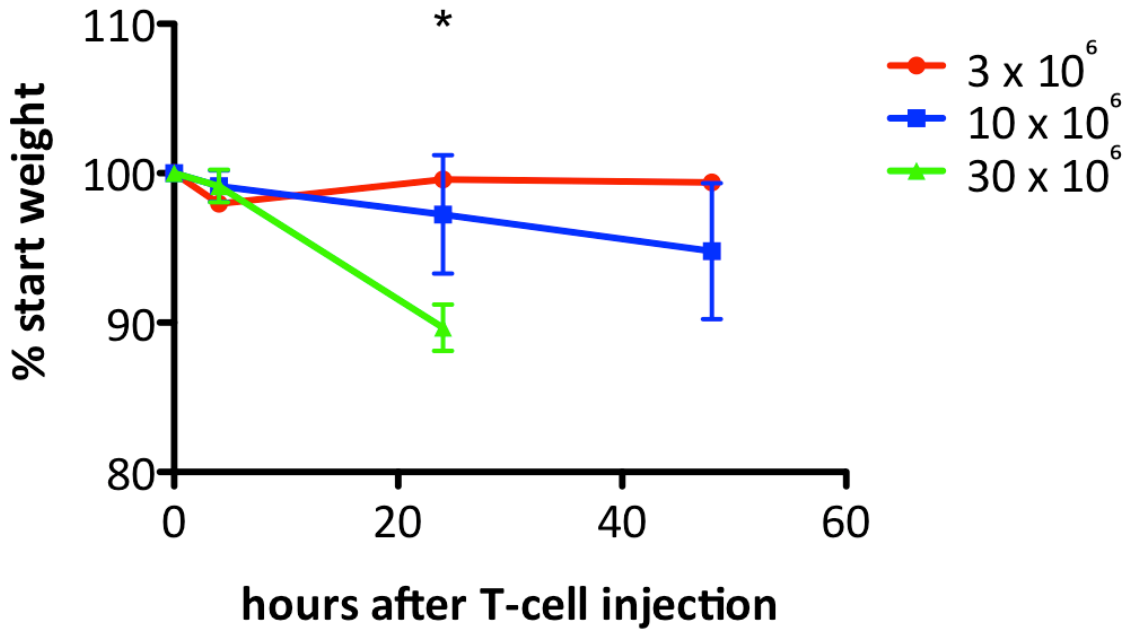

Figure 4-5 Weight loss induced in tumour-free mice by intra-peritoneal T4 immunotherapy

Serial weight measurement of tumour-free mice treated with 3×10^6 (red; n=2), 10×10^6 (blue; n=4) or 30×10^6 (green; n=4) $T4^+$ T-cells (% mean ± SD). Results are a combination of two independent experiments. All 4 mice treated with 30×10^6 $T4^+$ T-cells died within 30 hours after T-cell administration. * = $p<0.01$ comparing weight of mice treated with 30×10^6 $T4^+$ T-cells after 24 hours with their start weight (0 hours). Weight changes in mice treated with 3×10^6 or 10×10^6 $T4^+$ T-cells are not significant at any stage.

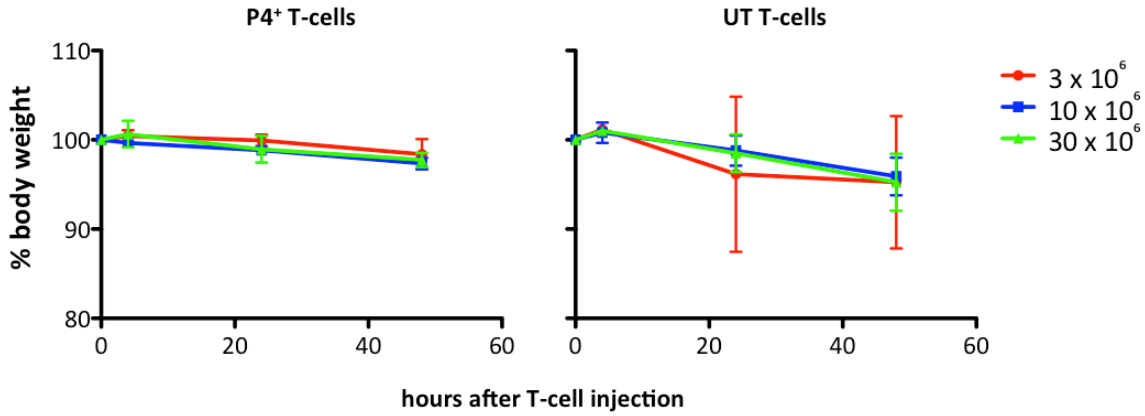

Figure 4-6 Monitoring of weight in tumour-free mice treated with $P4^+$ or UT T-cells
Serial weight measurements were performed in tumour-free mice treated with 3 x 10^6 (red), 10 x 10^6 (blue) or 30 x 10^6 (green) $P4^+$ or UT T-cells (n=2 for all groups) (% mean ± SD). No significant weight loss was detected at any point.

To investigate whether this rapid, dose dependent weight loss could be attributed to CRS, circulating cytokine levels were measured at several time-points. Blood samples were taken at 4, 24 and 48 hours after T-cell administration. Human and mouse cytokine levels were measured using a cytometric bead assay (IL-2, IL-4, IL-6, IL-10, IL-17A, IFNγ), or ELISA (hIL-2, hIFNγ, mIL-6). Cytokine levels at 4 and 24 hours after $T4^+$ T-cell administration are shown here. Circulating cytokine levels at 48 hours in mice treated with 3 x 10^6 or 10 x 10^6 $T4^+$ T-cells were all below detection level (data not shown). Additionally, circulating cytokine levels (hIL-2, hIFNγ and mIL-6) in mice treated with $P4^+$ or UT T-cells were all below detection level at all tested time points (data not shown).

High levels of human IL-2, human IFNγ and mouse IL-6 were detected in mice treated with 30 x 10^6 $T4^+$ T-cells (see Figure 4-7 and Figure 4-8). Low levels of hIL-17A were detected amongst all treatment doses (see Figure 4-7). Low level of mIL-10 was detected in one of the mice treated with 30 x 10^6 $T4^+$ T-cells (see Figure 4-8). In man, elevated levels of IL-2, IL-10, IFNγ, TNF and IL-6 have been reported in relation to T-cell therapy (240, 317, 319, 320, 327, 445, 450, 477). Treatment with the anti-IL-6R antibody Tocilizumab has achieved rapid relief of side effects in patients, suggesting a key role for IL-6 in the CRS-related toxicities. Blocking of mouse IL-6 in this model would be useful to determine whether mIL-6 plays a similar role in this pre-clinical model. At the time of printing this thesis, the murine equivalent (MR16-1 (588)) is being acquired. In a mouse model of graft-versus-host disease (GvHD) after allogeneic

bone marrow transplantation, treatment with MR16-1 resulted in a reduction of the GvHD induced mortality, while preserving the graft-versus-tumour response (589). The antibody would allow us to determine whether blocking IL-6R is equally efficient in relieving side effects in SCID/Beige mice as Tocilizumab is in man.

Interleukin-6 is principally produced by macrophages, which led to the hypothesis that the high levels of IL-2 produced by the $T4^{+}$ T-cells induced mIL-6 production by the macrophages in the intra-peritoneal cavity. To determine whether macrophages are influential in this pre-clinical model, further toxicity experiments were conducted in mice in which macrophages were depleted first, using liposomal clodronate.

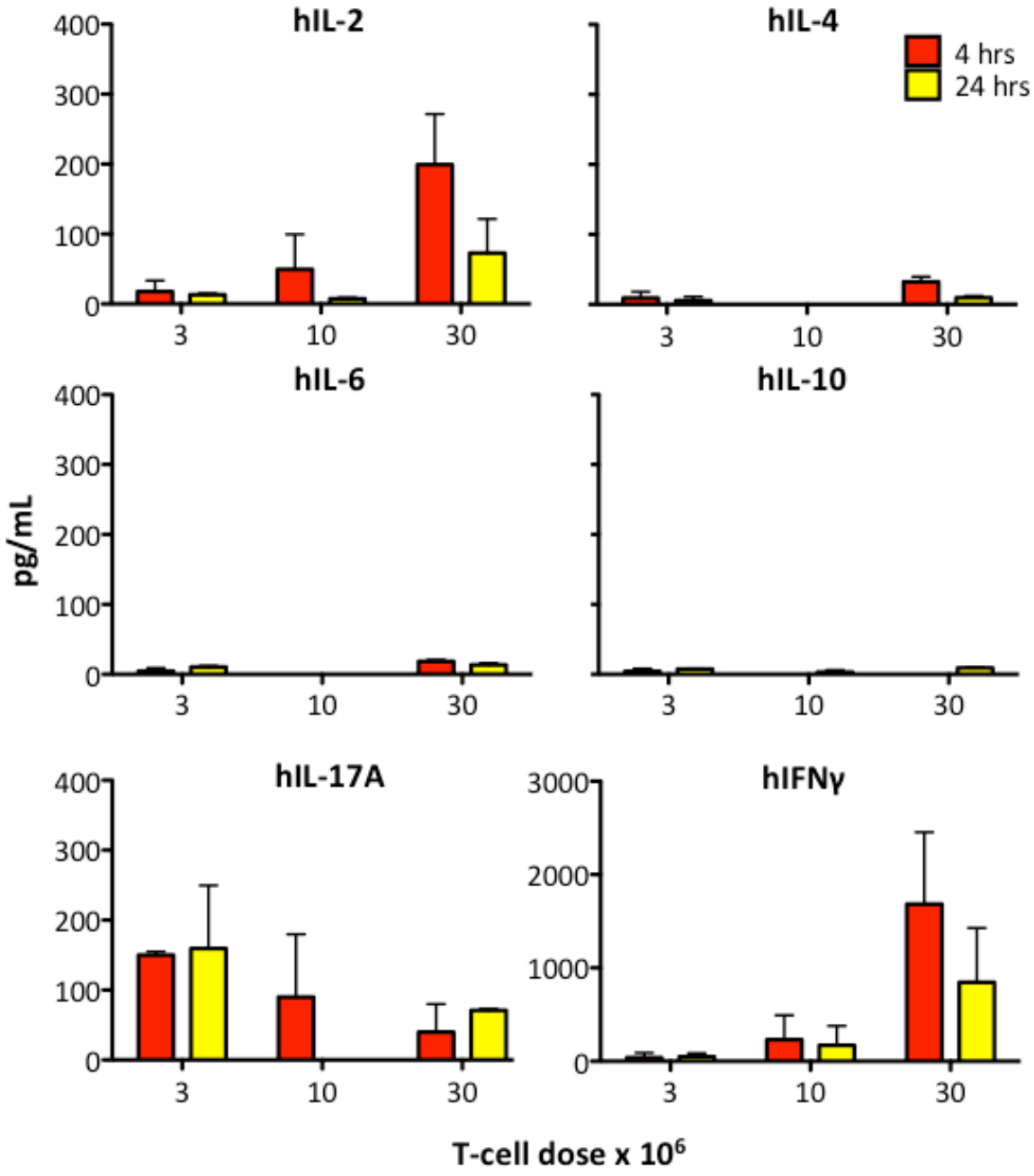

Figure 4-7 Circulating human cytokine concentrations in mice following IP administration of $T4^+$ T-cells.

Human circulating cytokine levels were quantified at 4 (red) and 24 (yellow) hours after T-cell administration in mice treated with escalating doses of T4 immunotherapy (n=4 for human IL-2 and IFNγ; n=2 for all remaining cytokines) data show mean ± SD. Human IL-2 and IFNγ levels were determined using cytometric bead array (n=2) or ELISA (n=2), all other cytokines were measured using cytometric bead array.

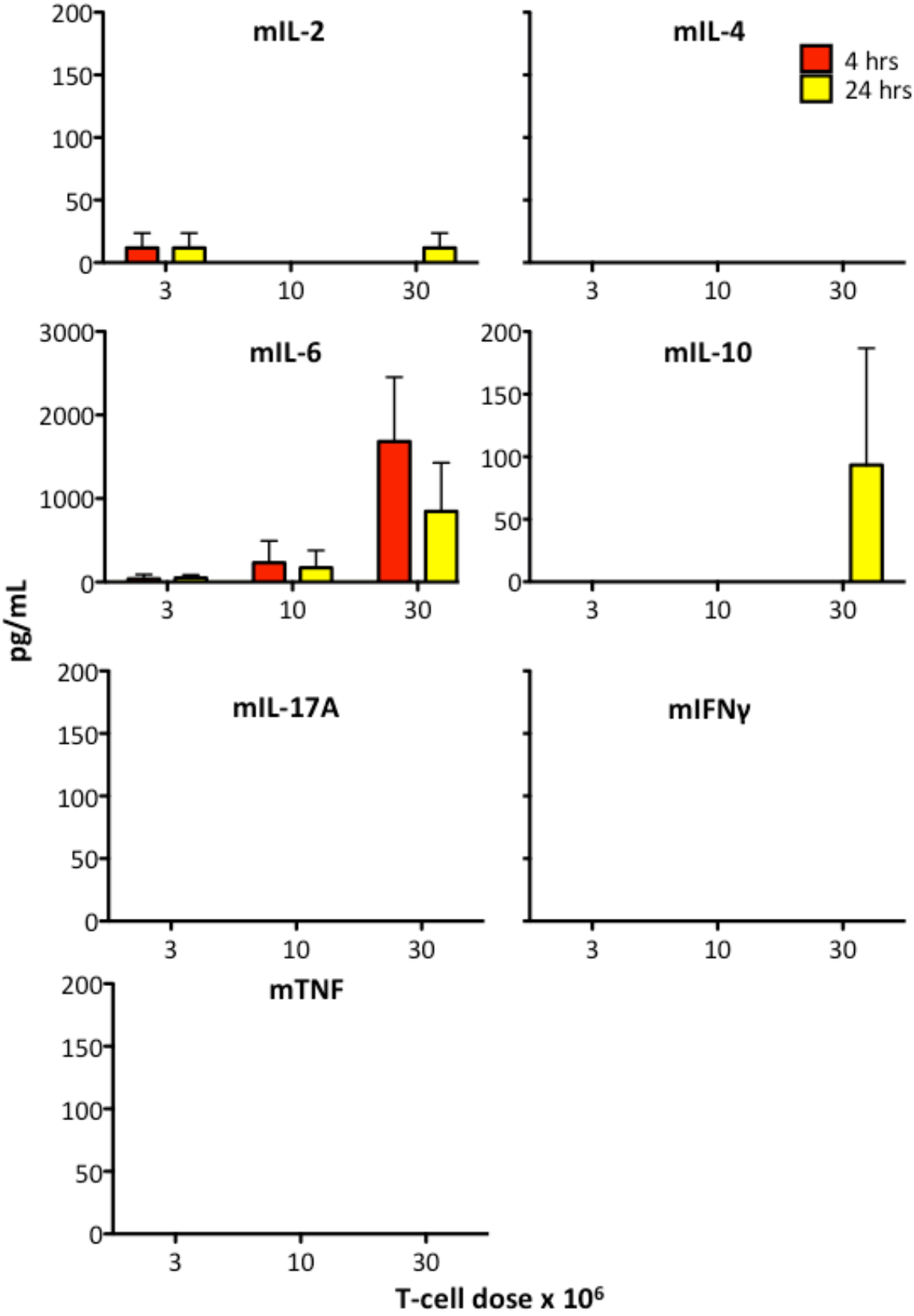

Figure 4-8 Circulating mouse cytokine concentrations in mice following IP administration of $T4^+$ T-cells

Mouse circulating cytokine levels at 4 (red) and 24 (yellow) hours after T-cell administration in mice treated with escalating doses of T4 immunotherapy (n=4 for mouse IL-6; n=2 for all remaining cytokines) data show mean ± SD. Mouse IL-6 levels were determined using cytometric bead array (n=2) or ELISA (n=2). All other cytokines were measured with a cytometric bead array.

4.2.5 Influence of Macrophages on Cytokine Release Syndrome

Liposomes are lipid vesicles consisting of concentric phospholipid bilayers and may be used to encapsulate hydrophilic molecules, including clodronate. Clodronate is a bisphosphonate, which is used in treatment of (secondary) bone cancer. Clodronate has a short half-life in circulation, but due to its hydrophilic nature, it does not easily cross the phospholipid bilayer liposome or cell membrane. When macrophages take up liposomal clodronate (LC) through phagocytosis, it accumulates within the cell until the liposomes are digested and the clodronate is released. At certain intracellular concentrations, clodronate induces the apoptosis of macrophages. Neither the liposomes nor the clodronate is toxic to other cell types, allowing for specific macrophage depletion (590-592).

To ensure maximal macrophage depletion, mice were treated with two doses of LC (or liposomal PBS (LP) as control) prior to $T4^+$ T-cell administration (see Table 4-3). Four days prior to T-cell administration, mice received a dose of 1mg LC/ 10g body weight. Three days later (one day prior to T-cell administration) mice received an additional dose of 0.5mg LC/ 10g body weight. To determine the efficacy of macrophage depletion, the amount of $CD45^+$ $F4/80^+$ cells in the IP cavity of $T4^+$ treated mice was determined using flow cytometry. Treatment with liposomal clodronate resulted in a lower absolute number of $CD45^+$ $F4/80^+$ cells in the intra-peritoneal cavity compared to the content in control mice treated with LP (see Figure 4-9).

Table 4-3 Design of 'Macrophage depletion' study

Number Mice	LC (day -4)	LP (day -1)	$T4^+$ T-cells	$P4^+$ T-cells
1 male	Dose 1: 1mg/10g Dose 2: 0.5mg/10g	-	30×10^6	-
2 male	-	Dose 1: 1mg/10g Dose 2: 0.5mg/10g	30×10^6	-
2 male	Dose 1: 1mg/10g Dose 2: 0.5mg/10g	-	-	30×10^6
2 male	-	Dose 1: 1mg/10g Dose 2: 0.5mg/10g	-	30×10^6

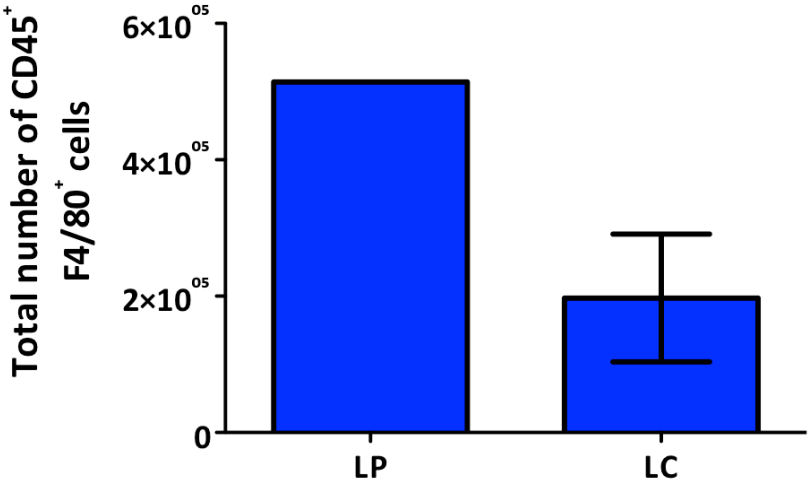

Figure 4-9 Peritoneal macrophage content in mice treated with liposomal clodronate.
Total macrophage content in IP cavity after liposomal PBS (LP) or liposomal clodronate (LC) treatment. Total cells were counted and macrophage content was determined based on $CD45^+$ $F4/80^+$ content. LP, n=1; LC, n=2. Data shown mean ± SD for LC.

Mice received a dose of 30 x 10^6 $T4^+$ or $P4^+$ T-cells, after which weight, behaviour and circulating cytokines were monitored as described in the previous experiment. Severe weight loss was seen in the mouse treated with 30 x 10^6 $T4^+$ T-cells without macrophage depletion, whereas no weight loss was seen in mice that were macrophage depleted prior to T-cell treatment (see Figure 4-10). Weight remained stable in mice treated with $P4^+$ T-cells, independent of macrophage content (see Figure 4-10).

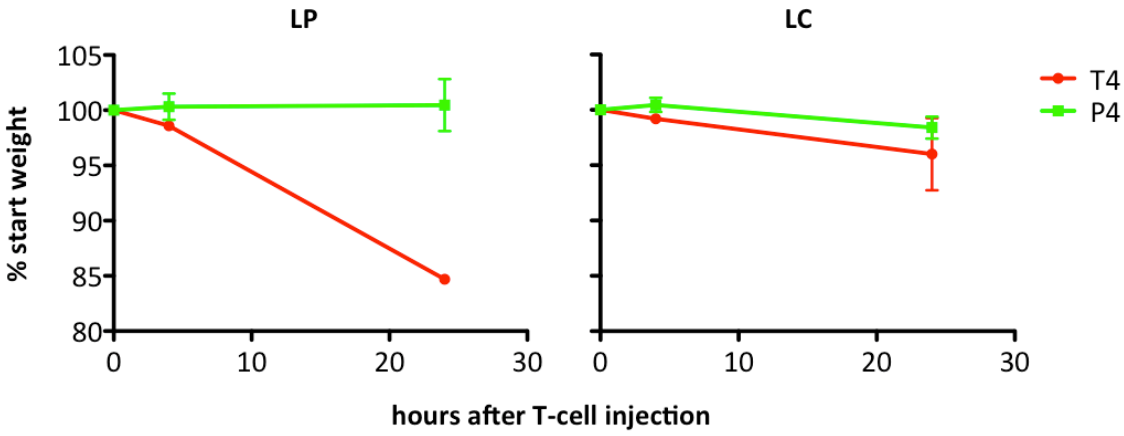

Figure 4-10 Weight loss induced by $T4^+$ T-cells in tumour-free mice with(out) macrophage depletion
Mice were treated with liposomal PBS (LP) or liposomal clodronate (LC) prior to administration of 30 x 10^6 $T4^+$ or $P4^+$ T-cells. Weight was measured at 0, 4 and 24 hours post T-cell administration. LP + T4 n=1; all other conditions n=2.

Blood samples were obtained at 4 and 24 hours after T-cell injections. Circulating levels of mouse IL-6 (mIL-6) was determined by ELISA. High mIL-6 levels were detected in the mouse treated with liposomal PBS (LP), at an equivalent level as previously measured in non-tumour bearing mice. In mice treated with liposomal clodronate prior to $T4^+$ T-cell administration (see Figure 4-11 and Figure 4-8), low levels of mIL-6 were detected 4 hours after $T4^+$ T-cell administration, which decreased to levels below the detection limit 24 hours after $T4^+$ T-cell administration. No detectable levels of mIL-6 were seen in any of the control mice treated with $P4^+$ T-cells (see Figure 4-11). These results suggest that measured mIL-6 levels are indeed produced by macrophages, and that elimination of macrophages reduced mIL-6 production and consequently reduces the toxicity related to CRS.

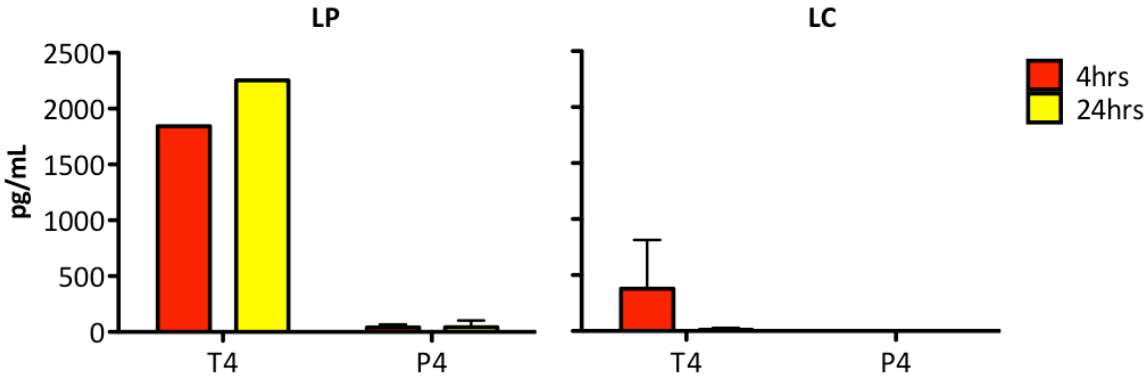

Figure 4-11 Circulating mouse Interleukin-6 following IP administration of 30 x 10^6 $T4/P4^+$ T-cells.

Prior to T-cell administration, mice were treated with two doses liposomal PBS (LP) or liposomal clodronate (LC). Mice received 1µg/10g body weight 4 days prior to T-cell administration and 0.5µg/10g body weight 1 day prior to T-cell administration. Mice received 30 x 10^6 $T4^+/P4^+$ T-cells IP. Blood samples were collected at 4 and 24 hours post T-cell administration. LP+T4 n=1, all other conditions n=2 (mean ± SD). Cytokine levels were determined by ELISA.

In mice bearing advanced SKOV3 tumours, the lower dose of 10 x 10^6 $T4^+$ T-cells was able to induce severe toxicity, whereas in non-tumour bearing animals severe toxicity was only detected with the high dose of 30 x 10^6 $T4^+$ T-cells. Toxicity of the lower dose in mice with a high tumour burden could be due to an increased presence of ErbB-expressing cells. However, SKOV3 tumours are associated with a substantial influx of macrophages (see Figure 4-12). When comparing macrophage content in SKOV3 tumour bearing mice with the macrophage content in tumour-free mice, a significantly higher amount of macrophages is detected in SKOV3 tumour-bearing

mice. This increased macrophage content could also contribute to the increased toxicity at a lower $T4^+$ T-cell dose.

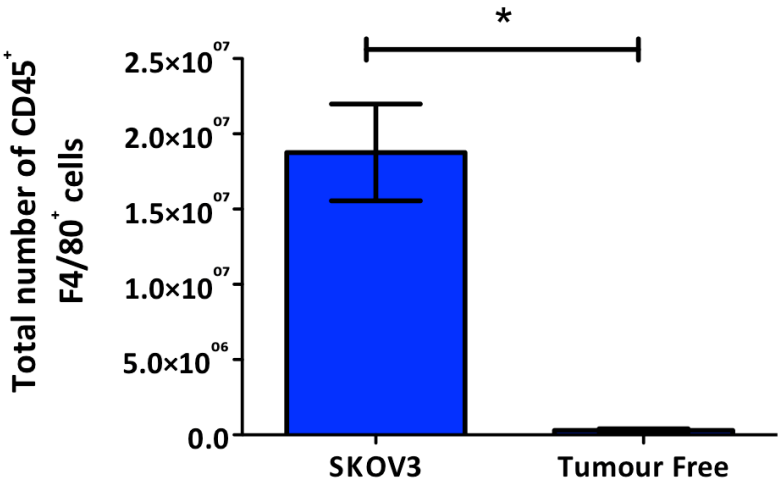

Figure 4-12 Macrophage content in the peritoneal cavity of SKOV3 tumour-bearing and tumour-free mice

Macrophage content in the peritoneal cavity was determined in mice with 14 days-established SKOV3 intra-peritoneal tumours (n=3; mean ± SD; left bar) compared to tumour free mice (n=3; mean ± SD; right bar). * = $p<0.01$

4.2.6 Cytokine Release Syndrome does not occur after Peri-Tumoural T4 Immunotherapy

The pre-clinical results presented above raise concerns that T4 immunotherapy may induce CRS in man. In a phase-I clinical trial, we aim to treat patients with locally recurrent HNSCC by intra-tumoural injection of $T4^+$ T-cells. To determine whether this route of administration could also induce CRS, cytokine levels were compared between mice treated with $T4^+$ T-cells using the peri-tumoural (PT) or intra-peritoneal (IP) routes (see Table 4-4). Mice had 14 day established IP or 27 day established SC HN3luc tumours and were treated with 5 x 10^6 or 10 x 10^6 $T4^+$ T-cells IP or 10 x 10^6 $T4^+$ T-cells PT. Control mice were treated with 10 x 10^6 UT T-cells. Additionally, non-tumour bearing mice were treated with 10 x 10^6 $T4^+$ T-cells (either IP or SC) to determine whether tumour burden is influential to cytokine production in both settings.

Table 4-4 Design of 'Peri-tumoural T4 treatment'-study

Number Mice	HN3 IP	HN3 SC	T-cells IP	T-cells PT
2 male	10 x 10^6	-	10 x 10^6 $T4^+$	-
2 male	10 x 10^6	-	10 x 10^6 UT	-
2 male	-	10 x 10^6	-	10 x 10^6 $T4^+$
2 male	-	10 x 10^6	-	10 x 10^6 UT
2 male	-	-	10 x 10^6 $T4^+$	-
2 male	-	-	-	10 x 10^6 $T4^+$

Efficacy and weight loss of mice treated with 10 x 10^6 $T4^+$ T-cells have been described in paragraph 4.2.3. Functionality of $T4^+$ T-cells after subcutaneous/peri-tumoural administration was confirmed with BLI tumour size measurement. As depicted in Figure 4-13, SC tumour burden was reduced after $T4^+$ T-cell administration; further tumour growth was seen in control mice treated with UT T-cells. In contrast to IP $T4^+$ T-cell administration (Figure 4-4), no significant weight loss was observed after SC/PT $T4^+$ T-cell administration (see Figure 4-14). At 24 hours after IP treatment, high circulating IFNγ levels were detected. Only background levels of IFNγ were detected at the same time-points after SC/PT treatment. These results suggest that CRS induced by $T4^+$ T-cells dose and route dependent, but independent of tumour burden

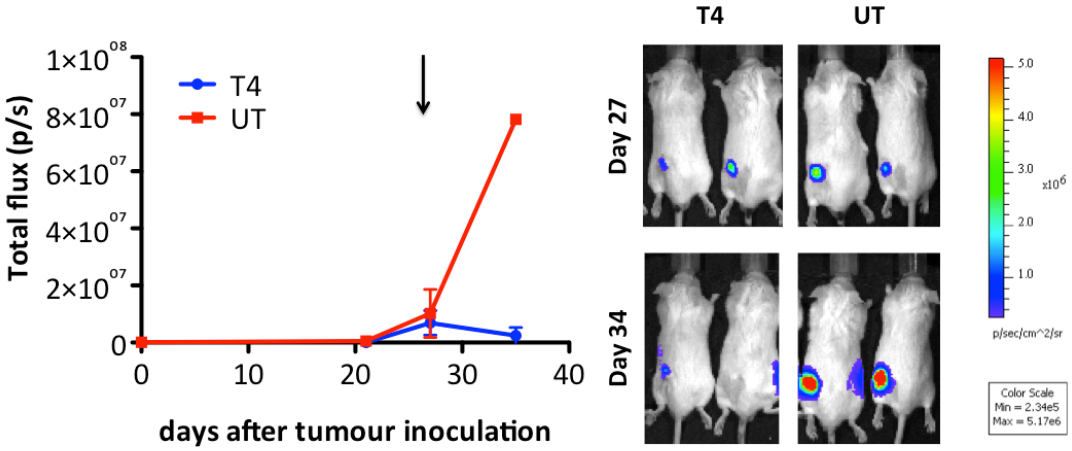

Figure 4-13 Intra-tumoural treatment of subcutaneous HN3luc tumours with 10 x 10^6 $T4^+$ T-cells

A: Mice with 27 day-established subcutaneous HN3luc tumours were treated with 10 x 10^6 $T4^+$ or UT T-cells (as indicated by the arrow). Mice were treated peri-tumoural when the tumour size did not allow for intra-tumoural injection. Serial BLI to monitor tumour growth and treatment efficacy. **B:** images of mice at the day of T-cell administration (day 27) and 7 days post treatment (day 34). All mice are shown on the same scale.

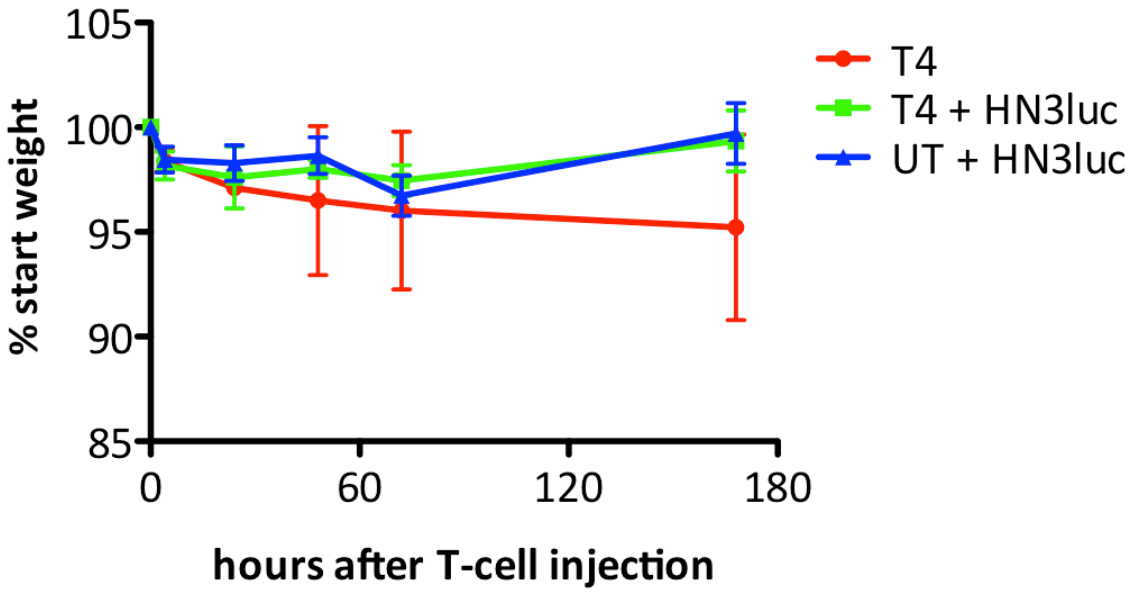

Figure 4-14 Serial weight measurements of mice following intra-tumoural treatment with 10 x 10^6 $T4^+$ T-cells

Serial weight measurements of (non) tumour-bearing mice after PT/SC treatment with 10 x 10^6 $T4^+$ (shown in red and green) or UT T-cells (blue)(mean ± SD)(n=2).

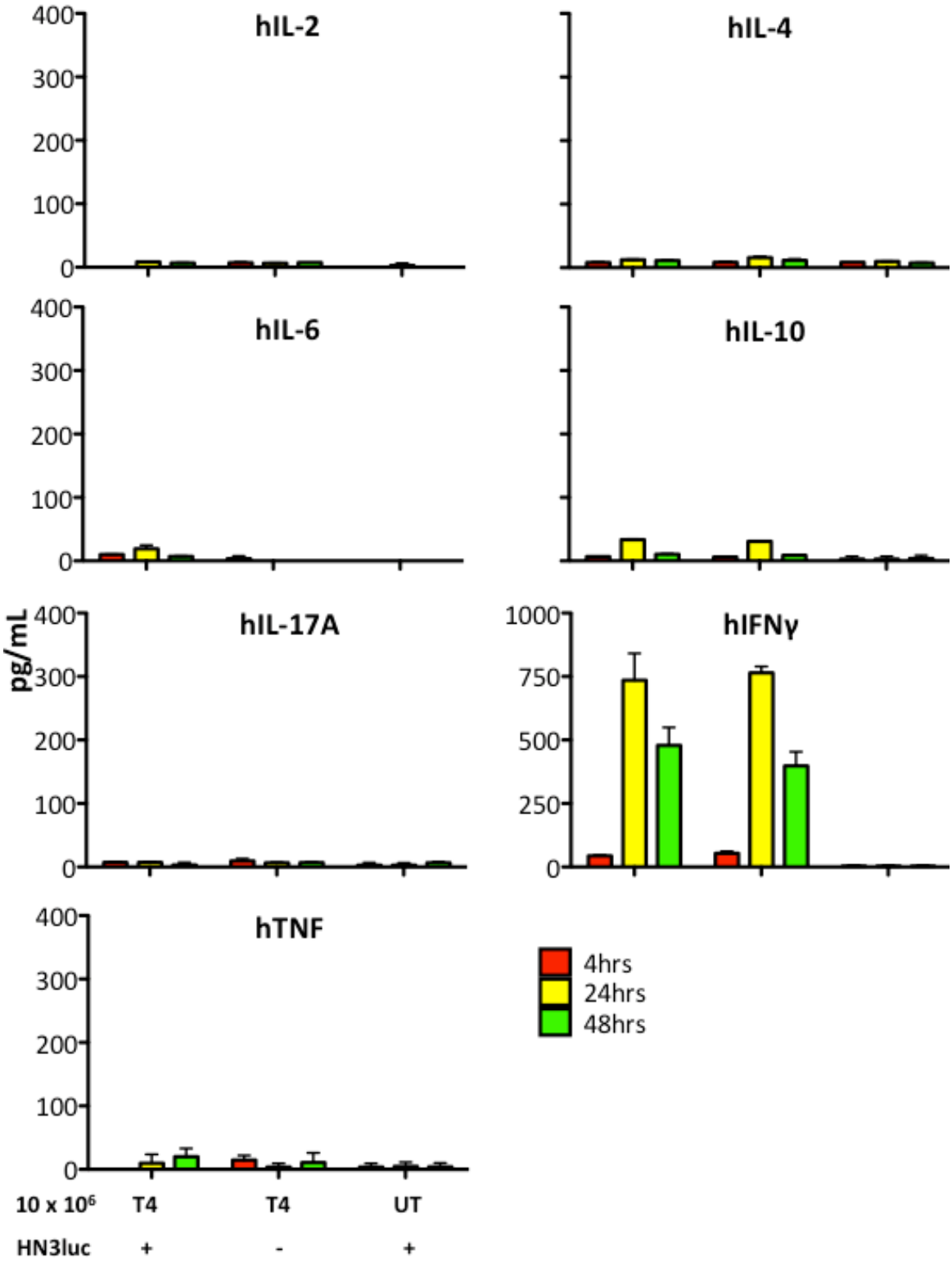

Figure 4-15 Human circulating cytokine levels after IP T4 immunotherapy administration

HN3luc tumour-bearing or tumour-free mice were treated with 10 x 10^6 $T4^+$ T-cells or UT T-cells through intra-peritoneal administration (n=2). Blood samples were collected at 4 (red), 24 (yellow) and 48 (green) hours post T-cell administration. Circulating cytokine levels were determined by cytometric bead array.

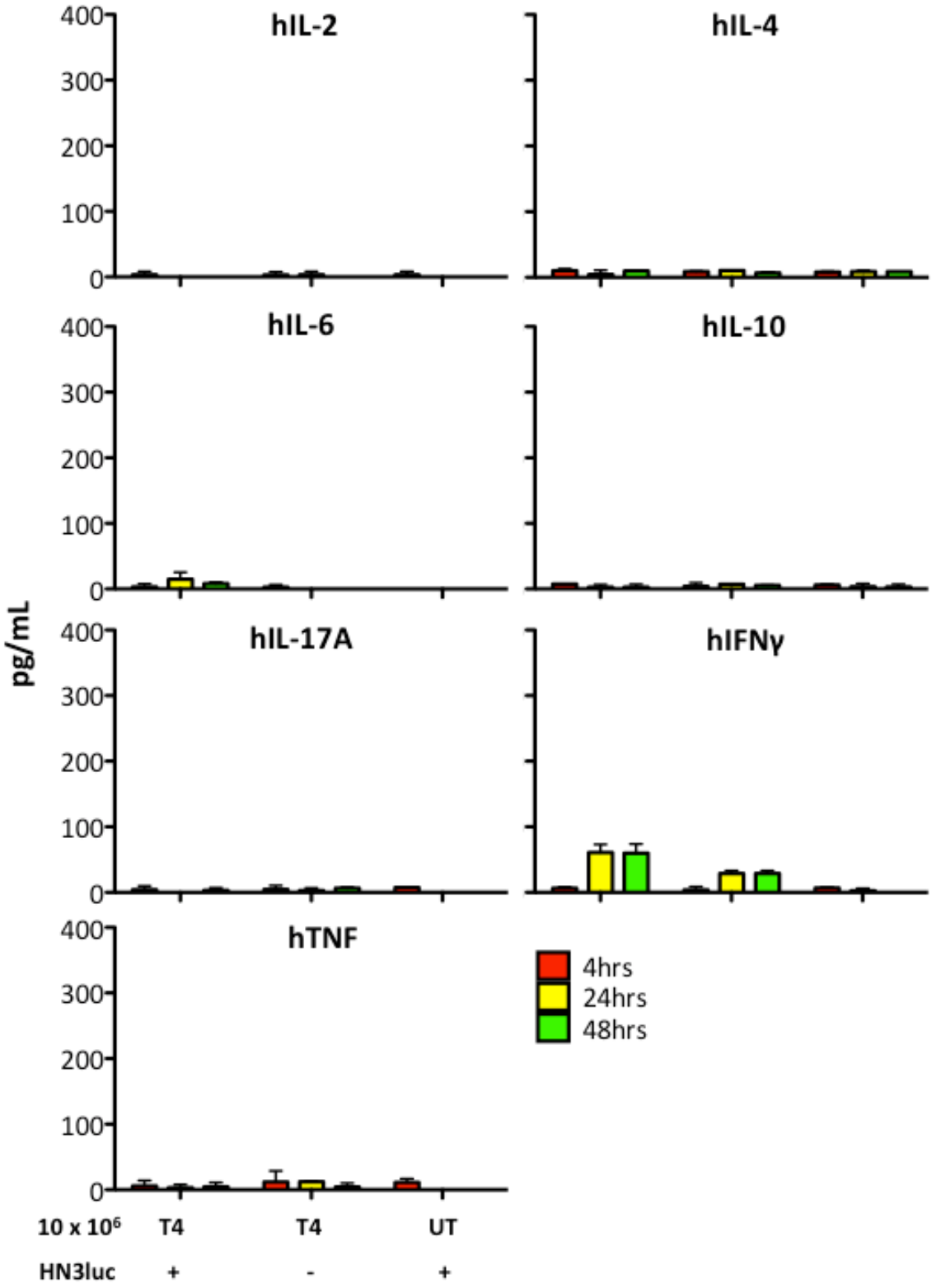

Figure 4-16 Human circulating cytokine levels after PT T4 immunotherapy administration

HN3luc tumour-bearing and non-tumour bearing mice were treated with 10 x 10^6 $T4^+$ T-cells or UT T-cells through peri-tumoural or subcutaneous administration (n=2). Blood samples were collected at 4 (red), 24 (yellow) and 48 (green) hours post T-cell administration. Circulating cytokine levels were determined by cytometric bead array.

4.3 Discussion

Cytokine release syndrome and the onset of a cytokine storm can cause severe complications in relation to infections as well as immunotherapies. Several Phase I clinical trials have shown the occurrence of cytokine storms in response to CAR-mediated adoptive T-cell transfer (240, 317, 320, 321, 445). The most severe cytokine storm was seen in a trial using ErbB2 re-targeted T-cells, in which the cytokine storm resulted in lethal multiple organ failure (240).

In relation to T4 immunotherapy, no severe toxicity had been seen in efficacy studies as well as studies focussing on the potential 'on-target'-toxicity (as described in paragraph 3.2.10). No toxicity was seen after IV or SC/PT administration of high doses (20×10^6) $T4^+$ T-cells. In contrast, in an IP xenograft model of ovarian cancer (using the fast-growing $ErbB^+$ tumour cell line SKOV3), treatment with $T4^+$ T-cells led to consistent, transient weight loss (see Figure 4-1). Furthermore, treatment of animals with high SKOV3 tumour burden resulted in lethal toxicity (see Figure 4-2). When animals bearing HN3luc intra-peritoneal tumours were treated with $T4^+$ T-cells, transient weight loss was also induced. However, this weight loss was also seen in non-tumour bearing animals. This finding suggests that human $T4^+$ T-cells can engage mouse ErbB receptors on non-transformed cells within the peritoneal cavity (see Figure 4-4). The administration of escalating doses of T-cells in non-tumour bearing animals resulting in rapid weight loss, triggered within hours after T-cell administration. At the highest treatment dose (30×10^6 $T4^+$ T-cells), toxicity was lethal (see Figure 4-5). Analysis of circulating cytokines revealed that the toxicity was due to cytokine release syndrome. Within four hours after T-cell administration, elevated levels of human IL-2, human IFNγ and mouse IL-6 were detected (see Figure 4-6 and Figure 4-7). The severity of the induced cytokine release syndrome, and the fact that it is only induced after intra-peritoneal T-cell administration might be a reflection of the magnitude of target recognition within tumour deposits and/or serosal cells within the peritoneal cavity, followed by systemic cytokine absorption. Three elements would support this hypothesis. First, CAR^+ T-cells reside within the peritoneal cavity after IP administration, without detectable re-location to other anatomic sites (460). Second, ErbB1 is expressed by normal mesothelial cells, providing a potential source of $T4^+$ T-cell stimulation in the peritoneal cavity (593). Third, preliminary data suggests that efficacy and toxicity increase when the T-cell are administered in a larger injection

volume. The resulting increase in IP pressure may increase the absorption of small molecules, including cytokines, and exert pro-inflammatory effects leading to increased production of IL-6 and other cytokines (594). The influence of the injection volume would also explain why no CRS-related toxicity was seen in previous studies in which mice were treated with high doses of T28ζ^{+}/T4^{+} T-cells (299).

Phase I clinical trials in CAR-mediated ACT have implicated IL-6 as an important factor in the occurrence of toxicity. The severity of cytokine release syndrome was reversed in patients by treatment with the anti-IL-6R antibody, Tocilizumab (317, 321). To determine whether IL-6 is a similarly important factor in the mouse model, blockage of mouse IL-6 or IL-6R is required. Tocilizumab does not cross the species barrier. A murine equivalent is being sourced which would allow for the evaluation of the effect of mIL-6R blockage in this model.

It has been suggested that monocytes and macrophages also play a role in the cascade resulting in cytokine release syndrome (575, 577). SCID/Beige mice are not completely immunodeficient, in that the mice still have functional macrophages (587). Therefore it was hypothesized that the mIL-6 was produced by the mouse macrophages present in the intra-peritoneal cavity, leading to clinical manifestations of CRS. Two results support this hypothesis. First, depletion of macrophages prior to T4^{+} T-cell administration eliminated IL-6 production and weight loss (see Figure 4-10 and Figure 4-11). Second, intra-peritoneal SKOV3 tumours are associated with a heavy influx of macrophages (see Figure 4-12). The higher macrophage content combined with the high expression of ErbB receptors on the tumour tissue could have contributed to the lethality of the toxicities seen at a T-cell dose of 10 x 10^{6} T4^{+} cells, whereas the same dose was not toxic in mice with an HN3luc tumour burden and a three fold higher dose was required to induce similar toxicity in non-tumour bearing mice.

Human IFNγ levels were also elevated in a dose-dependent manner after intra-peritoneal T4^{+} T-cell administration. In human, intravenous administration of IFNγ is associated with toxicities including fatigue, fevers, chills, anorexia, occasional nausea and vomiting, headaches, mild hypotension and granulocytopenia (595, 596). However, the influence of elevated IFNγ levels to toxicity can not be evaluated in this model because IFNγ is species-specific with respect to receptor binding and biological activity (597).

The absence of cytokine release syndrome in response to PT/SC T-cell administration is encouraging for the safe application in patients with HNSCC through intra-tumoural T-cell administration. However, due to the limitations of the pre-clinical mouse model, careful monitoring of circulating cytokine levels and clinical signs of cytokine release syndrome is of great importance.

CHAPTER 5

DEVELOPMENT OF A GMP-COMPLIANT TRANSDUCTION AND EXPANSION METHOD

5.1 Introduction

The pre-clinical toxicity studies discussed in the previous chapters suggest that T4 immunotherapy could have therapeutic potential in the treatment of HNSCC. To determine the safety of T4 immunotherapy in man, we aim to conduct a Phase-I clinical trial, treating patients with local recurrent HNSCC with intra-tumoural T-cell administration (EudraCT Number: 2012-001654-25; Clinicaltrials.gov Number: NCT01818323; REC Number: 12/LO/1843).

The primary aims of the study are:

1. Determine the dose limiting toxicities for T4 immunotherapy in HNSCC.
2. Determine a safe and feasible recommended dose for Phase-II testing.

Secondary objectives include:

1. Investigation of serum cytokine levels.
2. Persistence of $T4^+$ T-cells.
3. Assessment of preliminary anti-tumour activity.
4. Investigate the tumour ErbB phenotype before and after treatment.
5. Investigate the effect of T4 immunotherapy upon immune reactivity against endogenous tumour antigens.
6. Investigate the immunomodulatory effects of metronomic cyclophosphamide.

The trial is designed in a 3+3 format. In this format, the maximum administered dose occurs when two out of three (or two out of six with cohort expansion) patients experience a dose-limiting toxicity (DLT). If this occurs, the maximum tolerated dose (MTD) will be identified as the dose of the cohort below the maximum administered dose. When one DLT occurs in a cohort of three patients, the cohort is expanded with at least three additional patients (598).

The starting dose will be 1×10^7 $T4^+$ T-cells, which will be increased to 1×10^9 $T4^+$ T-cells over 5 dose escalating steps (see Table 5-1). If the MTD is not defined after completion of the dose escalation, a final cohort will be treated with 50mg cyclophosphamide for 14 days prior to T4 immunotherapy administration.

Table 5-1 Dose escalation protocol T4 immunotherapy

Notes	Dose level (cohort number)	Target dose (cells) [§]	Acceptable dose range (cells)[§]	Injection volume (mL)
	-1*	3×10^6	3×10^6	1 ± 0.2
Starting dose level	1	1×10^7	$3 \times 10^6 - 1 \times 10^7$	1 ± 0.2
	2	3×10^7	$1.1 - 3 \times 10^7$	1 ± 0.2
	3	1×10^8	$3.1 - 10 \times 10^7$	1 ± 0.2
	4	3×10^8	$1.1 - 3 \times 10^8$	1 ± 0.2
Final dose level	5	1×10^9 ⌘	$3.1 - 10 \times 10^8$	1 ± 0.2
Lymphodepletion❖	6	1×10^9 ⌘	$3.1 - 10 \times 10^8$	1 ± 0.2

[§] Indicated dose levels refer to the number of $T4^+$ T-cells, not total cell number.

* a '-1' dose level has been included in case dose de-escalation is required from dose level 1.

⌘ Maximum of $1x10^9$ total cells, which is the greatest number that can be accommodated within the injection volume.

❖ Cyclophosphamide 50mg PO once daily for 14 days prior to T4 immunotherapy

In order to be able to apply T4 immunotherapy, a good manufacturing process (GMP) compliant culture process had to be developed. The GMP manufacture of cell products is not without technical challenges. Most commonly, a leukapheresis product is used which is then processed in a highly time consuming and labour intensive open process, within Grade A isolators (599-602). Due to the requirement of highly specialised equipment, manufacturing is limited to specialised facilities, is costly, at risk of contamination due to the open processing, and not readily amendable to upscaling. Additionally, gene transfer efficiency is variable and when below specification, this can lead to difficulty in the release of poorly transduced cell products (320). With these challenges in mind, I aimed to design a robust production protocol for T4 immunotherapy under GMP.

The described process has been developed in collaboration with Dr MC van Schalkwyk and Mrs L Bosshard-Carter. The majority of the equipment and materials used are readily available for GMP production, allowing for easy translation of the process to other cell manufacturing protocols. Here, an outline of the process is described, as it will be performed within the Clinical Research Facility (CRF) GMP Unit, 15th Floor, Tower Wing, Guy's Hospital in accordance with the MIA(IMP) provisions granted to the facility (licence number 11387).

5.2 List of Materials

An overview of the most important materials required is given in Table 5-2.

Table 5-2 Table of Materials required for process

Product Name	Company
Culture Bags	
VueLife 197-AC culture bag	CellGenix GmbH
VueLife 118-C culture bag	CellGenix GmbH
MACS GMP Cell Differentiation Bag 3000mL	Miltenyi Biotech
MACS Cell Expansion Bag 100mL	Miltenyi Biotech
Pouches	
AK100 sample pouch 5mL	Biosafe
Media and Serum	
X-VIVO15 media	Lonza
Human AB Serum	Seralab
Stable L-Glutamine	PAA
Cytokines	
GMP-grade IL-4	Gentaur
IL-2: Aldesleukin (proleukin)	Novartis
Other	
N-Labstix	Siemens
CD3/CD28 CTS Dynabeads	Invitrogen
RetroNectin 2.5mg GMP-grade	Takara
GMP Grade SFG-T4 virus	Eufets
Luer Syringes	BD Plastipak
Sepax Manifold CS900.2	Biosafe
Sepax Manifold CS600.1	Biosafe
BacT/ALERT Microbial detection system	bioMérieux
Saline 0.9% w/v 500mL	Baxter
Trucount tubes	BD Biosciences
Equipment	
Grade A Isolator	Amercare
TSCD II sterile tubing welder	Terumo
T-SEAL II sterile sealing device	Terumo
Sepax 2 closed automated cell separation platform	Biosafe
Dynal MPC-1	Invitrogen
Dynal ClinExVivo MPC magnet	Invitrogen
Plasmatherm	Genesis

5.3 GMP-Compliant Production Process

The cell production is a 15-day process from phlebotomy to T-cell administration to the patient. The protocol can be divided into five major elements (see Figure 5-1); PBMC isolation and activation (day 1), transduction (day 4), expansion (day 5-13), de-beading (day 14) and preparation of final cell product (day 15). The process during these five elements is described below.

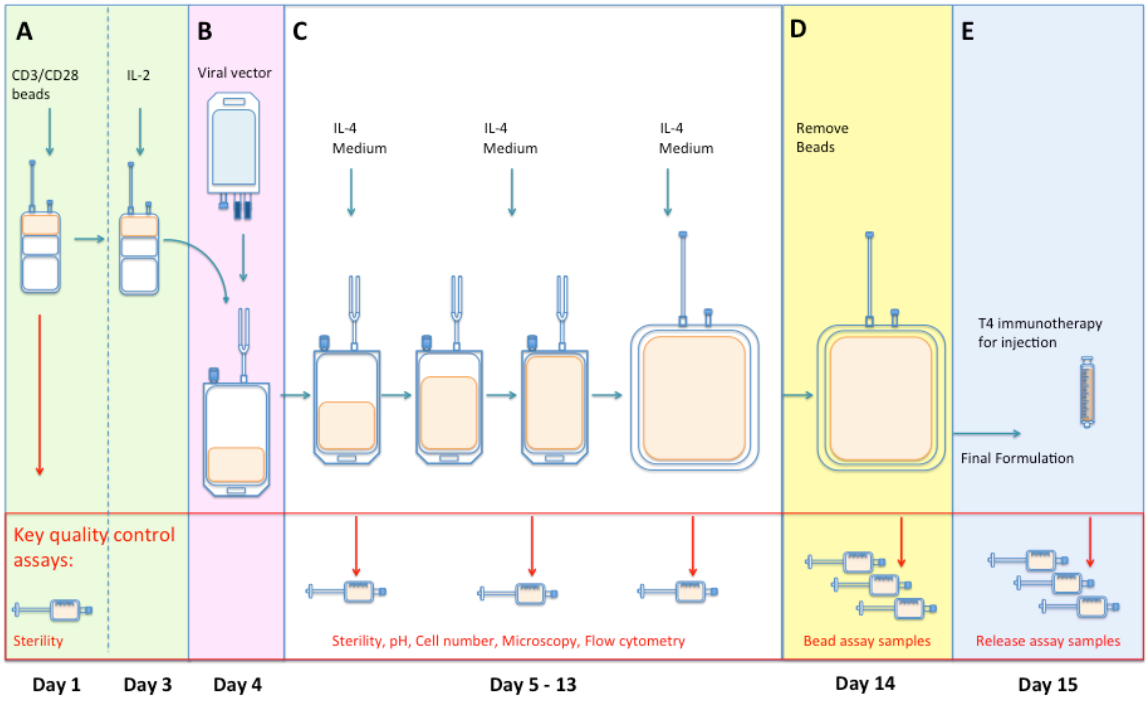

Figure 5-1 Schematic overview of GMP T-cell Transduction and Expansion protocol
A: PBMCs are isolated from whole blood using the Sepax closed automated cell separation platform and activated using CD3/CD28 CTS paramagnetic beads on day 1. **B**: Activated T-cells are transduced on day 4. **C**: Transduced cells are expanded using Interleukin-4 (day 5-13). **D**: Cell-culture is de-beaded on day 14. **F**: The final cell product is formulated and administered to the patient on day 15.

5.3.1 Day 1 – PBMC Isolation and T-cell Activation

The first day of the process consists of two elements, the isolation and activation of the patient's T-cells, and the preparation of the RetroNectin (RN)-coated transduction bag (see Figure 5-1 B).

Peripheral blood mononuclear cells are isolated with the 'NeatCell' protocol on a Sepax 2 closed automated cell separation platform using the CS900.2 single-use manifold. Using the 'small final volume'-option, PBMCs are re-suspended in 10mL complete media and the final product is presented in a 20mL syringe that is connected to the single-use manifold. The PBMCs are transferred to a MACS GMP cell expansion bag, through sterile welding and sealing. A sample of approximately 0.5mL is retained in the syringe to allow for cell enumeration. The cell number is determined using a Scepter automated cell counter. Cells are re-suspened to a final concentration of 3 x 10^6 cells/ml.

Paramagnetic CD3/CD28 CTS ClinExVivo T-cells activation beads are used for T-cell activation. The required amount of beads is calculated based on a ratio of 3 beads per cell. Within the isolator, beads are washed 3x using the complete media on a Dynal magnetic particle concentrator (MPC)-1. Beads are re-suspended at a concentration of 400 x 10^6 beads/mL and the required amount (rounded to the nearest 100µL) is added to the MACS GMP cell expansion bag through injection through the needle port. At this point samples are taken again to allow for sterility testing. The MACS GMP cell expansion bag containing the cells and beads is incubated at 37°C, 5% CO_2 and saturated humidity for until further use (on day 3).

Preparation of the RetroNectin-coated 197-AC VueLife bag

A 197-AC VueLife bag is coated with RetroNectin (RN) within the isolator. The bag is coated with 2.5mg RN, which is a ratio of approximately 5µg/cm^2. To achieve this, 2.5mg of lyophilized RN is dissolved in a total volume of 150mL saline (0.9% w/v). The first 100mL saline is directly injected into the VueLife bag, using Luer syringes and needles. The final 50mL saline is drawn up in a syringe, after which a needle is added and approximately 2mL of the saline is added to the lyophilized RN. After ensuring the RN is completely dissolved, it is drawn back up into the syringe and the 50mL RN-containing saline is added to the VueLife bag. The bag is massaged to facilitate even distribution of the RN and stored at 4°C until transduction at day 4 of the process.

5.3.2 Day 3 – Preparation of T-cell Transduction

On the day prior to T-cell transduction, 100U/mL IL-2 is added to the T-cell culture (see Figure 5-1 B). The amount of IL-2 required is based on the total culture volume and rounded off to the nearest 1000U.

5.3.3 Day 4 – Transduction of T-cells

On day 4, activated T-cells are transduced with clinical grade SFG-T4 viral vector (see Figure 5-1 C). The vector has been produced under GMP conditions by EUFETS GmbH, and is at a viral titre of 2.77 x 10^6 infectious units (IU)/mL. The virus is presented in serum-free, phenol red-free X-VIVO10 media, and stored in 60mL aliquots in 150mL Flexboy bags at -80°C until the day of use. The viral vector is thawed using the Plasmatherm and the complete content is transferred into the RN-coated VueLife bag. Cell density in the MACS GMP cell expansion bag is determined and a maximum total of 40 x 10^6 cells are added to the VueLife bag. The 197-AC VueLife bag is incubated at 37°C, 5%CO_2 and saturated humidity. The bag is turned twice at 15 minute-intervals to stimulate cell and virion engagement at both sides of the bag. There is no centrifugation step required at this stage.

5.3.4 Day 5-13 Expansion of Transduced T-cells

The required amount of media and cytokine required during the expansion period is determined based on cell density and the pH of the media. Both are determined on a daily basis. At regular fixed intervals, IL-4 is added irrespective of cell density or pH. When the culture volume exceeds 500mL total volume, the cell culture is transferred to a 3000mL MACS GMP cell differentiation bag through sterile welding, gravitational flow and sterile sealing. On day 8, additional samples are taken to allow for interim sterility and transduction rate assessment.

5.3.5 Day 14 – De-Beading of Cell Culture

On the day prior to T-cell administration to the patient, the cell-culture is de-beaded using a Dynal ClinExvivo MPC magnet (see Figure 5-1 E). Prior to de-beading, pH and cell density is determined and, if required, media and cytokines are added. To ensure maximal bead removal, the cell culture is passed over the primary and secondary

magnet twice, through a series of connected transfer bags by gravitational flow (see Figure 5-2).

Prior to de-beading, a sample is taken using an AK100 sample pouch to function as a positive control in the enumeration of residual Dynabeads (described in paragraph 5.4). The cell culture bag is welded onto one of two tubing lines of a 1000mL transfer bag. The second line of the transfer bag is welded onto one of two lines of a 2000mL transfer bag (the 'collection'-bag). The second line of the collection-bag is sealed-closed. The cell culture bag is hung onto the bag stand of the magnet. The 1000mL transfer bag is placed on the primary magnet bed. The tubing connecting the two transfer bags is coiled around the secondary magnet. Approximately a quarter of the cell culture volume is passed into the transfer bag and allowed to set for three minutes. Clamps are placed on the tubes connecting the bags to prevent continuous flow. After three minutes the culture is allowed to flow into the collection-bag, passing the secondary magnet in the process. The process is repeated three more times, allowing the complete culture to be passed over the magnets. The entire process is repeated a second time. For this, the 'collection-bag' is welded onto a new 1000mL transfer bag. The second line of the transfer bag is connected to a 3000mL MACS GMP cell differentiation bag. Finally, a 200mL aliquot of complete media is welded onto the transfer bag and placed on the bag stand. The media is allowed to flow through with the aim to remove any remaining T-cells that may be loosely attached to the retained beads. The cell culture bag incubated at 37°C, 5%CO_2 and saturated humidity until further use.

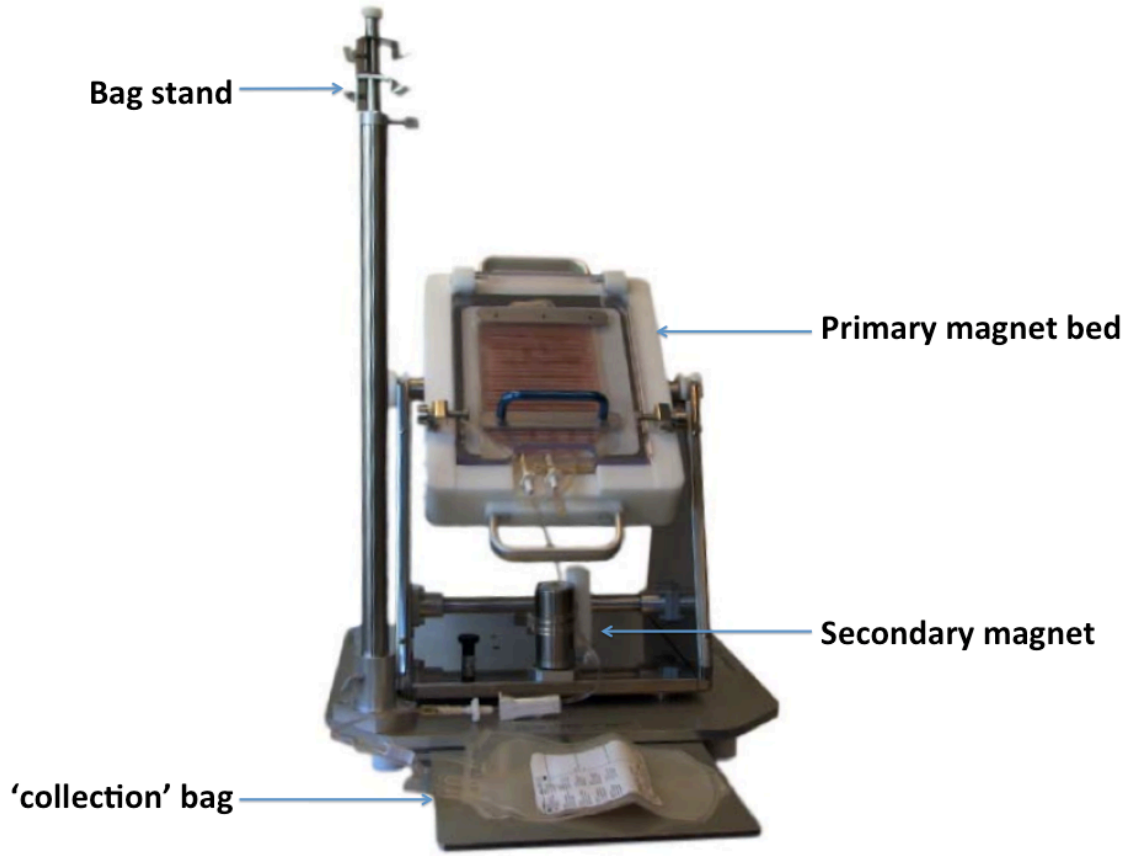

Figure 5-2 Overview of Dynal ClinExVivo MPC magnet
Cell culture is de-beaded using the Dynal ClinExVivo MPC magnet (603). The cell culture bag is placed on the bag stand, one third of the culture volume is transferred into the transfer bag placed on the primary magnet bed, remaining there for three minutes. The cell culture is then passed on into the 'collection' bag, passing the secondary magnet in the process.

5.3.6 Day 15 – Preparation of the Final Cell Product

At the final day of the process, the cell culture is concentrated to the required concentration, and all release criteria are verified (see Figure 5-1 E). Samples for release criteria testing are removed using AK-100 sample pouches. The release assays are performed and reviewed by the Qualified Person within two and a half hours. When release of the product is approved, the final formulation is transferred to the administering physician. The cell product is then immediately administered by intra-tumoural injection.

5.4 Release Criteria Assessment

To allow for release of the product, the end of production quality control assays have to be performed on the day of release (day 15).

Table 5-3 Overview of Quality Control Assays

Release Criteria	Timepoint	Method
≥ 70% cell viability	Day 15	DAPI staining and flow cytometry
≥ 10^7 $T4^+$ cells	Day 15	Flow cytometry
≥ 2 fold-increase in cell number	Day 15	Cell count, compared to number transduced cells on day 3
Cell surface phenotype ≥10% $T28\zeta^+$	Day 15	Flow cytometry
Bacterial, fungal and mycoplasma sterility	Day 1, 8 and 15	BacT/ALERT, fungal and mycoplasma testing.
Residual beads < 333,000 per mL	Day 15	Flow cytometry

Bacterial, fungal and mycoplasma sterility testing of the final product are performed according to the European Pharmacopeia by Wickenham Laboratories (Gosport, UK) and Mycoplasma Experience (Reigate, UK). Due to the duration of sterility testing (6 – 28 days), interim samples (taken at day 1 and day 8) are required to be negative at the day of release. Results of sterility testing on the final product will be used retrospectively.

All flow cytometry assays are performed by the staff of the Immune Monitoring Laboratory, NIHR Biomedical Research Centre at Guy's and St Thomas' NHS Foundation Trust and King's College London. Cell viability is determined using DAPI staining, and absolute number of viable cells is determined using Trucount beads. The proportion of $T4^+$ T-cells is determined by staining for T28ζ (using biotinylated anti-human EGF followed by PE-conjugated streptavidin). All flow cytometry assays were validated for accuracy and inter-observer variability (data not shown).

Traditionally, enumeration of residual CD3/CD28 CTS Dynabeads is determined using haemocytometer-based manual counting (604, 605). However, this approach is subjective and has a high inter-observer variability. For more reliable and consistent results, Dr van Schalkwyk developed a novel flow cytometric assay, based on the autofluorescence of the Dynabeads (see Figure 5-3 A). In short, samples are taken

before (day 14) and after (day 15) de-beading of the cell culture. Cells are lysed using 10% Triton X-100. An aliquot of each sample is transferred to a Trucount tube and analysed following the gating strategy shown in Figure 5-3. The auto-fluorescence of the Dynabeads is detected in the PerCP-Cy5.5 and APC channels using a BD FACSCanto II flow cytometer. Parameters are set to count 1000 events within the 'Trucount gate' The sample obtained prior to de-beading is used as a positive control and to create the 'Dynabead gate'. Both before and after samples are analysed in the same manner (see Figure 5-3 B). The number of residual beads is calculated using the following formula:

$$\frac{\text{no of beads in 'Dynabead gate'}}{\text{no of beads in 'Trucount gate'}} \times \frac{\text{no of Trucount beads per test}}{\text{test volume}} = \text{absolute bead count}$$

The assay was validated using several known concentrations of Dynabeads (ranging from 500,000 – 800 beads/mL) based on dilutions of original manufacturer's stock. The assay was verified using multiple sample sets, performed by two individual operators. Bead enumeration using this method proved to be accurate and consistent over the full range of concentrations tested (data not shown).

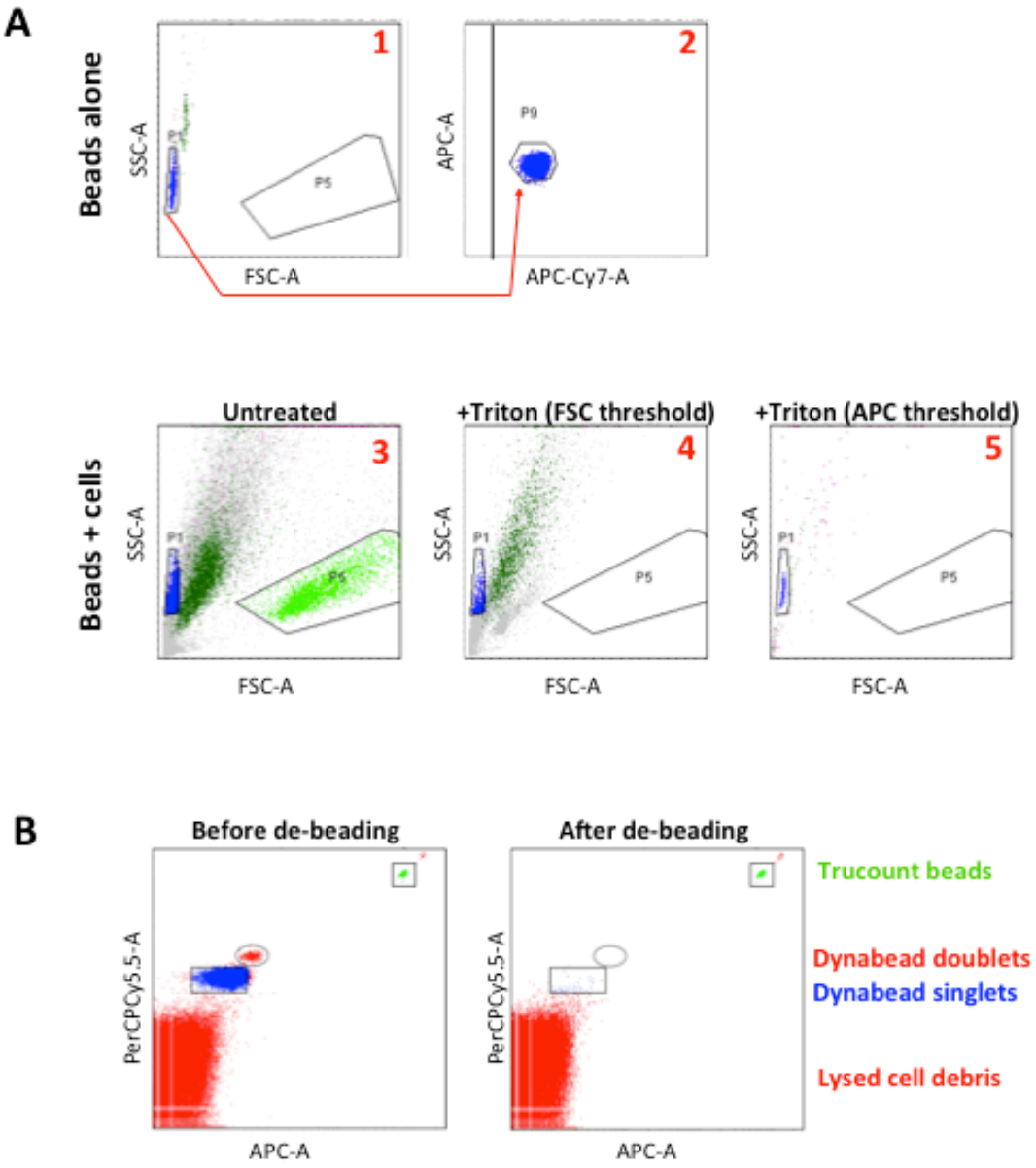

Figure 5-3 Enumeration of residual CD3/CD28 CTS Dynabeads

A: Dynabeads fall within a discrete gate (blue) in the forward (FSC-A) v side scatter (SSC-A) plot (1). Dynabeads are autofluorescent, meaning that a threshold can be set in any one of several fluorescence channels to eliminate non-fluorescent debris (2). When Dynabead-containing T-cell cultures are analysed, there is overlap between beads (blue) and dead cells (grey and dark green) (3). In this plot, viable T-cells are seen in the gate on the right (light green). Following lysis of T-cells with Triton X-100 and setting of a FSC threshold, unacceptable overlap still occurs between Dynabeads and cell debris (4). However, by setting a threshold based on fluorescence, Dynabeads can be clearly visualised as a discrete and separate population (5). **B**: Enumeration of Dynabeads in samples before and after de-beading using Trucount tubes. Owing to their autofluorescence, Dynabeads fall into a discrete gate compared to Trucount beads and lysed cell debris. Data are normalised to the number of Trucount beads counted in a separate gate, allowing the generation of an absolute count.

5.5 Transduction of Patient Samples

The closed production process was developed to achieve reproducible transduction and expansion of T-cells for clinical application. All pre-clinical work had been performed using PBMCs derived from healthy donor blood. In order to determine whether successful transduction and expansion could also be achieved using (often immunodeprived) patient blood, samples were obtained from HNSCC patients. The recruitment of patient donors was approved by the Guy's Hospital Research Ethics Committee (09/H0707/086; Generation of clinical grade T-cells for adoptive cell therapy). A total of seven patient samples were successfully transduced and expanded. Due to the limited availability of the clinical-grade virus produced by EUFETS, samples were transduced with non-clinical grade virus, which was produced, aliquotted and stored in a similar manner. One patient sample (patient 05) failed, in which no viable T-cells remained after transduction. Successful expansion (Figure 5-4) and enrichment (Figure 5-5) of six patients samples was achieved. All samples passed the tested release assay criteria. All samples showed at least a 2 fold-increase in total cell number on day 15 compared to day 4 (see Figure 5-4). Also, in all cases the minimum of 10% $T4^+$ cells was achieved (ranging between 16.4%, patient 02 and 94.5%, patient 01) (see Figure 5-5). In all six patient samples, the minimum dose of 1 x 10^7 $T4^+$ T-cells was achieved at the end of the 15-day culture period (see Table 5-4). No contamination was detected in any of the samples (data not shown).

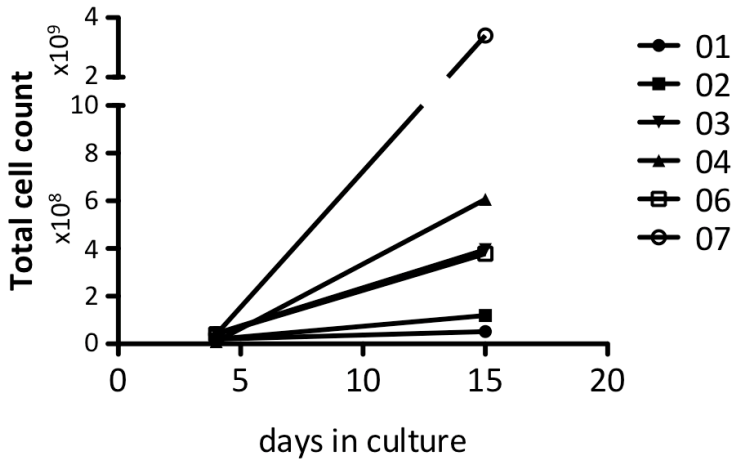

Figure 5-4 Expansion total cell count patient samples using closed GMP process
Expansion of total amount of cells from day 4 (amount of cells transduced) to the final day of production (day 15). NOTE: Amount of transduced cells was 20 x 10^6 in patients 01 and 02. For all other patients, 40 x 10^6 T-cells were transduced.

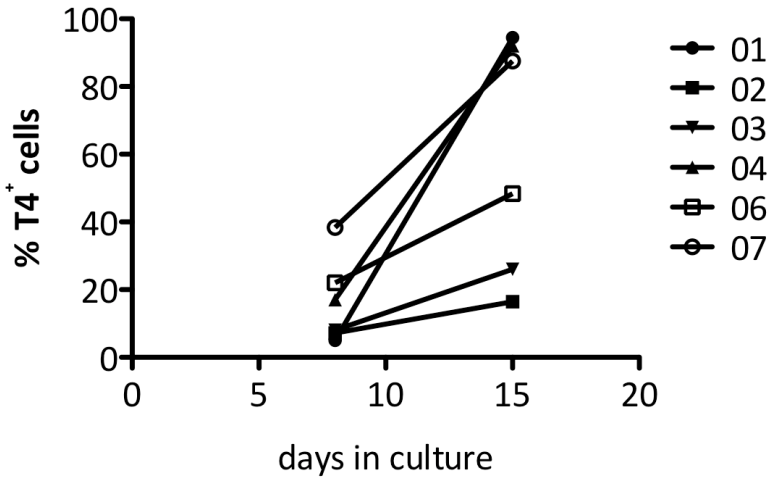

Figure 5-5 Enrichment of $T4^+$ cells in patient samples using closed GMP process
Amount of $T4^+$ T-cells is determined on day 8 (4 days after T-cell transduction) and day 15 (day of product release) using flow cytometry.

Table 5-4 Expansion of total $T4^+$ T-cells

	01	02	03	04	06	07
Day 8	1.00×10^6	1.44×10^6	3.50×10^6	1.70×10^6	8.8×10^6	1.54×10^7
Day 15	4.91×10^7	1.97×10^7	1.03×10^8	5.58×10^8	1.83×10^8	2.98×10^9

Total $T4^+$ T-cells are calculated based on total cell count multiplied by the transduction rate as determined by flow cytometry

To determine the functionality of $T4^+$ T-cells from patient samples, 1×10^6 total cells were co-cultivated with confluent monolayers (24 wells) HN3 tumour cells. Figure 5-6 presents representative crystal violet monolayer destruction assays performed using T-cells from the highest (patient 01) and lowest (patient 02) transduced samples. Monolayer destruction was visualised after 24 hours of co-cultivation. Within this period, complete monolayer destruction was achieved by the T-cells derived from patient 01, and partial monolayer destruction was achieved by the T-cells derived from patient 02. The difference in magnitude of monolayer destruction can most likely be attributed to the difference in absolute $T4^+$ T-cell content. Additional to monolayer destruction, cytokine production (IL-2 and IFNy) after 24 hours of co-cultivation were measured (see Figure 5-7) in five of the six successfully transduced samples. A significantly higher cytokine production, for both IL-2 and IFNy was measured when $T4^+$ T-cells were exposed to $ErbB^+$ HN3 tumour cells, compared to T-cells which were not exposed to any target.

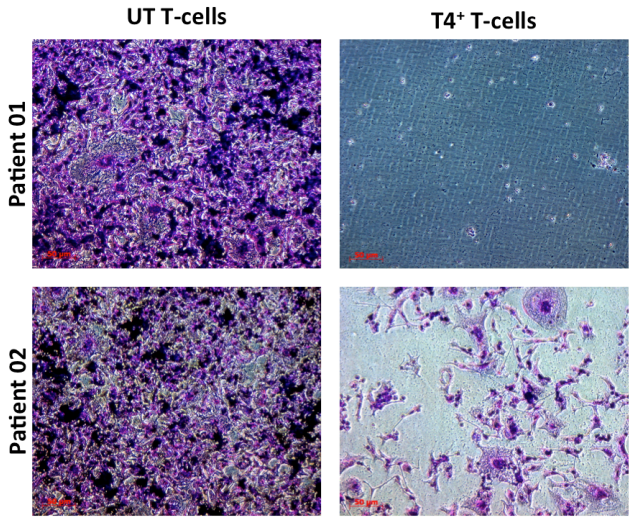

Figure 5-6 Monolayer destruction after 24 hour co-cultivation using crystal violet
T4 transduced or untransduced (UT) patient T-cells (1 x 10^6) were co-cultivated with confluent HN3 monolayers (24 well) for 24 hours. Monolayer destruction was visualised using crystal violet staining.

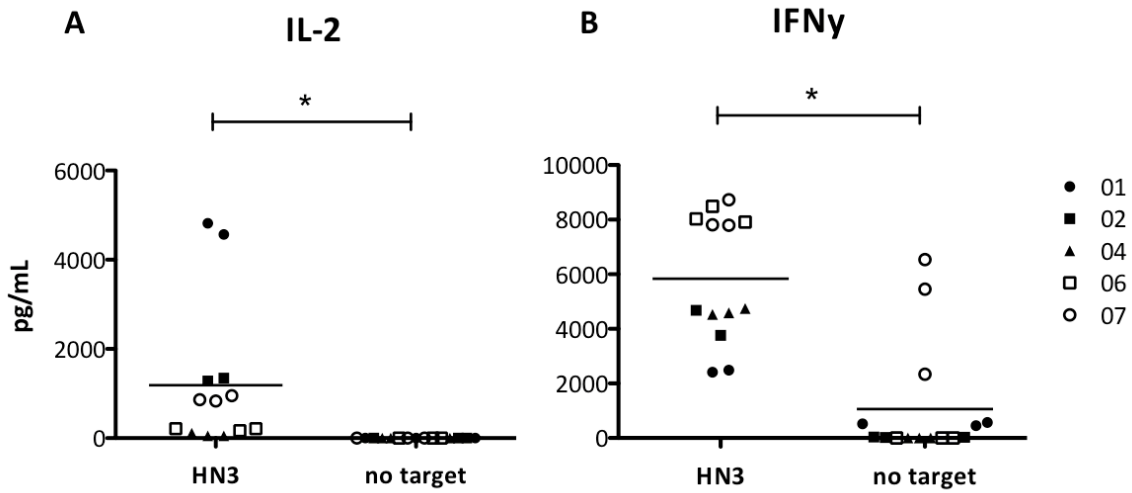

Figure 5-7 Cytokine production co-cultivation patient samples with tumour monolayers
IL-2 (**A**) and IFNγ (**B**) production in supernatants of co-cultivation of 1 x 10^6 T4-transduced T-cells with a confluent (24 well) HN3 monolayer or T4 transduced T-cells alone. Cytokine production is measured after 24 hours by ELISA. N=3 per patient sample, bar represents overall average of all samples. * = $p < 0.05$

5.6 Discussion

The production of cell therapy products under GMP is not without challenges. Challenges arise both from the quality of patient's PBMCs as well as the production process. Adoptive cell therapy products have been produced successfully from HNSCC patient PBMCs. Lymphokine-activated killer cells, IL-2 activated TILs, and tumour specific cytotoxic T-cells have been successfully cultured and expanded (264, 268). However, it has also been reported that PBMCs from HNSCC patients have been can undergo spontaneous apoptosis upon *in vitro* culture for as little as 12-24 hours (226). We aimed to develop a robust GMP-compliant cell manufacturing process for the production of T4 immunotherapy. Six out of seven patient samples were successfully transduced and expanded. All resulting products were of the required quality for the application in a clinical trial and were functional *in vitro*. The successful transduction of six patient samples confirms the applicability of the developed GMP-compliant manufacturing process. Additionally, it shows that the transduction and expansion of HNSCC PBMCs for clinical application is feasible.

CHAPTER 6

DISCUSSION

The main aim of this PhD was to determine the potential toxicity of T4 immunotherapy, through the use of *in vitro* and *in vivo* pre-clinical models. I also set out to compare potential toxicity that could be induced by intra-tumoural $T4^+$ T-cell administration, making comparison with other routes of delivery.

The 5-year survival rate for HNSCC has remained stable at approximately 60% over the past 5 decades (3-5). Treatment options for patients who present with locally advanced disease at diagnosis (which comprises about two-thirds of patients) is limited and at least 50% of patients relapse after initial treatment (5, 34). Adoptive cell therapy could be an attractive additional treatment option for these patients. Head and neck tumours are generally significantly infiltrated by immune cells (221, 222). However, the functionality of tumour infiltrating lymphocytes is often impaired due to low or absent ζ-chain expression, decreased proliferation and lack of IL-2 production (221, 223-225). Impaired immune function (based on the level of ζ-chain expression in TILs and the number of intra-tumoural DCs) has been correlated to poor survival. Enhancement of immune function could therefore benefit patient survival. Adoptive cell therapy for HNSCC has achieved encouraging results in clinical trials (265, 266). Tumour necrosis was achieved with intra-tumoural injections of allogeneic, OK-432 activated splenocytes, without any toxic effects (265). Intra-tumoural injection of OK-432 activated autologous PBMCs combined with chemo- and radiotherapy complete remission was achieved in 35% of patients and partial remission in 53% of patients (266). These trials are promising for the application of ACT as (part of) pre-operative treatment. However, further improvement of HNSCC is required.

Overexpression of the tumour-associated antigen ErbB1 is seen in over 80% of HNSCC cases and is associated with poor prognosis (101-103). ErbB1 is a member of the ErbB receptor family, which are commonly overexpressed in cancers and therefore make interesting TAAs for targeted (immuno)therapies. The ErbB1 targeting mAb Cetuximab has been approved by the FDA and MHRA for treatment of locally advanced HNSCC (146). However, tumours can become resistant to Cetuximab. Resistance to targeted ErbB therapies may be reduced by targeting of multiple ErbB receptor family members within a single treatment regimen (128, 174).

T4 immunotherapy re-targets T-cells against the extended ErbB receptor family through the expression in T-cells of T28ζ, a chimeric antigen receptor (299). The CAR is

co-expressed with 4αβ to allow for selective expansion of the transduced T-cell population by their culture in IL-4 (391). T4 immunotherapy has been shown to effectively control tumour growth in several xenograft models (299, 358). However, targeting of the ErbB receptor family using adoptively infused T-cells carries a significant risk of inducing severe toxicity. Targeting of the ErbB receptor family with monoclonal antibodies (such as Cetuximab and Herceptin) has been associated with a range of toxicities including skin rash (152-155) and cardiac toxicity (520, 521). Adoptive cell therapies using CAR-mediated re-directed T-cells has also induced severe adverse events, including on-target toxicity to healthy tissues or the induction of a cytokine storm, resulting in multiple organ failure (240, 317, 366, 477).

In a forthcoming phase-I clinical trial, we aim to determine the maximum tolerated dose of intra-tumoural T4 immunotherapy in patients with locally recurrent head and neck squamous cell carcinoma. The data contained within this thesis comprises much of the pre-clinical safety testing that has been carried out in preparation for this trial. The main conclusion which can be drawn from *in vitro* toxicity analysis is that $T4^+$ T-cells can be activated by, and destroy healthy $ErbB^+$ tissue. Both primary cardiac myocytes and pulmonary endothelial cells induced T-cell activation when co-cultivated with $T4^+$ T-cells. This evidence of toxicity was expected based on the ErbB expression profile of these cell types and the cardiac and endothelial toxicities reported following the administration of ErbB targeted treatments (240, 520, 521). However, this toxicity will only occur *in vivo* if $T4^+$ T-cell migration leads to an encounter with healthy $ErbB^+$ tissue. In order to determine this, pre-clinical *in vivo* models are required.

The main conclusion that arises from the pre-clinical *in vivo* toxicity assessment I have undertaken is that T4 immunotherapy can induce severe toxicity. Importantly however, this toxicity is dependent upon route of administration and therapeutic dose. These findings suggest that there is a window of therapeutic opportunity whereby anti-tumour efficacy can be achieved without the induction of severe toxicity.

In vivo pre-clinical toxicity studies were performed in the immunodeficient SCID/Beige mouse model. The use of this mouse model is appropriate for four reasons. First, the regulatory authorities require pre-clinical toxicity to be assessed with the exact medicinal product to be evaluated in man, meaning human $T4^+$ T-cells in this

case. Second, I have shown that human $T4^+$ T-cells can be activated by both $ErbB^+$ tumour and non-transformed mouse cells, suggesting that these T-cells could potentially be activated *in vivo* when encountering healthy $ErbB^+$ tissue. Third, the migration pattern of human $T4^+$ T-cells after IV injection was shown to be similar in mouse and in man (460, 547, 548). Based upon these considerations, I anticipated that pre-clinical toxicity studies in SCID/Beige mice would be able to indicate which organs could be at risk of toxicity in forthcoming clinical studies. Fourth, activated human T-cells are able to elicit severe toxicity in mice, best exemplified by xenogeneic graft versus host disease (537).

Intra-venous administration of 20×10^6 $T4^+$ T-cells did not result in any severe toxicity, despite the expression of ErbB-receptors detected on the pulmonary endothelial cells. Extensive histopathological analysis did not show any abnormality or the presence of infiltrated T-cells in any of the organs assessed. Previous clinical trials involving the IV administration of ErbB targeted T-cells have resulted in toxicities that have ranged from absent to severe (240, 547). Specifically, *ex-vivo* expanded ErbB2-specific cytotoxic T-cell clones did not induce any toxicity, despite their initial accumulation in the lungs, whereas T-cells re-targeted against ErbB2 with a third-generation CAR induced a lethal cytokine storm after recognition of ErbB2 expression in the lungs. The differences in toxicity might have been due to the intensity of CAR-mediated T-cell activation versus TCR-mediated T-cell activation. Additionally, it could have been influenced by the dose of T-cells administered (2.65×10^9 CTLs versus 1×10^{10} CAR T-cells respectively) (240, 547). Cell density has been reported to influence the level of cytokine production within the TGN1412 clinical trial experience, in which pre-cultivation of human PBMCs at higher density was shown to increase cytokine production (585, 586). The fact that severe toxicity could also be induced through IP administration of $T4^+$ T-cells confirms that toxicity can be induced in this model, suggesting that the absence of toxicity after IV T-cell administration is real and not due to an inappropriate clinical model.

Intra-peritoneal administration of T4 immunotherapy was shown to be able to induce severe, lethal, cytokine release syndrome in SCID/Beige mice. I hypothesize that the severity of the induced CRS is dependent on four factors; the dose of T-cells administered, the injection volume, the magnitude of ErbB recognition and the

interaction with macrophages within the peritoneal cavity. Several of the results presented here and published clinical trial experience provides support for this hypothesis. First, as mentioned previously, the density of T-cells has been shown to have an influence on the level of cytokine production and therefore on the severity of the induced CRS (586). Clinical trials have shown a timely relation between T-cell expansion and the onset of toxicity, which would explain why higher T-cell doses (and therefore higher cell density within the peritoneal cavity) induce more severe CRS (445). Second, increased injection volumes result in an increased pressure IP, which in turn increases the absorption of small molecules, including cytokines (594). This allows for the inflammation to 'spill over' into the systemic circulation. Third, the magnitude of ErbB recognition is a combination of the expression levels on healthy tissue (593) and the level of tumour burden. A dose of 10 x 10^6 $T4^+$ T-cells proved to result in lethal toxicity in animals with a high SKOV3luc tumour burden, whereas a similar dose did not elicit any toxicity in animals with a lower HN3luc tumour burden. In man, tumour burden at the moment of T-cell administration has also been correlated to the resulting level of cytokine production (317). Finally, I have presented data in this thesis that suggest that human $T4^+$ T-cells interact with (mouse) macrophages in the peritoneal cavity, resulting in the production of IL-6. In clinical trials, IL-6 has been indicated as a key player in CRS (317, 321). Intra-peritoneal administration of $T4^+$ T-cells was shown to induce the production of mouse IL-6 by the macrophages present in the peritoneal cavity. Intra-peritoneal SKOV3luc tumours are associated with an increased influx of macrophages. The higher peritoneal macrophage content may have contributed to the more severe toxicity seen in animals with a SKOV3luc tumour compared to tumour-free or HN3luc tumour bearing animals after treatment with the same T-cell dose. Depletion of macrophages in tumour-free animals resulted in reduced levels of circulating mIL-6 as well as reduced weight loss, confirming the contribution of macrophages to the kinetics of CRS. In clinical trials, reducing IL-6 signalling has also resulted in lessened toxicity. Furthermore, administration of the IL-6 receptor blocking antibody Tocilizumab has shown to rapidly alleviate the symptoms of CRS (317, 321).

In spite of the toxicity seen after IP $T4^+$ T-cell administration, anti-tumour efficacy has been seen with lower doses (7.5 x 10^6 $T4^+$ T-cells) without the induction of

any toxicity. This suggests that there is a window of therapeutic opportunity in which efficacy can be achieved without the induction of severe toxicity.

The occurrence of such severe CRS in mice raises concerns for the safety of T4 immunotherapy application in man. In a Phase-I clinical trial we aim to treat patients with locally recurrent HNSCC by administration of intra-tumoural injections of T4 immunotherapy. Within the first cohorts, patients will not receive lymphodepleting chemotherapy prior to T-cell administration. Previous clinical trials using allogeneic spleen cells or autologous PBMCs have proven the feasibility of intra-tumoural T-cell administration of patients with HNSCC (265, 266). In mice, after IT/PT T-cell administration, T-cells reside in the area of injection and do not migrate to a significant degree. This lack of T-cell migration should greatly reduce the risk of cardiac- or epithelial-toxicity. No elevation of circulating cytokines (human IL-2 and mouse IL-6) was detected after IT/PT T-cell administration. Low levels of human IFNγ were detected in these mice, suggesting functionality of transferred T-cells (which was also confirmed by a reduction in tumour burden). However cytokine production was not sufficient to induce adverse events.

The absence of toxicity after IT/PT T-cell administration is encouraging for the initiation of the planned Phase-I clinical trial. However, caution must nevertheless be taken. Although SCID/Beige mice can manifest the effects of human $T4^+$ T-cell-dependent toxicity, the model has limitations which could affect the translation of these results to the clinic. First, human $T4^+$ T-cells have a very limited life-span in SCID/Beige mice (5 days), whereas prolonged survival (of up to four years) of transfused T-cells has been reported in man (327, 372). The discrepancy in *in vivo* longevity makes the model insufficient to determine whether persistence of the $T4^+$ T-cell population could result in extended migration after PT/IT administration, which could lead to 'on-target' toxicity at a later time-point. Besides a lack of persistence, the model also does not allow for *in vivo* expansion of the transfused T-cell population. Therefore, it does not estimate whether expansion of the CAR^+ T-cell population could lead to late-onset toxicity in a dose-dependent manner. Second, the first cohorts of patients within the trial will not receive a lymphodepleting regimen prior to T-cell administration. Without lymphodepletion, the regulatory component of the immune system will remain to be present, as well as the so-called 'cytokine sinks'. This could

reduce the severity of CRS. Besides the regulatory immune component, the effector component will also remain intact without lymphodepletion. Cytokine production by transfused T-cells may induce an endogenous immune response. This endogenous immune response might be favourable for the anti-tumour efficacy, however, it might also enhance CRS. Third, not all cytokines produced in the detected CRS cross the species barrier (such as human IFNγ and mouse IL-6). Lack of cross-species recognition of these cytokines means that the effect of these cytokines on toxicity and T-cell functionality can not be incorporated, whereas they could be influential in man (595, 596). The use of an immunocompetent mouse model could be used to overcome some of the shortcomings of the SCID/Beige xenograft model.

Despite these shortcomings, the SCID/Beige mouse model has proven to be a useful tool to study the kinetics and risks of CRS in response to T4 immunotherapy. Additional studies using the anti mIL-6R antibody MR16-1 could further elucidate the role of IL-6 in the pathogenesis of CRS. Additionally it provides a model in which alternative interventions can be explored to reduce the risk of CRS without limiting the efficacy of CAR-mediated adoptive T-cell therapy.

As mentioned previously, human $T4^+$ T-cells only showed limited persistence in mice. Prolonged persistence of circulating $T4^+$ T-cells could result in ErbB recognition on healthy tissue at a time-point after clinical efficacy has already been achieved. Therefore, studies to develop a selective elimination system to eradicate the $T4^+$ T-cell population should be performed. Such systems could include the incorporation of a suicide gene such as HSV-TK (Herpes-Simplex Virus Thymidine Kinase) or the use of the NBI-3001 chimeric protein, in which IL-4 is coupled to pseudomonas exotoxin (606, 607). Treatment with NBI-3001 would rely on the high affinity of IL-4 to 4αβ, resulting in selective elimination of $4\alpha\beta^+$ T-cells.

In order to effectively execute the planned Phase-I clinical trial, a stable, GMP-compliant transduction and expansion method is required. Previously it has been reported that PBMCs derived from HNSCC patients can undergo spontaneous apoptosis in culture. We have developed a robust process, in which all manufactured cell products were of the required clinical standard.

In summary, T4 immunotherapy has potent anti-tumour activity. However, there is a risk of toxicity due to targeting of healthy $ErbB^{+}$ tissue as well as the potential induction of a cytokine storm. The pre-clinical data presented in this thesis argue that is likely to be a therapeutic window within which anti-tumour efficacy can be achieved without the induction of severe toxicity. The available pre-clinical efficacy and toxicity data, combined with the robust GMP-manufacture protocol and the availability of the target patient population, paves the way for instigating a Phase-I clinical trial in man.

Appendix 1 – Primers

FWD junction 1	GTG TGC ATG TAC ATC GAG GCA
REV junction 1	ATA GGG GAC TTG GAC AAA GGT G
FWD junction 2	ACA CCT ACG ACG CCC TTC ACA
REV junction 2	CGT AGC GCT TCA TGG CTT TGT
FWD junction 3	AGG GCT ACG GCC TGA CAG AAA
REV junction 3	GTC GAT GAG AGC GTT TGT AGC

Appendix 2 – Supplementary Figures

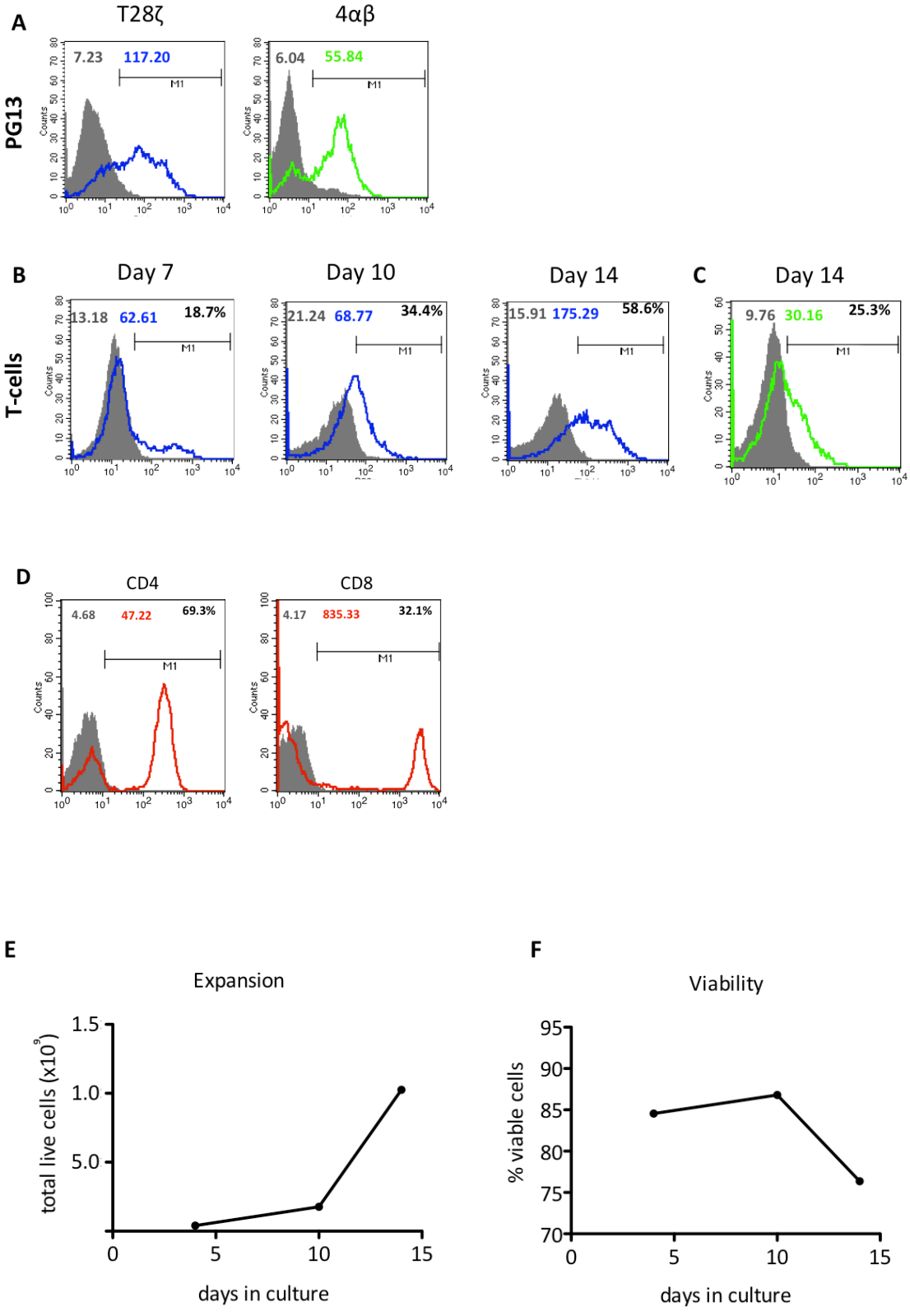

Supplementary Figure 1 P4 expression in PG13 packaging cells and T-cells

A: Expression of P28ζ (open blue histogram) and 4αβ (open green histogram) was detected on the surface of PG13 packaging cells using flow cytometry Filled grey histograms show untransduced PG13 stained with the same protocol. MFIs are indicated by the grey/coloured numbers **B:** Expression of P28ζ was detected on the surface of T4-transduced primary human T-cells using flow cytometry (open blue histograms). Cells were analysed at multiple days after transduction to determine enrichment of the transduced population in cultured media supplemented with IL-4. Filled grey histograms show untransduced T-cells stained with the same protocol. MFIs are indicated by the grey/coloured numbers **C:** Expression of 4αβ (open green histogram) on T-cells transduced with T4. To determine expression of 4αβ on day 14 cells were cultured in media supplemented with IL-2 24 hours prior to analysis. Filled grey histogram shows untransduced T-cells stained with the same protocol. **D:** Proportion of CD4/CD8 content within the entire cell population, determined on day 14 of culture. **E:** Expansion of total cell population during culture based on trypan blue exclusion. **F:** Viability of total cell population during culture, based on live/dead gating within the FSC/SSC scatter.

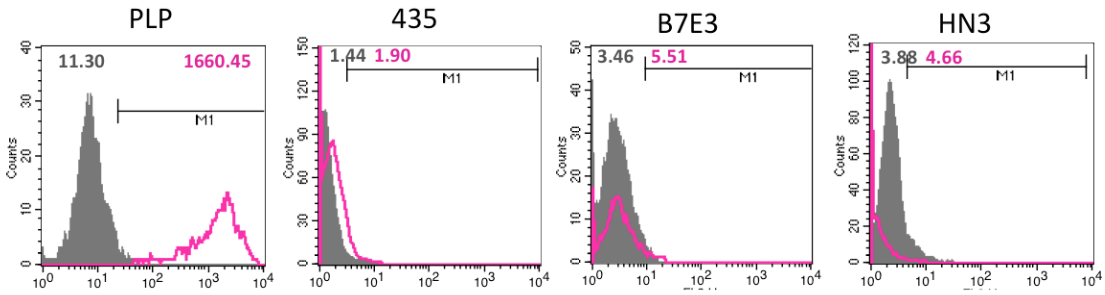

Supplementary Figure 2 PSMA expression in human and mouse tumour cell lines

PSMA expression was determined by flow cytometry. Cells were stained with the mouse-anti human PSMA primary antibody followed by goat-anti-mouse IgG PE-conjugated secondary antibody. PSMA (open pink histograms, MFI represented by pink number) is compared to cells stained with the secondary antibody alone (filled grey histograms, MFI represented by grey number).

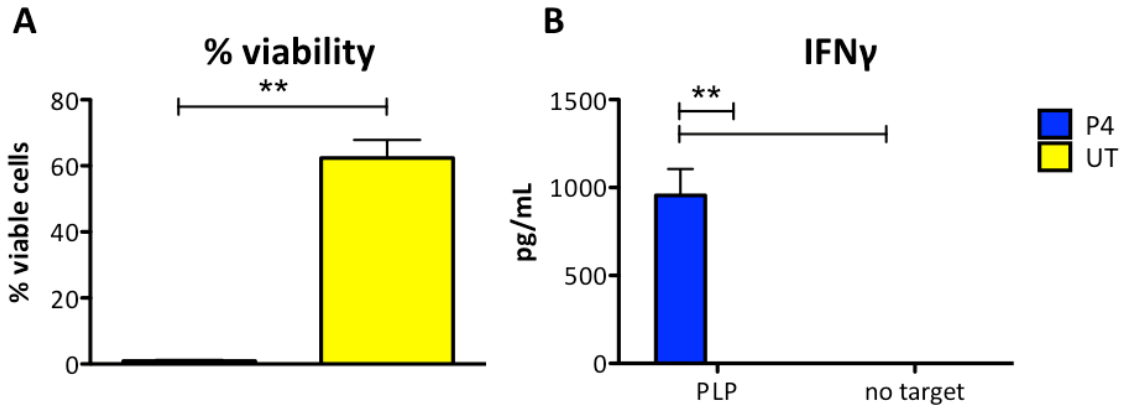

Supplementary Figure 3 Cytotoxicity of P4$^+$ T-cells

Functionality of P4$^+$ T-cells was confirmed by the co-cultivation of 1 x 10^6 P4$^+$ T-cells with a confluent monolayer (24 well plate) of the PSMA$^+$ prostate cancer cell line PLP. **A:** 1 x 10^6 P4$^+$ T-cells were co-cultivated with a confluent monolayer of PLP tumour cell line for 24 hours. Residual monolayer was quantified using an MTT assay. Amount of residual monolayer is presented as % of confluent monolayer without T-cells. Data shown mean ± SD of n=3. ** = p<0.001. **B:** IFNγ levels in the supernatant of co-cultivations (as described in **A**) were detected using ELISA. Data shown mean ± SD of n=6. ** = p<0.001.

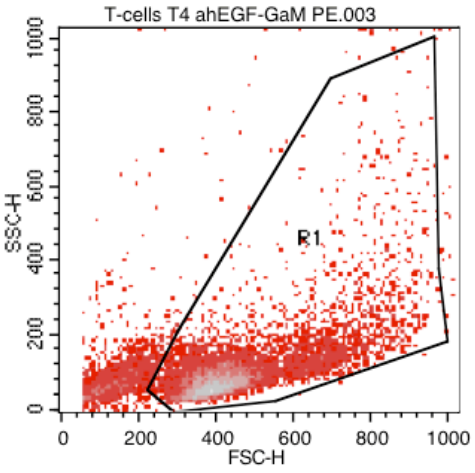

Region	Events	% Gated	% Total	X Mean	X Geo Mean	Y Mean	Y Geo Mean	Px,Py
R1	8402	84.02	84.02	453.60	436.42	113.85	96.66	1, 2

Supplementary Figure 4 Live/dead gating cell product toxicity study

Cell viability of>70% is on of the release criteria at the final day of the 14-day culture process for the production of T4 immunotherapy. For the toxicity study, the amount of viable cells was determined based on their location in the forward/side scatter. A gate was drawn around the viable cells (R1) and the % cells within the gate was calculated (% Gated; 84.02%)

Appendix 3 – Dose Conversion

The conversion of the $T4^+$ T-cell dose given to mice, to the corresponding dose in human (human equivalent dose; HED) was based on the normalisation of body surface area (BSA) as described by Reagan-Shaw et al. (608).

Adult human	weight	70kg
	BSA	$1.6m^2$
	K_m factor	44
Mouse	weight	0.02kg
	BSA	$0.007m^2$
	K_m factor	3

$$\text{HED (mg/kg)} = \text{animal dose (mg/kg)} \times \frac{\text{animal } K_m}{\text{human } K_m}$$

$$\text{HED (cells/kg)} = \text{mouse dose (cells/kg)} \times \frac{\text{mouse } K_m}{\text{human } K_m}$$

Dose administered to mice: 20×10^6 total T-cells (51% transduced)

20×10^6 cells x 0.02kg = 1000×10^6 T-cells/kg

$$\text{HED (cells/kg)} = 1000 \times 10^6 \times \frac{3}{44} = 68 \times 10^6 \text{ cells/kg}$$

Total dose adult human = HED x weight

68×10^6 x 70kg = **4.8×10^9 cells**

4.8×10^9 total T-cells x 51% transduced = **2.4×10^9 $T4^+$ T-cells**

Appendix 4 - Histopathology Reports

Toxicity Study

Table 0-1 Reference mouse coding route of T-cell administration

	IV	PT/SC
Male	C3M3 C3M4 C3M5	C2M1 C2M2 C2M3
Female	C5M1 C5M2 C5M3	C8M1 C8M2 C8M3

89 Queen Street
Newton Abbot
Devon • TQ12 2BG • U.K.

Abbey Veterinary Services

RAPID DIAGNOSTIC HISTOPATHOLOGY & CYTOLOGY

Trevor J Whitbread BSc. BVSc. Dip ECVP MRCVS
Judith Hargreaves MVB FRCPath MRCVS
Malcolm Silkstone BVSc. Dip ACVP MRCVS
Ines Hoffmann Tierärztin MSc. MRCVS
Sonja A Rivers BVetMed MSc. Dip ACVP MRCVS
Richard Fox BVetMed Dip ECVP MRCVS
Lucy Oldroyd BSc. BVMS Dip ACVP MACVS MRCVS

Tel: + 44 (0)1626 353598
e.mail: admin@abbeyvetservices.co.uk
Web: www.abbeyvetservices.co.uk
Fax: + 44 (0)1626 335135

Kings College London
St Thomas Street
London Bridge
London
SE1 9RT

KINSTT

Our Ref: 79129G
TJW/SW
Owner's Name: UNKNOWN {228783}
Animal's Name: C3M3
02/02/2012

REF: C3M3

MACROSCOPIC

3 x tubes containing general internal organs
1 x tube labelled skull and left leg

MICROSCOPIC

Cerebrum:	NAD
Cerebellum:	NAD
Skeletal muscle:	NAD
Spinal cord:	NAD
Bone marrow:	NAD
Cortical bone:	NAD
Vertebral muscle:	NAD
Heart:	NAD
Lung:	NAD
Oesophagus:	NAD
Testis:	NAD
Salivary gland:	NAD
Kidney:	NAD
Liver:	NAD
Pancreas:	NAD
Small intestine:	NAD
Large intestine:	NAD
Spleen:	NAD
Stomach:	NAD
Lymph node:	NAD
Bronchial lymph node:	NAD
Lacrimal gland:	NAD
Eye:	NAD
Testis:	NAD

T J Whitbread BSc. BVSc. MRCVS DipECVP

Abbey Veterinary Services

RAPID DIAGNOSTIC HISTOPATHOLOGY & CYTOLOGY

89 Queen Street
Newton Abbot
Devon • TQ12 2BG • U.K.

Trevor J Whitbread BSc. BVSc. Dip ECVP MRCVS
Judith Hargreaves MVB FRCPath MRCVS
Malcolm Silkstone BVSc. Dip ACVP MRCVS
Ines Hoffmann Tierärztin MSc. MRCVS
Sonja A Rivers BVetMed MSc. Dip ACVP MRCVS
Richard Fox BVetMed Dip ECVP MRCVS
Lucy Oldroyd BSc. BVMS Dip ACVP MACVS MRCVS

Tel: + 44 (0)1626 353598
e.mail: admin@abbeyvetservices.co.uk
Web: www.abbeyvetservices.co.uk
Fax: + 44 (0)1626 335135

Kings College London
St Thomas Street
London Bridge
London
SE1 9RT

KINSTT

Our Ref: 79125G
TJW/SW
Owner's Name: UNKNOWN {228783}
Animal's Name: C3M4
02/02/2012

REF: C3M4

MACROSCOPIC
3 x tubes with internal organs
1 x tube with skull and left leg

MICROSCOPIC

Cerebrum:	NAD
Cerebellum:	NAD
Spinal cord:	NAD
Bone marrow:	NAD
Cortical bone:	NAD
Vertebral muscle:	NAD
Skeletal muscle:	NAD
Heart:	NAD
Lung:	NAD – mild collapse
Oesophagus:	NAD
Testis:	NAD
Salivary gland:	NAD
Kidney:	NAD
Liver:	NAD
Pancreas:	NAD
Small intestine:	NAD
Large intestine:	NAD
Spleen:	NAD
Stomach:	NAD
Lymph node:	NAD
Bronchial lymph node:	NAD
Adrenal:	NAD
Testis:	NAD

T J Whitbread BSc. BVSc. MRCVS DipECVP

Abbey Veterinary Services

RAPID DIAGNOSTIC HISTOPATHOLOGY & CYTOLOGY

89 Queen Street
Newton Abbot
Devon • TQ12 2BG • U.K.

Trevor J Whitbread BSc. BVSc. Dip ECVP MRCVS
Judith Hargreaves MVB FRCPath MRCVS
Malcolm Silkstone BVSc. Dip ACVP MRCVS
Ines Hoffmann Tierärztin MSc. MRCVS
Sonja A Rivers BVetMed MSc. Dip ACVP MRCVS
Richard Fox BVetMed Dip ECVP MRCVS
Lucy Oldroyd BSc. BVMS Dip ACVP MACVS MRCVS

Tel: + 44 (0)1626 353598
e.mail: admin@abbeyvetservices.co.uk
Web: www.abbeyvetservices.co.uk
Fax: + 44 (0)1626 335135

Kings College London
St Thomas Street
London Bridge
London
SE1 9RT

KINSTT

Our Ref: 79126G
TJW/SW
Owner's Name: UNKNOWN {228783}
Animal's Name: C3M5
02/02/2012

REF: C3M5

MACROSCOPIC

3 x tubes containing general internal organs
1 x tube containing skull and left leg

MICROSCOPIC

Cerebellum:	NAD
Cerebrum:	NAD
Spinal cord:	NAD
Bone marrow:	NAD
Cortical bone:	NAD
Vertebral muscle:	NAD
Heart:	NAD
Lung:	Markedly collapsed, no pneumonia or inflammation.
Oesophagus:	NAD
Testis:	NAD
Salivary gland:	NAD
Kidney:	NAD
Liver:	NAD
Pancreas:	NAD
Small intestine:	NAD
Large intestine:	NAD
Spleen:	NAD
Stomach:	NAD
Lymph node:	NAD
Bronchial lymph node:	NAD
Skeletal muscle:	NAD

T J Whitbread BSc. BVSc. MRCVS DipECVP

89 Queen Street
Newton Abbot
Devon • TQ12 2BG • U.K.

Abbey Veterinary Services

RAPID DIAGNOSTIC HISTOPATHOLOGY & CYTOLOGY

Trevor J Whitbread BSc. BVSc. Dip ECVP MRCVS
Judith Hargreaves MVB FRCPath MRCVS
Malcolm Silkstone BVSc. Dip ACVP MRCVS
Ines Hoffmann Tierärztin MSc. MRCVS
Sonja A Rivers BVetMed MSc. Dip ACVP MRCVS
Richard Fox BVetMed Dip ECVP MRCVS
Lucy Oldroyd BSc. BVMS Dip ACVP MACVS MRCVS

Tel: + 44 (0)1626 353598
e.mail: admin@abbeyvetservices.co.uk
Web: www.abbeyvetservices.co.uk
Fax: + 44 (0)1626 335135

Kings College London
St Thomas Street
London Bridge
London
SE1 9RT

KINSTT

Our Ref: 79132G
TJW/LH
Owner's Name: UNKNOWN {228783}
Animal's Name: C5M1
30/01/2012

OUR REF: C5M1

MACROSCOPIC
3 x tubes containing general organs
1 x tube containing skull + L leg

MICROSCOPIC

Cerebrum:	NAD
Cerebellum:	NAD
Spinal cord:	NAD
Skeletal muscle:	NAD
Bone marrow:	NAD
Cortical bone:	NAD
Vertebral muscle:	NAD
Heart:	NAD
Lung:	Moderate collapse. No inflammation or consolidation. Moderate very patchy thickening of alveolar walls.
Oesophagus:	NAD – Large numbers of bacteria in keratin of the lumen.
Ovary:	NAD
Uterus:	NAD
Salivary gland:	NAD
Adrenal:	NAD
Kidney:	NAD
Liver:	NAD
Pancreas:	NAD
Small intestine:	NAD
Large intestine:	NAD
Spleen:	NAD
Stomach:	NAD
Lymph node:	NAD
Bronchial lymph node:	NAD

T J Whitbread BSc. BVSc. MRCVS DipECVP

89 Queen Street
Newton Abbot
Devon • TQ12 2BG • U.K.

Abbey Veterinary Services

RAPID DIAGNOSTIC HISTOPATHOLOGY & CYTOLOGY

Trevor J Whitbread BSc. BVSc. Dip ECVP MRCVS
Judith Hargreaves MVB FRCPath MRCVS
Malcolm Silkstone BVSc. Dip ACVP MRCVS
Ines Hoffmann Tierärztin MSc. MRCVS
Sonja A Rivers BVetMed MSc. Dip ACVP MRCVS
Richard Fox BVetMed Dip ECVP MRCVS
Lucy Oldroyd BSc. BVMS Dip ACVP MACVS MRCVS

Tel: + 44 (0)1626 353598
e.mail: admin@abbeyvetservices.co.uk
Web: www.abbeyvetservices.co.uk
Fax: + 44 (0)1626 335135

Kings College London
St Thomas Street
London Bridge
London
SE1 9RT

KINSTT

Our Ref: 79136G
TJW/LH
Owner's Name: UNKNOWN {228783}
Animal's Name: C5M2
30/01/2012

REF: C5M2

MACROSCOPIC

3 x tubes containing general organs
1 x tube containing skull + L leg

MICROSCOPIC

Spinal cord:	NAD
Skeletal muscle:	NAD
Bone marrow:	NAD
Cortical bone:	NAD
Vertebral muscle:	NAD
Heart:	NAD
Lung:	Congestion, blood in alveolar spaces. Mild collapse. Mild alveolar wall thickening.
Oesophagus:	NAD
Ovary:	NAD
Uterus:	NAD
Salivary gland:	NAD
Kidney:	NAD
Liver:	NAD
Pancreas:	NAD
Small intestine:	NAD
Large intestine:	NAD
Spleen:	NAD
Stomach:	NAD but large numbers of bacteria within the lumen
Lymph node:	NAD
Bronchial lymph node:	NAD

T J Whitbread BSc. BVSc. MRCVS DipECVP

89 Queen Street
Newton Abbot
Devon • TQ12 2BG • U.K.

Abbey Veterinary Services

RAPID DIAGNOSTIC HISTOPATHOLOGY & CYTOLOGY

Trevor J Whitbread BSc. BVSc. Dip ECVP MRCVS
Judith Hargreaves MVB FRCPath MRCVS
Malcolm Silkstone BVSc. Dip ACVP MRCVS
Ines Hoffmann Tierärztin MSc. MRCVS
Sonja A Rivers BVetMed MSc. Dip ACVP MRCVS
Richard Fox BVetMed Dip ECVP MRCVS
Lucy Oldroyd BSc. BVMS Dip ACVP MACVS MRCVS

Tel: + 44 (0)1626 353598
e.mail: admin@abbeyvetservices.co.uk
Web: www.abbeyvetservices.co.uk
Fax: + 44 (0)1626 335135

Kings College London
St Thomas Street
London Bridge
London
SE1 9RT

KINSTT

Our Ref: 79130G
TJW/SW
Owner's Name: UNKNOWN {228783}
Animal's Name: C5M3
02/02/2012

REF: C5M3

MACROSCOPIC

3 x tubes containing general organs
1 x tube containing head and leg

MICROSCOPIC

Cerebrum:	NAD
Cerebellum:	NAD
Spinal cord:	NAD
Skeletal muscle:	NAD
Bone marrow:	NAD
Cortical bone:	NAD
Vertebral muscle:	NAD
Heart:	NAD
Lung:	NAD – Minimal collapse, no inflammation.
Oesophagus:	NAD
Ovary:	NAD
Uterus:	NAD
Salivary gland:	NAD
Kidney:	NAD
Liver:	Very mild hepatocellular vacuolation, otherwise normal.
Pancreas:	NAD
Small intestine:	NAD
Large intestine:	NAD
Spleen:	NAD
Stomach:	NAD
Lymph node:	NAD
Bronchial lymph node:	NAD

T J Whitbread BSc. BVSc. MRCVS DipECVP

Abbey Veterinary Services

RAPID DIAGNOSTIC HISTOPATHOLOGY & CYTOLOGY

89 Queen Street
Newton Abbot
Devon • TQ12 2BG • U.K.

Trevor J Whitbread BSc. BVSc. Dip ECVP MRCVS
Judith Hargreaves MVB FRCPath MRCVS
Malcolm Silkstone BVSc. Dip ACVP MRCVS
Ines Hoffmann Tierärztin MSc. MRCVS
Sonja A Rivers BVetMed MSc. Dip ACVP MRCVS
Richard Fox BVetMed Dip ECVP MRCVS
Lucy Oldroyd BSc. BVMS Dip ACVP MACVS MRCVS

Tel: + 44 (0)1626 353598
e.mail: admin@abbeyvetservices.co.uk
Web: www.abbeyvetservices.co.uk
Fax: + 44 (0)1626 335135

Kings College London
St Thomas Street
London Bridge
London
SE1 9RT

KINSTT

Our Ref: 79135G
TJW/SW
Owner's Name: UNKNOWN {228783}
Animal's Name: C2M1
18/01/2012

REF: C2MI

MACROSCOPIC

3 x tubes containing general organs
1 x tube containing skull and leg.

MICROSCOPIC

Cerebrum:	NAD
Cerebellum:	NAD
Skeletal muscle:	NAD
Spinal cord:	NAD
Bone marrow:	NAD
Cortical bone:	NAD
Vertebral muscle:	NAD
Heart:	NAD
Lung:	Moderate artefactual collapse. Mild increased background of alveolar walls. A small number of haemosiderophages within the wall, not in the alveolar space.
Oesophagus:	NAD
Lymph node:	NAD
Salivary gland:	NAD
Kidney:	Mild vacuolation of tubule cells. Glomeruli are normal.
Liver:	NAD
Pancreas:	NAD
Small intestine:	NAD in all areas.
Large intestine:	Mucosal folds are normal in appearance.
Stomach:	NAD
Testis:	NAD

T J Whitbread BSc. BVSc. MRCVS DipECVP

Abbey Veterinary Services

RAPID DIAGNOSTIC HISTOPATHOLOGY & CYTOLOGY

89 Queen Street
Newton Abbot
Devon • TQ12 2BG • U.K.

Trevor J Whitbread BSc. BVSc. Dip ECVP MRCVS
Judith Hargreaves MVB FRCPath MRCVS
Malcolm Silkstone BVSc. Dip ACVP MRCVS
Ines Hoffmann Tierärztin MSc. MRCVS
Sonja A Rivers BVetMed MSc. Dip ACVP MRCVS
Richard Fox BVetMed Dip ECVP MRCVS
Lucy Oldroyd BSc. BVMS Dip ACVP MACVS MRCVS

Tel: + 44 (0)1626 353598
e.mail: admin@abbeyvetservices.co.uk
Web: www.abbeyvetservices.co.uk
Fax: + 44 (0)1626 335135

Kings College London
St Thomas Street
London Bridge
London
SE1 9RT

KINSTT

Our Ref: 79134G
TJW/LH
Owner's Name: UNKNOWN {228783}
Animal's Name: C2M2
30/01/2012

REF: C2M2

MACROSCOPIC
3 x tubes of general organs
1 x tube skin + L leg

MICROSCOPIC

Cerebellum:	NAD
Cerebrum:	NAD
Skeletal muscle:	NAD
Spinal cord:	NAD
Bone marrow:	NAD
Cortical bone:	NAD
Vertebral muscle:	NAD
Heart:	NAD
Lung:	Very congested (CO_2 euthanasia?). Some collapse. Mild thickening of alveolar walls. No exudation or consolidation.
Oesophagus:	NAD
Salivary gland:	NAD
Kidney:	Mild vacuolation of tubules. No other change.
Liver:	NAD
Pancreas:	NAD
Small intestine:	NAD
Large intestine:	NAD
Stomach:	NAD
Testis:	NAD
Spleen:	There is normal red pulp with EMH but white pulp is severely depleted of lymphoid cells.
Lymph node:	Severe depletion of lymphocytes, no follicle centres. A concentration of histiocytic cells, including in the subcapsular sinus and karyorrhexis.

T J Whitbread BSc. BVSc. MRCVS DipECVP

Abbey Veterinary Services

RAPID DIAGNOSTIC HISTOPATHOLOGY & CYTOLOGY

89 Queen Street
Newton Abbot
Devon • TQ12 2BG • U.K.

Trevor J Whitbread BSc. BVSc. Dip ECVP MRCVS
Judith Hargreaves MVB FRCPath MRCVS
Malcolm Silkstone BVSc. Dip ACVP MRCVS
Ines Hoffmann Tierärztin MSc. MRCVS
Sonja A Rivers BVetMed MSc. Dip ACVP MRCVS
Richard Fox BVetMed Dip ECVP MRCVS
Lucy Oldroyd BSc. BVMS Dip ACVP MACVS MRCVS

Tel: + 44 (0)1626 353598
e.mail: admin@abbeyvetservices.co.uk
Web: www.abbeyvetservices.co.uk
Fax: + 44 (0)1626 335135

Kings College London
St Thomas Street
London Bridge
London
SE1 9RT

KINSTT

Our Ref: 79133G
TJW/LH
Owner's Name: UNKNOWN {228783}
Animal's Name: C2M3
30/01/2012

REF: C2M3

MACROSCOPIC

3 x tubes containing general organs
1 x tube containing skull + L leg

MICROSCOPIC

Cerebrum:	NAD
Cerebellum:	NAD
Skeletal muscle:	NAD
Spinal cord:	NAD
Bone marrow:	NAD
Cortical bone:	NAD
Vertebral muscle:	NAD
Heart:	NAD
Lung:	Marked collapse. Artefactual haemorrhage. Mild patchy increased alveolar wall thickness. No consolidation.
Oesophagus:	NAD
Salivary gland:	NAD
Kidney:	NAD
Liver:	NAD
Pancreas:	NAD
Small intestine:	NAD
Large intestine:	NAD
Stomach:	NAD
Lymph node:	Depleted of lymphoid cells with histiocytic cells and pyknosis and karyorrhexis
Testis:	NAD

T J Whitbread BSc. BVSc. MRCVS DipECVP

Abbey Veterinary Services

RAPID DIAGNOSTIC HISTOPATHOLOGY & CYTOLOGY

89 Queen Street
Newton Abbot
Devon • TQ12 2BG • U.K.

Trevor J Whitbread BSc. BVSc. Dip ECVP MRCVS
Judith Hargreaves MVB FRCPath MRCVS
Malcolm Silkstone BVSc. Dip ACVP MRCVS
Ines Hoffmann Tierärztin MSc. MRCVS
Sonja A Rivers BVetMed MSc. Dip ACVP MRCVS
Richard Fox BVetMed Dip ECVP MRCVS
Lucy Oldroyd BSc. BVMS Dip ACVP MACVS MRCVS

Tel: + 44 (0)1626 353598
e.mail: admin@abbeyvetservices.co.uk
Web: www.abbeyvetservices.co.uk
Fax: + 44 (0)1626 335135

Kings College London
St Thomas Street
London Bridge
London
SE1 9RT

KINSTT

Our Ref: 79128G
TJW/SW
Owner's Name: UNKNOWN {228783}
Animal's Name: C8M1
02/02/2012

REF: C8M1

MACROSCOPIC

3 x tubes containing general internal organs
1 x tube containing skull and left leg

MICROSCOPIC

Cerebellum:	NAD
Cerebrum:	NAD
Spinal cord:	NAD
Skeletal muscle:	NAD
Bone marrow:	NAD
Cortical bone:	NAD
Vertebral muscle:	NAD
Heart:	NAD
Lung:	NAD
Oesophagus:	NAD
Ovary:	-
Uterus:	NAD
Salivary gland:	NAD
Kidney:	NAD
Liver:	NAD
Pancreas:	NAD
Small intestine:	NAD
Large intestine:	NAD
Spleen:	NAD
Stomach:	NAD
Lymph node:	NAD
Bronchial lymph node:	NAD

T J Whitbread BSc. BVSc. MRCVS DipECVP

Abbey Veterinary Services

RAPID DIAGNOSTIC HISTOPATHOLOGY & CYTOLOGY

89 Queen Street
Newton Abbot
Devon • TQ12 2BG • U.K.

Trevor J Whitbread BSc. BVSc. Dip ECVP MRCVS
Judith Hargreaves MVB FRCPath MRCVS
Malcolm Silkstone BVSc. Dip ACVP MRCVS
Ines Hoffmann Tierärztin MSc. MRCVS
Sonja A Rivers BVetMed MSc. Dip ACVP MRCVS
Richard Fox BVetMed Dip ECVP MRCVS
Lucy Oldroyd BSc. BVMS Dip ACVP MACVS MRCVS

Tel: + 44 (0)1626 353598
e.mail: admin@abbeyvetservices.co.uk
Web: www.abbeyvetservices.co.uk
Fax: + 44 (0)1626 335135

Kings College London
St Thomas Street
London Bridge
London
SE1 9RT

KINSTT

Our Ref: 79131G
TJW/LH
Owner's Name: UNKNOWN {228783}
Animal's Name: C8M2
30/01/2012

REF: C8M2

MACROSCOPIC

3 x tubes containing general organs
1 x tube containing head + legs

MICROSCOPIC

Cerebrum:	NAD
Cerebellum:	NAD
Spinal cord:	NAD
Skeletal muscle:	NAD
Bone marrow:	NAD
Cortical bone:	NAD
Vertebral muscle:	NAD
Heart:	NAD
Lung:	Only mild collapse. Otherwise NAD.
Oesophagus:	NAD
Ovary:	NAD
Uterus:	NAD
Salivary gland:	NAD
Kidney:	NAD
Liver:	NAD
Pancreas:	NAD
Small intestine:	NAD
Large intestine:	NAD
Spleen:	NAD
Stomach:	NAD
Lymph node:	NAD
Bronchial lymph node:	NAD

There are some small clusters of neutrophils and mononuclear cells within surface parts and mesenteric fat.

T J Whitbread BSc. BVSc. MRCVS DipECVP

Abbey Veterinary Services

RAPID DIAGNOSTIC HISTOPATHOLOGY & CYTOLOGY

89 Queen Street
Newton Abbot
Devon • TQ12 2BG • U.K.

Trevor J Whitbread BSc. BVSc. Dip ECVP MRCVS
Judith Hargreaves MVB FRCPath MRCVS
Malcolm Silkstone BVSc. Dip ACVP MRCVS
Ines Hoffmann Tierärztin MSc. MRCVS
Sonja A Rivers BVetMed MSc. Dip ACVP MRCVS
Richard Fox BVetMed Dip ECVP MRCVS
Lucy Oldroyd BSc. BVMS Dip ACVP MACVS MRCVS

Tel: + 44 (0)1626 353598
e.mail: admin@abbeyvetservices.co.uk
Web: www.abbeyvetservices.co.uk
Fax: + 44 (0)1626 335135

Kings College London
St Thomas Street
London Bridge
London
SE1 9RT

KINSTT

Our Ref: 79127G
TJW/SW
Owner's Name: UNKNOWN {228783}
Animal's Name: C8M3
02/02/2012

REF: C8M3

MACROSCOPIC

3 x tubes containing general internal organs
1 x tube containing skull and left leg

MICROSCOPIC

Cerebellum:	NAD
Cerebrum:	NAD
Spinal cord:	NAD
Bone marrow:	NAD
Cortical bone:	NAD
Vertebral muscle:	NAD
Heart:	NAD
Lung:	NAD – moderate collapse
Oesophagus:	NAD
Ovary:	NAD
Uterus:	NAD
Salivary gland:	NAD
Kidney:	NAD
Liver:	NAD
Pancreas:	NAD
Small intestine:	NAD
Large intestine:	NAD
Spleen:	NAD
Stomach:	NAD
Lymph node:	NAD
Bronchial lymph node:	NAD
Skeletal muscle:	NAD

T J Whitbread BSc. BVSc. MRCVS DipECVP

Appendix 5 - Histopathology Reports

SAEs IP treatment Ovarian Cancer

Abbey Veterinary Services

RAPID DIAGNOSTIC HISTOPATHOLOGY & CYTOLOGY

89 Queen Street
Newton Abbot
Devon · TQ12 2BG · U.K.

Trevor J Whitbread BSc. BVSc. Dip ECVP MRCVS
Judith Hargreaves MVB FRCPath MRCVS
Malcolm Silkstone BVSc. Dip ACVP MRCVS
Ines Hoffmann Tierärztin MSc. MRCVS
Sonja A Rivers BVetMed MSc. Dip ACVP MRCVS
Richard Fox BVetMed Dip ECVP MRCVS
Lucy Oldroyd BSc. BVMS Dip ACVP MACVS MRCVS

Tel: + 44 (0)1626 353598
e.mail: admin@abbeyvetservices.co.uk
Web: www.abbeyvetservices.co.uk
Fax: + 44 (0)1626 335135

FAO: Lynsey Whilding
Imperial College London
Du Cane Road
London IMPDUC
W12 0NN

Our Ref: 95766G
TJW/JM
Owner's Name: NOT GIVEN 239203
Animal's Name: MICE 34299/34301
13/06/2012

Post results

MACROSCOPIC

6 mice carcasses

MICROSCOPIC

I have processed two from each container but have so far not processed the third from each in case we need to do other types of testing on those.

34299.
Mouse B. These tissues are very badly autolysed. I have taken a selection of the internal organs.

The liver shows some mild vacuolation but I can see no antemortem degeneration or signs of infection. This is still fairly well preserved.

The renal tissue is almost totally autolysed. There is no outline of any significant alteration in overall architecture and I can see no indication for inflammation.

The lung has collapsed but there is no underlying pathology.

Heart muscle is normal.

The muscle surrounding the gut at different levels within the alimentary system is normal but I cannot comment fully on the epithelial lining because it is totally autolysed.

Mouse C. These tissues are much better preserved although there is still marked autolytic change in some of the samples.

The spleen is badly autolysed but there is accumulation of haemosiderin. I do not get the impression there has been active necrosis here and the cells that remain are mostly of course small lymphocytes as one would expect. They are unremarkable.

The gut is slightly better preserved but not very well, again with no obvious pathology.

34301.
Mouse E. These are much better preserved.

The liver is very vacuolated but there is no necrosis or inflammation.

The spleen has slightly degenerated but again there is a lot of EMH, a lot of haemosiderin accumulation. Cell density is perhaps slightly less than normal but I can see in the background small lymphocytes and some plasma cells but nothing that has the appearance of any pathological change.

The kidney is badly autolysed. I can't see any active necrosis but I have been slightly suspicious at one or two of the tubules but not enough to be definitive I am afraid.

The gut is better preserved but there is also mesenteric fat of course, where there is inflammation. This is principally on the surface, mostly neutrophilic but also extending into the deeper parts of the fat. There is a small number of mononuclear cells.

The other tissues are either badly autolysed or unremarkable.

Mouse F. The spleen is much better preserved than the others. Again there is a lot of EMH and some haemosiderin storage. The other lymphoid cells present are unremarkable and I can see no convincing necrosis and no inflammation.

The gut is better preserved but I can see no degeneration or inflammation of any significance and the large bowel of course has a large number of bacteria as is normally seen. Some of these are present in quite large numbers in the deeper crypts. This could be artefactual. I will carry out some special stains to investigate this further.

COMMENT

I can see nothing very striking here as to cause of death. There is a peritonitis and of course this has had IP injection. I wonder whether the carrier for the cells is actually slightly irritant.

I can see no abnormality within the lymphoid organs although most of those are autolysed.

There are very large numbers of bacteria within the lumen of the large bowel but that is an area where one normally sees bacteria. I can see no indication that these bacteria are causing any specific damage to the gut itself but I must say they do seem to be deeper into the glands than I would often expect to see.

To be certain of the absence of any structural change freshly preserved tissue would really be necessary and under those circumstances I would suggest euthanasia of animals that are beginning to look sick. We are of course only looking at structural change histologically. Toxic changes such as clostridium for example can be per acute but normally do show some changes histologically within the gut and I can see nothing convincing here. I can see no evidence in the liver for the presence of anaemia although can't be ruled out but it is obviously difficult to obtain sufficient blood for full examination.

T J Whitbread BSc. BVSc. MRCVS DipECVP

REFERENCES

1. Curado MP, Hashibe M. Recent changes in the epidemiology of head and neck cancer. Current opinion in oncology. 2009 May;21(3):194-200. PubMed PMID: 19363341.
2. Parkin DM, Bray F, Ferlay J, Pisani P. Global cancer statistics, 2002. CA: a cancer journal for clinicians. 2005 Mar-Apr;55(2):74-108. PubMed PMID: 15761078.
3. Warnakulasuriya S. Global epidemiology of oral and oropharyngeal cancer. Oral oncology. 2009 Apr-May;45(4-5):309-16. PubMed PMID: 18804401. Epub 2008/09/23. eng.
4. Murdoch D. Standard, and novel cytotoxic and molecular-targeted, therapies for HNSCC: an evidence-based review. Current opinion in oncology. 2007 May;19(3):216-21. PubMed PMID: 17414639. Epub 2007/04/07. eng.
5. Argiris A, Karamouzis MV, Raben D, Ferris RL. Head and neck cancer. Lancet. 2008 May 17;371(9625):1695-709. PubMed PMID: 18486742.
6. Jeannon JP, Ofu E, Balfour A, Bowman J, Simo R. The natural history of untreated squamous cell carcinoma of the head and neck: how we do it. Clin Otolaryngol. 2011 Aug;36(4):384-8. PubMed PMID: 21848553. Epub 2011/08/19. eng.
7. Leemans CR, Braakhuis BJ, Brakenhoff RH. The molecular biology of head and neck cancer. Nature reviews Cancer. 2011 Jan;11(1):9-22. PubMed PMID: 21160525.
8. Blot WJ, McLaughlin JK, Winn DM, Austin DF, Greenberg RS, Preston-Martin S, et al. Smoking and drinking in relation to oral and pharyngeal cancer. Cancer research. 1988 Jun 1;48(11):3282-7. PubMed PMID: 3365707.
9. Ide R, Mizoue T, Fujino Y, Hoshiyama Y, Sakata K, Tamakoshi A, et al. Cigarette smoking, alcohol drinking, and oral and pharyngeal cancer mortality in Japan. Oral diseases. 2008 May;14(4):314-9. PubMed PMID: 18449960.
10. Lee YC, Boffetta P, Sturgis EM, Wei Q, Zhang ZF, Muscat J, et al. Involuntary smoking and head and neck cancer risk: pooled analysis in the International Head and Neck Cancer Epidemiology Consortium. Cancer epidemiology, biomarkers & prevention : a publication of the American Association for Cancer Research, cosponsored by the American Society of Preventive Oncology. 2008 Aug;17(8):1974-81. PubMed PMID: 18708387. Pubmed Central PMCID: 2561190.
11. Freedman ND, Abnet CC, Leitzmann MF, Hollenbeck AR, Schatzkin A. Prospective investigation of the cigarette smoking-head and neck cancer association by sex. Cancer. 2007 Oct 1;110(7):1593-601. PubMed PMID: 17724671.
12. Bosetti C, Gallus S, Peto R, Negri E, Talamini R, Tavani A, et al. Tobacco smoking, smoking cessation, and cumulative risk of upper aerodigestive tract cancers. American journal of epidemiology. 2008 Feb 15;167(4):468-73. PubMed PMID: 18056925.
13. Sapkota A, Gajalakshmi V, Jetly DH, Roychowdhury S, Dikshit RP, Brennan P, et al. Smokeless tobacco and increased risk of hypopharyngeal and laryngeal cancers: a multicentric case-control study from India. International journal of cancer Journal international du cancer. 2007 Oct 15;121(8):1793-8. PubMed PMID: 17583577.
14. Hashibe M, Brennan P, Chuang SC, Boccia S, Castellsague X, Chen C, et al. Interaction between tobacco and alcohol use and the risk of head and neck cancer: pooled analysis in the International Head and Neck Cancer Epidemiology Consortium. Cancer epidemiology, biomarkers & prevention : a publication of the American

Association for Cancer Research, cosponsored by the American Society of Preventive Oncology. 2009 Feb;18(2):541-50. PubMed PMID: 19190158. Pubmed Central PMCID: 3051410.
15. La Vecchia C, Zhang ZF, Altieri A. Alcohol and laryngeal cancer: an update. European journal of cancer prevention : the official journal of the European Cancer Prevention Organisation. 2008 Apr;17(2):116-24. PubMed PMID: 18287868.
16. D'Souza G, Kreimer AR, Viscidi R, Pawlita M, Fakhry C, Koch WM, et al. Case-control study of human papillomavirus and oropharyngeal cancer. The New England journal of medicine. 2007 May 10;356(19):1944-56. PubMed PMID: 17494927.
17. Herrero R, Castellsague X, Pawlita M, Lissowska J, Kee F, Balaram P, et al. Human papillomavirus and oral cancer: the International Agency for Research on Cancer multicenter study. Journal of the National Cancer Institute. 2003 Dec 3;95(23):1772-83. PubMed PMID: 14652239.
18. Applebaum KM, Furniss CS, Zeka A, Posner MR, Smith JF, Bryan J, et al. Lack of association of alcohol and tobacco with HPV16-associated head and neck cancer. Journal of the National Cancer Institute. 2007 Dec 5;99(23):1801-10. PubMed PMID: 18042931.
19. Gillison ML, D'Souza G, Westra W, Sugar E, Xiao W, Begum S, et al. Distinct risk factor profiles for human papillomavirus type 16-positive and human papillomavirus type 16-negative head and neck cancers. Journal of the National Cancer Institute. 2008 Mar 19;100(6):407-20. PubMed PMID: 18334711.
20. Licitra L, Perrone F, Bossi P, Suardi S, Mariani L, Artusi R, et al. High-risk human papillomavirus affects prognosis in patients with surgically treated oropharyngeal squamous cell carcinoma. Journal of clinical oncology : official journal of the American Society of Clinical Oncology. 2006 Dec 20;24(36):5630-6. PubMed PMID: 17179101.
21. Ragin CC, Taioli E. Survival of squamous cell carcinoma of the head and neck in relation to human papillomavirus infection: review and meta-analysis. International journal of cancer Journal international du cancer. 2007 Oct 15;121(8):1813-20. PubMed PMID: 17546592.
22. Yoshizaki T, Kondo S, Wakisaka N, Murono S, Endo K, Sugimoto H, et al. Pathogenic role of Epstein-Barr virus latent membrane protein-1 in the development of nasopharyngeal carcinoma. Cancer letters. 2013 May 17. PubMed PMID: 23689138.
23. Lin JC, Wang WY, Chen KY, Wei YH, Liang WM, Jan JS, et al. Quantification of plasma Epstein-Barr virus DNA in patients with advanced nasopharyngeal carcinoma. The New England journal of medicine. 2004 Jun 10;350(24):2461-70. PubMed PMID: 15190138.
24. Polesel J, Franceschi S, Talamini R, Negri E, Barzan L, Montella M, et al. Tobacco smoking, alcohol drinking, and the risk of different histological types of nasopharyngeal cancer in a low-risk population. Oral oncology. 2011 Jun;47(6):541-5. PubMed PMID: 21478046.
25. Vaughan TL, Shapiro JA, Burt RD, Swanson GM, Berwick M, Lynch CF, et al. Nasopharyngeal cancer in a low-risk population: defining risk factors by histological type. Cancer epidemiology, biomarkers & prevention : a publication of the American Association for Cancer Research, cosponsored by the American Society of Preventive Oncology. 1996 Aug;5(8):587-93. PubMed PMID: 8824359.
26. Hiraki A, Matsuo K, Suzuki T, Kawase T, Tajima K. Teeth loss and risk of cancer at 14 common sites in Japanese. Cancer epidemiology, biomarkers & prevention : a publication of the American Association for Cancer Research, cosponsored by the

American Society of Preventive Oncology. 2008 May;17(5):1222-7. PubMed PMID: 18483345.
27. Guha N, Boffetta P, Wunsch Filho V, Eluf Neto J, Shangina O, Zaridze D, et al. Oral health and risk of squamous cell carcinoma of the head and neck and esophagus: results of two multicentric case-control studies. American journal of epidemiology. 2007 Nov 15;166(10):1159-73. PubMed PMID: 17761691.
28. Freedman ND, Park Y, Subar AF, Hollenbeck AR, Leitzmann MF, Schatzkin A, et al. Fruit and vegetable intake and head and neck cancer risk in a large United States prospective cohort study. International journal of cancer Journal international du cancer. 2008 May 15;122(10):2330-6. PubMed PMID: 18092323.
29. De Stefani E, Boffetta P, Ronco AL, Deneo-Pellegrini H, Acosta G, Mendilaharsu M. Dietary patterns and risk of laryngeal cancer: an exploratory factor analysis in Uruguayan men. International journal of cancer Journal international du cancer. 2007 Sep 1;121(5):1086-91. PubMed PMID: 17437274.
30. Conway DI, Petticrew M, Marlborough H, Berthiller J, Hashibe M, Macpherson LM. Socioeconomic inequalities and oral cancer risk: a systematic review and meta-analysis of case-control studies. International journal of cancer Journal international du cancer. 2008 Jun 15;122(12):2811-9. PubMed PMID: 18351646.
31. Sharma AK, Kies MS. Pocket Guide to TNM staging of head and neck cancer and neck dissection classification. Third Edition ed. Deschler DG, Day T, editors. Alexandria, VA: American Academy of Otolaryngology - Head and Neck Surgery Foundation, Inc.; 2008.
32. Braakhuis BJ, Brakenhoff RH, Leemans CR. Treatment choice for locally advanced head and neck cancers on the basis of risk factors: biological risk factors. Annals of oncology : official journal of the European Society for Medical Oncology / ESMO. 2012 Sep;23 Suppl 10:x173-7. PubMed PMID: 22987957.
33. Adelstein DJ, Li Y, Adams GL, Wagner H, Jr., Kish JA, Ensley JF, et al. An intergroup phase III comparison of standard radiation therapy and two schedules of concurrent chemoradiotherapy in patients with unresectable squamous cell head and neck cancer. Journal of clinical oncology : official journal of the American Society of Clinical Oncology. 2003 Jan 1;21(1):92-8. PubMed PMID: 12506176.
34. Weber RS, Berkey BA, Forastiere A, Cooper J, Maor M, Goepfert H, et al. Outcome of salvage total laryngectomy following organ preservation therapy: the Radiation Therapy Oncology Group trial 91-11. Archives of otolaryngology--head & neck surgery. 2003 Jan;129(1):44-9. PubMed PMID: 12525193.
35. Burtness B, Goldwasser MA, Flood W, Mattar B, Forastiere AA, Eastern Cooperative Oncology G. Phase III randomized trial of cisplatin plus placebo compared with cisplatin plus cetuximab in metastatic/recurrent head and neck cancer: an Eastern Cooperative Oncology Group study. Journal of clinical oncology : official journal of the American Society of Clinical Oncology. 2005 Dec 1;23(34):8646-54. PubMed PMID: 16314626.
36. Vermorken JB, Mesia R, Rivera F, Remenar E, Kawecki A, Rottey S, et al. Platinum-based chemotherapy plus cetuximab in head and neck cancer. The New England journal of medicine. 2008 Sep 11;359(11):1116-27. PubMed PMID: 18784101.
37. Trotti A, Bellm LA, Epstein JB, Frame D, Fuchs HJ, Gwede CK, et al. Mucositis incidence, severity and associated outcomes in patients with head and neck cancer receiving radiotherapy with or without chemotherapy: a systematic literature review. Radiotherapy and oncology : journal of the European Society for Therapeutic Radiology and Oncology. 2003 Mar;66(3):253-62. PubMed PMID: 12742264.

38. List MA, Siston A, Haraf D, Schumm P, Kies M, Stenson K, et al. Quality of life and performance in advanced head and neck cancer patients on concomitant chemoradiotherapy: a prospective examination. Journal of clinical oncology : official journal of the American Society of Clinical Oncology. 1999 Mar;17(3):1020-8. PubMed PMID: 10071297.
39. Abendstein H, Nordgren M, Boysen M, Jannert M, Silander E, Ahlner-Elmqvist M, et al. Quality of life and head and neck cancer: a 5 year prospective study. The Laryngoscope. 2005 Dec;115(12):2183-92. PubMed PMID: 16369164.
40. Dirix P, Nuyts S, Van den Bogaert W. Radiation-induced xerostomia in patients with head and neck cancer: a literature review. Cancer. 2006 Dec 1;107(11):2525-34. PubMed PMID: 17078052.
41. Fang F, Chen P, Chen XC, Li J, Wen YJ, Wei YQ. Humoral immunity responses against EGFR-positive tumor cells induced by xenogeneic EGFR expressed in the yeast Pichia pastoris. International journal of molecular medicine. 2009 Feb;23(2):181-8. PubMed PMID: 19148541.
42. Kraus MH, Issing W, Miki T, Popescu NC, Aaronson SA. Isolation and characterization of ERBB3, a third member of the ERBB/epidermal growth factor receptor family: evidence for overexpression in a subset of human mammary tumors. Proceedings of the National Academy of Sciences of the United States of America. 1989 Dec;86(23):9193-7. PubMed PMID: 2687875. Pubmed Central PMCID: 298460.
43. Plowman GD, Culouscou JM, Whitney GS, Green JM, Carlton GW, Foy L, et al. Ligand-specific activation of HER4/p180erbB4, a fourth member of the epidermal growth factor receptor family. Proceedings of the National Academy of Sciences of the United States of America. 1993 Mar 1;90(5):1746-50. PubMed PMID: 8383326. Pubmed Central PMCID: 45956.
44. Yamamoto T, Ikawa S, Akiyama T, Semba K, Nomura N, Miyajima N, et al. Similarity of protein encoded by the human c-erb-B-2 gene to epidermal growth factor receptor. Nature. 1986 Jan 16-22;319(6050):230-4. PubMed PMID: 3003577.
45. Guy PM, Platko JV, Cantley LC, Cerione RA, Carraway KL, 3rd. Insect cell-expressed p180erbB3 possesses an impaired tyrosine kinase activity. Proceedings of the National Academy of Sciences of the United States of America. 1994 Aug 16;91(17):8132-6. PubMed PMID: 8058768. Pubmed Central PMCID: 44559.
46. Burgess AW, Cho HS, Eigenbrot C, Ferguson KM, Garrett TP, Leahy DJ, et al. An open-and-shut case? Recent insights into the activation of EGF/ErbB receptors. Molecular cell. 2003 Sep;12(3):541-52. PubMed PMID: 14527402.
47. Junttila TT, Sundvall M, Maatta JA, Elenius K. Erbb4 and its isoforms: selective regulation of growth factor responses by naturally occurring receptor variants. Trends in cardiovascular medicine. 2000 Oct;10(7):304-10. PubMed PMID: 11343971.
48. de Bono JS, Rowinsky EK. The ErbB receptor family: a therapeutic target for cancer. Trends in molecular medicine. 2002;8(4 Suppl):S19-26. PubMed PMID: 11927283.
49. Mandruzzato S, Brasseur F, Andry G, Boon T, van der Bruggen P. A CASP-8 mutation recognized by cytolytic T lymphocytes on a human head and neck carcinoma. The Journal of experimental medicine. 1997 Aug 29;186(5):785-93. PubMed PMID: 9271594. Pubmed Central PMCID: 2199018.
50. Modjtahedi H, Moscatello DK, Box G, Green M, Shotton C, Lamb DJ, et al. Targeting of cells expressing wild-type EGFR and type-III mutant EGFR (EGFRvIII) by anti-EGFR MAb ICR62: a two-pronged attack for tumour therapy. International journal

of cancer Journal international du cancer. 2003 Jun 10;105(2):273-80. PubMed PMID: 12673691.
51. Kass ES, Greiner JW, Kantor JA, Tsang KY, Guadagni F, Chen Z, et al. Carcinoembryonic antigen as a target for specific antitumor immunotherapy of head and neck cancer. Cancer research. 2002 Sep 1;62(17):5049-57. PubMed PMID: 12208760.
52. Kienstra MA, Neel HB, Strome SE, Roche P. Identification of NY-ESO-1, MAGE-1, and MAGE-3 in head and neck squamous cell carcinoma. Head & neck. 2003 Jun;25(6):457-63. PubMed PMID: 12784237.
53. Scanlan MJ, Gure AO, Jungbluth AA, Old LJ, Chen YT. Cancer/testis antigens: an expanding family of targets for cancer immunotherapy. Immunological reviews. 2002 Oct;188:22-32. PubMed PMID: 12445278.
54. Albers A, Abe K, Hunt J, Wang J, Lopez-Albaitero A, Schaefer C, et al. Antitumor activity of human papillomavirus type 16 E7-specific T cells against virally infected squamous cell carcinoma of the head and neck. Cancer research. 2005 Dec 1;65(23):11146-55. PubMed PMID: 16322265.
55. Davidson HC, Leibowitz MS, Lopez-Albaitero A, Ferris RL. Immunotherapy for head and neck cancer. Oral oncology. 2009 Sep;45(9):747-51. PubMed PMID: 19442565. Epub 2009/05/16. eng.
56. Wong RW. Transgenic and knock-out mice for deciphering the roles of EGFR ligands. Cellular and molecular life sciences : CMLS. 2003 Jan;60(1):113-8. PubMed PMID: 12613661.
57. Gassmann M, Casagranda F, Orioli D, Simon H, Lai C, Klein R, et al. Aberrant neural and cardiac development in mice lacking the ErbB4 neuregulin receptor. Nature. 1995 Nov 23;378(6555):390-4. PubMed PMID: 7477376.
58. Lee KF, Simon H, Chen H, Bates B, Hung MC, Hauser C. Requirement for neuregulin receptor erbB2 in neural and cardiac development. Nature. 1995 Nov 23;378(6555):394-8. PubMed PMID: 7477377.
59. Riethmacher D, Sonnenberg-Riethmacher E, Brinkmann V, Yamaai T, Lewin GR, Birchmeier C. Severe neuropathies in mice with targeted mutations in the ErbB3 receptor. Nature. 1997 Oct 16;389(6652):725-30. PubMed PMID: 9338783.
60. Threadgill DW, Dlugosz AA, Hansen LA, Tennenbaum T, Lichti U, Yee D, et al. Targeted disruption of mouse EGF receptor: effect of genetic background on mutant phenotype. Science. 1995 Jul 14;269(5221):230-4. PubMed PMID: 7618084.
61. Miettinen PJ, Berger JE, Meneses J, Phung Y, Pedersen RA, Werb Z, et al. Epithelial immaturity and multiorgan failure in mice lacking epidermal growth factor receptor. Nature. 1995 Jul 27;376(6538):337-41. PubMed PMID: 7630400.
62. Linggi B, Carpenter G. ErbB receptors: new insights on mechanisms and biology. Trends in cell biology. 2006 Dec;16(12):649-56. PubMed PMID: 17085050.
63. Bajaj M, Waterfield MD, Schlessinger J, Taylor WR, Blundell T. On the tertiary structure of the extracellular domains of the epidermal growth factor and insulin receptors. Biochimica et biophysica acta. 1987 Nov 26;916(2):220-6. PubMed PMID: 3676333.
64. Lax I, Johnson A, Howk R, Sap J, Bellot F, Winkler M, et al. Chicken epidermal growth factor (EGF) receptor: cDNA cloning, expression in mouse cells, and differential binding of EGF and transforming growth factor alpha. Molecular and cellular biology. 1988 May;8(5):1970-8. PubMed PMID: 3260329. Pubmed Central PMCID: 363375.
65. Bouyain S, Longo PA, Li S, Ferguson KM, Leahy DJ. The extracellular region of ErbB4 adopts a tethered conformation in the absence of ligand. Proceedings of the

National Academy of Sciences of the United States of America. 2005 Oct 18;102(42):15024-9. PubMed PMID: 16203964. Pubmed Central PMCID: 1257738.
66. Cho HS, Leahy DJ. Structure of the extracellular region of HER3 reveals an interdomain tether. Science. 2002 Aug 23;297(5585):1330-3. PubMed PMID: 12154198.
67. Ferguson KM, Berger MB, Mendrola JM, Cho HS, Leahy DJ, Lemmon MA. EGF activates its receptor by removing interactions that autoinhibit ectodomain dimerization. Molecular cell. 2003 Feb;11(2):507-17. PubMed PMID: 12620237.
68. Garrett TP, McKern NM, Lou M, Elleman TC, Adams TE, Lovrecz GO, et al. Crystal structure of a truncated epidermal growth factor receptor extracellular domain bound to transforming growth factor alpha. Cell. 2002 Sep 20;110(6):763-73. PubMed PMID: 12297049.
69. Ogiso H, Ishitani R, Nureki O, Fukai S, Yamanaka M, Kim JH, et al. Crystal structure of the complex of human epidermal growth factor and receptor extracellular domains. Cell. 2002 Sep 20;110(6):775-87. PubMed PMID: 12297050.
70. Garrett TP, McKern NM, Lou M, Elleman TC, Adams TE, Lovrecz GO, et al. The crystal structure of a truncated ErbB2 ectodomain reveals an active conformation, poised to interact with other ErbB receptors. Molecular cell. 2003 Feb;11(2):495-505. PubMed PMID: 12620236.
71. Cho HS, Mason K, Ramyar KX, Stanley AM, Gabelli SB, Denney DW, Jr., et al. Structure of the extracellular region of HER2 alone and in complex with the Herceptin Fab. Nature. 2003 Feb 13;421(6924):756-60. PubMed PMID: 12610629.
72. Di Fiore PP, Pierce JH, Kraus MH, Segatto O, King CR, Aaronson SA. erbB-2 is a potent oncogene when overexpressed in NIH/3T3 cells. Science. 1987 Jul 10;237(4811):178-82. PubMed PMID: 2885917.
73. Graus-Porta D, Beerli RR, Daly JM, Hynes NE. ErbB-2, the preferred heterodimerization partner of all ErbB receptors, is a mediator of lateral signaling. The EMBO journal. 1997 Apr 1;16(7):1647-55. PubMed PMID: 9130710. Pubmed Central PMCID: 1169769.
74. Klapper LN, Glathe S, Vaisman N, Hynes NE, Andrews GC, Sela M, et al. The ErbB-2/HER2 oncoprotein of human carcinomas may function solely as a shared coreceptor for multiple stroma-derived growth factors. Proceedings of the National Academy of Sciences of the United States of America. 1999 Apr 27;96(9):4995-5000. PubMed PMID: 10220407. Pubmed Central PMCID: 21805.
75. Penuel E, Akita RW, Sliwkowski MX. Identification of a region within the ErbB2/HER2 intracellular domain that is necessary for ligand-independent association. The Journal of biological chemistry. 2002 Aug 9;277(32):28468-73. PubMed PMID: 12000754.
76. Lemmon MA. Ligand-induced ErbB receptor dimerization. Experimental cell research. 2009 Feb 15;315(4):638-48. PubMed PMID: 19038249. Pubmed Central PMCID: 2667204.
77. Tao RH, Maruyama IN. All EGF(ErbB) receptors have preformed homo- and heterodimeric structures in living cells. Journal of cell science. 2008 Oct 1;121(Pt 19):3207-17. PubMed PMID: 18782861.
78. Liu P, Sudhaharan T, Koh RM, Hwang LC, Ahmed S, Maruyama IN, et al. Investigation of the dimerization of proteins from the epidermal growth factor receptor family by single wavelength fluorescence cross-correlation spectroscopy. Biophysical journal. 2007 Jul 15;93(2):684-98. PubMed PMID: 17468161. Pubmed Central PMCID: 1896234.

79. Moriki T, Maruyama H, Maruyama IN. Activation of preformed EGF receptor dimers by ligand-induced rotation of the transmembrane domain. Journal of molecular biology. 2001 Aug 31;311(5):1011-26. PubMed PMID: 11531336.
80. Smith SO, Smith C, Shekar S, Peersen O, Ziliox M, Aimoto S. Transmembrane interactions in the activation of the Neu receptor tyrosine kinase. Biochemistry. 2002 Jul 30;41(30):9321-32. PubMed PMID: 12135353.
81. Warren CM, Landgraf R. Signaling through ERBB receptors: multiple layers of diversity and control. Cellular signalling. 2006 Jul;18(7):923-33. PubMed PMID: 16460914.
82. Jorissen RN, Walker F, Pouliot N, Garrett TP, Ward CW, Burgess AW. Epidermal growth factor receptor: mechanisms of activation and signalling. Experimental cell research. 2003 Mar 10;284(1):31-53. PubMed PMID: 12648464.
83. Pawson T. Specificity in signal transduction: from phosphotyrosine-SH2 domain interactions to complex cellular systems. Cell. 2004 Jan 23;116(2):191-203. PubMed PMID: 14744431.
84. Olayioye MA, Graus-Porta D, Beerli RR, Rohrer J, Gay B, Hynes NE. ErbB-1 and ErbB-2 acquire distinct signaling properties dependent upon their dimerization partner. Molecular and cellular biology. 1998 Sep;18(9):5042-51. PubMed PMID: 9710588. Pubmed Central PMCID: 109089.
85. Yarden Y, Sliwkowski MX. Untangling the ErbB signalling network. Nature reviews Molecular cell biology. 2001 Feb;2(2):127-37. PubMed PMID: 11252954.
86. Soltoff SP, Cantley LC. p120cbl is a cytosolic adapter protein that associates with phosphoinositide 3-kinase in response to epidermal growth factor in PC12 and other cells. The Journal of biological chemistry. 1996 Jan 5;271(1):563-7. PubMed PMID: 8550620.
87. Schlessinger J. Cell signaling by receptor tyrosine kinases. Cell. 2000 Oct 13;103(2):211-25. PubMed PMID: 11057895.
88. Sorkin A, Von Zastrow M. Signal transduction and endocytosis: close encounters of many kinds. Nature reviews Molecular cell biology. 2002 Aug;3(8):600-14. PubMed PMID: 12154371.
89. Miaczynska M, Pelkmans L, Zerial M. Not just a sink: endosomes in control of signal transduction. Current opinion in cell biology. 2004 Aug;16(4):400-6. PubMed PMID: 15261672.
90. Lin SY, Makino K, Xia W, Matin A, Wen Y, Kwong KY, et al. Nuclear localization of EGF receptor and its potential new role as a transcription factor. Nature cell biology. 2001 Sep;3(9):802-8. PubMed PMID: 11533659.
91. Pinkas-Kramarski R, Soussan L, Waterman H, Levkowitz G, Alroy I, Klapper L, et al. Diversification of Neu differentiation factor and epidermal growth factor signaling by combinatorial receptor interactions. The EMBO journal. 1996 May 15;15(10):2452-67. PubMed PMID: 8665853. Pubmed Central PMCID: 450177.
92. Riese DJ, 2nd, van Raaij TM, Plowman GD, Andrews GC, Stern DF. The cellular response to neuregulins is governed by complex interactions of the erbB receptor family. Molecular and cellular biology. 1995 Oct;15(10):5770-6. PubMed PMID: 7565730. Pubmed Central PMCID: 230829.
93. Takikita M, Xie R, Chung JY, Cho H, Ylaya K, Hong SM, et al. Membranous expression of Her3 is associated with a decreased survival in head and neck squamous cell carcinoma. Journal of translational medicine. 2011;9:126. PubMed PMID: 21801427. Pubmed Central PMCID: 3162511.

94. Lewis TS, Shapiro PS, Ahn NG. Signal transduction through MAP kinase cascades. Advances in cancer research. 1998;74:49-139. PubMed PMID: 9561267.
95. Blenis J. Signal transduction via the MAP kinases: proceed at your own RSK. Proceedings of the National Academy of Sciences of the United States of America. 1993 Jul 1;90(13):5889-92. PubMed PMID: 8392180. Pubmed Central PMCID: 46831.
96. Chan TO, Rittenhouse SE, Tsichlis PN. AKT/PKB and other D3 phosphoinositide-regulated kinases: kinase activation by phosphoinositide-dependent phosphorylation. Annual review of biochemistry. 1999;68:965-1014. PubMed PMID: 10872470.
97. Burgering BM, Coffer PJ. Protein kinase B (c-Akt) in phosphatidylinositol-3-OH kinase signal transduction. Nature. 1995 Aug 17;376(6541):599-602. PubMed PMID: 7637810.
98. Newton AC, Johnson JE. Protein kinase C: a paradigm for regulation of protein function by two membrane-targeting modules. Biochimica et biophysica acta. 1998 Aug 21;1376(2):155-72. PubMed PMID: 9748550.
99. Song JI, Grandis JR. STAT signaling in head and neck cancer. Oncogene. 2000 May 15;19(21):2489-95. PubMed PMID: 10851047.
100. Bromberg J, Darnell JE, Jr. The role of STATs in transcriptional control and their impact on cellular function. Oncogene. 2000 May 15;19(21):2468-73. PubMed PMID: 10851045.
101. Rubin Grandis J, Melhem MF, Barnes EL, Tweardy DJ. Quantitative immunohistochemical analysis of transforming growth factor-alpha and epidermal growth factor receptor in patients with squamous cell carcinoma of the head and neck. Cancer. 1996 Sep 15;78(6):1284-92. PubMed PMID: 8826952.
102. Temam S, Kawaguchi H, El-Naggar AK, Jelinek J, Tang H, Liu DD, et al. Epidermal growth factor receptor copy number alterations correlate with poor clinical outcome in patients with head and neck squamous cancer. Journal of clinical oncology : official journal of the American Society of Clinical Oncology. 2007 Jun 1;25(16):2164-70. PubMed PMID: 17538160.
103. Chung CH, Ely K, McGavran L, Varella-Garcia M, Parker J, Parker N, et al. Increased epidermal growth factor receptor gene copy number is associated with poor prognosis in head and neck squamous cell carcinomas. Journal of clinical oncology : official journal of the American Society of Clinical Oncology. 2006 Sep 1;24(25):4170-6. PubMed PMID: 16943533.
104. Ratushny V, Astsaturov I, Burtness BA, Golemis EA, Silverman JS. Targeting EGFR resistance networks in head and neck cancer. Cellular signalling. 2009 Aug;21(8):1255-68. PubMed PMID: 19258037. Pubmed Central PMCID: 2770888.
105. Slaughter DP, Southwick HW, Smejkal W. Field cancerization in oral stratified squamous epithelium; clinical implications of multicentric origin. Cancer. 1953 Sep;6(5):963-8. PubMed PMID: 13094644.
106. Rodrigo JP, Ramos S, Lazo PS, Alvarez I, Suarez C. Amplification of ERBB oncogenes in squamous cell carcinomas of the head and neck. European journal of cancer. 1996 Oct;32A(11):2004-10. PubMed PMID: 8943688.
107. Grandis JR, Tweardy DJ. Elevated levels of transforming growth factor alpha and epidermal growth factor receptor messenger RNA are early markers of carcinogenesis in head and neck cancer. Cancer research. 1993 Aug 1;53(15):3579-84. PubMed PMID: 8339264.
108. Psyrri A, Yu Z, Weinberger PM, Sasaki C, Haffty B, Camp R, et al. Quantitative determination of nuclear and cytoplasmic epidermal growth factor receptor expression in oropharyngeal squamous cell cancer by using automated quantitative

analysis. Clinical cancer research : an official journal of the American Association for Cancer Research. 2005 Aug 15;11(16):5856-62. PubMed PMID: 16115926.
109. Rubin Grandis J, Tweardy DJ, Melhem MF. Asynchronous modulation of transforming growth factor alpha and epidermal growth factor receptor protein expression in progression of premalignant lesions to head and neck squamous cell carcinoma. Clinical cancer research : an official journal of the American Association for Cancer Research. 1998 Jan;4(1):13-20. PubMed PMID: 9516947.
110. Shin DM, Ro JY, Hong WK, Hittelman WN. Dysregulation of epidermal growth factor receptor expression in premalignant lesions during head and neck tumorigenesis. Cancer research. 1994 Jun 15;54(12):3153-9. PubMed PMID: 8205534.
111. Batra SK, Castelino-Prabhu S, Wikstrand CJ, Zhu X, Humphrey PA, Friedman HS, et al. Epidermal growth factor ligand-independent, unregulated, cell-transforming potential of a naturally occurring human mutant EGFRvIII gene. Cell growth & differentiation : the molecular biology journal of the American Association for Cancer Research. 1995 Oct;6(10):1251-9. PubMed PMID: 8845302.
112. Bigner SH, Humphrey PA, Wong AJ, Vogelstein B, Mark J, Friedman HS, et al. Characterization of the epidermal growth factor receptor in human glioma cell lines and xenografts. Cancer research. 1990 Dec 15;50(24):8017-22. PubMed PMID: 2253244.
113. Sok JC, Coppelli FM, Thomas SM, Lango MN, Xi S, Hunt JL, et al. Mutant epidermal growth factor receptor (EGFRvIII) contributes to head and neck cancer growth and resistance to EGFR targeting. Clinical cancer research : an official journal of the American Association for Cancer Research. 2006 Sep 1;12(17):5064-73. PubMed PMID: 16951222.
114. Grandis JR, Sok JC. Signaling through the epidermal growth factor receptor during the development of malignancy. Pharmacology & therapeutics. 2004 Apr;102(1):37-46. PubMed PMID: 15056497.
115. Pedersen MW, Meltorn M, Damstrup L, Poulsen HS. The type III epidermal growth factor receptor mutation. Biological significance and potential target for anti-cancer therapy. Annals of oncology : official journal of the European Society for Medical Oncology / ESMO. 2001 Jun;12(6):745-60. PubMed PMID: 11484948.
116. Wheeler SE, Suzuki S, Thomas SM, Sen M, Leeman-Neill RJ, Chiosea SI, et al. Epidermal growth factor receptor variant III mediates head and neck cancer cell invasion via STAT3 activation. Oncogene. 2010 Sep 16;29(37):5135-45. PubMed PMID: 20622897. Pubmed Central PMCID: 2940981.
117. Tzahar E, Waterman H, Chen X, Levkowitz G, Karunagaran D, Lavi S, et al. A hierarchical network of interreceptor interactions determines signal transduction by Neu differentiation factor/neuregulin and epidermal growth factor. Molecular and cellular biology. 1996 Oct;16(10):5276-87. PubMed PMID: 8816440. Pubmed Central PMCID: 231527.
118. Alimandi M, Romano A, Curia MC, Muraro R, Fedi P, Aaronson SA, et al. Cooperative signaling of ErbB3 and ErbB2 in neoplastic transformation and human mammary carcinomas. Oncogene. 1995 May 4;10(9):1813-21. PubMed PMID: 7538656.
119. Wallasch C, Weiss FU, Niederfellner G, Jallal B, Issing W, Ullrich A. Heregulin-dependent regulation of HER2/neu oncogenic signaling by heterodimerization with HER3. The EMBO journal. 1995 Sep 1;14(17):4267-75. PubMed PMID: 7556068. Pubmed Central PMCID: 394510.

120. Chausovsky A, Waterman H, Elbaum M, Yarden Y, Geiger B, Bershadsky AD. Molecular requirements for the effect of neuregulin on cell spreading, motility and colony organization. Oncogene. 2000 Feb 17;19(7):878-88. PubMed PMID: 10702796.
121. Sardari Y, Pardis S, Tadbir AA, Ashraf MJ, Fattahi MJ, Ebrahimi H, et al. HER2/neu expression in head and neck squamous cell carcinoma patients is not significantly elevated. Asian Pacific journal of cancer prevention : APJCP. 2012;13(6):2891-6. PubMed PMID: 22938479.
122. Field JK, Spandidos DA, Yiagnisis M, Gosney JR, Papadimitriou K, Stell PM. C-erbB-2 expression in squamous cell carcinoma of the head and neck. Anticancer research. 1992 May-Jun;12(3):613-9. PubMed PMID: 1377893.
123. Craven JM, Pavelic ZP, Stambrook PJ, Pavelic L, Gapany M, Kelley DJ, et al. Expression of c-erbB-2 gene in human head and neck carcinoma. Anticancer research. 1992 Nov-Dec;12(6B):2273-6. PubMed PMID: 1363518.
124. Riviere A, Becker J, Loning T. Comparative investigation of c-erbB2/neu expression in head and neck tumors and mammary cancer. Cancer. 1991 Apr 15;67(8):2142-9. PubMed PMID: 1672262.
125. Kearsley JH, Leonard JH, Walsh MD, Wright GR. A comparison of epidermal growth factor receptor (EGFR) and c-erbB-2 oncogene expression in head and neck squamous cell carcinomas. Pathology. 1991 Jul;23(3):189-94. PubMed PMID: 1685773.
126. Cavalot A, Martone T, Roggero N, Brondino G, Pagano M, Cortesina G. Prognostic impact of HER-2/neu expression on squamous head and neck carcinomas. Head & neck. 2007 Jul;29(7):655-64. PubMed PMID: 17315173.
127. Ibrahim SO, Vasstrand EN, Liavaag PG, Johannessen AC, Lillehaug JR. Expression of c-erbB proto-oncogene family members in squamous cell carcinoma of the head and neck. Anticancer research. 1997 Nov-Dec;17(6D):4539-46. PubMed PMID: 9494565.
128. Xia W, Lau YK, Zhang HZ, Xiao FY, Johnston DA, Liu AR, et al. Combination of EGFR, HER-2/neu, and HER-3 is a stronger predictor for the outcome of oral squamous cell carcinoma than any individual family members. Clinical cancer research : an official journal of the American Association for Cancer Research. 1999 Dec;5(12):4164-74. PubMed PMID: 10632356.
129. Hoffmann TK, Ballo H, Braunstein S, Van Lierop A, Wagenmann M, Bier H. Serum level and tissue expression of c-erbB-1 and c-erbB-2 proto-oncogene products in patients with squamous cell carcinoma of the head and neck. Oral oncology. 2001 Jan;37(1):50-6. PubMed PMID: 11120483.
130. Ming W, Hua Q, Tao Z, Zhang D. [Expression and significance of ErbB3 and ErbB4 in patients with laryngeal squamous cell carcinomas]. Lin chuang er bi yan hou tou jing wai ke za zhi = Journal of clinical otorhinolaryngology, head, and neck surgery. 2007 Aug;21(15):706-8. PubMed PMID: 17969526.
131. Dorsey K, Agulnik M. Promising New Molecular Targeted Therapies in Head and Neck Cancer. Drugs. 2013 Feb 26. PubMed PMID: 23440867.
132. Karamouzis MV, Grandis JR, Argiris A. Therapies directed against epidermal growth factor receptor in aerodigestive carcinomas. JAMA : the journal of the American Medical Association. 2007 Jul 4;298(1):70-82. PubMed PMID: 17609492.
133. Kawamoto T, Sato JD, Le A, Polikoff J, Sato GH, Mendelsohn J. Growth stimulation of A431 cells by epidermal growth factor: identification of high-affinity receptors for epidermal growth factor by an anti-receptor monoclonal antibody. Proceedings of the National Academy of Sciences of the United States of America. 1983 Mar;80(5):1337-41. PubMed PMID: 6298788. Pubmed Central PMCID: 393592.

134. Gill GN, Kawamoto T, Cochet C, Le A, Sato JD, Masui H, et al. Monoclonal anti-epidermal growth factor receptor antibodies which are inhibitors of epidermal growth factor binding and antagonists of epidermal growth factor binding and antagonists of epidermal growth factor-stimulated tyrosine protein kinase activity. The Journal of biological chemistry. 1984 Jun 25;259(12):7755-60. PubMed PMID: 6330079.
135. Dittmann K, Mayer C, Rodemann HP. Inhibition of radiation-induced EGFR nuclear import by C225 (Cetuximab) suppresses DNA-PK activity. Radiotherapy and oncology : journal of the European Society for Therapeutic Radiology and Oncology. 2005 Aug;76(2):157-61. PubMed PMID: 16024112.
136. Bernier J, Bentzen SM, Vermorken JB. Molecular therapy in head and neck oncology. Nature reviews Clinical oncology. 2009 May;6(5):266-77. PubMed PMID: 19390553.
137. Goldstein NI, Prewett M, Zuklys K, Rockwell P, Mendelsohn J. Biological efficacy of a chimeric antibody to the epidermal growth factor receptor in a human tumor xenograft model. Clinical cancer research : an official journal of the American Association for Cancer Research. 1995 Nov;1(11):1311-8. PubMed PMID: 9815926.
138. Fan Z, Lu Y, Wu X, Mendelsohn J. Antibody-induced epidermal growth factor receptor dimerization mediates inhibition of autocrine proliferation of A431 squamous carcinoma cells. The Journal of biological chemistry. 1994 Nov 4;269(44):27595-602. PubMed PMID: 7961676.
139. Sato JD, Kawamoto T, Le AD, Mendelsohn J, Polikoff J, Sato GH. Biological effects in vitro of monoclonal antibodies to human epidermal growth factor receptors. Molecular biology & medicine. 1983 Dec;1(5):511-29. PubMed PMID: 6094961.
140. Huang SM, Bock JM, Harari PM. Epidermal growth factor receptor blockade with C225 modulates proliferation, apoptosis, and radiosensitivity in squamous cell carcinomas of the head and neck. Cancer research. 1999 Apr 15;59(8):1935-40. PubMed PMID: 10213503.
141. Prewett M, Rothman M, Waksal H, Feldman M, Bander NH, Hicklin DJ. Mouse-human chimeric anti-epidermal growth factor receptor antibody C225 inhibits the growth of human renal cell carcinoma xenografts in nude mice. Clinical cancer research : an official journal of the American Association for Cancer Research. 1998 Dec;4(12):2957-66. PubMed PMID: 9865906.
142. Lopez-Albaitero A, Ferris RL. Immune activation by epidermal growth factor receptor specific monoclonal antibody therapy for head and neck cancer. Archives of otolaryngology--head & neck surgery. 2007 Dec;133(12):1277-81. PubMed PMID: 18086972.
143. Lopez-Albaitero A, Lee SC, Morgan S, Grandis JR, Gooding WE, Ferrone S, et al. Role of polymorphic Fc gamma receptor IIIa and EGFR expression level in cetuximab mediated, NK cell dependent in vitro cytotoxicity of head and neck squamous cell carcinoma cells. Cancer immunology, immunotherapy : CII. 2009 Nov;58(11):1853-64. PubMed PMID: 19319529. Pubmed Central PMCID: 3426289.
144. Taylor RJ, Chan SL, Wood A, Voskens CJ, Wolf JS, Lin W, et al. FcgammaRIIIa polymorphisms and cetuximab induced cytotoxicity in squamous cell carcinoma of the head and neck. Cancer immunology, immunotherapy : CII. 2009 Jul;58(7):997-1006. PubMed PMID: 18979096.
145. Kondo N, Tsukuda M, Sakakibara A, Takahashi H, Hyakusoku H, Komatsu M, et al. Combined molecular targeted drug therapy for EGFR and HER-2 in head and neck squamous cell carcinoma cell lines. International journal of oncology. 2012 Jun;40(6):1805-12. PubMed PMID: 22344385.

146. Bonner JA, Harari PM, Giralt J, Azarnia N, Shin DM, Cohen RB, et al. Radiotherapy plus cetuximab for squamous-cell carcinoma of the head and neck. The New England journal of medicine. 2006 Feb 9;354(6):567-78. PubMed PMID: 16467544.
147. Robert F, Ezekiel MP, Spencer SA, Meredith RF, Bonner JA, Khazaeli MB, et al. Phase I study of anti--epidermal growth factor receptor antibody cetuximab in combination with radiation therapy in patients with advanced head and neck cancer. Journal of clinical oncology : official journal of the American Society of Clinical Oncology. 2001 Jul 1;19(13):3234-43. PubMed PMID: 11432891.
148. Bonner JA, Harari PM, Giralt J, Cohen RB, Jones CU, Sur RK, et al. Radiotherapy plus cetuximab for locoregionally advanced head and neck cancer: 5-year survival data from a phase 3 randomised trial, and relation between cetuximab-induced rash and survival. The lancet oncology. 2010 Jan;11(1):21-8. PubMed PMID: 19897418.
149. Baselga J, Trigo JM, Bourhis J, Tortochaux J, Cortes-Funes H, Hitt R, et al. Phase II multicenter study of the antiepidermal growth factor receptor monoclonal antibody cetuximab in combination with platinum-based chemotherapy in patients with platinum-refractory metastatic and/or recurrent squamous cell carcinoma of the head and neck. Journal of clinical oncology : official journal of the American Society of Clinical Oncology. 2005 Aug 20;23(24):5568-77. PubMed PMID: 16009950.
150. Herbst RS, Arquette M, Shin DM, Dicke K, Vokes EE, Azarnia N, et al. Phase II multicenter study of the epidermal growth factor receptor antibody cetuximab and cisplatin for recurrent and refractory squamous cell carcinoma of the head and neck. Journal of clinical oncology : official journal of the American Society of Clinical Oncology. 2005 Aug 20;23(24):5578-87. PubMed PMID: 16009949.
151. Vermorken JB, Trigo J, Hitt R, Koralewski P, Diaz-Rubio E, Rolland F, et al. Open-label, uncontrolled, multicenter phase II study to evaluate the efficacy and toxicity of cetuximab as a single agent in patients with recurrent and/or metastatic squamous cell carcinoma of the head and neck who failed to respond to platinum-based therapy. Journal of clinical oncology : official journal of the American Society of Clinical Oncology. 2007 Jun 1;25(16):2171-7. PubMed PMID: 17538161.
152. Baselga J, Pfister D, Cooper MR, Cohen R, Burtness B, Bos M, et al. Phase I studies of anti-epidermal growth factor receptor chimeric antibody C225 alone and in combination with cisplatin. Journal of clinical oncology : official journal of the American Society of Clinical Oncology. 2000 Feb;18(4):904-14. PubMed PMID: 10673534.
153. Shin DM, Donato NJ, Perez-Soler R, Shin HJ, Wu JY, Zhang P, et al. Epidermal growth factor receptor-targeted therapy with C225 and cisplatin in patients with head and neck cancer. Clinical cancer research : an official journal of the American Association for Cancer Research. 2001 May;7(5):1204-13. PubMed PMID: 11350885.
154. Busam KJ, Capodieci P, Motzer R, Kiehn T, Phelan D, Halpern AC. Cutaneous side-effects in cancer patients treated with the antiepidermal growth factor receptor antibody C225. The British journal of dermatology. 2001 Jun;144(6):1169-76. PubMed PMID: 11422037.
155. Ang KK, Zhang QE, Rosenthal DI, Nguyen-Tan P, Sherman EJ, Weber RS, et al. A randomized phase III trial (RTOG 0522) of concurrent accelerated radiation plus cisplatin with or without cetuximab for stage III-IV head and neck squamous cell carcinomas (HNC) (abstract no. 5500). Journal of clinical oncology : official journal of the American Society of Clinical Oncology. 2011;29(Suppl.).

156. Stintzing S, Kapaun C, Laubender RP, Jung A, Neumann J, Modest DP, et al. Prognostic value of cetuximab-related skin toxicity in metastatic colorectal cancer patients and its correlation with parameters of the epidermal growth factor receptor signal transduction pathway: results from a randomized trial of the GERMAN AIO CRC Study Group. International journal of cancer Journal international du cancer. 2013 Jan 1;132(1):236-45. PubMed PMID: 22644776.
157. Sugiura Y, Nemoto E, Kawai O, Ohkubo Y, Fusegawa H, Kaseda S. Skin rash by gefitinib is a sign of favorable outcomes for patients of advanced lung adenocarcinoma in Japanese patients. SpringerPlus. 2013 Dec;2(1):22. PubMed PMID: 23420789. Pubmed Central PMCID: 3569587.
158. Chiu CH, Tsai CM, Chen YM, Chiang SC, Liou JL, Perng RP. Gefitinib is active in patients with brain metastases from non-small cell lung cancer and response is related to skin toxicity. Lung cancer. 2005 Jan;47(1):129-38. PubMed PMID: 15603863.
159. Wacker B, Nagrani T, Weinberg J, Witt K, Clark G, Cagnoni PJ. Correlation between development of rash and efficacy in patients treated with the epidermal growth factor receptor tyrosine kinase inhibitor erlotinib in two large phase III studies. Clinical cancer research : an official journal of the American Association for Cancer Research. 2007 Jul 1;13(13):3913-21. PubMed PMID: 17606725.
160. Klinghammer K, Knodler M, Schmittel A, Budach V, Keilholz U, Tinhofer I. Association of epidermal growth factor receptor polymorphism, skin toxicity, and outcome in patients with squamous cell carcinoma of the head and neck receiving cetuximab-docetaxel treatment. Clinical cancer research : an official journal of the American Association for Cancer Research. 2010 Jan 1;16(1):304-10. PubMed PMID: 20028750.
161. Cohen EE, Lingen MW, Martin LE, Harris PL, Brannigan BW, Haserlat SM, et al. Response of some head and neck cancers to epidermal growth factor receptor tyrosine kinase inhibitors may be linked to mutation of ERBB2 rather than EGFR. Clinical cancer research : an official journal of the American Association for Cancer Research. 2005 Nov 15;11(22):8105-8. PubMed PMID: 16299242.
162. Pfister DG, Su YB, Kraus DH, Wolden SL, Lis E, Aliff TB, et al. Concurrent cetuximab, cisplatin, and concomitant boost radiotherapy for locoregionally advanced, squamous cell head and neck cancer: a pilot phase II study of a new combined-modality paradigm. Journal of clinical oncology : official journal of the American Society of Clinical Oncology. 2006 Mar 1;24(7):1072-8. PubMed PMID: 16505426.
163. Kondo N, Ishiguro Y, Kimura M, Sano D, Fujita K, Sakakibara A, et al. Antitumor effect of gefitinib on head and neck squamous cell carcinoma enhanced by trastuzumab. Oncology reports. 2008 Aug;20(2):373-8. PubMed PMID: 18636200.
164. Yang XD, Jia XC, Corvalan JR, Wang P, Davis CG. Development of ABX-EGF, a fully human anti-EGF receptor monoclonal antibody, for cancer therapy. Critical reviews in oncology/hematology. 2001 Apr;38(1):17-23. PubMed PMID: 11255078.
165. Machiels JP, Subramanian S, Ruzsa A, Repassy G, Lifirenko I, Flygare A, et al. Zalutumumab plus best supportive care versus best supportive care alone in patients with recurrent or metastatic squamous-cell carcinoma of the head and neck after failure of platinum-based chemotherapy: an open-label, randomised phase 3 trial. The lancet oncology. 2011 Apr;12(4):333-43. PubMed PMID: 21377930.
166. Cohen EE, Rosen F, Stadler WM, Recant W, Stenson K, Huo D, et al. Phase II trial of ZD1839 in recurrent or metastatic squamous cell carcinoma of the head and neck. Journal of clinical oncology : official journal of the American Society of Clinical Oncology. 2003 May 15;21(10):1980-7. PubMed PMID: 12743152.

167. Stewart JS, Cohen EE, Licitra L, Van Herpen CM, Khorprasert C, Soulieres D, et al. Phase III study of gefitinib compared with intravenous methotrexate for recurrent squamous cell carcinoma of the head and neck [corrected]. Journal of clinical oncology : official journal of the American Society of Clinical Oncology. 2009 Apr 10;27(11):1864-71. PubMed PMID: 19289630.
168. Soulieres D, Senzer NN, Vokes EE, Hidalgo M, Agarwala SS, Siu LL. Multicenter phase II study of erlotinib, an oral epidermal growth factor receptor tyrosine kinase inhibitor, in patients with recurrent or metastatic squamous cell cancer of the head and neck. Journal of clinical oncology : official journal of the American Society of Clinical Oncology. 2004 Jan 1;22(1):77-85. PubMed PMID: 14701768.
169. Siu LL, Soulieres D, Chen EX, Pond GR, Chin SF, Francis P, et al. Phase I/II trial of erlotinib and cisplatin in patients with recurrent or metastatic squamous cell carcinoma of the head and neck: a Princess Margaret Hospital phase II consortium and National Cancer Institute of Canada Clinical Trials Group Study. Journal of clinical oncology : official journal of the American Society of Clinical Oncology. 2007 Jun 1;25(16):2178-83. PubMed PMID: 17538162.
170. Harari PM, Allen GW, Bonner JA. Biology of interactions: antiepidermal growth factor receptor agents. Journal of clinical oncology : official journal of the American Society of Clinical Oncology. 2007 Sep 10;25(26):4057-65. PubMed PMID: 17827454.
171. Allegra CJ, Jessup JM, Somerfield MR, Hamilton SR, Hammond EH, Hayes DF, et al. American Society of Clinical Oncology provisional clinical opinion: testing for KRAS gene mutations in patients with metastatic colorectal carcinoma to predict response to anti-epidermal growth factor receptor monoclonal antibody therapy. Journal of clinical oncology : official journal of the American Society of Clinical Oncology. 2009 Apr 20;27(12):2091-6. PubMed PMID: 19188670.
172. Di Nicolantonio F, Martini M, Molinari F, Sartore-Bianchi A, Arena S, Saletti P, et al. Wild-type BRAF is required for response to panitumumab or cetuximab in metastatic colorectal cancer. Journal of clinical oncology : official journal of the American Society of Clinical Oncology. 2008 Dec 10;26(35):5705-12. PubMed PMID: 19001320.
173. De Roock W, Claes B, Bernasconi D, De Schutter J, Biesmans B, Fountzilas G, et al. Effects of KRAS, BRAF, NRAS, and PIK3CA mutations on the efficacy of cetuximab plus chemotherapy in chemotherapy-refractory metastatic colorectal cancer: a retrospective consortium analysis. The lancet oncology. 2010 Aug;11(8):753-62. PubMed PMID: 20619739.
174. Rabinowits G, Haddad RI. Overcoming resistance to EGFR inhibitor in head and neck cancer: a review of the literature. Oral oncology. 2012 Nov;48(11):1085-9. PubMed PMID: 22840785.
175. Quesnelle KM, Grandis JR. Dual kinase inhibition of EGFR and HER2 overcomes resistance to cetuximab in a novel in vivo model of acquired cetuximab resistance. Clinical cancer research : an official journal of the American Association for Cancer Research. 2011 Sep 15;17(18):5935-44. PubMed PMID: 21791633. Pubmed Central PMCID: 3426303.
176. Yonesaka K, Zejnullahu K, Okamoto I, Satoh T, Cappuzzo F, Souglakos J, et al. Activation of ERBB2 signaling causes resistance to the EGFR-directed therapeutic antibody cetuximab. Science translational medicine. 2011 Sep 7;3(99):99ra86. PubMed PMID: 21900593. Pubmed Central PMCID: 3268675.
177. Ritter CA, Perez-Torres M, Rinehart C, Guix M, Dugger T, Engelman JA, et al. Human breast cancer cells selected for resistance to trastuzumab in vivo overexpress

epidermal growth factor receptor and ErbB ligands and remain dependent on the ErbB receptor network. Clinical cancer research : an official journal of the American Association for Cancer Research. 2007 Aug 15;13(16):4909-19. PubMed PMID: 17699871.
178. Erjala K, Sundvall M, Junttila TT, Zhang N, Savisalo M, Mali P, et al. Signaling via ErbB2 and ErbB3 associates with resistance and epidermal growth factor receptor (EGFR) amplification with sensitivity to EGFR inhibitor gefitinib in head and neck squamous cell carcinoma cells. Clinical cancer research : an official journal of the American Association for Cancer Research. 2006 Jul 1;12(13):4103-11. PubMed PMID: 16818711.
179. Piechocki MP, Yoo GH, Dibbley SK, Lonardo F. Breast cancer expressing the activated HER2/neu is sensitive to gefitinib in vitro and in vivo and acquires resistance through a novel point mutation in the HER2/neu. Cancer research. 2007 Jul 15;67(14):6825-43. PubMed PMID: 17638894.
180. Sergina NV, Rausch M, Wang D, Blair J, Hann B, Shokat KM, et al. Escape from HER-family tyrosine kinase inhibitor therapy by the kinase-inactive HER3. Nature. 2007 Jan 25;445(7126):437-41. PubMed PMID: 17206155. Pubmed Central PMCID: 3025857.
181. Bottaro DP, Rubin JS, Faletto DL, Chan AM, Kmiecik TE, Vande Woude GF, et al. Identification of the hepatocyte growth factor receptor as the c-met proto-oncogene product. Science. 1991 Feb 15;251(4995):802-4. PubMed PMID: 1846706.
182. Engelman JA, Zejnullahu K, Mitsudomi T, Song Y, Hyland C, Park JO, et al. MET amplification leads to gefitinib resistance in lung cancer by activating ERBB3 signaling. Science. 2007 May 18;316(5827):1039-43. PubMed PMID: 17463250.
183. Riedel F, Gotte K, Schwalb J, Wirtz H, Bergler W, Hormann K. Serum levels of vascular endothelial growth factor in patients with head and neck cancer. European archives of oto-rhino-laryngology : official journal of the European Federation of Oto-Rhino-Laryngological Societies. 2000;257(6):332-6. PubMed PMID: 10993554.
184. Smith BD, Smith GL, Carter D, Sasaki CT, Haffty BG. Prognostic significance of vascular endothelial growth factor protein levels in oral and oropharyngeal squamous cell carcinoma. Journal of clinical oncology : official journal of the American Society of Clinical Oncology. 2000 May;18(10):2046-52. PubMed PMID: 10811669.
185. Cohen EE, Davis DW, Karrison TG, Seiwert TY, Wong SJ, Nattam S, et al. Erlotinib and bevacizumab in patients with recurrent or metastatic squamous-cell carcinoma of the head and neck: a phase I/II study. The lancet oncology. 2009 Mar;10(3):247-57. PubMed PMID: 19201650. Pubmed Central PMCID: 2768532.
186. Abbas AK, Lichtman AH. Basic Immunology, Functions and Disorders of the Immune System. Third Edition ed. Philadelphia: Saunders Elsevier; 2009.
187. Griesemer AD, Sorenson EC, Hardy MA. The role of the thymus in tolerance. Transplantation. 2010 Sep 15;90(5):465-74. PubMed PMID: 20555306. Pubmed Central PMCID: 2933313.
188. Ramsdell F, Fowlkes BJ. Clonal deletion versus clonal anergy: the role of the thymus in inducing self tolerance. Science. 1990 Jun 15;248(4961):1342-8. PubMed PMID: 1972593.
189. Azuma M, Cayabyab M, Buck D, Phillips JH, Lanier LL. CD28 interaction with B7 costimulates primary allogeneic proliferative responses and cytotoxicity mediated by small, resting T lymphocytes. The Journal of experimental medicine. 1992 Feb 1;175(2):353-60. PubMed PMID: 1370679. Pubmed Central PMCID: 2119127.

190. Jenkins MK, Taylor PS, Norton SD, Urdahl KB. CD28 delivers a costimulatory signal involved in antigen-specific IL-2 production by human T cells. Journal of immunology. 1991 Oct 15;147(8):2461-6. PubMed PMID: 1717561.
191. Croft M. Costimulation of T cells by OX40, 4-1BB, and CD27. Cytokine & growth factor reviews. 2003 Jun-Aug;14(3-4):265-73. PubMed PMID: 12787564.
192. Kim YJ, Han MK, Broxmeyer HE. 4-1BB regulates NKG2D costimulation in human cord blood CD8+ T cells. Blood. 2008 Feb 1;111(3):1378-86. PubMed PMID: 18024793. Pubmed Central PMCID: 2214739.
193. Itoh M, Takahashi T, Sakaguchi N, Kuniyasu Y, Shimizu J, Otsuka F, et al. Thymus and autoimmunity: production of CD25+CD4+ naturally anergic and suppressive T cells as a key function of the thymus in maintaining immunologic self-tolerance. Journal of immunology. 1999 May 1;162(9):5317-26. PubMed PMID: 10228007.
194. Sakaguchi S, Sakaguchi N, Asano M, Itoh M, Toda M. Immunologic self-tolerance maintained by activated T cells expressing IL-2 receptor alpha-chains (CD25). Breakdown of a single mechanism of self-tolerance causes various autoimmune diseases. Journal of immunology. 1995 Aug 1;155(3):1151-64. PubMed PMID: 7636184.
195. Ehrlich P. Ueber den jetzigen stand der karzinomforschung. Ned tijdschr Geneeskd. 1909;5:273-90.
196. Old LJ, Boyse EA. Immunology of Experimental Tumors. Annual review of medicine. 1964;15:167-86. PubMed PMID: 14139934.
197. Klein G. Tumor antigens. Annual review of microbiology. 1966;20:223-52. PubMed PMID: 5330233.
198. Burnet M. Cancer; a biological approach. I. The processes of control. British medical journal. 1957 Apr 6;1(5022):779-86. PubMed PMID: 13404306. Pubmed Central PMCID: 1973174.
199. Burnet M. Cancer: a biological approach. III. Viruses associated with neoplastic conditions. IV. Practical applications. British medical journal. 1957 Apr 13;1(5023):841-7. PubMed PMID: 13413231. Pubmed Central PMCID: 1973618.
200. Penn I. Posttransplant malignancies. Transplantation proceedings. 1999 Feb-Mar;31(1-2):1260-2. PubMed PMID: 10083562.
201. Birkeland SA, Storm HH, Lamm LU, Barlow L, Blohme I, Forsberg B, et al. Cancer risk after renal transplantation in the Nordic countries, 1964-1986. International journal of cancer Journal international du cancer. 1995 Jan 17;60(2):183-9. PubMed PMID: 7829213.
202. Sheil AG. Cancer after transplantation. World journal of surgery. 1986 Jun;10(3):389-96. PubMed PMID: 3524027.
203. Penn I. Malignant melanoma in organ allograft recipients. Transplantation. 1996 Jan 27;61(2):274-8. PubMed PMID: 8600636.
204. Clark WH, Jr., Elder DE, Guerry Dt, Braitman LE, Trock BJ, Schultz D, et al. Model predicting survival in stage I melanoma based on tumor progression. Journal of the National Cancer Institute. 1989 Dec 20;81(24):1893-904. PubMed PMID: 2593166.
205. Clemente CG, Mihm MC, Jr., Bufalino R, Zurrida S, Collini P, Cascinelli N. Prognostic value of tumor infiltrating lymphocytes in the vertical growth phase of primary cutaneous melanoma. Cancer. 1996 Apr 1;77(7):1303-10. PubMed PMID: 8608507.
206. Rilke F, Colnaghi MI, Cascinelli N, Andreola S, Baldini MT, Bufalino R, et al. Prognostic significance of HER-2/neu expression in breast cancer and its relationship to

other prognostic factors. International journal of cancer Journal international du cancer. 1991 Aug 19;49(1):44-9. PubMed PMID: 1678734.
207. Deligdisch L, Jacobs AJ, Cohen CJ. Histologic correlates of virulence in ovarian adenocarcinoma. II. Morphologic correlates of host response. American journal of obstetrics and gynecology. 1982 Dec 15;144(8):885-9. PubMed PMID: 6890770.
208. Lipponen PK, Eskelinen MJ, Jauhiainen K, Harju E, Terho R. Tumour infiltrating lymphocytes as an independent prognostic factor in transitional cell bladder cancer. European journal of cancer. 1992;29A(1):69-75. PubMed PMID: 1445749.
209. Naito Y, Saito K, Shiiba K, Ohuchi A, Saigenji K, Nagura H, et al. CD8+ T cells infiltrated within cancer cell nests as a prognostic factor in human colorectal cancer. Cancer research. 1998 Aug 15;58(16):3491-4. PubMed PMID: 9721846.
210. Epstein NA, Fatti LP. Prostatic carcinoma: some morphological features affecting prognosis. Cancer. 1976 May;37(5):2455-65. PubMed PMID: 1260728.
211. Jass JR. Lymphocytic infiltration and survival in rectal cancer. Journal of clinical pathology. 1986 Jun;39(6):585-9. PubMed PMID: 3722412. Pubmed Central PMCID: 499954.
212. Shankaran V, Ikeda H, Bruce AT, White JM, Swanson PE, Old LJ, et al. IFNgamma and lymphocytes prevent primary tumour development and shape tumour immunogenicity. Nature. 2001 Apr 26;410(6832):1107-11. PubMed PMID: 11323675.
213. Street SE, Trapani JA, MacGregor D, Smyth MJ. Suppression of lymphoma and epithelial malignancies effected by interferon gamma. The Journal of experimental medicine. 2002 Jul 1;196(1):129-34. PubMed PMID: 12093877. Pubmed Central PMCID: 2194011.
214. Smyth MJ, Thia KY, Street SE, Cretney E, Trapani JA, Taniguchi M, et al. Differential tumor surveillance by natural killer (NK) and NKT cells. The Journal of experimental medicine. 2000 Feb 21;191(4):661-8. PubMed PMID: 10684858. Pubmed Central PMCID: 2195840.
215. Dunn GP, Bruce AT, Ikeda H, Old LJ, Schreiber RD. Cancer immunoediting: from immunosurveillance to tumor escape. Nature immunology. 2002 Nov;3(11):991-8. PubMed PMID: 12407406.
216. Seliger B. Strategies of tumor immune evasion. BioDrugs : clinical immunotherapeutics, biopharmaceuticals and gene therapy. 2005;19(6):347-54. PubMed PMID: 16392887.
217. Algarra I, Garcia-Lora A, Cabrera T, Ruiz-Cabello F, Garrido F. The selection of tumor variants with altered expression of classical and nonclassical MHC class I molecules: implications for tumor immune escape. Cancer immunology, immunotherapy : CII. 2004 Oct;53(10):904-10. PubMed PMID: 15069585.
218. Garcia-Lora A, Martinez M, Algarra I, Gaforio JJ, Garrido F. MHC class I-deficient metastatic tumor variants immunoselected by T lymphocytes originate from the coordinated downregulation of APM components. International journal of cancer Journal international du cancer. 2003 Sep 10;106(4):521-7. PubMed PMID: 12845647.
219. Grandis JR, Falkner DM, Melhem MF, Gooding WE, Drenning SD, Morel PA. Human leukocyte antigen class I allelic and haplotype loss in squamous cell carcinoma of the head and neck: clinical and immunogenetic consequences. Clinical cancer research : an official journal of the American Association for Cancer Research. 2000 Jul;6(7):2794-802. PubMed PMID: 10914726.
220. Lopez-Albaitero A, Nayak JV, Ogino T, Machandia A, Gooding W, DeLeo AB, et al. Role of antigen-processing machinery in the in vitro resistance of squamous cell

carcinoma of the head and neck cells to recognition by CTL. Journal of immunology. 2006 Mar 15;176(6):3402-9. PubMed PMID: 16517708.
221. Whiteside TL. Immunobiology and immunotherapy of head and neck cancer. Current oncology reports. 2001 Jan;3(1):46-55. PubMed PMID: 11123869.
222. Goldman SA, Baker E, Weyant RJ, Clarke MR, Myers JN, Lotze MT. Peritumoral CD1a-positive dendritic cells are associated with improved survival in patients with tongue carcinoma. Archives of otolaryngology--head & neck surgery. 1998 Jun;124(6):641-6. PubMed PMID: 9639473.
223. Reichert TE, Day R, Wagner EM, Whiteside TL. Absent or low expression of the zeta chain in T cells at the tumor site correlates with poor survival in patients with oral carcinoma. Cancer research. 1998 Dec 1;58(23):5344-7. PubMed PMID: 9850063.
224. Reichert TE, Rabinowich H, Johnson JT, Whiteside TL. Human immune cells in the tumor microenvironment: mechanisms responsible for signaling and functional defects. Journal of immunotherapy. 1998;21:295-306.
225. Young MR, Wright MA, Lozano Y, Matthews JP, Benefield J, Prechel MM. Mechanisms of immune suppression in patients with head and neck cancer: influence on the immune infiltrate of the cancer. International journal of cancer Journal international du cancer. 1996 Jul 29;67(3):333-8. PubMed PMID: 8707405.
226. Saito T, Kuss I, Dworacki G, Gooding W, Johnson JT, Whiteside TL. Spontaneous ex vivo apoptosis of peripheral blood mononuclear cells in patients with head and neck cancer. Clinical cancer research : an official journal of the American Association for Cancer Research. 1999 Jun;5(6):1263-73. PubMed PMID: 10389908.
227. Hoffmann TK, Dworacki G, Tsukihiro T, Meidenbauer N, Gooding W, Johnson JT, et al. Spontaneous apoptosis of circulating T lymphocytes in patients with head and neck cancer and its clinical importance. Clinical cancer research : an official journal of the American Association for Cancer Research. 2002 Aug;8(8):2553-62. PubMed PMID: 12171883.
228. Gastman BR, Atarshi Y, Reichert TE, Saito T, Balkir L, Rabinowich H, et al. Fas ligand is expressed on human squamous cell carcinomas of the head and neck, and it promotes apoptosis of T lymphocytes. Cancer research. 1999 Oct 15;59(20):5356-64. PubMed PMID: 10537320.
229. Sato T, Irie S, Kitada S, Reed JC. FAP-1: a protein tyrosine phosphatase that associates with Fas. Science. 1995 Apr 21;268(5209):411-5. PubMed PMID: 7536343.
230. van Herpen CM, De Mulder PH. Locoregional immunotherapy in cancer patients: review of clinical studies. Annals of oncology : official journal of the European Society for Medical Oncology / ESMO. 2000 Oct;11(10):1229-39. PubMed PMID: 11106110.
231. Rosenberg SA, Yang JC, Restifo NP. Cancer immunotherapy: moving beyond current vaccines. Nature medicine. 2004 Sep;10(9):909-15. PubMed PMID: 15340416. Pubmed Central PMCID: 1435696.
232. Mule JJ, Shu S, Schwarz SL, Rosenberg SA. Adoptive immunotherapy of established pulmonary metastases with LAK cells and recombinant interleukin-2. Science. 1984 Sep 28;225(4669):1487-9. PubMed PMID: 6332379.
233. Hawkins MJ, Atkins MB, Dutcher JP, Fisher RI, Weiss GR, Margolin KA, et al. A phase II clinical trial of interleukin-2 and lymphokine-activated killer cells in advanced colorectal carcinoma. Journal of immunotherapy with emphasis on tumor immunology : official journal of the Society for Biological Therapy. 1994 Jan;15(1):74-8. PubMed PMID: 8110733.

234. Fisher RI, Coltman CA, Jr., Doroshow JH, Rayner AA, Hawkins MJ, Mier JW, et al. Metastatic renal cancer treated with interleukin-2 and lymphokine-activated killer cells. A phase II clinical trial. Annals of internal medicine. 1988 Apr;108(4):518-23. PubMed PMID: 3258138.
235. Dutcher JP, Creekmore S, Weiss GR, Margolin K, Markowitz AB, Roper M, et al. A phase II study of interleukin-2 and lymphokine-activated killer cells in patients with metastatic malignant melanoma. Journal of clinical oncology : official journal of the American Society of Clinical Oncology. 1989 Apr;7(4):477-85. PubMed PMID: 2647913.
236. Besser MJ, Shapira-Frommer R, Treves AJ, Zippel D, Itzhaki O, Hershkovitz L, et al. Clinical responses in a phase II study using adoptive transfer of short-term cultured tumor infiltration lymphocytes in metastatic melanoma patients. Clinical cancer research : an official journal of the American Association for Cancer Research. 2010 May 1;16(9):2646-55. PubMed PMID: 20406835.
237. Dudley ME, Yang JC, Sherry R, Hughes MS, Royal R, Kammula U, et al. Adoptive cell therapy for patients with metastatic melanoma: evaluation of intensive myeloablative chemoradiation preparative regimens. Journal of clinical oncology : official journal of the American Society of Clinical Oncology. 2008 Nov 10;26(32):5233-9. PubMed PMID: 18809613. Pubmed Central PMCID: 2652090.
238. Joseph RW, Peddareddigari VR, Liu P, Miller PW, Overwijk WW, Bekele NB, et al. Impact of clinical and pathologic features on tumor-infiltrating lymphocyte expansion from surgically excised melanoma metastases for adoptive T-cell therapy. Clinical cancer research : an official journal of the American Association for Cancer Research. 2011 Jul 15;17(14):4882-91. PubMed PMID: 21632855. Pubmed Central PMCID: 3139726.
239. Bendle GM, Linnemann C, Hooijkaas AI, Bies L, de Witte MA, Jorritsma A, et al. Lethal graft-versus-host disease in mouse models of T cell receptor gene therapy. Nature medicine. 2010 May;16(5):565-70, 1p following 70. PubMed PMID: 20400962.
240. Morgan RA, Yang JC, Kitano M, Dudley ME, Laurencot CM, Rosenberg SA. Case report of a serious adverse event following the administration of T cells transduced with a chimeric antigen receptor recognizing ERBB2. Molecular therapy : the journal of the American Society of Gene Therapy. 2010 Apr;18(4):843-51. PubMed PMID: 20179677. Pubmed Central PMCID: 2862534.
241. Lamers CH, Sleijfer S, van Steenbergen S, van Elzakker P, van Krimpen B, Groot C, et al. Treatment of metastatic renal cell carcinoma with CAIX CAR-engineered T cells: clinical evaluation and management of on-target toxicity. Molecular therapy : the journal of the American Society of Gene Therapy. 2013 Apr;21(4):904-12. PubMed PMID: 23423337.
242. Lamers CH, Willemsen R, van Elzakker P, van Steenbergen-Langeveld S, Broertjes M, Oosterwijk-Wakka J, et al. Immune responses to transgene and retroviral vector in patients treated with ex vivo-engineered T cells. Blood. 2011 Jan 6;117(1):72-82. PubMed PMID: 20889925.
243. Mule JJ, Shu S, Rosenberg SA. The anti-tumor efficacy of lymphokine-activated killer cells and recombinant interleukin 2 in vivo. Journal of immunology. 1985 Jul;135(1):646-52. PubMed PMID: 3889158.
244. Ettinghausen SE, Lipford EH, 3rd, Mule JJ, Rosenberg SA. Recombinant interleukin 2 stimulates in vivo proliferation of adoptively transferred lymphokine-activated killer (LAK) cells. Journal of immunology. 1985 Nov;135(5):3623-35. PubMed PMID: 3900213.

245. Lafreniere R, Rosenberg SA. Adoptive immunotherapy of murine hepatic metastases with lymphokine activated killer (LAK) cells and recombinant interleukin 2 (RIL 2) can mediate the regression of both immunogenic and nonimmunogenic sarcomas and an adenocarcinoma. Journal of immunology. 1985 Dec;135(6):4273-80. PubMed PMID: 3877766.
246. Mule JJ, Yang J, Shu S, Rosenberg SA. The anti-tumor efficacy of lymphokine-activated killer cells and recombinant interleukin 2 in vivo: direct correlation between reduction of established metastases and cytolytic activity of lymphokine-activated killer cells. Journal of immunology. 1986 May 15;136(10):3899-909. PubMed PMID: 2871106.
247. Shiloni E, Lafreniere R, Mule JJ, Schwarz SL, Rosenberg SA. Effect of immunotherapy with allogeneic lymphokine-activated killer cells and recombinant interleukin 2 on established pulmonary and hepatic metastases in mice. Cancer research. 1986 Nov;46(11):5633-40. PubMed PMID: 3489526.
248. Rosenberg SA, Lotze MT, Muul LM, Leitman S, Chang AE, Ettinghausen SE, et al. Observations on the systemic administration of autologous lymphokine-activated killer cells and recombinant interleukin-2 to patients with metastatic cancer. The New England journal of medicine. 1985 Dec 5;313(23):1485-92. PubMed PMID: 3903508.
249. Hayes RL, Arbit E, Odaimi M, Pannullo S, Scheff R, Kravchinskiy D, et al. Adoptive cellular immunotherapy for the treatment of malignant gliomas. Critical reviews in oncology/hematology. 2001 Jul-Aug;39(1-2):31-42. PubMed PMID: 11418300.
250. Dillman RO, Duma CM, Ellis RA, Cornforth AN, Schiltz PM, Sharp SL, et al. Intralesional lymphokine-activated killer cells as adjuvant therapy for primary glioblastoma. Journal of immunotherapy. 2009 Nov-Dec;32(9):914-9. PubMed PMID: 19816190.
251. Rosenberg SA, Lotze MT, Yang JC, Topalian SL, Chang AE, Schwartzentruber DJ, et al. Prospective randomized trial of high-dose interleukin-2 alone or in conjunction with lymphokine-activated killer cells for the treatment of patients with advanced cancer. Journal of the National Cancer Institute. 1993 Apr 21;85(8):622-32. PubMed PMID: 8468720.
252. Rosenberg SA, Spiess P, Lafreniere R. A new approach to the adoptive immunotherapy of cancer with tumor-infiltrating lymphocytes. Science. 1986 Sep 19;233(4770):1318-21. PubMed PMID: 3489291.
253. Muul LM, Spiess PJ, Director EP, Rosenberg SA. Identification of specific cytolytic immune responses against autologous tumor in humans bearing malignant melanoma. Journal of immunology. 1987 Feb 1;138(3):989-95. PubMed PMID: 3100623.
254. Kradin RL, Kurnick JT, Lazarus DS, Preffer FI, Dubinett SM, Pinto CE, et al. Tumour-infiltrating lymphocytes and interleukin-2 in treatment of advanced cancer. Lancet. 1989 Mar 18;1(8638):577-80. PubMed PMID: 2564111.
255. Rosenberg SA, Yang JC, Topalian SL, Schwartzentruber DJ, Weber JS, Parkinson DR, et al. Treatment of 283 consecutive patients with metastatic melanoma or renal cell cancer using high-dose bolus interleukin 2. JAMA : the journal of the American Medical Association. 1994 Mar 23-30;271(12):907-13. PubMed PMID: 8120958.
256. Rosenberg SA, Yannelli JR, Yang JC, Topalian SL, Schwartzentruber DJ, Weber JS, et al. Treatment of patients with metastatic melanoma with autologous tumor-infiltrating lymphocytes and interleukin 2. Journal of the National Cancer Institute. 1994 Aug 3;86(15):1159-66. PubMed PMID: 8028037.

257. Atkins MB, Sparano J, Fisher RI, Weiss GR, Margolin KA, Fink KI, et al. Randomized phase II trial of high-dose interleukin-2 either alone or in combination with interferon alfa-2b in advanced renal cell carcinoma. Journal of clinical oncology : official journal of the American Society of Clinical Oncology. 1993 Apr;11(4):661-70. PubMed PMID: 8478661.
258. Fyfe GA, Fisher RI, Rosenberg SA, Sznol M, Parkinson DR, Louie AC. Long-term response data for 255 patients with metastatic renal cell carcinoma treated with high-dose recombinant interleukin-2 therapy. Journal of clinical oncology : official journal of the American Society of Clinical Oncology. 1996 Aug;14(8):2410-1. PubMed PMID: 8708739.
259. Geertsen PF, Hermann GG, von der Maase H, Steven K. Treatment of metastatic renal cell carcinoma by continuous intravenous infusion of recombinant interleukin-2: a single-center phase II study. Journal of clinical oncology : official journal of the American Society of Clinical Oncology. 1992 May;10(5):753-9. PubMed PMID: 1569448.
260. Rosenberg SA, Packard BS, Aebersold PM, Solomon D, Topalian SL, Toy ST, et al. Use of tumor-infiltrating lymphocytes and interleukin-2 in the immunotherapy of patients with metastatic melanoma. A preliminary report. The New England journal of medicine. 1988 Dec 22;319(25):1676-80. PubMed PMID: 3264384.
261. Dudley ME, Wunderlich J, Nishimura MI, Yu D, Yang JC, Topalian SL, et al. Adoptive transfer of cloned melanoma-reactive T lymphocytes for the treatment of patients with metastatic melanoma. Journal of immunotherapy. 2001 Jul-Aug;24(4):363-73. PubMed PMID: 11565838.
262. Radvanyi LG, Bernatchez C, Zhang M, Fox PS, Miller P, Chacon J, et al. Specific lymphocyte subsets predict response to adoptive cell therapy using expanded autologous tumor-infiltrating lymphocytes in metastatic melanoma patients. Clinical cancer research : an official journal of the American Association for Cancer Research. 2012 Dec 15;18(24):6758-70. PubMed PMID: 23032743. Pubmed Central PMCID: 3525747.
263. Dudley ME, Gross CA, Somerville RP, Hong Y, Schaub NP, Rosati SF, et al. Randomized selection design trial evaluating CD8+-enriched versus unselected tumor-infiltrating lymphocytes for adoptive cell therapy for patients with melanoma. Journal of clinical oncology : official journal of the American Society of Clinical Oncology. 2013 Jun 10;31(17):2152-9. PubMed PMID: 23650429. Pubmed Central PMCID: 3731980.
264. Tsukuda M, Mochimatsu I, Sakumoto M, Furukawa S, Yuyama S, Yanoma S, et al. Autologous tumor cell killing activity of tumor-associated lymphocytes in patients with head and neck carcinomas. Biotherapy. 1993;6(2):155-61. PubMed PMID: 8398575. Epub 1993/01/01. eng.
265. Kubota E, Katano M, Imamura H, Kurokawa H, Katsuki T, Yamamoto H, et al. Locoregional immunotherapy of head and neck cancers utilizing allogeneic spleen cells--a report of 2 cases. Biotherapy. 1993;6(3):175-82. PubMed PMID: 8292459.
266. Kubota E, Katano M, Kurokawa H, Imamura H, Katsuki T, Yamamoto H, et al. Tumoricidal effect of human PBMC following stimulation with OK-432 and its application for locoregional immunotherapy in head and neck cancer patients. Journal of cranio-maxillo-facial surgery : official publication of the European Association for Cranio-Maxillo-Facial Surgery. 1993 Jan;21(1):30-7. PubMed PMID: 8445052.
267. Yasumura S, Weidmann E, Hirabayashi H, Johnson JT, Herberman RB, Whiteside TL. HLA restriction and T-cell-receptor V beta gene expression of cytotoxic T lymphocytes reactive with human squamous-cell carcinoma of the head and neck.

International journal of cancer Journal international du cancer. 1994 May 1;57(3):297-305. PubMed PMID: 8168988.
268. Yasumura S, Hirabayashi H, Schwartz DR, Toso JF, Johnson JT, Herberman RB, et al. Human cytotoxic T-cell lines with restricted specificity for squamous cell carcinoma of the head and neck. Cancer research. 1993 Mar 15;53(6):1461-8. PubMed PMID: 8443824.
269. To WC, Wood BG, Krauss JC, Strome M, Esclamado RM, Lavertu P, et al. Systemic adoptive T-cell immunotherapy in recurrent and metastatic carcinoma of the head and neck: a phase 1 study. Archives of otolaryngology--head & neck surgery. 2000 Oct;126(10):1225-31. PubMed PMID: 11031409.
270. Riechelmann H, Wiesneth M, Schauwecker P, Reinhardt P, Gronau S, Schmitt A, et al. Adoptive therapy of head and neck squamous cell carcinoma with antibody coated immune cells: a pilot clinical trial. Cancer immunology, immunotherapy : CII. 2007 Sep;56(9):1397-406. PubMed PMID: 17273869. Epub 2007/02/03. eng.
271. Dembic Z, Haas W, Weiss S, McCubrey J, Kiefer H, von Boehmer H, et al. Transfer of specificity by murine alpha and beta T-cell receptor genes. Nature. 1986 Mar 20-26;320(6059):232-8. PubMed PMID: 2421164.
272. Clay TM, Custer MC, Sachs J, Hwu P, Rosenberg SA, Nishimura MI. Efficient transfer of a tumor antigen-reactive TCR to human peripheral blood lymphocytes confers anti-tumor reactivity. Journal of immunology. 1999 Jul 1;163(1):507-13. PubMed PMID: 10384155.
273. Zhao Y, Zheng Z, Robbins PF, Khong HT, Rosenberg SA, Morgan RA. Primary human lymphocytes transduced with NY-ESO-1 antigen-specific TCR genes recognize and kill diverse human tumor cell lines. Journal of immunology. 2005 Apr 1;174(7):4415-23. PubMed PMID: 15778407. Pubmed Central PMCID: 2174604.
274. Cohen CJ, Zheng Z, Bray R, Zhao Y, Sherman LA, Rosenberg SA, et al. Recognition of fresh human tumor by human peripheral blood lymphocytes transduced with a bicistronic retroviral vector encoding a murine anti-p53 TCR. Journal of immunology. 2005 Nov 1;175(9):5799-808. PubMed PMID: 16237072. Pubmed Central PMCID: 1473968.
275. Kuball J, Schmitz FW, Voss RH, Ferreira EA, Engel R, Guillaume P, et al. Cooperation of human tumor-reactive CD4+ and CD8+ T cells after redirection of their specificity by a high-affinity p53A2.1-specific TCR. Immunity. 2005 Jan;22(1):117-29. PubMed PMID: 15664164.
276. Tsuji T, Yasukawa M, Matsuzaki J, Ohkuri T, Chamoto K, Wakita D, et al. Generation of tumor-specific, HLA class I-restricted human Th1 and Tc1 cells by cell engineering with tumor peptide-specific T-cell receptor genes. Blood. 2005 Jul 15;106(2):470-6. PubMed PMID: 15790789.
277. Xue SA, Gao L, Thomas S, Hart DP, Xue JZ, Gillmore R, et al. Development of a Wilms' tumor antigen-specific T-cell receptor for clinical trials: engineered patient's T cells can eliminate autologous leukemia blasts in NOD/SCID mice. Haematologica. 2010 Jan;95(1):126-34. PubMed PMID: 19679884. Pubmed Central PMCID: 2805729.
278. Schaft N, Willemsen RA, de Vries J, Lankiewicz B, Essers BW, Gratama JW, et al. Peptide fine specificity of anti-glycoprotein 100 CTL is preserved following transfer of engineered TCR alpha beta genes into primary human T lymphocytes. Journal of immunology. 2003 Feb 15;170(4):2186-94. PubMed PMID: 12574392.
279. Stanislawski T, Voss RH, Lotz C, Sadovnikova E, Willemsen RA, Kuball J, et al. Circumventing tolerance to a human MDM2-derived tumor antigen by TCR gene transfer. Nature immunology. 2001 Oct;2(10):962-70. PubMed PMID: 11577350.

280. Frankel TL, Burns WR, Peng PD, Yu Z, Chinnasamy D, Wargo JA, et al. Both CD4 and CD8 T cells mediate equally effective in vivo tumor treatment when engineered with a highly avid TCR targeting tyrosinase. Journal of immunology. 2010 Jun 1;184(11):5988-98. PubMed PMID: 20427771.
281. Roszkowski JJ, Lyons GE, Kast WM, Yee C, Van Besien K, Nishimura MI. Simultaneous generation of CD8+ and CD4+ melanoma-reactive T cells by retroviral-mediated transfer of a single T-cell receptor. Cancer research. 2005 Feb 15;65(4):1570-6. PubMed PMID: 15735047.
282. Johnson LA, Morgan RA, Dudley ME, Cassard L, Yang JC, Hughes MS, et al. Gene therapy with human and mouse T-cell receptors mediates cancer regression and targets normal tissues expressing cognate antigen. Blood. 2009 Jul 16;114(3):535-46. PubMed PMID: 19451549. Pubmed Central PMCID: 2929689.
283. Parkhurst MR, Joo J, Riley JP, Yu Z, Li Y, Robbins PF, et al. Characterization of genetically modified T-cell receptors that recognize the CEA:691-699 peptide in the context of HLA-A2.1 on human colorectal cancer cells. Clinical cancer research : an official journal of the American Association for Cancer Research. 2009 Jan 1;15(1):169-80. PubMed PMID: 19118044. Pubmed Central PMCID: 3474199.
284. Morgan RA, Dudley ME, Wunderlich JR, Hughes MS, Yang JC, Sherry RM, et al. Cancer regression in patients after transfer of genetically engineered lymphocytes. Science. 2006 Oct 6;314(5796):126-9. PubMed PMID: 16946036. Pubmed Central PMCID: 2267026.
285. Chhabra A. MHC class I TCR engineered anti-tumor CD4 T cells: implications for cancer immunotherapy. Endocrine, metabolic & immune disorders drug targets. 2009 Dec;9(4):344-52. PubMed PMID: 19807670.
286. Ferrara J, Reddy P, Paczesny S. Immunotherapy through T-cell receptor gene transfer induces severe graft-versus-host disease. Immunotherapy. 2010 Nov;2(6):791-4. PubMed PMID: 21091111. Pubmed Central PMCID: 3448368.
287. Linette GP, Stadtmauer EA, Maus MV, Rapoport AP, Levine BL, Emery L, et al. Cardiovascular toxicity and titin cross-reactivity of affinity enhanced T cells in myeloma and melanoma. Blood. 2013 Jun 14. PubMed PMID: 23770775.
288. Holler PD, Chlewicki LK, Kranz DM. TCRs with high affinity for foreign pMHC show self-reactivity. Nature immunology. 2003 Jan;4(1):55-62. PubMed PMID: 12469116.
289. Kuwana Y, Asakura Y, Utsunomiya N, Nakanishi M, Arata Y, Itoh S, et al. Expression of chimeric receptor composed of immunoglobulin-derived V regions and T-cell receptor-derived C regions. Biochemical and biophysical research communications. 1987 Dec 31;149(3):960-8. PubMed PMID: 3122749.
290. Gross G, Gorochov G, Waks T, Eshhar Z. Generation of effector T cells expressing chimeric T cell receptor with antibody type-specificity. Transplantation proceedings. 1989 Feb;21(1 Pt 1):127-30. PubMed PMID: 2784887.
291. Gross G, Waks T, Eshhar Z. Expression of immunoglobulin-T-cell receptor chimeric molecules as functional receptors with antibody-type specificity. Proceedings of the National Academy of Sciences of the United States of America. 1989 Dec;86(24):10024-8. PubMed PMID: 2513569. Pubmed Central PMCID: 298636.
292. Eshhar Z, Waks T, Gross G, Schindler DG. Specific activation and targeting of cytotoxic lymphocytes through chimeric single chains consisting of antibody-binding domains and the gamma or zeta subunits of the immunoglobulin and T-cell receptors. Proceedings of the National Academy of Sciences of the United States of America. 1993 Jan 15;90(2):720-4. PubMed PMID: 8421711. Pubmed Central PMCID: 45737.

293. Eshhar Z, Waks T, Bendavid A, Schindler DG. Functional expression of chimeric receptor genes in human T cells. Journal of immunological methods. 2001 Feb 1;248(1-2):67-76. PubMed PMID: 11223069.
294. Sadelain M. T-cell engineering for cancer immunotherapy. Cancer journal. 2009 Nov-Dec;15(6):451-5. PubMed PMID: 20010162.
295. Jena B, Dotti G, Cooper LJ. Redirecting T-cell specificity by introducing a tumor-specific chimeric antigen receptor. Blood. 2010 Aug 19;116(7):1035-44. PubMed PMID: 20439624. Pubmed Central PMCID: 2938125.
296. Altenschmidt U, Kahl R, Moritz D, Schnierle BS, Gerstmayer B, Wels W, et al. Cytolysis of tumor cells expressing the Neu/erbB-2, erbB-3, and erbB-4 receptors by genetically targeted naive T lymphocytes. Clinical cancer research : an official journal of the American Association for Cancer Research. 1996 Jun;2(6):1001-8. PubMed PMID: 9816261.
297. Muniappan A, Banapour B, Lebkowski J, Talib S. Ligand-mediated cytolysis of tumor cells: use of heregulin-zeta chimeras to redirect cytotoxic T lymphocytes. Cancer gene therapy. 2000 Jan;7(1):128-34. PubMed PMID: 10678365.
298. Pameijer CR, Navanjo A, Meechoovet B, Wagner JR, Aguilar B, Wright CL, et al. Conversion of a tumor-binding peptide identified by phage display to a functional chimeric T cell antigen receptor. Cancer gene therapy. 2007 Jan;14(1):91-7. PubMed PMID: 17024231.
299. Davies DM, Foster J, Van Der Stegen SJ, Parente-Pereira AC, Chiapero-Stanke L, Delinassios GJ, et al. Flexible targeting of ErbB dimers that drive tumorigenesis by using genetically engineered T cells. Molecular medicine. 2012;18:565-76. PubMed PMID: 22354215. Pubmed Central PMCID: 3388141. Epub 2012/02/23. eng.
300. Zhang T, Wu MR, Sentman CL. An NKp30-based chimeric antigen receptor promotes T cell effector functions and antitumor efficacy in vivo. Journal of immunology. 2012 Sep 1;189(5):2290-9. PubMed PMID: 22851709. Pubmed Central PMCID: 3633481.
301. Sharifzadeh Z, Rahbarizadeh F, Shokrgozar MA, Ahmadvand D, Mahboudi F, Jamnani FR, et al. Genetically engineered T cells bearing chimeric nanoconstructed receptors harboring TAG-72-specific camelid single domain antibodies as targeting agents. Cancer letters. 2012 Aug 16. PubMed PMID: 22902507.
302. Urbanska K, Lanitis E, Poussin M, Lynn RC, Gavin BP, Kelderman S, et al. A universal strategy for adoptive immunotherapy of cancer through use of a novel T-cell antigen receptor. Cancer research. 2012 Apr 1;72(7):1844-52. PubMed PMID: 22315351. Pubmed Central PMCID: 3319867.
303. Chmielewski M, Hombach A, Heuser C, Adams GP, Abken H. T cell activation by antibody-like immunoreceptors: increase in affinity of the single-chain fragment domain above threshold does not increase T cell activation against antigen-positive target cells but decreases selectivity. Journal of immunology. 2004 Dec 15;173(12):7647-53. PubMed PMID: 15585893.
304. Kershaw MH, Westwood JA, Parker LL, Wang G, Eshhar Z, Mavroukakis SA, et al. A phase I study on adoptive immunotherapy using gene-modified T cells for ovarian cancer. Clinical cancer research : an official journal of the American Association for Cancer Research. 2006 Oct 15;12(20 Pt 1):6106-15. PubMed PMID: 17062687. Pubmed Central PMCID: 2154351.
305. Wilkie S, Picco G, Foster J, Davies DM, Julien S, Cooper L, et al. Retargeting of human T cells to tumor-associated MUC1: the evolution of a chimeric antigen receptor. Journal of immunology. 2008 Apr 1;180(7):4901-9. PubMed PMID: 18354214.

306. Cheung NK, Guo HF, Modak S, Cheung IY. Anti-idiotypic antibody facilitates scFv chimeric immune receptor gene transduction and clonal expansion of human lymphocytes for tumor therapy. Hybridoma and hybridomics. 2003 Aug;22(4):209-18. PubMed PMID: 14511566.
307. Weijtens ME, Willemsen RA, Valerio D, Stam K, Bolhuis RL. Single chain Ig/gamma gene-redirected human T lymphocytes produce cytokines, specifically lyse tumor cells, and recycle lytic capacity. Journal of immunology. 1996 Jul 15;157(2):836-43. PubMed PMID: 8752936.
308. Brentjens RJ, Santos E, Nikhamin Y, Yeh R, Matsushita M, La Perle K, et al. Genetically targeted T cells eradicate systemic acute lymphoblastic leukemia xenografts. Clinical cancer research : an official journal of the American Association for Cancer Research. 2007 Sep 15;13(18 Pt 1):5426-35. PubMed PMID: 17855649.
309. Cooper LJ, Al-Kadhimi Z, Serrano LM, Pfeiffer T, Olivares S, Castro A, et al. Enhanced antilymphoma efficacy of CD19-redirected influenza MP1-specific CTLs by cotransfer of T cells modified to present influenza MP1. Blood. 2005 Feb 15;105(4):1622-31. PubMed PMID: 15507526.
310. Cooper LJ, Topp MS, Serrano LM, Gonzalez S, Chang WC, Naranjo A, et al. T-cell clones can be rendered specific for CD19: toward the selective augmentation of the graft-versus-B-lineage leukemia effect. Blood. 2003 Feb 15;101(4):1637-44. PubMed PMID: 12393484.
311. Kochenderfer JN, Wilson WH, Janik JE, Dudley ME, Stetler-Stevenson M, Feldman SA, et al. Eradication of B-lineage cells and regression of lymphoma in a patient treated with autologous T cells genetically engineered to recognize CD19. Blood. 2010 Nov 18;116(20):4099-102. PubMed PMID: 20668228. Pubmed Central PMCID: 2993617.
312. Kochenderfer JN, Yu Z, Frasheri D, Restifo NP, Rosenberg SA. Adoptive transfer of syngeneic T cells transduced with a chimeric antigen receptor that recognizes murine CD19 can eradicate lymphoma and normal B cells. Blood. 2010 Nov 11;116(19):3875-86. PubMed PMID: 20631379. Pubmed Central PMCID: 2981541.
313. Loskog A, Giandomenico V, Rossig C, Pule M, Dotti G, Brenner MK. Addition of the CD28 signaling domain to chimeric T-cell receptors enhances chimeric T-cell resistance to T regulatory cells. Leukemia. 2006 Oct;20(10):1819-28. PubMed PMID: 16932339.
314. Roessig C, Scherer SP, Baer A, Vormoor J, Rooney CM, Brenner MK, et al. Targeting CD19 with genetically modified EBV-specific human T lymphocytes. Annals of hematology. 2002;81 Suppl 2:S42-3. PubMed PMID: 12611072.
315. Cheadle EJ, Hawkins RE, Batha H, O'Neill AL, Dovedi SJ, Gilham DE. Natural expression of the CD19 antigen impacts the long-term engraftment but not antitumor activity of CD19-specific engineered T cells. Journal of immunology. 2010 Feb 15;184(4):1885-96. PubMed PMID: 20089697.
316. Davila ML, Kloss CC, Gunset G, Sadelain M. CD19 CAR-Targeted T Cells Induce Long-Term Remission and B Cell Aplasia in an Immunocompetent Mouse Model of B Cell Acute Lymphoblastic Leukemia. PloS one. 2013;8(4):e61338. PubMed PMID: 23585892. Pubmed Central PMCID: 3621858.
317. Brentjens RJ, Davila ML, Riviere I, Park J, Wang X, Cowell LG, et al. CD19-targeted T cells rapidly induce molecular remissions in adults with chemotherapy-refractory acute lymphoblastic leukemia. Science translational medicine. 2013 Mar 20;5(177):177ra38. PubMed PMID: 23515080.

318. Laurin D, Marin V, Biagi E, Pizzitola I, Agostoni V, Gallot G, et al. Upregulation of adhesion molecules on leukemia targets improves the efficacy of cytotoxic T cells transduced with chimeric anti-CD19 receptor. Journal of immunotherapy. 2013 Apr;36(3):181-9. PubMed PMID: 23502765.
319. Kochenderfer JN, Dudley ME, Feldman SA, Wilson WH, Spaner DE, Maric I, et al. B-cell depletion and remissions of malignancy along with cytokine-associated toxicity in a clinical trial of anti-CD19 chimeric-antigen-receptor-transduced T cells. Blood. 2012 Mar 22;119(12):2709-20. PubMed PMID: 22160384. Pubmed Central PMCID: 3327450.
320. Kalos M, Levine BL, Porter DL, Katz S, Grupp SA, Bagg A, et al. T cells with chimeric antigen receptors have potent antitumor effects and can establish memory in patients with advanced leukemia. Science translational medicine. 2011 Aug 10;3(95):95ra73. PubMed PMID: 21832238. Pubmed Central PMCID: 3393096. Epub 2011/08/13. eng.
321. Grupp SA, Kalos M, Barrett D, Aplenc R, Porter DL, Rheingold SR, et al. Chimeric antigen receptor-modified T cells for acute lymphoid leukemia. The New England journal of medicine. 2013 Apr 18;368(16):1509-18. PubMed PMID: 23527958.
322. Jensen MC, Popplewell L, Cooper LJ, DiGiusto D, Kalos M, Ostberg JR, et al. Antitransgene rejection responses contribute to attenuated persistence of adoptively transferred CD20/CD19-specific chimeric antigen receptor redirected T cells in humans. Biology of blood and marrow transplantation : journal of the American Society for Blood and Marrow Transplantation. 2010 Sep;16(9):1245-56. PubMed PMID: 20304086. Pubmed Central PMCID: 3383803.
323. Mihara K, Yanagihara K, Takigahira M, Kitanaka A, Imai C, Bhattacharyya J, et al. Synergistic and persistent effect of T-cell immunotherapy with anti-CD19 or anti-CD38 chimeric receptor in conjunction with rituximab on B-cell non-Hodgkin lymphoma. British journal of haematology. 2010 Oct;151(1):37-46. PubMed PMID: 20678160.
324. Jensen M, Tan G, Forman S, Wu AM, Raubitschek A. CD20 is a molecular target for scFvFc:zeta receptor redirected T cells: implications for cellular immunotherapy of CD20+ malignancy. Biology of blood and marrow transplantation : journal of the American Society for Blood and Marrow Transplantation. 1998;4(2):75-83. PubMed PMID: 9763110.
325. Wang J, Press OW, Lindgren CG, Greenberg P, Riddell S, Qian X, et al. Cellular immunotherapy for follicular lymphoma using genetically modified CD20-specific CD8+ cytotoxic T lymphocytes. Molecular therapy : the journal of the American Society of Gene Therapy. 2004 Apr;9(4):577-86. PubMed PMID: 15093188.
326. Wang J, Jensen M, Lin Y, Sui X, Chen E, Lindgren CG, et al. Optimizing adoptive polyclonal T cell immunotherapy of lymphomas, using a chimeric T cell receptor possessing CD28 and CD137 costimulatory domains. Human gene therapy. 2007 Aug;18(8):712-25. PubMed PMID: 17685852.
327. Till BG, Jensen MC, Wang J, Qian X, Gopal AK, Maloney DG, et al. CD20-specific adoptive immunotherapy for lymphoma using a chimeric antigen receptor with both CD28 and 4-1BB domains: pilot clinical trial results. Blood. 2012 Apr 26;119(17):3940-50. PubMed PMID: 22308288. Pubmed Central PMCID: 3350361.
328. James SE, Greenberg PD, Jensen MC, Lin Y, Wang J, Till BG, et al. Antigen sensitivity of CD22-specific chimeric TCR is modulated by target epitope distance from the cell membrane. Journal of immunology. 2008 May 15;180(10):7028-38. PubMed PMID: 18453625. Pubmed Central PMCID: 2585549.
329. Haso W, Lee DW, Shah NN, Stetler-Stevenson M, Yuan CM, Pastan IH, et al. Anti-CD22-chimeric antigen receptors targeting B-cell precursor acute lymphoblastic

leukemia. Blood. 2013 Feb 14;121(7):1165-74. PubMed PMID: 23243285. Pubmed Central PMCID: 3575759.
330. Giordano Attianese GM, Marin V, Hoyos V, Savoldo B, Pizzitola I, Tettamanti S, et al. In vitro and in vivo model of a novel immunotherapy approach for chronic lymphocytic leukemia by anti-CD23 chimeric antigen receptor. Blood. 2011 May 5;117(18):4736-45. PubMed PMID: 21406718. Pubmed Central PMCID: 3100686.
331. Maliar A, Servais C, Waks T, Chmielewski M, Lavy R, Altevogt P, et al. Redirected T cells that target pancreatic adenocarcinoma antigens eliminate tumors and metastases in mice. Gastroenterology. 2012 Nov;143(5):1375-84 e1-5. PubMed PMID: 22819865.
332. Hombach A, Heuser C, Sircar R, Tillmann T, Diehl V, Pohl C, et al. An anti-CD30 chimeric receptor that mediates CD3-zeta-independent T-cell activation against Hodgkin's lymphoma cells in the presence of soluble CD30. Cancer research. 1998 Mar 15;58(6):1116-9. PubMed PMID: 9515791.
333. Savoldo B, Rooney CM, Di Stasi A, Abken H, Hombach A, Foster AE, et al. Epstein Barr virus specific cytotoxic T lymphocytes expressing the anti-CD30zeta artificial chimeric T-cell receptor for immunotherapy of Hodgkin disease. Blood. 2007 Oct 1;110(7):2620-30. PubMed PMID: 17507664. Pubmed Central PMCID: 1988944.
334. Di Stasi A, De Angelis B, Rooney CM, Zhang L, Mahendravada A, Foster AE, et al. T lymphocytes coexpressing CCR4 and a chimeric antigen receptor targeting CD30 have improved homing and antitumor activity in a Hodgkin tumor model. Blood. 2009 Jun 18;113(25):6392-402. PubMed PMID: 19377047. Pubmed Central PMCID: 2710932.
335. Schirrmann T, Pecher G. Specific targeting of CD33(+) leukemia cells by a natural killer cell line modified with a chimeric receptor. Leukemia research. 2005 Mar;29(3):301-6. PubMed PMID: 15661266.
336. Dutour A, Marin V, Pizzitola I, Valsesia-Wittmann S, Lee D, Yvon E, et al. In Vitro and In Vivo Antitumor Effect of Anti-CD33 Chimeric Receptor-Expressing EBV-CTL against CD33 Acute Myeloid Leukemia. Advances in hematology. 2012;2012:683065. PubMed PMID: 22272203. Pubmed Central PMCID: 3261457.
337. Marin V, Pizzitola I, Agostoni V, Attianese GM, Finney H, Lawson A, et al. Cytokine-induced killer cells for cell therapy of acute myeloid leukemia: improvement of their immune activity by expression of CD33-specific chimeric receptors. Haematologica. 2010 Dec;95(12):2144-52. PubMed PMID: 20713459. Pubmed Central PMCID: 2995574.
338. Mihara K, Yanagihara K, Takigahira M, Imai C, Kitanaka A, Takihara Y, et al. Activated T-cell-mediated immunotherapy with a chimeric receptor against CD38 in B-cell non-Hodgkin lymphoma. Journal of immunotherapy. 2009 Sep;32(7):737-43. PubMed PMID: 19561535.
339. Bhattacharyya J, Mihara K, Kitanaka A, Yanagihara K, Kubo T, Takei Y, et al. T-cell immunotherapy with a chimeric receptor against CD38 is effective in eradicating chemotherapy-resistant B-cell lymphoma cells overexpressing survivin induced by BMI-1. Blood cancer journal. 2012 Jun;2(6):e75. PubMed PMID: 22829977. Pubmed Central PMCID: 3389163.
340. Mihara K, Bhattacharyya J, Kitanaka A, Yanagihara K, Kubo T, Takei Y, et al. T-cell immunotherapy with a chimeric receptor against CD38 is effective in eliminating myeloma cells. Leukemia. 2012 Feb;26(2):365-7. PubMed PMID: 21836610.
341. Hekele A, Dall P, Moritz D, Wels W, Groner B, Herrlich P, et al. Growth retardation of tumors by adoptive transfer of cytotoxic T lymphocytes reprogrammed

by CD44v6-specific scFv:zeta-chimera. International journal of cancer Journal international du cancer. 1996 Oct 9;68(2):232-8. PubMed PMID: 8900434.
342. Dall P, Herrmann I, Durst B, Stoff-Khalili MA, Bauerschmitz G, Hanstein B, et al. In vivo cervical cancer growth inhibition by genetically engineered cytotoxic T cells. Cancer immunology, immunotherapy : CII. 2005 Jan;54(1):51-60. PubMed PMID: 15693139.
343. Shaffer DR, Savoldo B, Yi Z, Chow KK, Kakarla S, Spencer DM, et al. T cells redirected against CD70 for the immunotherapy of CD70-positive malignancies. Blood. 2011 Apr 21;117(16):4304-14. PubMed PMID: 21304103. Pubmed Central PMCID: 3087480.
344. Tettamanti S, Marin V, Pizzitola I, Magnani CF, Giordano Attianese GM, Cribioli E, et al. Targeting of acute myeloid leukaemia by cytokine-induced killer cells redirected with a novel CD123-specific chimeric antigen receptor. British journal of haematology. 2013 May;161(3):389-401. PubMed PMID: 23432359.
345. Darcy PK, Kershaw MH, Trapani JA, Smyth MJ. Expression in cytotoxic T lymphocytes of a single-chain anti-carcinoembryonic antigen antibody. Redirected Fas ligand-mediated lysis of colon carcinoma. European journal of immunology. 1998 May;28(5):1663-72. PubMed PMID: 9603473.
346. Haynes NM, Trapani JA, Teng MW, Jackson JT, Cerruti L, Jane SM, et al. Rejection of syngeneic colon carcinoma by CTLs expressing single-chain antibody receptors codelivering CD28 costimulation. Journal of immunology. 2002 Nov 15;169(10):5780-6. PubMed PMID: 12421958.
347. Nolan KF, Yun CO, Akamatsu Y, Murphy JC, Leung SO, Beecham EJ, et al. Bypassing immunization: optimized design of "designer T cells" against carcinoembryonic antigen (CEA)-expressing tumors, and lack of suppression by soluble CEA. Clinical cancer research : an official journal of the American Association for Cancer Research. 1999 Dec;5(12):3928-41. PubMed PMID: 10632322.
348. Sheen AJ, Sherlock DJ, Irlam J, Hawkins RE, Gilham DE. T lymphocytes isolated from patients with advanced colorectal cancer are suitable for gene immunotherapy approaches. British journal of cancer. 2003 Apr 7;88(7):1119-27. PubMed PMID: 12671714. Pubmed Central PMCID: 2376387.
349. Chmielewski M, Maliar A, Eshhar Z, Abken H. CAR's made it to the pancreas. Oncoimmunology. 2012 Nov 1;1(8):1387-9. PubMed PMID: 23243602. Pubmed Central PMCID: 3518511.
350. Chmielewski M, Hahn O, Rappl G, Nowak M, Schmidt-Wolf IH, Hombach AA, et al. T cells that target carcinoembryonic antigen eradicate orthotopic pancreatic carcinomas without inducing autoimmune colitis in mice. Gastroenterology. 2012 Oct;143(4):1095-107 e2. PubMed PMID: 22750462.
351. Ohno M, Natsume A, Ichiro Iwami K, Iwamizu H, Noritake K, Ito D, et al. Retrovirally engineered T-cell-based immunotherapy targeting type III variant epidermal growth factor receptor, a glioma-associated antigen. Cancer science. 2010 Dec;101(12):2518-24. PubMed PMID: 20880333.
352. Shen CJ, Yang YX, Han EQ, Cao N, Wang YF, Wang Y, et al. Chimeric antigen receptor containing ICOS signaling domain mediates specific and efficient antitumor effect of T cells against EGFRvIII expressing glioma. Journal of hematology & oncology. 2013 May 9;6(1):33. PubMed PMID: 23656794.
353. Morgan RA, Johnson LA, Davis JL, Zheng Z, Woolard KD, Reap EA, et al. Recognition of glioma stem cells by genetically modified T cells targeting EGFRvIII and

development of adoptive cell therapy for glioma. Human gene therapy. 2012 Oct;23(10):1043-53. PubMed PMID: 22780919. Pubmed Central PMCID: 3472555.
354. Meier R, Golovko D, Tavri S, Henning TD, Knopp C, Piontek G, et al. Depicting adoptive immunotherapy for prostate cancer in an animal model with magnetic resonance imaging. Magnetic resonance in medicine : official journal of the Society of Magnetic Resonance in Medicine / Society of Magnetic Resonance in Medicine. 2011 Mar;65(3):756-63. PubMed PMID: 20928869.
355. Ren-Heidenreich L, Mordini R, Hayman GT, Siebenlist R, LeFever A. Comparison of the TCR zeta-chain with the FcR gamma-chain in chimeric TCR constructs for T cell activation and apoptosis. Cancer immunology, immunotherapy : CII. 2002 Oct;51(8):417-23. PubMed PMID: 12202902.
356. Shirasu N, Yamada H, Shibaguchi H, Kuroki M, Kuroki M. Molecular characterization of a fully human chimeric T-cell antigen receptor for tumor-associated antigen EpCAM. Journal of biomedicine & biotechnology. 2012;2012:853879. PubMed PMID: 22547929. Pubmed Central PMCID: 3324174.
357. Daly T, Royal RE, Kershaw MH, Treisman J, Wang G, Li W, et al. Recognition of human colon cancer by T cells transduced with a chimeric receptor gene. Cancer gene therapy. 2000 Feb;7(2):284-91. PubMed PMID: 10770638.
358. Parente-Pereira AC, Whilding LM, Brewig N, van der Stegen SJC, Davies DM, Wilkie S, et al. Synergistic Chemoimmunotherapy of Epithelial Ovarian Cancer Using ErbB-Retargeted T Cells Combined with Carboplatin. Journal of immunology. 2013 Sep 1;191(5):2437-45. PubMed PMID: 23898037.
359. Ahmed N, Salsman VS, Kew Y, Shaffer D, Powell S, Zhang YJ, et al. HER2-specific T cells target primary glioblastoma stem cells and induce regression of autologous experimental tumors. Clinical cancer research : an official journal of the American Association for Cancer Research. 2010 Jan 15;16(2):474-85. PubMed PMID: 20068073.
360. Pinthus JH, Waks T, Kaufman-Francis K, Schindler DG, Harmelin A, Kanety H, et al. Immuno-gene therapy of established prostate tumors using chimeric receptor-redirected human lymphocytes. Cancer research. 2003 May 15;63(10):2470-6. PubMed PMID: 12750268.
361. Stancovski I, Schindler DG, Waks T, Yarden Y, Sela M, Eshhar Z. Targeting of T lymphocytes to Neu/HER2-expressing cells using chimeric single chain Fv receptors. Journal of immunology. 1993 Dec 1;151(11):6577-82. PubMed PMID: 7902379.
362. Teng MW, Kershaw MH, Moeller M, Smyth MJ, Darcy PK. Immunotherapy of cancer using systemically delivered gene-modified human T lymphocytes. Human gene therapy. 2004 Jul;15(7):699-708. PubMed PMID: 15242530.
363. Wilkie S, van Schalkwyk MC, Hobbs S, Davies DM, van der Stegen SJ, Pereira AC, et al. Dual targeting of ErbB2 and MUC1 in breast cancer using chimeric antigen receptors engineered to provide complementary signaling. J Clin Immunol. 2012 Oct;32(5):1059-70. PubMed PMID: 22526592. Epub 2012/04/25. eng.
364. Zhao Y, Wang QJ, Yang S, Kochenderfer JN, Zheng Z, Zhong X, et al. A herceptin-based chimeric antigen receptor with modified signaling domains leads to enhanced survival of transduced T lymphocytes and antitumor activity. Journal of immunology. 2009 Nov 1;183(9):5563-74. PubMed PMID: 19843940.
365. Gattenlohner S, Marx A, Markfort B, Pscherer S, Landmeier S, Juergens H, et al. Rhabdomyosarcoma lysis by T cells expressing a human autoantibody-based chimeric receptor targeting the fetal acetylcholine receptor. Cancer research. 2006 Jan 1;66(1):24-8. PubMed PMID: 16397210.

366. Lamers CH, Sleijfer S, Vulto AG, Kruit WH, Kliffen M, Debets R, et al. Treatment of metastatic renal cell carcinoma with autologous T-lymphocytes genetically retargeted against carbonic anhydrase IX: first clinical experience. Journal of clinical oncology : official journal of the American Society of Clinical Oncology. 2006 May 1;24(13):e20-2. PubMed PMID: 16648493.
367. Weijtens ME, Willemsen RA, van Krimpen BA, Bolhuis RL. Chimeric scFv/gamma receptor-mediated T-cell lysis of tumor cells is coregulated by adhesion and accessory molecules. International journal of cancer Journal international du cancer. 1998 Jul 17;77(2):181-7. PubMed PMID: 9650549.
368. Lamers CH, Langeveld SC, Groot-van Ruijven CM, Debets R, Sleijfer S, Gratama JW. Gene-modified T cells for adoptive immunotherapy of renal cell cancer maintain transgene-specific immune functions in vivo. Cancer immunology, immunotherapy : CII. 2007 Dec;56(12):1875-83. PubMed PMID: 17479266.
369. Schroten C, Kraaij R, Veldhoven JL, Berrevoets CA, den Bakker MA, Ma Q, et al. T cell activation upon exposure to patient-derived tumor tissue: a functional assay to select patients for adoptive T cell therapy. Journal of immunological methods. 2010 Jul 31;359(1-2):11-20. PubMed PMID: 20460126.
370. Pule MA, Savoldo B, Myers GD, Rossig C, Russell HV, Dotti G, et al. Virus-specific T cells engineered to coexpress tumor-specific receptors: persistence and antitumor activity in individuals with neuroblastoma. Nature medicine. 2008 Nov;14(11):1264-70. PubMed PMID: 18978797. Pubmed Central PMCID: 2749734.
371. Rossig C, Bollard CM, Nuchtern JG, Merchant DA, Brenner MK. Targeting of G(D2)-positive tumor cells by human T lymphocytes engineered to express chimeric T-cell receptor genes. International journal of cancer Journal international du cancer. 2001 Oct 15;94(2):228-36. PubMed PMID: 11668503.
372. Louis CU, Savoldo B, Dotti G, Pule M, Yvon E, Myers GD, et al. Antitumor activity and long-term fate of chimeric antigen receptor-positive T cells in patients with neuroblastoma. Blood. 2011 Dec 1;118(23):6050-6. PubMed PMID: 21984804. Pubmed Central PMCID: 3234664.
373. Yvon E, Del Vecchio M, Savoldo B, Hoyos V, Dutour A, Anichini A, et al. Immunotherapy of metastatic melanoma using genetically engineered GD2-specific T cells. Clinical cancer research : an official journal of the American Association for Cancer Research. 2009 Sep 15;15(18):5852-60. PubMed PMID: 19737958. Pubmed Central PMCID: 2745508.
374. Lo AS, Ma Q, Liu DL, Junghans RP. Anti-GD3 chimeric sFv-CD28/T-cell receptor zeta designer T cells for treatment of metastatic melanoma and other neuroectodermal tumors. Clinical cancer research : an official journal of the American Association for Cancer Research. 2010 May 15;16(10):2769-80. PubMed PMID: 20460472.
375. Yun CO, Nolan KF, Beecham EJ, Reisfeld RA, Junghans RP. Targeting of T lymphocytes to melanoma cells through chimeric anti-GD3 immunoglobulin T-cell receptors. Neoplasia. 2000 Sep-Oct;2(5):449-59. PubMed PMID: 11191112. Pubmed Central PMCID: 1507984.
376. Willemsen RA, Ronteltap C, Chames P, Debets R, Bolhuis RL. T cell retargeting with MHC class I-restricted antibodies: the CD28 costimulatory domain enhances antigen-specific cytotoxicity and cytokine production. Journal of immunology. 2005 Jun 15;174(12):7853-8. PubMed PMID: 15944290.

377. Schuberth PC, Jakka G, Jensen SM, Wadle A, Gautschi F, Haley D, et al. Effector memory and central memory NY-ESO-1-specific re-directed T cells for treatment of multiple myeloma. Gene therapy. 2013 Apr;20(4):386-95. PubMed PMID: 22739387.
378. Burns WR, Zhao Y, Frankel TL, Hinrichs CS, Zheng Z, Xu H, et al. A high molecular weight melanoma-associated antigen-specific chimeric antigen receptor redirects lymphocytes to target human melanomas. Cancer research. 2010 Apr 15;70(8):3027-33. PubMed PMID: 20395199. Pubmed Central PMCID: 3245576.
379. Kahlon KS, Brown C, Cooper LJ, Raubitschek A, Forman SJ, Jensen MC. Specific recognition and killing of glioblastoma multiforme by interleukin 13-zetakine redirected cytolytic T cells. Cancer research. 2004 Dec 15;64(24):9160-6. PubMed PMID: 15604287.
380. Brown CE, Starr R, Aguilar B, Shami AF, Martinez C, D'Apuzzo M, et al. Stem-like tumor-initiating cells isolated from IL13Ralpha2 expressing gliomas are targeted and killed by IL13-zetakine-redirected T Cells. Clinical cancer research : an official journal of the American Association for Cancer Research. 2012 Apr 15;18(8):2199-209. PubMed PMID: 22407828. Pubmed Central PMCID: 3578382.
381. Kong S, Sengupta S, Tyler B, Bais AJ, Ma Q, Doucette S, et al. Suppression of human glioma xenografts with second-generation IL13R-specific chimeric antigen receptor-modified T cells. Clinical cancer research : an official journal of the American Association for Cancer Research. 2012 Nov 1;18(21):5949-60. PubMed PMID: 22966020.
382. Westwood JA, Smyth MJ, Teng MW, Moeller M, Trapani JA, Scott AM, et al. Adoptive transfer of T cells modified with a humanized chimeric receptor gene inhibits growth of Lewis-Y-expressing tumors in mice. Proceedings of the National Academy of Sciences of the United States of America. 2005 Dec 27;102(52):19051-6. PubMed PMID: 16365285. Pubmed Central PMCID: 1323148.
383. Peinert S, Prince HM, Guru PM, Kershaw MH, Smyth MJ, Trapani JA, et al. Gene-modified T cells as immunotherapy for multiple myeloma and acute myeloid leukemia expressing the Lewis Y antigen. Gene therapy. 2010 May;17(5):678-86. PubMed PMID: 20200563.
384. Mezzanzanica D, Canevari S, Mazzoni A, Figini M, Colnaghi MI, Waks T, et al. Transfer of chimeric receptor gene made of variable regions of tumor-specific antibody confers anticarbohydrate specificity on T cells. Cancer gene therapy. 1998 Nov-Dec;5(6):401-7. PubMed PMID: 9917095.
385. Westwood JA, Murray WK, Trivett M, Haynes NM, Solomon B, Mileshkin L, et al. The Lewis-Y carbohydrate antigen is expressed by many human tumors and can serve as a target for genetically redirected T cells despite the presence of soluble antigen in serum. Journal of immunotherapy. 2009 Apr;32(3):292-301. PubMed PMID: 19242371.
386. Neeson P, Shin A, Tainton KM, Guru P, Prince HM, Harrison SJ, et al. Ex vivo culture of chimeric antigen receptor T cells generates functional CD8+ T cells with effector and central memory-like phenotype. Gene therapy. 2010 Sep;17(9):1105-16. PubMed PMID: 20428216.
387. Carpenito C, Milone MC, Hassan R, Simonet JC, Lakhal M, Suhoski MM, et al. Control of large, established tumor xenografts with genetically retargeted human T cells containing CD28 and CD137 domains. Proceedings of the National Academy of Sciences of the United States of America. 2009 Mar 3;106(9):3360-5. PubMed PMID: 19211796. Pubmed Central PMCID: 2651342.

388. Lanitis E, Poussin M, Hagemann IS, Coukos G, Sandaltzopoulos R, Scholler N, et al. Redirected antitumor activity of primary human lymphocytes transduced with a fully human anti-mesothelin chimeric receptor. Molecular therapy : the journal of the American Society of Gene Therapy. 2012 Mar;20(3):633-43. PubMed PMID: 22127019. Pubmed Central PMCID: 3293635.
389. Moon EK, Carpenito C, Sun J, Wang LC, Kapoor V, Predina J, et al. Expression of a functional CCR2 receptor enhances tumor localization and tumor eradication by retargeted human T cells expressing a mesothelin-specific chimeric antibody receptor. Clinical cancer research : an official journal of the American Association for Cancer Research. 2011 Jul 15;17(14):4719-30. PubMed PMID: 21610146. Pubmed Central PMCID: 3612507.
390. Bakhtiari SH, Rahbarizadeh F, Hasannia S, Ahmadvand D, Iri-Sofla FJ, Rasaee MJ. Anti-MUC1 nanobody can redirect T-body cytotoxic effector function. Hybridoma. 2009 Apr;28(2):85-92. PubMed PMID: 19249993.
391. Wilkie S, Burbridge SE, Chiapero-Stanke L, Pereira AC, Cleary S, van der Stegen SJ, et al. Selective expansion of chimeric antigen receptor-targeted T-cells with potent effector function using interleukin-4. The Journal of biological chemistry. 2010 Aug 13;285(33):25538-44. PubMed PMID: 20562098. Pubmed Central PMCID: 2919118. Epub 2010/06/22. eng.
392. Sanchez C, Chan R, Bajgain P, Rambally S, Palapattu G, Mims M, et al. Combining T-cell immunotherapy and anti-androgen therapy for prostate cancer. Prostate cancer and prostatic diseases. 2013 Jan 8. PubMed PMID: 23295316.
393. Chekmasova AA, Rao TD, Nikhamin Y, Park KJ, Levine DA, Spriggs DR, et al. Successful eradication of established peritoneal ovarian tumors in SCID-Beige mice following adoptive transfer of T cells genetically targeted to the MUC16 antigen. Clinical cancer research : an official journal of the American Association for Cancer Research. 2010 Jul 15;16(14):3594-606. PubMed PMID: 20628030. Pubmed Central PMCID: 2907178.
394. Park JR, Digiusto DL, Slovak M, Wright C, Naranjo A, Wagner J, et al. Adoptive transfer of chimeric antigen receptor re-directed cytolytic T lymphocyte clones in patients with neuroblastoma. Molecular therapy : the journal of the American Society of Gene Therapy. 2007 Apr;15(4):825-33. PubMed PMID: 17299405. Epub 2007/02/15. eng.
395. Gilham DE, O'Neil A, Hughes C, Guest RD, Kirillova N, Lehane M, et al. Primary polyclonal human T lymphocytes targeted to carcino-embryonic antigens and neural cell adhesion molecule tumor antigens by CD3zeta-based chimeric immune receptors. Journal of immunotherapy. 2002 Mar-Apr;25(2):139-51. PubMed PMID: 12074044.
396. Gonzalez S, Naranjo A, Serrano LM, Chang WC, Wright CL, Jensen MC. Genetic engineering of cytolytic T lymphocytes for adoptive T-cell therapy of neuroblastoma. The journal of gene medicine. 2004 Jun;6(6):704-11. PubMed PMID: 15170741.
397. Zhang T, Lemoi BA, Sentman CL. Chimeric NK-receptor-bearing T cells mediate antitumor immunotherapy. Blood. 2005 Sep 1;106(5):1544-51. PubMed PMID: 15890688. Pubmed Central PMCID: 1895219.
398. Barber A, Rynda A, Sentman CL. Chimeric NKG2D expressing T cells eliminate immunosuppression and activate immunity within the ovarian tumor microenvironment. Journal of immunology. 2009 Dec 1;183(11):6939-47. PubMed PMID: 19915047. Pubmed Central PMCID: 2825039.
399. Morgenroth A, Cartellieri M, Schmitz M, Gunes S, Weigle B, Bachmann M, et al. Targeting of tumor cells expressing the prostate stem cell antigen (PSCA) using

genetically engineered T-cells. The Prostate. 2007 Jul 1;67(10):1121-31. PubMed PMID: 17492652.
400. Kloss CC, Condomines M, Cartellieri M, Bachmann M, Sadelain M. Combinatorial antigen recognition with balanced signaling promotes selective tumor eradication by engineered T cells. Nature biotechnology. 2013 Jan;31(1):71-5. PubMed PMID: 23242161.
401. Katari UL, Keirnan JM, Worth AC, Hodges SE, Leen AM, Fisher WE, et al. Engineered T cells for pancreatic cancer treatment. HPB : the official journal of the International Hepato Pancreato Biliary Association. 2011 Sep;13(9):643-50. PubMed PMID: 21843265. Pubmed Central PMCID: 3183449.
402. Gong MC, Latouche JB, Krause A, Heston WD, Bander NH, Sadelain M. Cancer patient T cells genetically targeted to prostate-specific membrane antigen specifically lyse prostate cancer cells and release cytokines in response to prostate-specific membrane antigen. Neoplasia. 1999 Jun;1(2):123-7. PubMed PMID: 10933046. Pubmed Central PMCID: 1508130.
403. Maher J, Brentjens RJ, Gunset G, Riviere I, Sadelain M. Human T-lymphocyte cytotoxicity and proliferation directed by a single chimeric TCRzeta /CD28 receptor. Nature biotechnology. 2002 Jan;20(1):70-5. PubMed PMID: 11753365.
404. Zhong XS, Matsushita M, Plotkin J, Riviere I, Sadelain M. Chimeric antigen receptors combining 4-1BB and CD28 signaling domains augment PI3kinase/AKT/Bcl-XL activation and CD8+ T cell-mediated tumor eradication. Molecular therapy : the journal of the American Society of Gene Therapy. 2010 Feb;18(2):413-20. PubMed PMID: 19773745. Pubmed Central PMCID: 2839303.
405. Hudecek M, Schmitt TM, Baskar S, Lupo-Stanghellini MT, Nishida T, Yamamoto TN, et al. The B-cell tumor-associated antigen ROR1 can be targeted with T cells modified to express a ROR1-specific chimeric antigen receptor. Blood. 2010 Nov 25;116(22):4532-41. PubMed PMID: 20702778. Pubmed Central PMCID: 2996114.
406. McGuinness RP, Ge Y, Patel SD, Kashmiri SV, Lee HS, Hand PH, et al. Anti-tumor activity of human T cells expressing the CC49-zeta chimeric immune receptor. Human gene therapy. 1999 Jan 20;10(2):165-73. PubMed PMID: 10022542.
407. Hombach A, Heuser C, Sircar R, Tillmann T, Diehl V, Kruis W, et al. T cell targeting of TAG72+ tumor cells by a chimeric receptor with antibody-like specificity for a carbohydrate epitope. Gastroenterology. 1997 Oct;113(4):1163-70. PubMed PMID: 9322511.
408. Hombach A, Sircar R, Heuser C, Tillmann T, Diehl V, Kruis W, et al. Chimeric anti-TAG72 receptors with immunoglobulin constant Fc domains and gamma or zeta signalling chains. International journal of molecular medicine. 1998 Jul;2(1):99-103. PubMed PMID: 9854151.
409. Warren RS, Bergsland EK, Pennathur-Das R, Nemu-naitis J, Venook AP, Hege KM. Clinical studies of regional and systemic gene therapy with autologous CC49-z modified T-cells in colorectal cancer metastatic to the liver. Cancer gene therapy: Stockton Press; 1998. p. S1-S2.
410. Niederman TM, Ghogawala Z, Carter BS, Tompkins HS, Russell MM, Mulligan RC. Antitumor activity of cytotoxic T lymphocytes engineered to target vascular endothelial growth factor receptors. Proceedings of the National Academy of Sciences of the United States of America. 2002 May 14;99(10):7009-14. PubMed PMID: 11997459. Pubmed Central PMCID: 124519.
411. Kershaw MH, Westwood JA, Zhu Z, Witte L, Libutti SK, Hwu P. Generation of gene-modified T cells reactive against the angiogenic kinase insert domain-containing

receptor (KDR) found on tumor vasculature. Human gene therapy. 2000 Dec 10;11(18):2445-52. PubMed PMID: 11119416.
412. Hwu P, Shafer GE, Treisman J, Schindler DG, Gross G, Cowherd R, et al. Lysis of ovarian cancer cells by human lymphocytes redirected with a chimeric gene composed of an antibody variable region and the Fc receptor gamma chain. The Journal of experimental medicine. 1993 Jul 1;178(1):361-6. PubMed PMID: 8315392. Pubmed Central PMCID: 2191075.
413. Kershaw MH, Westwood JA, Hwu P. Dual-specific T cells combine proliferation and antitumor activity. Nature biotechnology. 2002 Dec;20(12):1221-7. PubMed PMID: 12415288.
414. Kandalaft LE, Powell DJ, Jr., Coukos G. A phase I clinical trial of adoptive transfer of folate receptor-alpha redirected autologous T cells for recurrent ovarian cancer. Journal of translational medicine. 2012;10:157. PubMed PMID: 22863016. Pubmed Central PMCID: 3439340.
415. Song DG, Ye Q, Carpenito C, Poussin M, Wang LP, Ji C, et al. In vivo persistence, tumor localization, and antitumor activity of CAR-engineered T cells is enhanced by costimulatory signaling through CD137 (4-1BB). Cancer research. 2011 Jul 1;71(13):4617-27. PubMed PMID: 21546571.
416. Vera J, Savoldo B, Vigouroux S, Biagi E, Pule M, Rossig C, et al. T lymphocytes redirected against the kappa light chain of human immunoglobulin efficiently kill mature B lymphocyte-derived malignant cells. Blood. 2006 Dec 1;108(12):3890-7. PubMed PMID: 16926291. Pubmed Central PMCID: 1895462.
417. Jiang HR, Gilham DE, Mulryan K, Kirillova N, Hawkins RE, Stern PL. Combination of vaccination and chimeric receptor expressing T cells provides improved active therapy of tumors. Journal of immunology. 2006 Oct 1;177(7):4288-98. PubMed PMID: 16982863.
418. Moritz D, Groner B. A spacer region between the single chain antibody- and the CD3 zeta-chain domain of chimeric T cell receptor components is required for efficient ligand binding and signaling activity. Gene therapy. 1995 Oct;2(8):539-46. PubMed PMID: 8593604.
419. Guest RD, Hawkins RE, Kirillova N, Cheadle EJ, Arnold J, O'Neill A, et al. The role of extracellular spacer regions in the optimal design of chimeric immune receptors: evaluation of four different scFvs and antigens. Journal of immunotherapy. 2005 May-Jun;28(3):203-11. PubMed PMID: 15838376.
420. Moritz D, Wels W, Mattern J, Groner B. Cytotoxic T lymphocytes with a grafted recognition specificity for ERBB2-expressing tumor cells. Proceedings of the National Academy of Sciences of the United States of America. 1994 May 10;91(10):4318-22. PubMed PMID: 7910405. Pubmed Central PMCID: 43776.
421. Hudecek M, Lupo Stanghellini MT, Kosasih PL, Sommermeyer D, Jensen M, Rader C, et al. Receptor affinity and extracellular domain modifications affect tumor recognition by ROR1-specific chimeric antigen receptor T-cells. Clinical cancer research : an official journal of the American Association for Cancer Research. 2013 Apr 25. PubMed PMID: 23620405.
422. Hudecek M, Silva A, Kosasih PL, Chen YY, Turtle CJ, Jensen MC, et al. The Non-Signaling Extracellular Spacer Domain of CD19-Specific Chimeric Antigen Receptors Is Decisive for in Vivo Anti-Tumor Activity. 54th ASH Annual Meeting and Exposition; December 8-11, 2012; Atlanta, GA2012.

423. Patel SD, Moskalenko M, Smith D, Maske B, Finer MH, McArthur JG. Impact of chimeric immune receptor extracellular protein domains on T cell function. Gene therapy. 1999 Mar;6(3):412-9. PubMed PMID: 10435091.
424. Hombach A, Heuser C, Gerken M, Fischer B, Lewalter K, Diehl V, et al. T cell activation by recombinant FcepsilonRI gamma-chain immune receptors: an extracellular spacer domain impairs antigen-dependent T cell activation but not antigen recognition. Gene therapy. 2000 Jun;7(12):1067-75. PubMed PMID: 10871757.
425. Hombach A, Hombach AA, Abken H. Adoptive immunotherapy with genetically engineered T cells: modification of the IgG1 Fc 'spacer' domain in the extracellular moiety of chimeric antigen receptors avoids 'off-target' activation and unintended initiation of an innate immune response. Gene therapy. 2010 Oct;17(10):1206-13. PubMed PMID: 20555360.
426. Weijtens ME, Hart EH, Bolhuis RL. Functional balance between T cell chimeric receptor density and tumor associated antigen density: CTL mediated cytolysis and lymphokine production. Gene therapy. 2000 Jan;7(1):35-42. PubMed PMID: 10680014.
427. Badou A, Savignac M, Moreau M, Leclerc C, Foucras G, Cassar G, et al. Weak TCR stimulation induces a calcium signal that triggers IL-4 synthesis, stronger TCR stimulation induces MAP kinases that control IFN-gamma production. European journal of immunology. 2001 Aug;31(8):2487-96. PubMed PMID: 11500833.
428. Bridgeman JS, Hawkins RE, Bagley S, Blaylock M, Holland M, Gilham DE. The optimal antigen response of chimeric antigen receptors harboring the CD3zeta transmembrane domain is dependent upon incorporation of the receptor into the endogenous TCR/CD3 complex. Journal of immunology. 2010 Jun 15;184(12):6938-49. PubMed PMID: 20483753.
429. Borst J, Coligan JE, Oettgen H, Pessano S, Malin R, Terhorst C. The delta- and epsilon-chains of the human T3/T-cell receptor complex are distinct polypeptides. Nature. 1984 Nov 29-Dec 5;312(5993):455-8. PubMed PMID: 6239105.
430. Howard FD, Moingeon P, Moebius U, McConkey DJ, Yandava B, Gennert TE, et al. The CD3 zeta cytoplasmic domain mediates CD2-induced T cell activation. The Journal of experimental medicine. 1992 Jul 1;176(1):139-45. PubMed PMID: 1351920. Pubmed Central PMCID: 2119282.
431. Weissman AM, Hou D, Orloff DG, Modi WS, Seuanez H, O'Brien SJ, et al. Molecular cloning and chromosomal localization of the human T-cell receptor zeta chain: distinction from the molecular CD3 complex. Proceedings of the National Academy of Sciences of the United States of America. 1988 Dec;85(24):9709-13. PubMed PMID: 2974162. Pubmed Central PMCID: 282845.
432. Irving BA, Weiss A. The cytoplasmic domain of the T cell receptor zeta chain is sufficient to couple to receptor-associated signal transduction pathways. Cell. 1991 Mar 8;64(5):891-901. PubMed PMID: 1705867.
433. Haynes NM, Snook MB, Trapani JA, Cerruti L, Jane SM, Smyth MJ, et al. Redirecting mouse CTL against colon carcinoma: superior signaling efficacy of single-chain variable domain chimeras containing TCR-zeta vs Fc epsilon RI-gamma. Journal of immunology. 2001 Jan 1;166(1):182-7. PubMed PMID: 11123291.
434. Krause A, Guo HF, Latouche JB, Tan C, Cheung NK, Sadelain M. Antigen-dependent CD28 signaling selectively enhances survival and proliferation in genetically modified activated human primary T lymphocytes. The Journal of experimental medicine. 1998 Aug 17;188(4):619-26. PubMed PMID: 9705944. Pubmed Central PMCID: 2213361.

435. Alvarez-Vallina L, Hawkins RE. Antigen-specific targeting of CD28-mediated T cell co-stimulation using chimeric single-chain antibody variable fragment-CD28 receptors. European journal of immunology. 1996 Oct;26(10):2304-9. PubMed PMID: 8898938.
436. Finney HM, Lawson AD, Bebbington CR, Weir AN. Chimeric receptors providing both primary and costimulatory signaling in T cells from a single gene product. Journal of immunology. 1998 Sep 15;161(6):2791-7. PubMed PMID: 9743337.
437. Hombach A, Wieczarkowiecz A, Marquardt T, Heuser C, Usai L, Pohl C, et al. Tumor-specific T cell activation by recombinant immunoreceptors: CD3 zeta signaling and CD28 costimulation are simultaneously required for efficient IL-2 secretion and can be integrated into one combined CD28/CD3 zeta signaling receptor molecule. Journal of immunology. 2001 Dec 1;167(11):6123-31. PubMed PMID: 11714771.
438. Kofler DM, Chmielewski M, Rappl G, Hombach A, Riet T, Schmidt A, et al. CD28 costimulation Impairs the efficacy of a redirected t-cell antitumor attack in the presence of regulatory t cells which can be overcome by preventing Lck activation. Molecular therapy : the journal of the American Society of Gene Therapy. 2011 Apr;19(4):760-7. PubMed PMID: 21326215. Pubmed Central PMCID: 3070115.
439. Finney HM, Akbar AN, Lawson AD. Activation of resting human primary T cells with chimeric receptors: costimulation from CD28, inducible costimulator, CD134, and CD137 in series with signals from the TCR zeta chain. Journal of immunology. 2004 Jan 1;172(1):104-13. PubMed PMID: 14688315.
440. Pule MA, Straathof KC, Dotti G, Heslop HE, Rooney CM, Brenner MK. A chimeric T cell antigen receptor that augments cytokine release and supports clonal expansion of primary human T cells. Molecular therapy : the journal of the American Society of Gene Therapy. 2005 Nov;12(5):933-41. PubMed PMID: 15979412.
441. Imai C, Mihara K, Andreansky M, Nicholson IC, Pui CH, Geiger TL, et al. Chimeric receptors with 4-1BB signaling capacity provoke potent cytotoxicity against acute lymphoblastic leukemia. Leukemia. 2004 Apr;18(4):676-84. PubMed PMID: 14961035.
442. Song DG, Ye Q, Poussin M, Harms GM, Figini M, Powell DJ, Jr. CD27 costimulation augments the survival and antitumor activity of redirected human T cells in vivo. Blood. 2012 Jan 19;119(3):696-706. PubMed PMID: 22117050.
443. Altvater B, Landmeier S, Pscherer S, Temme J, Juergens H, Pule M, et al. 2B4 (CD244) signaling via chimeric receptors costimulates tumor-antigen specific proliferation and in vitro expansion of human T cells. Cancer immunology, immunotherapy : CII. 2009 Dec;58(12):1991-2001. PubMed PMID: 19360406.
444. Kowolik CM, Topp MS, Gonzalez S, Pfeiffer T, Olivares S, Gonzalez N, et al. CD28 costimulation provided through a CD19-specific chimeric antigen receptor enhances in vivo persistence and antitumor efficacy of adoptively transferred T cells. Cancer research. 2006 Nov 15;66(22):10995-1004. PubMed PMID: 17108138.
445. Porter DL, Levine BL, Kalos M, Bagg A, June CH. Chimeric antigen receptor-modified T cells in chronic lymphoid leukemia. The New England journal of medicine. 2011 Aug 25;365(8):725-33. PubMed PMID: 21830940. Pubmed Central PMCID: 3387277.
446. Savoldo B, Ramos CA, Liu E, Mims MP, Keating MJ, Carrum G, et al. CD28 costimulation improves expansion and persistence of chimeric antigen receptor-modified T cells in lymphoma patients. The Journal of clinical investigation. 2011 May;121(5):1822-6. PubMed PMID: 21540550. Pubmed Central PMCID: 3083795.
447. Geiger TL, Nguyen P, Leitenberg D, Flavell RA. Integrated src kinase and costimulatory activity enhances signal transduction through single-chain chimeric

receptors in T lymphocytes. Blood. 2001 Oct 15;98(8):2364-71. PubMed PMID: 11588032.
448. Hombach AA, Heiders J, Foppe M, Chmielewski M, Abken H. OX40 costimulation by a chimeric antigen receptor abrogates CD28 and IL-2 induced IL-10 secretion by redirected CD4(+) T cells. Oncoimmunology. 2012 Jul 1;1(4):458-66. PubMed PMID: 22754764. Pubmed Central PMCID: 3382912.
449. Sadelain M, Brentjens R, Riviere I. The promise and potential pitfalls of chimeric antigen receptors. Current opinion in immunology. 2009 Apr;21(2):215-23. PubMed PMID: 19327974.
450. Brentjens R, Yeh R, Bernal Y, Riviere I, Sadelain M. Treatment of chronic lymphocytic leukemia with genetically targeted autologous T cells: case report of an unforeseen adverse event in a phase I clinical trial. Molecular therapy : the journal of the American Society of Gene Therapy. 2010 Apr;18(4):666-8. PubMed PMID: 20357779. Pubmed Central PMCID: 2862525.
451. Wingens M, Walma T, van Ingen H, Stortelers C, van Leeuwen JE, van Zoelen EJ, et al. Structural analysis of an epidermal growth factor/transforming growth factor-alpha chimera with unique ErbB binding specificity. The Journal of biological chemistry. 2003 Oct 3;278(40):39114-23. PubMed PMID: 12869572.
452. Campion SR, Niyogi SK. Interaction of epidermal growth factor with its receptor. Progress in nucleic acid research and molecular biology. 1994;49:353-83. PubMed PMID: 7863010.
453. Groenen LC, Nice EC, Burgess AW. Structure-function relationships for the EGF/TGF-alpha family of mitogens. Growth factors. 1994;11(4):235-57. PubMed PMID: 7779404.
454. Stortelers C, van der Woning SP, Jacobs-Oomen S, Wingens M, van Zoelen EJ. Selective formation of ErbB-2/ErbB-3 heterodimers depends on the ErbB-3 affinity of epidermal growth factor-like ligands. The Journal of biological chemistry. 2003 Apr 4;278(14):12055-63. PubMed PMID: 12556529.
455. Barbacci EG, Guarino BC, Stroh JG, Singleton DH, Rosnack KJ, Moyer JD, et al. The structural basis for the specificity of epidermal growth factor and heregulin binding. The Journal of biological chemistry. 1995 Apr 21;270(16):9585-9. PubMed PMID: 7721889.
456. Stortelers C, Souriau C, van Liempt E, van de Poll ML, van Zoelen EJ. Role of the N-terminus of epidermal growth factor in ErbB-2/ErbB-3 binding studied by phage display. Biochemistry. 2002 Jul 9;41(27):8732-41. PubMed PMID: 12093292.
457. Stortelers C, van De Poll ML, Lenferink AE, Gadellaa MM, van Zoelen C, van Zoelen EJ. Epidermal growth factor contains both positive and negative determinants for interaction with ErbB-2/ErbB-3 heterodimers. Biochemistry. 2002 Apr 2;41(13):4292-301. PubMed PMID: 11914075.
458. Chavez AR, Buchser W, Basse PH, Liang X, Appleman LJ, Maranchie JK, et al. Pharmacologic administration of interleukin-2. Annals of the New York Academy of Sciences. 2009 Dec;1182:14-27. PubMed PMID: 20074271.
459. Banchereau J, Briere F, Galizzi JP, Miossec P, Rousset F. Human interleukin 4. Journal of lipid mediators and cell signalling. 1994 Feb;9(1):43-53. PubMed PMID: 8032715.
460. Parente-Pereira AC, Burnet J, Ellison D, Foster J, Davies DM, van der Stegen S, et al. Trafficking of CAR-engineered human T cells following regional or systemic adoptive transfer in SCID beige mice. J Clin Immunol. 2011 Aug;31(4):710-8. PubMed PMID: 21505816. Epub 2011/04/21. eng.

461. Beppu M, Ikebe T, Shirasuna K. The inhibitory effects of immunosuppressive factors, dexamethasone and interleukin-4, on NF-kappaB-mediated protease production by oral cancer. Biochimica et biophysica acta. 2002 Jan 2;1586(1):11-22. PubMed PMID: 11781145.
462. Herzberg F, Schoning M, Schirner M, Topp M, Thiel E, Kreuser ED. IL-4 and TNF-alpha induce changes in integrin expression and adhesive properties and decrease the lung-colonizing potential of HT-29 colon carcinoma cells. Clinical & experimental metastasis. 1996 Mar;14(2):165-75. PubMed PMID: 8605730.
463. Morisaki T, Yuzuki DH, Lin RT, Foshag LJ, Morton DL, Hoon DS. Interleukin 4 receptor expression and growth inhibition of gastric carcinoma cells by interleukin 4. Cancer research. 1992 Nov 1;52(21):6059-65. PubMed PMID: 1394231.
464. Volpert OV, Fong T, Koch AE, Peterson JD, Waltenbaugh C, Tepper RI, et al. Inhibition of angiogenesis by interleukin 4. The Journal of experimental medicine. 1998 Sep 21;188(6):1039-46. PubMed PMID: 9743522. Pubmed Central PMCID: 2212547.
465. Myers JN, Yasumura S, Suminami Y, Hirabayashi H, Lin W, Johnson JT, et al. Growth stimulation of human head and neck squamous cell carcinoma cell lines by interleukin 4. Clinical cancer research : an official journal of the American Association for Cancer Research. 1996 Jan;2(1):127-35. PubMed PMID: 9816099.
466. Schuler T, Qin Z, Ibe S, Noben-Trauth N, Blankenstein T. T helper cell type 1-associated and cytotoxic T lymphocyte-mediated tumor immunity is impaired in interleukin 4-deficient mice. The Journal of experimental medicine. 1999 Mar 1;189(5):803-10. PubMed PMID: 10049944. Pubmed Central PMCID: 2192943.
467. Lathers DM, Young MR. Increased aberrance of cytokine expression in plasma of patients with more advanced squamous cell carcinoma of the head and neck. Cytokine. 2004 Mar 7;25(5):220-8. PubMed PMID: 15036248.
468. Mojtahedi Z, Khademi B, Yehya A, Talebi A, Fattahi MJ, Ghaderi A. Serum levels of interleukins 4 and 10 in head and neck squamous cell carcinoma. The Journal of laryngology and otology. 2012 Feb;126(2):175-9. PubMed PMID: 21888745.
469. Sparano A, Lathers DM, Achille N, Petruzzelli GJ, Young MR. Modulation of Th1 and Th2 cytokine profiles and their association with advanced head and neck squamous cell carcinoma. Otolaryngology--head and neck surgery : official journal of American Academy of Otolaryngology-Head and Neck Surgery. 2004 Nov;131(5):573-6. PubMed PMID: 15523428.
470. de Oliveira MV, Fraga CA, Gomez RS, Paula AM. Immunohistochemical expression of interleukin-4, -6, -8, and -12 in inflammatory cells in surrounding invasive front of oral squamous cell carcinoma. Head & neck. 2009 Nov;31(11):1439-46. PubMed PMID: 19424975.
471. Franca CM, Barros FM, Lotufo MA, Fernandes KP, Borra RC. Response of peripheral blood mononuclear cells to conditioned medium from cultured oral squamous cell carcinomas. Brazilian oral research. 2011 Sep-Oct;25(5):414-20. PubMed PMID: 22031054.
472. Mann EA, Spiro JD, Chen LL, Kreutzer DL. Cytokine expression by head and neck squamous cell carcinomas. American journal of surgery. 1992 Dec;164(6):567-73. PubMed PMID: 1463101.
473. Mehrotra R, Varricchio F, Husain SR, Puri RK. Head and neck cancers, but not benign lesions, express interleukin-4 receptors in situ. Oncology reports. 1998 Jan-Feb;5(1):45-8. PubMed PMID: 9458290.
474. Vairaktaris E, Yannopoulos A, Vassiliou S, Serefoglou Z, Vylliotis A, Nkenke E, et al. Strong association of interleukin-4 (-590 C/T) polymorphism with increased risk for

oral squamous cell carcinoma in Europeans. Oral surgery, oral medicine, oral pathology, oral radiology, and endodontics. 2007 Dec;104(6):796-802. PubMed PMID: 17428692.
475. Werkmeister R, Fillies T, Gaertner C, Joos U, Berdel WE. A clinical phase I/II trial of rhIL-4 applied topically in patients with oral squamous cell carcinomas to assess safety and therapeutic activity. Oncology reports. 2005 Mar;13(3):449-52. PubMed PMID: 15706415.
476. Pries R, Wollenberg B. Cytokines in head and neck cancer. Cytokine & growth factor reviews. 2006 Jun;17(3):141-6. PubMed PMID: 16540364.
477. Grupp SA, Kalos M, Barrett D, Aplenc R, Porter DL, Rheingold SR, et al. Chimeric Antigen Receptor-Modified T Cells for Acute Lymphoid Leukemia. The New England journal of medicine. 2013 Mar 25. PubMed PMID: 23527958.
478. Till BG, Jensen MC, Wang J, Chen EY, Wood BL, Greisman HA, et al. Adoptive immunotherapy for indolent non-Hodgkin lymphoma and mantle cell lymphoma using genetically modified autologous CD20-specific T cells. Blood. 2008 Sep 15;112(6):2261-71. PubMed PMID: 18509084. Pubmed Central PMCID: 2532803.
479. Brentjens RJ, Riviere I, Park JH, Davila ML, Wang X, Stefanski J, et al. Safety and persistence of adoptively transferred autologous CD19-targeted T cells in patients with relapsed or chemotherapy refractory B-cell leukemias. Blood. 2011 Nov 3;118(18):4817-28. PubMed PMID: 21849486. Pubmed Central PMCID: 3208293.
480. Gattinoni L, Finkelstein SE, Klebanoff CA, Antony PA, Palmer DC, Spiess PJ, et al. Removal of homeostatic cytokine sinks by lymphodepletion enhances the efficacy of adoptively transferred tumor-specific CD8+ T cells. The Journal of experimental medicine. 2005 Oct 3;202(7):907-12. PubMed PMID: 16203864. Pubmed Central PMCID: 1397916.
481. NationalCancerInstitute. Common Toxicity Criteria version 4.03 2013 [01/07/2013]. Available from: http://ctep.cancer.gov/protocolDevelopment/electronic_applications/ctc.htm.
482. SpringerReferences. Cytokine Release Syndrome 2013 [cited 2013 28 May]. Available from: http://www.springerreference.com/docs/html/chapterdbid/38111.html.
483. Ferreira FL, Bota DP, Bross A, Melot C, Vincent JL. Serial evaluation of the SOFA score to predict outcome in critically ill patients. JAMA : the journal of the American Medical Association. 2001 Oct 10;286(14):1754-8. PubMed PMID: 11594901.
484. Pandharipande PP, Shintani AK, Hagerman HE, St Jacques PJ, Rice TW, Sanders NW, et al. Derivation and validation of Spo2/Fio2 ratio to impute for Pao2/Fio2 ratio in the respiratory component of the Sequential Organ Failure Assessment score. Critical care medicine. 2009 Apr;37(4):1317-21. PubMed PMID: 19242333.
485. Liu H, Moy P, Kim S, Xia Y, Rajasekaran A, Navarro V, et al. Monoclonal antibodies to the extracellular domain of prostate-specific membrane antigen also react with tumor vascular endothelium. Cancer research. 1997 Sep 1;57(17):3629-34. PubMed PMID: 9288760.
486. Gaken J, Jiang J, Daniel K, van Berkel E, Hughes C, Kuiper M, et al. Fusagene vectors: a novel strategy for the expression of multiple genes from a single cistron. Gene therapy. 2000 Dec;7(23):1979-85. PubMed PMID: 11175308.
487. Donnelly ML, Hughes LE, Luke G, Mendoza H, ten Dam E, Gani D, et al. The 'cleavage' activities of foot-and-mouth disease virus 2A site-directed mutants and naturally occurring '2A-like' sequences. The Journal of general virology. 2001 May;82(Pt 5):1027-41. PubMed PMID: 11297677.

488. Szymczak AL, Workman CJ, Wang Y, Vignali KM, Dilioglou S, Vanin EF, et al. Correction of multi-gene deficiency in vivo using a single 'self-cleaving' 2A peptide-based retroviral vector. Nature biotechnology. 2004 May;22(5):589-94. PubMed PMID: 15064769.
489. Donnelly ML, Luke G, Mehrotra A, Li X, Hughes LE, Gani D, et al. Analysis of the aphthovirus 2A/2B polyprotein 'cleavage' mechanism indicates not a proteolytic reaction, but a novel translational effect: a putative ribosomal 'skip'. The Journal of general virology. 2001 May;82(Pt 5):1013-25. PubMed PMID: 11297676.
490. Sambrook J, Russel DW. Molecular Cloning A Laboratory Manual. Third Edition ed. New York: Cold Spring Harbor Laboratory Press; 2001.
491. Birnboim HC, Doly J. A rapid alkaline extraction procedure for screening recombinant plasmid DNA. Nucleic acids research. 1979 Nov 24;7(6):1513-23. PubMed PMID: 388356. Pubmed Central PMCID: 342324.
492. Melzak KA, Sherwood CS, Turner RFB, Haynes CA. Driving Forces for DNA Adsorption to Silica in Perchlorate Solutions. Journal of Colloid and Interface Science. 1996 (181):635-44.
493. Sanger F, Nicklen S, Coulson AR. DNA sequencing with chain-terminating inhibitors. Proceedings of the National Academy of Sciences of the United States of America. 1977 Dec;74(12):5463-7. PubMed PMID: 271968. Pubmed Central PMCID: 431765.
494. PromoCell. Endothelial Cells (Microvascular) 2012 [14/06/2013]. Instruction Manual]. Available from: http://www.promocell.com/fileadmin/promocell/PDF/C-12281.pdf.
495. PromoCell. Cardiac Myocytes 2013 [14/06/2013]. Instruction Manual]. Available from: http://www.promocell.com/fileadmin/promocell/PDF/C-12810.pdf.
496. CellBiologics. Mouse Lung Microvascular Endothelial Cells/BALB-5011 2013 [14/06/2013]. Available from: http://www.cellbiologics.com/product_info.php?products_id=86.
497. Morgenstern JP, Land H. Advanced mammalian gene transfer: high titre retroviral vectors with multiple drug selection markers and a complementary helper-free packaging cell line. Nucleic acids research. 1990 Jun 25;18(12):3587-96. PubMed PMID: 2194165. Pubmed Central PMCID: 331014.
498. Vogt PK. Retroviral virions and genomes. In: Varmus HE, editor. Retroviruses. New York: Cold Spring Harbor Laboratory Press; 1997. p. 27-70.
499. Schwartzberg P, Colicelli J, Goff SP. Construction and analysis of deletion mutations in the pol gene of Moloney murine leukemia virus: a new viral function required for productive infection. Cell. 1984 Jul;37(3):1043-52. PubMed PMID: 6204767.
500. Rein A, McClure MR, Rice NR, Luftig RB, Schultz AM. Myristylation site in Pr65gag is essential for virus particle formation by Moloney murine leukemia virus. Proceedings of the National Academy of Sciences of the United States of America. 1986 Oct;83(19):7246-50. PubMed PMID: 3489936. Pubmed Central PMCID: 386692.
501. Gorelick RJ, Henderson LE, Hanser JP, Rein A. Point mutants of Moloney murine leukemia virus that fail to package viral RNA: evidence for specific RNA recognition by a "zinc finger-like" protein sequence. Proceedings of the National Academy of Sciences of the United States of America. 1988 Nov;85(22):8420-4. PubMed PMID: 3141927. Pubmed Central PMCID: 282469.
502. Oshima M, Muriaux D, Mirro J, Nagashima K, Dryden K, Yeager M, et al. Effects of blocking individual maturation cleavages in murine leukemia virus gag. Journal of

virology. 2004 Feb;78(3):1411-20. PubMed PMID: 14722296. Pubmed Central PMCID: 321369.
503. Alberts B, Bray D, Hopkin K, Johnson A, Lewis J, Raff M, et al. Essential Cell Biology. 3rd Edition ed: Garland Science; 2009.
504. Swanstrom R, Willis JW. Synthesis, assembly and processing of viral proteins. In: Varmus HE, editor. Retroviruses. New York: Cold Spring Harbor Laboratory Press; 1997.
505. Ory DS, Neugeboren BA, Mulligan RC. A stable human-derived packaging cell line for production of high titer retrovirus/vesicular stomatitis virus G pseudotypes. Proceedings of the National Academy of Sciences of the United States of America. 1996 Oct 15;93(21):11400-6. PubMed PMID: 8876147. Pubmed Central PMCID: 38069.
506. Graham FL, Smiley J, Russell WC, Nairn R. Characteristics of a human cell line transformed by DNA from human adenovirus type 5. The Journal of general virology. 1977 Jul;36(1):59-74. PubMed PMID: 886304.
507. Gossen M, Bujard H. Tight control of gene expression in mammalian cells by tetracycline-responsive promoters. Proceedings of the National Academy of Sciences of the United States of America. 1992 Jun 15;89(12):5547-51. PubMed PMID: 1319065. Pubmed Central PMCID: 49329.
508. Miller AD, Garcia JV, von Suhr N, Lynch CM, Wilson C, Eiden MV. Construction and properties of retrovirus packaging cells based on gibbon ape leukemia virus. Journal of virology. 1991 May;65(5):2220-4. PubMed PMID: 1850008. Pubmed Central PMCID: 240569.
509. Riviere I, Brose K, Mulligan RC. Effects of retroviral vector design on expression of human adenosine deaminase in murine bone marrow transplant recipients engrafted with genetically modified cells. Proceedings of the National Academy of Sciences of the United States of America. 1995 Jul 18;92(15):6733-7. PubMed PMID: 7624312. Pubmed Central PMCID: 41403.
510. Zhao Y, Low W, Collins MK. Improved safety and titre of murine leukaemia virus (MLV)-based retroviral vectors. Gene therapy. 2000 Feb;7(4):300-5. PubMed PMID: 10694810.
511. Hanenberg H, Xiao XL, Dilloo D, Hashino K, Kato I, Williams DA. Colocalization of retrovirus and target cells on specific fibronectin fragments increases genetic transduction of mammalian cells. Nature medicine. 1996 Aug;2(8):876-82. PubMed PMID: 8705856.
512. Pollok KE, Hanenberg H, Noblitt TW, Schroeder WL, Kato I, Emanuel D, et al. High-efficiency gene transfer into normal and adenosine deaminase-deficient T lymphocytes is mediated by transduction on recombinant fibronectin fragments. Journal of virology. 1998 Jun;72(6):4882-92. PubMed PMID: 9573255. Pubmed Central PMCID: 110042.
513. Mosmann T. Rapid colorimetric assay for cellular growth and survival: application to proliferation and cytotoxicity assays. Journal of immunological methods. 1983 Dec 16;65(1-2):55-63. PubMed PMID: 6606682.
514. Nakatsu T, Ichiyama S, Hiratake J, Saldanha A, Kobashi N, Sakata K, et al. Structural basis for the spectral difference in luciferase bioluminescence. Nature. 2006 Mar 16;440(7082):372-6. PubMed PMID: 16541080.
515. O'Neill K, Lyons SK, Gallagher WM, Curran KM, Byrne AT. Bioluminescent imaging: a critical tool in pre-clinical oncology research. The Journal of pathology. 2010 Feb;220(3):317-27. PubMed PMID: 19967724.

516. Inouye S. Firefly luciferase: an adenylate-forming enzyme for multicatalytic functions. Cellular and molecular life sciences : CMLS. 2010 Feb;67(3):387-404. PubMed PMID: 19859663.
517. Josephy PD, Eling T, Mason RP. The horseradish peroxidase-catalyzed oxidation of 3,5,3',5'-tetramethylbenzidine. Free radical and charge-transfer complex intermediates. The Journal of biological chemistry. 1982 Apr 10;257(7):3669-75. PubMed PMID: 6277943.
518. Junttila TT, Akita RW, Parsons K, Fields C, Lewis Phillips GD, Friedman LS, et al. Ligand-independent HER2/HER3/PI3K complex is disrupted by trastuzumab and is effectively inhibited by the PI3K inhibitor GDC-0941. Cancer cell. 2009 May 5;15(5):429-40. PubMed PMID: 19411071.
519. Arnould L, Gelly M, Penault-Llorca F, Benoit L, Bonnetain F, Migeon C, et al. Trastuzumab-based treatment of HER2-positive breast cancer: an antibody-dependent cellular cytotoxicity mechanism? British journal of cancer. 2006 Jan 30;94(2):259-67. PubMed PMID: 16404427. Pubmed Central PMCID: 2361112.
520. Sawaki M, Mukai H, Tokudome N, Nakayama T, Taira N, Mizuno T, et al. Safety of adjuvant trastuzumab for HER-2-overexpressing elderly breast cancer patients: a multicenter cohort study. Breast cancer. 2012 Jul;19(3):253-8. PubMed PMID: 21526424.
521. Huszno J, Les D, Sarzyczny-Slota D, Nowara E. Cardiac side effects of trastuzumab in breast cancer patients - single centere experiences. Contemporary oncology. 2013;17(2):190-5. PubMed PMID: 23788989. Pubmed Central PMCID: 3685367.
522. Lemieux J, Diorio C, Cote MA, Provencher L, Barabe F, Jacob S, et al. Alcohol and HER2 Polymorphisms as Risk Factor for Cardiotoxicity in Breast Cancer Treated with Trastuzumab. Anticancer research. 2013 Jun;33(6):2569-76. PubMed PMID: 23749910.
523. Roca L, Dieras V, Roche H, Lappartient E, Kerbrat P, Cany L, et al. Correlation of HER2, FCGR2A, and FCGR3A gene polymorphisms with trastuzumab related cardiac toxicity and efficacy in a subgroup of patients from UNICANCER-PACS04 trial. Breast cancer research and treatment. 2013 Jun;139(3):789-800. PubMed PMID: 23780683.
524. de Azambuja E, Bedard PL, Suter T, Piccart-Gebhart M. Cardiac toxicity with anti-HER-2 therapies: what have we learned so far? Targeted oncology. 2009 Apr;4(2):77-88. PubMed PMID: 19418111.
525. Suter TM, Procter M, van Veldhuisen DJ, Muscholl M, Bergh J, Carlomagno C, et al. Trastuzumab-associated cardiac adverse effects in the herceptin adjuvant trial. Journal of clinical oncology : official journal of the American Society of Clinical Oncology. 2007 Sep 1;25(25):3859-65. PubMed PMID: 17646669.
526. Procter M, Suter TM, de Azambuja E, Dafni U, van Dooren V, Muehlbauer S, et al. Longer-term assessment of trastuzumab-related cardiac adverse events in the Herceptin Adjuvant (HERA) trial. Journal of clinical oncology : official journal of the American Society of Clinical Oncology. 2010 Jul 20;28(21):3422-8. PubMed PMID: 20530280.
527. Ghani EA, Kerr I, Dada R. Grade 3 trastuzumab-induced neutropenia in breast cancer patient. Journal of oncology pharmacy practice : official publication of the International Society of Oncology Pharmacy Practitioners. 2013 Jun 26. PubMed PMID: 23804626.
528. Oosterwijk E, Ruiter DJ, Hoedemaeker PJ, Pauwels EK, Jonas U, Zwartendijk J, et al. Monoclonal antibody G 250 recognizes a determinant present in renal-cell

carcinoma and absent from normal kidney. International journal of cancer Journal international du cancer. 1986 Oct 15;38(4):489-94. PubMed PMID: 2428759.
529. Steffens MG, Boerman OC, Oyen WJ, Kniest PH, Witjes JA, Oosterhof GO, et al. Intratumoral distribution of two consecutive injections of chimeric antibody G250 in primary renal cell carcinoma: implications for fractionated dose radioimmunotherapy. Cancer research. 1999 Apr 1;59(7):1615-9. PubMed PMID: 10197637.
530. Steffens MG, Oosterwijk-Wakka JC, Zegwaart-Hagemeier NE, Boerman OC, Debruyne FM, Corstens FH, et al. Immunohistochemical analysis of tumor antigen saturation following injection of monoclonal antibody G250. Anticancer research. 1999 Mar-Apr;19(2A):1197-200. PubMed PMID: 10368675.
531. Rajagopalan V, Zucker IH, Jones JA, Carlson M, Ma YJ. Cardiac ErbB-1/ErbB-2 mutant expression in young adult mice leads to cardiac dysfunction. American journal of physiology Heart and circulatory physiology. 2008 Aug;295(2):H543-54. PubMed PMID: 18599591.
532. Zhao YY, Sawyer DR, Baliga RR, Opel DJ, Han X, Marchionni MA, et al. Neuregulins promote survival and growth of cardiac myocytes. Persistence of ErbB2 and ErbB4 expression in neonatal and adult ventricular myocytes. The Journal of biological chemistry. 1998 Apr 24;273(17):10261-9. PubMed PMID: 9553078.
533. Prigent SA, Lemoine NR, Hughes CM, Plowman GD, Selden C, Gullick WJ. Expression of the c-erbB-3 protein in normal human adult and fetal tissues. Oncogene. 1992 Jul;7(7):1273-8. PubMed PMID: 1377811.
534. Srinivasan R, Poulsom R, Hurst HC, Gullick WJ. Expression of the c-erbB-4/HER4 protein and mRNA in normal human fetal and adult tissues and in a survey of nine solid tumour types. The Journal of pathology. 1998 Jul;185(3):236-45. PubMed PMID: 9771476.
535. Iwamoto R, Mekada E. ErbB and HB-EGF signaling in heart development and function. Cell structure and function. 2006;31(1):1-14. PubMed PMID: 16508205.
536. Press MF, Cordon-Cardo C, Slamon DJ. Expression of the HER-2/neu proto-oncogene in normal human adult and fetal tissues. Oncogene. 1990 Jul;5(7):953-62. PubMed PMID: 1973830.
537. Pino S, Brehm MA, Covassin-Barberis L, King M, Gott B, Chase TH, et al. Development of novel major histocompatibility complex class I and class II-deficient NOD-SCID IL2R gamma chain knockout mice for modeling human xenogeneic graft-versus-host disease. Methods in molecular biology. 2010;602:105-17. PubMed PMID: 20012395.
538. Ashida ER, Johnson AR, Lipsky PE. Human endothelial cell-lymphocyte interaction. Endothelial cells function as accessory cells necessary for mitogen-induced human T lymphocyte activation in vitro. The Journal of clinical investigation. 1981 May;67(5):1490-9. PubMed PMID: 6971878. Pubmed Central PMCID: 370717.
539. Bonfil RD, Vinyals A, Bustuoabad OD, Llorens A, Benavides FJ, Gonzalez-Garrigues M, et al. Stimulation of angiogenesis as an explanation of Matrigel-enhanced tumorigenicity. International journal of cancer Journal international du cancer. 1994 Jul 15;58(2):233-9. PubMed PMID: 7517919.
540. Topley P, Jenkins DC, Jessup EA, Stables JN. Effect of reconstituted basement membrane components on the growth of a panel of human tumour cell lines in nude mice. British journal of cancer. 1993 May;67(5):953-8. PubMed PMID: 8494729. Pubmed Central PMCID: 1968456.
541. De Keulenaer GW, Doggen K, Lemmens K. The vulnerability of the heart as a pluricellular paracrine organ: lessons from unexpected triggers of heart failure in

targeted ErbB2 anticancer therapy. Circulation research. 2010 Jan 8;106(1):35-46. PubMed PMID: 20056944.
542. Smith JM, Sporn MB, Roberts AB, Derynck R, Winkler ME, Gregory H. Human transforming growth factor-alpha causes precocious eyelid opening in newborn mice. Nature. 1985 Jun 6-12;315(6019):515-6. PubMed PMID: 3873618.
543. Abdullah NA, Torres BA, Basu M, Johnson HM. Differential effects of epidermal growth factor, transforming growth factor-alpha, and vaccinia virus growth factor in the positive regulation of IFN-gamma production. Journal of immunology. 1989 Jul 1;143(1):113-7. PubMed PMID: 2499624.
544. Carlsson T, Schindler FR, Hollerhage M, Depboylu C, Arias-Carrion O, Schnurrbusch S, et al. Systemic administration of neuregulin-1beta1 protects dopaminergic neurons in a mouse model of Parkinson's disease. Journal of neurochemistry. 2011 Jun;117(6):1066-74. PubMed PMID: 21517849.
545. Ibbotson KJ, Harrod J, Gowen M, D'Souza S, Smith DD, Winkler ME, et al. Human recombinant transforming growth factor alpha stimulates bone resorption and inhibits formation in vitro. Proceedings of the National Academy of Sciences of the United States of America. 1986 Apr;83(7):2228-32. PubMed PMID: 3485799. Pubmed Central PMCID: 323265.
546. Liu X, Gu X, Li Z, Li X, Li H, Chang J, et al. Neuregulin-1/erbB-activation improves cardiac function and survival in models of ischemic, dilated, and viral cardiomyopathy. Journal of the American College of Cardiology. 2006 Oct 3;48(7):1438-47. PubMed PMID: 17010808.
547. Bernhard H, Neudorfer J, Gebhard K, Conrad H, Hermann C, Nahrig J, et al. Adoptive transfer of autologous, HER2-specific, cytotoxic T lymphocytes for the treatment of HER2-overexpressing breast cancer. Cancer immunology, immunotherapy : CII. 2008 Feb;57(2):271-80. PubMed PMID: 17646988.
548. Read EJ, Keenan AM, Carter CS, Yolles PS, Davey RJ. In vivo traffic of indium-111-oxine labeled human lymphocytes collected by automated apheresis. Journal of nuclear medicine : official publication, Society of Nuclear Medicine. 1990 Jun;31(6):999-1006. PubMed PMID: 2112185.
549. Wagstaff J, Gibson C, Thatcher N, Ford WL, Sharma H, Crowther D. Human lymphocyte traffic assessed by indium-111 oxine labelling: clinical observations. Clinical and experimental immunology. 1981 Mar;43(3):443-9. PubMed PMID: 7285388. Pubmed Central PMCID: 1537191.
550. Fisher B, Packard BS, Read EJ, Carrasquillo JA, Carter CS, Topalian SL, et al. Tumor localization of adoptively transferred indium-111 labeled tumor infiltrating lymphocytes in patients with metastatic melanoma. Journal of clinical oncology : official journal of the American Society of Clinical Oncology. 1989 Feb;7(2):250-61. PubMed PMID: 2644399.
551. Cao YA, Bachmann MH, Beilhack A, Yang Y, Tanaka M, Swijnenburg RJ, et al. Molecular imaging using labeled donor tissues reveals patterns of engraftment, rejection, and survival in transplantation. Transplantation. 2005 Jul 15;80(1):134-9. PubMed PMID: 16003245.
552. Serrano LM, Pfeiffer T, Olivares S, Numbenjapon T, Bennitt J, Kim D, et al. Differentiation of naive cord-blood T cells into CD19-specific cytolytic effectors for posttransplantation adoptive immunotherapy. Blood. 2006 Apr 1;107(7):2643-52. PubMed PMID: 16352804. Pubmed Central PMCID: 1895371.

553. Barry SM, Johnson MA, Janossy G. Cytopathology or immunopathology? The puzzle of cytomegalovirus pneumonitis revisited. Bone marrow transplantation. 2000 Sep;26(6):591-7. PubMed PMID: 11035367.
554. Imashuku S. Clinical features and treatment strategies of Epstein-Barr virus-associated hemophagocytic lymphohistiocytosis. Critical reviews in oncology/hematology. 2002 Dec;44(3):259-72. PubMed PMID: 12467966.
555. Huang KJ, Su IJ, Theron M, Wu YC, Lai SK, Liu CC, et al. An interferon-gamma-related cytokine storm in SARS patients. Journal of medical virology. 2005 Feb;75(2):185-94. PubMed PMID: 15602737.
556. Yuen KY, Wong SS. Human infection by avian influenza A H5N1. Hong Kong medical journal = Xianggang yi xue za zhi / Hong Kong Academy of Medicine. 2005 Jun;11(3):189-99. PubMed PMID: 15951584.
557. Panelli MC, White R, Foster M, Martin B, Wang E, Smith K, et al. Forecasting the cytokine storm following systemic interleukin (IL)-2 administration. Journal of translational medicine. 2004 Jun 2;2(1):17. PubMed PMID: 15175100. Pubmed Central PMCID: 434535. Epub 2004/06/04. Eng.
558. Suntharalingam G, Perry MR, Ward S, Brett SJ, Castello-Cortes A, Brunner MD, et al. Cytokine storm in a phase 1 trial of the anti-CD28 monoclonal antibody TGN1412. The New England journal of medicine. 2006 Sep 7;355(10):1018-28. PubMed PMID: 16908486.
559. Hodi FS. Overcoming immunological tolerance to melanoma: Targeting CTLA-4. Asia-Pacific journal of clinical oncology. 2010 Mar;6 Suppl 1:S16-23. PubMed PMID: 20482528.
560. Suthanthiran M, Fotino M, Riggio RR, Cheigh JS, Stenzel KH. OKT3-associated adverse reactions: mechanistic basis and therapeutic options. American journal of kidney diseases : the official journal of the National Kidney Foundation. 1989 Nov;14(5 Suppl 2):39-44. PubMed PMID: 2530898.
561. Goldman M, Abramowicz D, De Pauw L, Alegre ML, Widera I, Vereerstraeten P, et al. OKT3-induced cytokine release attenuation by high-dose methylprednisolone. Lancet. 1989 Sep 30;2(8666):802-3. PubMed PMID: 2571039.
562. Chung CH. Managing premedications and the risk for reactions to infusional monoclonal antibody therapy. The oncologist. 2008 Jun;13(6):725-32. PubMed PMID: 18586928.
563. Bugelski PJ, Achuthanandam R, Capocasale RJ, Treacy G, Bouman-Thio E. Monoclonal antibody-induced cytokine-release syndrome. Expert review of clinical immunology. 2009 Sep;5(5):499-521. PubMed PMID: 20477639.
564. Tisoncik JR, Korth MJ, Simmons CP, Farrar J, Martin TR, Katze MG. Into the eye of the cytokine storm. Microbiology and molecular biology reviews : MMBR. 2012 Mar;76(1):16-32. PubMed PMID: 22390970. Pubmed Central PMCID: 3294426.
565. Levy MM, Fink MP, Marshall JC, Abraham E, Angus D, Cook D, et al. 2001 SCCM/ESICM/ACCP/ATS/SIS International Sepsis Definitions Conference. Critical care medicine. 2003 Apr;31(4):1250-6. PubMed PMID: 12682500.
566. Rubenfeld GD, Caldwell E, Peabody E, Weaver J, Martin DP, Neff M, et al. Incidence and outcomes of acute lung injury. The New England journal of medicine. 2005 Oct 20;353(16):1685-93. PubMed PMID: 16236739.
567. Frazier WJ, Hall MW. Immunoparalysis and adverse outcomes from critical illness. Pediatric clinics of North America. 2008 Jun;55(3):647-68, xi. PubMed PMID: 18501759. Pubmed Central PMCID: 2474674.

568. Mongkolsapaya J, Dejnirattisai W, Xu XN, Vasanawathana S, Tangthawornchaikul N, Chairunsri A, et al. Original antigenic sin and apoptosis in the pathogenesis of dengue hemorrhagic fever. Nature medicine. 2003 Jul;9(7):921-7. PubMed PMID: 12808447.
569. Beyersdorf N, Gaupp S, Balbach K, Schmidt J, Toyka KV, Lin CH, et al. Selective targeting of regulatory T cells with CD28 superagonists allows effective therapy of experimental autoimmune encephalomyelitis. The Journal of experimental medicine. 2005 Aug 1;202(3):445-55. PubMed PMID: 16061730. Pubmed Central PMCID: 2213080.
570. Tacke M, Hanke G, Hanke T, Hunig T. CD28-mediated induction of proliferation in resting T cells in vitro and in vivo without engagement of the T cell receptor: evidence for functionally distinct forms of CD28. European journal of immunology. 1997 Jan;27(1):239-47. PubMed PMID: 9022025.
571. Luhder F, Huang Y, Dennehy KM, Guntermann C, Muller I, Winkler E, et al. Topological requirements and signaling properties of T cell-activating, anti-CD28 antibody superagonists. The Journal of experimental medicine. 2003 Apr 21;197(8):955-66. PubMed PMID: 12707299. Pubmed Central PMCID: 2193880.
572. Abramowicz D, Schandene L, Goldman M, Crusiaux A, Vereerstraeten P, De Pauw L, et al. Release of tumor necrosis factor, interleukin-2, and gamma-interferon in serum after injection of OKT3 monoclonal antibody in kidney transplant recipients. Transplantation. 1989 Apr;47(4):606-8. PubMed PMID: 2523100.
573. Eastwood D, Bird C, Dilger P, Hockley J, Findlay L, Poole S, et al. Severity of the TGN1412 trial disaster cytokine storm correlated with IL-2 release. British journal of clinical pharmacology. 2013 May 23. PubMed PMID: 23701319.
574. Alwan LM, Grossmann K, Sageser D, Van Atta J, Agarwal N, Gilreath JA. Comparison of acute toxicity and mortality after two different dosing regimens of high-dose interleukin-2 for patients with metastatic melanoma. Targeted oncology. 2013 Apr 23. PubMed PMID: 23609056.
575. Sandilands GP, Wilson M, Huser C, Jolly L, Sands WA, McSharry C. Were monocytes responsible for initiating the cytokine storm in the TGN1412 clinical trial tragedy? Clinical and experimental immunology. 2010 Dec;162(3):516-27. PubMed PMID: 20964641. Pubmed Central PMCID: 3026555.
576. Klinger M, Brandl C, Zugmaier G, Hijazi Y, Bargou RC, Topp MS, et al. Immunopharmacologic response of patients with B-lineage acute lymphoblastic leukemia to continuous infusion of T cell-engaging CD19/CD3-bispecific BiTE antibody blinatumomab. Blood. 2012 Jun 28;119(26):6226-33. PubMed PMID: 22592608.
577. Teachey DT, Rheingold SR, Maude SL, Zugmaier G, Barrett DM, Seif AE, et al. Cytokine release syndrome after blinatumomab treatment related to abnormal macrophage activation and ameliorated with cytokine directed therapy. Blood. 2013 May 15. PubMed PMID: 23678006.
578. Rodriguez-Palmero M, Hara T, Thumbs A, Hunig T. Triggering of T cell proliferation through CD28 induces GATA-3 and promotes T helper type 2 differentiation in vitro and in vivo. European journal of immunology. 1999 Dec;29(12):3914-24. PubMed PMID: 10601999.
579. Eastwood D, Findlay L, Poole S, Bird C, Wadhwa M, Moore M, et al. Monoclonal antibody TGN1412 trial failure explained by species differences in CD28 expression on CD4+ effector memory T-cells. British journal of pharmacology. 2010 Oct;161(3):512-26. PubMed PMID: 20880392. Pubmed Central PMCID: 2990151.

580. Hunig T. The storm has cleared: lessons from the CD28 superagonist TGN1412 trial. Nature reviews Immunology. 2012 May;12(5):317-8. PubMed PMID: 22487653. Epub 2012/04/11. eng.
581. Stebbings R, Findlay L, Edwards C, Eastwood D, Bird C, North D, et al. "Cytokine storm" in the phase I trial of monoclonal antibody TGN1412: better understanding the causes to improve preclinical testing of immunotherapeutics. Journal of immunology. 2007 Sep 1;179(5):3325-31. PubMed PMID: 17709549.
582. Dustin ML, Olszowy MW, Holdorf AD, Li J, Bromley S, Desai N, et al. A novel adaptor protein orchestrates receptor patterning and cytoskeletal polarity in T-cell contacts. Cell. 1998 Sep 4;94(5):667-77. PubMed PMID: 9741631.
583. Sanchez-Lockhart M, Miller J. Engagement of CD28 outside of the immunological synapse results in up-regulation of IL-2 mRNA stability but not IL-2 transcription. Journal of immunology. 2006 Apr 15;176(8):4778-84. PubMed PMID: 16585571.
584. Thoulouze MI, Sol-Foulon N, Blanchet F, Dautry-Varsat A, Schwartz O, Alcover A. Human immunodeficiency virus type-1 infection impairs the formation of the immunological synapse. Immunity. 2006 May;24(5):547-61. PubMed PMID: 16713973.
585. Romer PS, Berr S, Avota E, Na SY, Battaglia M, ten Berge I, et al. Preculture of PBMCs at high cell density increases sensitivity of T-cell responses, revealing cytokine release by CD28 superagonist TGN1412. Blood. 2011 Dec 22;118(26):6772-82. PubMed PMID: 21931118.
586. Frigault MJ, June CH. Predicting cytokine storms: it's about density. Blood. 2011 Dec 22;118(26):6724-6. PubMed PMID: 22194391.
587. Xing Z, Zganiacz A, Wang J, Sharma SK. Enhanced protection against fatal mycobacterial infection in SCID beige mice by reshaping innate immunity with IFN-gamma transgene. Journal of immunology. 2001 Jul 1;167(1):375-83. PubMed PMID: 11418673.
588. Okazaki M, Yamada Y, Nishimoto N, Yoshizaki K, Mihara M. Characterization of anti-mouse interleukin-6 receptor antibody. Immunology letters. 2002 Dec 3;84(3):231-40. PubMed PMID: 12413742.
589. Tawara I, Koyama M, Liu C, Toubai T, Thomas D, Evers R, et al. Interleukin-6 modulates graft-versus-host responses after experimental allogeneic bone marrow transplantation. Clinical cancer research : an official journal of the American Association for Cancer Research. 2011 Jan 1;17(1):77-88. PubMed PMID: 21047980. Pubmed Central PMCID: 3058832.
590. Van Rooijen N, Sanders A. Liposome mediated depletion of macrophages: mechanism of action, preparation of liposomes and applications. Journal of immunological methods. 1994 Sep 14;174(1-2):83-93. PubMed PMID: 8083541. Epub 1994/09/14. eng.
591. Buiting AM, Van Rooijen N. Liposome mediated depletion of macrophages: an approach for fundamental studies. J Drug Target. 1994;2(5):357-62. PubMed PMID: 7704479. Epub 1994/01/01. eng.
592. Zeisberger SM, Odermatt B, Marty C, Zehnder-Fjallman AH, Ballmer-Hofer K, Schwendener RA. Clodronate-liposome-mediated depletion of tumour-associated macrophages: a new and highly effective antiangiogenic therapy approach. British journal of cancer. 2006 Aug 7;95(3):272-81. PubMed PMID: 16832418. Pubmed Central PMCID: 2360657. Epub 2006/07/13. eng.

593. Palmer U, Liu Z, Broome U, Klominek J. Epidermal growth factor receptor ligands are chemoattractants for normal human mesothelial cells. The European respiratory journal. 1999 Aug;14(2):405-11. PubMed PMID: 10515421.
594. Paniagua R, Ventura Mde J, Rodriguez E, Sil J, Galindo T, Hurtado ME, et al. Impact of fill volume on peritoneal clearances and cytokine appearance in peritoneal dialysis. Peritoneal dialysis international : journal of the International Society for Peritoneal Dialysis. 2004 Mar-Apr;24(2):156-62. PubMed PMID: 15119636.
595. Foon KA, Sherwin SA, Abrams PG, Stevenson HC, Holmes P, Maluish AE, et al. A phase I trial of recombinant gamma interferon in patients with cancer. Cancer immunology, immunotherapy : CII. 1985;20(3):193-7. PubMed PMID: 3933818.
596. Vadhan-Raj S, Al-Katib A, Bhalla R, Pelus L, Nathan CF, Sherwin SA, et al. Phase I trial of recombinant interferon gamma in cancer patients. Journal of clinical oncology : official journal of the American Society of Clinical Oncology. 1986 Feb;4(2):137-46. PubMed PMID: 3080551.
597. Gibbs VC, Williams SR, Gray PW, Schreiber RD, Pennica D, Rice G, et al. The extracellular domain of the human interferon gamma receptor interacts with a species-specific signal transducer. Molecular and cellular biology. 1991 Dec;11(12):5860-6. PubMed PMID: 1834931. Pubmed Central PMCID: 361734.
598. Le Tourneau C, Lee JJ, Siu LL. Dose escalation methods in phase I cancer clinical trials. Journal of the National Cancer Institute. 2009 May 20;101(10):708-20. PubMed PMID: 19436029. Pubmed Central PMCID: 2684552.
599. Porter DL, Levine BL, Bunin N, Stadtmauer EA, Luger SM, Goldstein S, et al. A phase 1 trial of donor lymphocyte infusions expanded and activated ex vivo via CD3/CD28 costimulation. Blood. 2006 Feb 15;107(4):1325-31. PubMed PMID: 16269610.
600. Lamers CH, van Elzakker P, Langeveld SC, Sleijfer S, Gratama JW. Process validation and clinical evaluation of a protocol to generate gene-modified T lymphocytes for imunogene therapy for metastatic renal cell carcinoma: GMP-controlled transduction and expansion of patient's T lymphocytes using a carboxy anhydrase IX-specific scFv transgene. Cytotherapy. 2006;8(6):542-53. PubMed PMID: 17148030.
601. Lamers CH, van Elzakker P, van Steenbergen SC, Sleijfer S, Debets R, Gratama JW. Retronectin-assisted retroviral transduction of primary human T lymphocytes under good manufacturing practice conditions: tissue culture bag critically determines cell yield. Cytotherapy. 2008;10(4):406-16. PubMed PMID: 18574773.
602. Hollyman D, Stefanski J, Przybylowski M, Bartido S, Borquez-Ojeda O, Taylor C, et al. Manufacturing validation of biologically functional T cells targeted to CD19 antigen for autologous adoptive cell therapy. Journal of immunotherapy. 2009 Feb-Mar;32(2):169-80. PubMed PMID: 19238016. Pubmed Central PMCID: 2683970.
603. Invitrogen. 2013 [13/06/2013]. Available from: http://www.invitrogen.com/etc/medialib/en/images/ics_organized/brands/Dynal/bigger-is-better.Par.38235.Image.180.306.1..gif.
604. Levine BL, Cotte J, Small CC, Carroll RG, Riley JL, Bernstein WB, et al. Large-scale production of CD4+ T cells from HIV-1-infected donors after CD3/CD28 costimulation. Journal of hematotherapy. 1998 Oct;7(5):437-48. PubMed PMID: 9829318.
605. MHRA. EU guidance on good manufacturing practice. London: Pharmaceutical Press; 2007.
606. Puri RK, Mehrotra PT, Leland P, Kreitman RJ, Siegel JP, Pastan I. A chimeric protein comprised of IL-4 and Pseudomonas exotoxin is cytotoxic for activated human

lymphocytes. Journal of immunology. 1994 Apr 1;152(7):3693-700. PubMed PMID: 8144944. Epub 1994/04/01. eng.
607. Garland L, Gitlitz B, Ebbinghaus S, Pan H, de Haan H, Puri RK, et al. Phase I trial of intravenous IL-4 pseudomonas exotoxin protein (NBI-3001) in patients with advanced solid tumors that express the IL-4 receptor. Journal of immunotherapy. 2005 Jul-Aug;28(4):376-81. PubMed PMID: 16000956. Epub 2005/07/08. eng.
608. Reagan-Shaw S, Nihal M, Ahmad N. Dose translation from animal to human studies revisited. FASEB journal : official publication of the Federation of American Societies for Experimental Biology. 2008 Mar;22(3):659-61. PubMed PMID: 17942826.